UNIVERSITY OF CALIFORNIA SAN DIEGO

Untangling Intertwined Pathways: Cholesterol Metabolism, APP Processing, and Tau Phosphorylation in Alzheimer's Disease

A dissertation submitted in partial fulfillment of the requirement
for the degree of Doctor of Philosophy

in

Biomedical Sciences

by

Vanessa Francine Langness

Committee in Charge:

Professor Lawrence S.B. Goldstein, Chair
Professor Don Cleveland
Professor Seth Field
Professor Shelley Halpain
Professor Edward Koo
Professor Samara Reck-Peterson

2019

The Dissertation of Vanessa Francine Langness is approved, and it is acceptable in quality and form for publication on microfilm and electronically:

Chair

University of California San Diego

2019

DEDICATION

To my family, my friends, and my pets.

EPIGRAPH

“Through our eyes, the universe is perceiving itself. Through our ears, the universe is listening to its harmonies.”

Allan Watts

TABLE OF CONTENTS

LIST OF ABBREVIATIONS

ABCA7 ATP-binding cassette sub-family A, member 7

AD Alzheimer's disease

AICD APP intracellular domain

APOE Apolipoprotein E

APOJ Apolipoprotein J

APP Amyloid Precursor Protein

APP^{dp} APP Duplication

Aβ Amyloid beta

ACAT Acyl-CoA cholesterol acyltransferase

BACE 1 β-secretase

BSI β-secretase inhibitor

BIV β-secretase inhibitor IV

BBR Berberine;

BiFC Bimolecular fluorescence complementation

BisTris 2-[bis(2-hydroxyethyl)amino]-2-(hydroxymethyl)propane-1,3-diol

CE Cholesterol Esters

CTF Amyloid Precursor Protein C-Terminal Fragment

CYP46A1 cholesterol 24-hydroxylase

DHCR7 Δ7-dehydrocholesterol reductase

DMEM Dulbecco's modified Eagle's medium

EOAD Early onset Alzheimer's disease

Farnesyl-PP Farnesyl-pyrophosphate

FAD Familial Alzheimer's disease

Farnesyl-PP Farnesyl-pyrophosphate

FBS Fetal bovine serum

FDA Food and Drug Administration

flAPP Full length APP

GXXXG Glycine-XXX-glycine

HDL High density lipoprotein

hiPSC Human Induced Pluripotent Stem Cell

HMGCR 3-hydroxy-3-methylglutaryl-CoA reductase

iPSC Induced pluripotent stem cell

KO Knock-out

LDL Low density lipoprotein

LDLR Low density lipoprotein receptor

LOAD Late onset Alzheimer's disease

LXR liver X receptor

MEF Mouse embryonic fibroblast.

MSD-ECL Meso Scale Discovery electrochemiluminescence

MVA Mevalonate

MVP mevalonate-5-phosphate

mTor mechanistic target of rapamycin

NDC Non-demented control

NPC Neural Progenitor Cell

NFT Neurofibrillary Tangles

RI ROCK inhibitor

PE phosphatidylethanolamine

PS1 Presenilin 1

PS2 Presenilin 2

pTau Hyperphosphorylated Tau protein

qRT-PCR quantitative RT-PCR

SAD Sporadic Alzheimer's disease

sAPP Soluble APP

SM sphingomyelin

SREBP Sterol-regulatory element-binding protein

Tfn Transferrin

UPS ubiquitin-proteasome system

VN Venus fluorophore N-terminus

VC Venus fluorophore C-terminus

WT Wild Type

LIST OF SUPPLEMENTAL FILES

Supplemental Table 1 Screening Data from Initial Screen, Related to Figure 1

Supplemental Table 3 Comparison of Primary and Secondary Screen Results, Related to Figure 1

Supplemental Table 4 Mass Spectrometry Results Comparing Protein Expression in Vehicle (DMSO) and Statin-Treated Neurons, Related to Figure 2

LIST OF FIGURES

LIST OF TABLES

ACKNOWLEDGEMENTS

I would like to acknowledge the support of Larry Goldstein, my thesis advisor. Larry is an incredibly kind person and a great leader. He gave me a lot of trust and freedom to explore and try different things in the lab. He was generous with his time and gave me a lot of scientific insight and guidance on my project. His guidance has pushed me to grow as a scientist and as a communicator of science. Larry also sent me to various conferences during my time in graduate school. This has allowed me to gain a broader understanding of our field. This has also given me the opportunity to refine my public speaking skills. Outside of that, it has given me the opportunity to travel to different countries and experience the world. Thank you for believing in me and for being so supportive of my career and my development as a scientist over the years.

I would also like to thank Don Cleveland, Seth Field, Shelley Halpain, Edward Koo, and Samara Reck-Peterson for serving on my committee. Their guidance on my project has been invaluable and their critiques have challenged me to become a better scientist. Their commitment to training the next generation of scientists is greatly appreciated.

Thank you to all of the members of the Goldstein lab, past and present for sharing your knowledge and expertise and for always challenging me to improve as a scientist and as a person. I would especially like to thank Rik van der Kant who took me under his wing in lab. Rik helped me to get started in the lab and he would often

go out of his way to engage me in regular scientific discussions. His scientific insight and mentorship really helped to shape my thesis project over the years and helped me to evolve into a better scientist. I would also like to thank Louie Wang for the opportunity to mentor him for his Master's thesis in our lab and for all of the important work he has done on this project. Thank you also to Lauren Fong for the important work she did on collaborative projects. Thank you to Angels Almenhar, Utpal Das, Rodrigo dos santos Chaves and Chao Shun Yang for scientific advice and encouragement.

Thank you to the Biomedical Sciences (BMS) Graduate Program for accepting me into the program and for creating a supportive and fun learning environment, for providing career development opportunities, and for giving me this opportunity to earn my PhD at UCSD. I am so grateful to have been a part of such a great program with such wonderful and supportive people. Thank you to my fellow BMS students for being so positive and friendly and for making me feel like I have a family away from home.

Thank you to my husband Jonathan for being my partner through all of this. Thank you for listening to me vent when I had bad days and thank you for celebrating with me on the good days. Thank you to my family and my husband's family for all of their support throughout the years. Thank you to my mom for being incredibly supportive of everything that I do and for always being there for me. I am grateful that you made sure I always had chemistry sets and microscopes to tinker with while growing up. Thank you to my dad who sometimes would take me out to look at the night sky through his telescope. Thank you both for taking me to the library and encouraging me to have a love of learning.

Thank you to Sluffy and Moose, my pets for being amazing creatures who have comforted me and have been great sources of support. Sluffy moved with me all the way from Denver and was a great cat and great companion. Moose has sat on my lap every day while I have been writing my dissertation. I call him my thesis support dog. I am pretty sure he deserves a PhD too once I defend. I will definitely call him Dr. Moose from now on.

Chapter 2, in full, is a reprint of the material as it appears in Cell Stem Cell 2019. Kant, R. van der, Langness, V. F., Herrera, C. M., Williams, D. A., Fong, L. K., Leestemaker, Y., Steenvoorden, E., Rynearson, K. D., Brouwers, J. F., Helms, J. B., Ovaa, H., Giera, M., Wagner, S. L., Bang, A. G., and Goldstein, L. S. B. (2019) The dissertation author was the co-first author on this paper.

Chapter 3, in full, is currently being prepared for submission for publication of the material. Langness, V. F., Kant, R. van der, Das, U., Wang, L., Chaves, R., Young, J., Goldstein, L. S. B. The dissertation author was the primary investigator and author of this material.

Chapter 4, in full, is a reprint of the material as it appears in JBC 2018. Fong, L. K., Yang, M. M., Chaves, R. dos S., Reyna, S. M., Langness, V. F., Woodruff, G., Roberts, E. A., Young, J. E., and Goldstein, L. S. B. (2018) Full-length amyloid precursor protein regulates lipoprotein metabolism and amyloid-β clearance in human astrocytes. *J. Biol. Chem.* 10.1074/jbc.RA117.000441 The dissertation author was a co-author on this paper.

VITA

2013 Bachelor of Science, Chemistry & Biology, Metropolitan State University of Denver

2019 Doctor of Philosophy, University of California San Diego

PUBLICATIONS

Vanessa Langness, Rik van der Kant, Utpal Das, Louie Wang, Rodrigo Chaves, Lawrence SB. Goldstein. “Cholesterol Lowering Drugs Reduce APP Processing to Aβ by inducing APP Dimerization ". Manuscript In Preparation

Kant, Rik van der*, **Vanessa F. Langness***, Cheryl M. Herrera, Daniel A. Williams, Lauren K. Fong, Yves Leestemaker, Evelyne Steenvoorden, et al. “Cholesterol Metabolism Is a Druggable Axis That Independently Regulates Tau and Amyloid-β in IPSC-Derived Alzheimer’s Disease Neurons.” *Cell Stem Cell* 24, no. 3 (March 7, 2019): 363-375.e9. https://doi.org/10.1016/j.stem.2018.12.013.
**Co-First Authors*

Fong, Lauren K., Max M. Yang, Rodrigo dos Santos Chaves, Sol M. Reyna, **Vanessa F. Langness**, Grace Woodruff, Elizabeth A. Roberts, Jessica E. Young, and Lawrence S. B. Goldstein. “Full-Length Amyloid Precursor Protein Regulates Lipoprotein Metabolism and Amyloid-β Clearance in Human Astrocytes.” *Journal of Biological Chemistry*, June 1, 2018, jbc.RA117.000441. https://doi.org/10.1074/jbc.RA117.000441.

ABSTRACT OF THE DISSERTATION

Untangling Intertwined Pathways:
Cholesterol Metabolism, APP Processing, and Tau Phosphorylation in Alzheimer's Disease

by

Vanessa Langness

Doctor of Philosophy in Biomedical Sciences

University of California San Diego, 2019

Professor Lawrence S.B. Goldstein, Chair

Alzheimer's disease (AD) is a progressive neurodegenerative disease that results in loss of neurons and synapses. The dementia associated with AD is devastating for families and poses an increasing social and economic burden as our

population ages. Currently there are no drugs available that can revert or even slow disease progression.

Brains from human patients with AD exhibit two defining pathological changes: 1) Accumulation of extracellular amyloid plaques which are composed of amyloid beta (Aß), and; 2) accumulation of intracellular neurofibrillary tangles which are made up of hyperphosphorylated tau (pTau) protein. These changes are thought to be toxic and contribute to the devastating neurodegeneration that occurs in AD. Recent developments in disease modeling using human induced pluripotent stem cells (hiPSCs) have allowed for modeling of Alzheimer's disease in human neurons in a dish. We can measure Aß and pTau levels in these hiPSC derived neurons allowing us to study how the levels of these proteins become dysregulated in AD.

Genetic, biochemical, pharmacological, and epidemiological data suggest a role for cholesterol in AD pathogenesis. Recent studies have shown that amyloid precursor protein (APP), the precursor to Aß contains a cholesterol binding site. We use cholesterol lowering drugs, CRISPR/CAS9 genome editing, and fluorescent complementation assays to study how cholesterol levels and mutations that abolish APP-Cholesterol binding influence Aß and pTau burden. Our data indicate that cholesterol metabolism influences levels of these toxic proteins. We also show that APP can influence cholesterol homeostasis by regulating transport of cholesterol between different cell types in the brain. Our work sheds light on a pathway which unites the variety of genetic and environmental factors that contribute to AD risk.

Targeting cholesterol metabolic pathways may be a promising approach in the search for drugs which can treat or prevent AD.

Chapter 1

Introduction

In 1907 Dr. Alois Alzheimer published what is widely accepted as the first characterization of the disease which was later named after him. He described the symptoms of Auguste Deter, a woman who was under his care at an “insane asylum” in Frankfurt Germany (1):

> The first symptom the 51-year-old woman showed was the idea that she was jealous of her husband. Soon she developed a rapid loss of memory. She was disoriented in her home, carried things from one place to another and hid them, sometimes she thought somebody was trying to kill her and started to cry loudly. In the institution her behavior showed all the signs of complete helplessness. She is completely disoriented in time and space. Sometimes she says that she does not understand anything and that everything is strange to her. Sometimes she greets the attending physician like company and asks to be excused for not having completed the household chores, sometimes she protests loudly that he intends to cut her, or she rebukes him vehemently with expressions which imply that she suspects him of dishonorable intentions. Then again she is completely delirious, drags around her bedding, calls her husband and daughter and seems to suffer from auditory hallucinations. Often she screamed for many hours... Her memory is seriously impaired. If objects are shown to her, she names them correctly, but almost immediately afterwards she has forgotten everything. When reading a test, she skips from line to line or reads by spelling the words individually, or by making them meaningless through her pronunciation. In writing, she repeats separate syllables many times, omits others, and quickly breaks down completely. In speaking, she uses gap-fills and a few paraphrased expressions (“milk-pourer’’ instead of cup); sometimes it is obvious that she cannot go on. Plainly, she does not understand certain questions. She does no longer remember the use of some objects. Her walk is unimpeded, she uses her hands equally well. Her patellar reflexes are normal. Her pupils react normally.(2)

Post-mortem observation of Deter’s brain revealed several features that distinguished it from a normal brain. Deter’s brain was atrophic, many neurons had completely disintegrated and in their place were a “tangle of fibrils”. Alzheimer also noted a parallel

process “deposition of a pathological metabolic substance in the neuron whose closer examination is still pending”.

This initial work set the foundation for later studies that characterized what we now know to be the key histological hallmarks of AD. The first hallmark is accumulation of extracellular plaques containing amyloid-β (Aβ) peptide in the brain. These amyloid plaques are surrounded by neurons that contain the second histopathological hallmark of AD: intracellular neurofibrillary tangles (NFTs) containing hyperphosphorylated tau (pTau). These changes are accompanied by brain atrophy and a loss of neurons and synapses in the neocortex, and hippocampus, as well as other subcortical regions of the brain (3, 4). Early studies showed a strong correlation of cognitive decline with amyloid and Tau pathology. Finding drugs that lower Aβ and pTau levels in the brain has been a major focus of researchers seeking to treat or prevent AD.

The amyloid cascade hypothesis was first proposed in the early 90’s by John Hardy and Dennis Selkoe. It states that deposition of Aβ peptide in the brain is toxic and that pTau, NFTs, the neuronal and synaptic loss, and dementia characteristic of AD are all a direct result of Aβ accumulation (4–6). The amyloid cascade hypothesis has been criticized because the number of amyloid plaques do not correlate well with the degree of cognitive impairment (7). However, the hypothesis has been refined since it was first proposed. Accumulation of soluble Aβ oligomers appear to correlate better with the degree of cognitive impairment. The current view in the field is that soluble Aβ oligomers are the neurotoxic species, not the plaques (8). Several drugs have been developed that were successful at reducing Aβ in the brain, but all of them

have failed to improve cognitive function in patients (5). This has caused many scientists to question whether Aβ is the toxic species in AD or whether its accumulation is an epiphenomenon. While Aβ oligomers likely do contribute to neurodegeneration, Aβ oligomers may accumulate late in the disease process. This may occur once many of the hard to reverse effects like neuron and synapse loss have already manifested. Whether Aβ accumulation causes AD, or whether it accumulates downstream of earlier pathogenic changes, gaining an understanding of the pathways that regulate Aβ production in the brain may give us clues into the early drivers of AD pathogenesis and could lead us to better drug targets. One major focus of my thesis work involved elucidating how Aβ production and pTau levels are regulated in cultured hiPSC derived neurons.

Aβ is Derived From Proteolytic Cleavage of Amyloid Precursor Protein

It is well established that Aβ is generated by proteolytic cleavage of its full-length precursor, amyloid precursor protein (APP) (9). Proteolytic processing of APP can occur by at least two pathways (Figure 1.1). In the amyloidogenic pathway, APP is first cleaved by β-secretase (BACE1) into two fragments, a membrane bound β-C-terminal fragment (βCTF) and soluble APP-β (sAPPβ). In the non-amyloidogenic pathway, APP is first cleaved by α-secretase into two fragments, a membrane bound α-C-terminal fragment (αCTF), and soluble APP-α (sAPPα). Both α- and β- CTF can be further cleaved by γ-secretase. Cleavage of αCTF by γ-secretase results in generation of the non-amyloidogenic peptide p3 and the AICD fragment. Cleavage of βCTF by γ-secretase results in generation of the amyloidogenic peptide Aβ and the

AICD fragment. γ-secretase can cut at slightly different locations within βCTF. Depending on where γ-secretase cuts, it can give rise to Aβ40 or the slightly longer Aβ42 fragment. Aβ42 is thought to be more pathogenic because it is more prone to toxic oligomer formation.

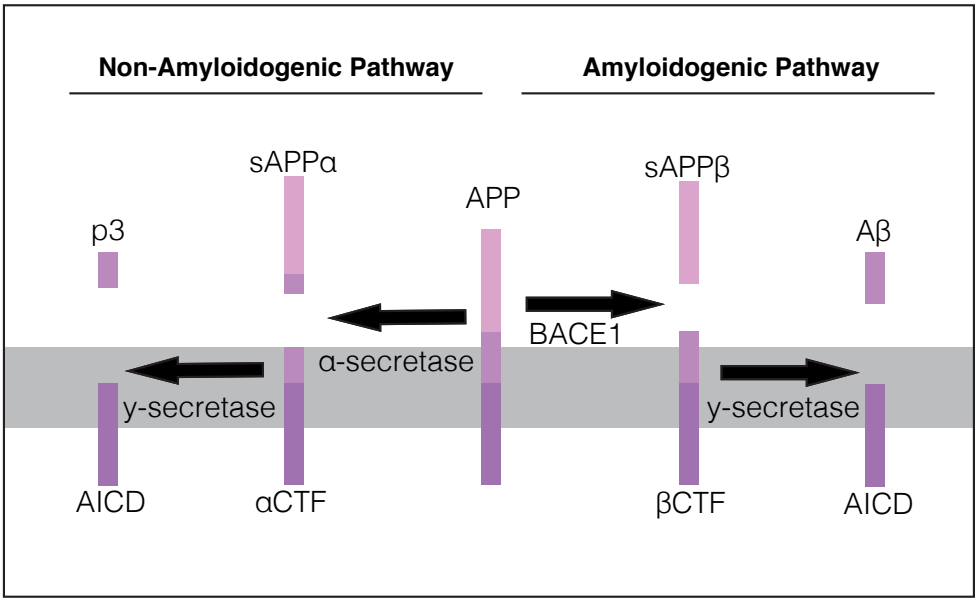

Figure 1.1: Diagram of APP Processing In the non-amyloidogenic pathway APP is processed first by α-secretase and then by y-secretase. In the Amyloidogenic pathway, APP is processed first by BACE1 and then by y-secretase.

What Causes Alzheimer's Disease?

Alzheimer's disease is a multifactorial disease that can be influenced by a variety of genetic and environmental risk factors. A small percentage (1-2%) of AD cases emerge from families that display an autosomal dominant pattern of inheritance. This form of Alzheimer's disease is called familial AD (FAD). People who have FAD tend to experience symptoms before the age of 60 and in this case the disease is referred to as early onset AD (EOAD). This early onset, familial form of AD is caused

by mutations in one of three genes: APP, Presenilin 1 (PS1), or Presenilin 2 (PS2) (1). Not surprisingly, all three of these genes are directly involved in regulation of APP processing to Aβ. PS1 and PS2 are two different isoforms of the catalytic subunit of y-secretase which cleaves APP to Aβ. These mutations can exert their effects in a variety of ways. Generally, they either increase total Aβ production, or they increase the ratio of the more oligomerization prone Aβ42 compared to the less oligomerization prone Aβ40 (10). Alternatively, a small subset of APP mutations that occur within the Aβ sequence, can increase the propensity of the Aβ peptide to aggregate into toxic oligomers (11). Emerging evidence shows that many of these mutations can also cause an accumulation of APP CTFs and that the CTFs can contribute to early changes that occur during AD pathogenesis (12). Nonetheless, it is clear that a severe and highly penetrant form of the disease emerges from mutations in genes involved in APP processing. Understanding the regulation and function of the proteins involved in this APP processing pathway is likely going to be crucial to making progress toward treating and preventing AD.

In contrast to FAD, Sporadic AD (SAD) is much more prevalent and tends to cause a late-onset form of the disease which is often referred to as late onset-AD (LOAD). SAD has a high level of heritability and can be caused by a variety of environmental and genetic risk factors.

While many genetic risk factors have been associated with SAD, the major genetic risk factor is the e4 allele of Apolipoprotein E (APOEe4). APOE encodes a

protein which is found on the surface of cholesterol and cholesteryl ester (CE) containing lipoproteins. It has a major role in regulation of cholesterol transport in the brain. APOE can bind to and promote clearance of excess Aβ. The APOEe4 allele might contribute to AD pathology by reducing Aβ clearance from the brain (13).

Striking clues about the physiological pathways that may contribute to AD emerge from the other genes that have been identified as AD risk factors. Apolipoprotein J (APOJ) (aka Clustrin) and ATP-binding cassette sub-family A, member 7 (ABCA7) variants have both been associated with AD risk through GWAS. Both APOJ and ABCA7 are thought to play important roles in cholesterol homeostasis (10). These observations have contributed to increasing interest in the role of cholesterol homeostasis in AD.

A variety of factors have been identified as contributors to AD risk. One of the major risk factors is age. Other risk factors that have been identified include traumatic brain injury, obesity, diabetes, hypertension, coronary artery disease, and high levels of dietary cholesterol (14) Many of these risk factors such as obesity, diabetes, and hypertension may result from complex interactions between genetic and environmental factors.

Cholesterol and AD

Our lab became interested in the connection between cholesterol and AD after we performed a drug screen aimed at finding FDA (Food and Drug Administration) approved compounds which could be repurposed to lower pTau levels in human iPSC

(hiPSC) derived neurons. Several cholesterol lowering drugs were identified as hits in this screen including efavirenz and a variety of statins. The details of this screen and the characterization of the effects of these drugs on AD relevant pathways are found in the second chapter.

One of the earliest clues connecting cholesterol with AD was identified in the early 1990's when researchers demonstrated that brains from individuals with coronary artery disease had higher levels of amyloid plaques compared to age-matched controls with no heart disease (15, 16). Coronary artery disease is typically caused by atherosclerosis which involves a build-up of cholesterol and fatty deposits which block arteries. High blood cholesterol levels is one of the major contributors to coronary artery disease risk. This link between coronary artery disease, AD, and cholesterol inspired a follow up study which showed that the brains of rabbits fed a diet high in cholesterol had increased accumulation of amyloid plaques (17). Brains of transgenic mice fed a diet high in cholesterol also showed an increase in amyloid pathology (18). Furthermore, epidemiology studies have shown a correlation between high levels of total cholesterol with AD risk (19). This line of research sparked interest in whether statins can lower the risk of AD. Several subsequent epidemiology studies showed that statin users are at a lower risk for AD (20–25). However, randomized clinical trials have failed to show a beneficial effect of statins for treatment of AD (26–30). The randomized clinical trials have known limitations such as insufficient follow-up times, exclusion of hyper-lipidemic patients, and short treatment time frames which could explain the lack of beneficial findings (31). Researchers have since firmly established that statins can

reduce Aβ levels (32–34). However, there is no current consensus on a mechanism. In the third chapter of this dissertation, we dig deeper into the mechanism using a combination of hiPSC derived neurons and fluorescence complementation assays. We show that cholesterol lowering drugs reduce APP processing to Aβ by increasing full length APP (flAPP) dimerization and inhibiting processing by BACE1 and y-secretase.

Cholesterol Metabolism in the Brain

De novo synthesis of cholesterol from the precursor acetyl CoA can occur in any nucleated cell via the mevalonate pathway. The rate limiting step of this pathway is the conversion of HMG CoA to mevalonate by HMGCR (35).

The brain contains almost 10x that of the average cholesterol content of other organs. Because of the inability of plasma lipoproteins to cross the blood brain barrier, cholesterol metabolism in the brain is separated from the rest of the body and the central nervous system (CNS) must synthesize its own cholesterol (36).

In the central nervous system, cholesterol and other lipids are transferred between different cell types by lipoproteins that resemble high density lipoprotein (HDL) in density and size (36). ApoE is the major apolipoprotein in the CNS and it plays a critical role in transport of cholesterol and other lipids between cells in the brain. ApoE is synthesized mainly in astrocytes and associates with lipoproteins containing cholesterol. ABCA7 and ABCA1 assist with lipidation of nascent apolipoproteins which are destined to be exported from the cell (37). Once secreted from astrocytes, the ApoE containing lipoproteins bind to LDL receptors on neurons and are taken into the cells by receptor mediated endocytosis. This cholesterol delivery from astrocytes is

thought to be involved in the growth and regeneration of damaged neurons (36) Neurons are capable of a low level of cholesterol synthesis, but not enough to support the high levels needed for proper neuronal function (38).

Once ApoE is endocytosed, it is transported to acidic compartments where cholesteryl esters contained in the lipoprotein are cleaved by acid lipases into free cholesterol. This free cholesterol can then be delivered to various membranes in the cell such as the ER or the PM. Excess brain cholesterol is removed by conversion into 24-hydroxycholesterol, which can cross the blood-brain barrier. After crossing the blood-brain barrier it is carried in plasma to the liver where it is excreted into bile (36). Excess cholesterol can also be stored in lipid droplets in the form of cholesteryl esters which can be hydrolyzed to free cholesterol if the cell becomes cholesterol starved (39).

In the third chapter of this dissertation, we show that flAPP plays a role in regulating cholesterol homeostasis by regulating astrocytic endocytosis of cholesterol containing low density lipoproteins. This may be one way that astrocytes regulate the amount of cholesterol available to the neurons. Our work sheds light on a pathway which unites the variety of genetic and environmental factors that contribute to AD risk. We propose that targeting cholesterol metabolic pathways is a promising approach to treating and preventing AD.

REFERENCES

1. Bondi, M. W., Edmonds, E. C., and Salmon, D. P. (2017) Alzheimer's Disease: Past, Present, and Future. *J Int Neuropsychol Soc*. **23**, 818–831

2. Alzheimer, A., Stelzmann, R. A., Schnitzlein, H. N., and Murtagh, F. R. (1995) An English translation of Alzheimer's 1907 paper, "Uber eine eigenartige Erkankung der Hirnrinde." *Clin Anat*. **8**, 429–431

3. Puglielli, L., Tanzi, R. E., and Kovacs, D. M. (2003) Alzheimer's disease: the cholesterol connection. *Nat. Neurosci.* **6**, 345–351

4. Hardy, J. A., and Higgins, G. A. (1992) Alzheimer's disease: the amyloid cascade hypothesis. *Science*. **256**, 184–185

5. Karran, E., Mercken, M., and De Strooper, B. (2011) The amyloid cascade hypothesis for Alzheimer's disease: an appraisal for the development of therapeutics. *Nat Rev Drug Discov*. **10**, 698–712

6. Drachman, D. A. (2014) The amyloid hypothesis, time to move on: Amyloid is the downstream result, not cause, of Alzheimer's disease. *Alzheimers Dement*. **10**, 372–380

7. Hardy, J., and Selkoe, D. J. (2002) The amyloid hypothesis of Alzheimer's disease: progress and problems on the road to therapeutics. *Science*. **297**, 353–356

8. Sengupta, U., Nilson, A. N., and Kayed, R. (2016) The Role of Amyloid-β Oligomers in Toxicity, Propagation, and Immunotherapy. *EBioMedicine*. **6**, 42–49

9. Grimm, M. O. W., Rothhaar, T. L., and Hartmann, T. (2012) The role of APP proteolytic processing in lipid metabolism. *Exp Brain Res*. **217**, 365–375

10. Van Cauwenberghe, C., Van Broeckhoven, C., and Sleegers, K. (2016) The genetic landscape of Alzheimer disease: clinical implications and perspectives. *Genetics in Medicine*. **18**, 421–430

11. Nilsberth, C., Westlind-Danielsson, A., Eckman, C. B., Condron, M. M., Axelman, K., Forsell, C., Stenh, C., Luthman, J., Teplow, D. B., Younkin, S. G., Näslund, J., and Lannfelt, L. (2001) The "Arctic" APP mutation (E693G) causes Alzheimer's disease by enhanced Aβ protofibril formation. *Nature Neuroscience*. **4**, 887–893

12. Kwart, D., Gregg, A., Scheckel, C., Murphy, E., Paquet, D., Duffield, M., Fak, J., Olsen, O., Darnell, R., and Tessier-Lavigne, M. (2019) A Large Panel of Isogenic

APP and PSEN1 Mutant Human iPSC Neurons Reveals Shared Endosomal Abnormalities Mediated by APP β-CTFs, Not Aβ. *Neuron*. 10.1016/j.neuron.2019.07.010

13. Castellano, J. M., Kim, J., Stewart, F. R., Jiang, H., DeMattos, R. B., Patterson, B. W., Fagan, A. M., Morris, J. C., Mawuenyega, K. G., Cruchaga, C., Goate, A. M., Bales, K. R., Paul, S. M., Bateman, R. J., and Holtzman, D. M. (2011) Human apoE isoforms differentially regulate brain amyloid-β peptide clearance. *Sci Transl Med*. **3**, 89ra57

14. Armstrong, R. A. (2019) Risk factors for Alzheimer's disease. *Folia Neuropathol*. **57**, 87–105

15. Sparks, D. L., Hunsaker, J. C., Scheff, S. W., Kryscio, R. J., Henson, J. L., and Markesbery, W. R. (1990) Cortical senile plaques in coronary artery disease, aging and Alzheimer's disease. *Neurobiology of Aging*. **11**, 601–607

16. Sparks, D. L., Martin, T. A., Gross, D. R., and Hunsaker, J. C. (2000) Link between heart disease, cholesterol, and Alzheimer's disease: A review. *Microscopy Research and Technique*. **50**, 287–290

17. Sparks, D. L., Scheff, S. W., Hunsaker, J. C., Liu, H., Landers, T., and Gross, D. R. (1994) Induction of Alzheimer-like β-Amyloid Immunoreactivity in the Brains of Rabbits with Dietary Cholesterol. *Experimental Neurology*. **126**, 88–94

18. Refolo, L. M., Malester, B., LaFrancois, J., Bryant-Thomas, T., Wang, R., Tint, G. S., Sambamurti, K., Duff, K., and Pappolla, M. A. (2000) Hypercholesterolemia accelerates the Alzheimer's amyloid pathology in a transgenic mouse model. *Neurobiol. Dis.* **7**, 321–331

19. Shepardson, N. E., Shankar, G. M., and Selkoe, D. J. (2011) Cholesterol Level and Statin Use in Alzheimer Disease: I. Review of Epidemiological and Preclinical Studies. *Arch Neurol*. **68**, 1239–1244

20. Li, G., Shofer, J. B., Rhew, I. C., Kukull, W. A., Peskind, E. R., McCormick, W., Bowen, J. D., Schellenberg, G. D., Crane, P. K., Breitner, J. C. S., and Larson, E. B. (2010) Age-varying association between statin use and incident Alzheimer's disease. *J Am Geriatr Soc*. **58**, 1311–1317

21. Wolozin, B., Kellman, W., Ruosseau, P., Celesia, G. G., and Siegel, G. (2000) Decreased prevalence of Alzheimer disease associated with 3-hydroxy-3-methyglutaryl coenzyme A reductase inhibitors. *Arch. Neurol.* **57**, 1439–1443

22. Lin, F.-C., Chuang, Y.-S., Hsieh, H.-M., Lee, T.-C., Chiu, K.-F., Liu, C.-K., and Wu, M.-T. (2015) Early Statin Use and the Progression of Alzheimer Disease. *Medicine (Baltimore)*. 10.1097/MD.0000000000002143

23. Zissimopoulos, J. M., Barthold, D., Brinton, R. D., and Joyce, G. (2017) Sex and Race Differences in the Association Between Statin Use and the Incidence of Alzheimer Disease. *JAMA Neurol*. **74**, 225–232

24. Jick, H., Zornberg, G. L., Jick, S. S., Seshadri, S., and Drachman, D. A. (2000) Statins and the risk of dementia. *Lancet*. **356**, 1627–1631

25. Haag, M. D. M., Hofman, A., Koudstaal, P. J., Stricker, B. H. C., and Breteler, M. M. B. (2009) Statins are associated with a reduced risk of Alzheimer disease regardless of lipophilicity. The Rotterdam Study. *J. Neurol. Neurosurg. Psychiatry*. **80**, 13–17

26. Feldman, H. H., Doody, R. S., Kivipelto, M., Sparks, D. L., Waters, D. D., Jones, R. W., Schwam, E., Schindler, R., Hey-Hadavi, J., DeMicco, D. A., Breazna, A., and LEADe Investigators (2010) Randomized controlled trial of atorvastatin in mild to moderate Alzheimer disease: LEADe. *Neurology*. **74**, 956–964

27. Sano, M., Bell, K. L., Galasko, D., Galvin, J. E., Thomas, R. G., van Dyck, C. H., and Aisen, P. S. (2011) A randomized, double-blind, placebo-controlled trial of simvastatin to treat Alzheimer disease. *Neurology*. **77**, 556–563

28. Santanello, N. C., Barber, B. L., Applegate, W. B., Elam, J., Curtis, C., Hunninghake, D. B., and Gordon, D. J. (1997) Effect of pharmacologic lipid lowering on health-related quality of life in older persons: results from the Cholesterol Reduction in Seniors Program (CRISP) Pilot Study. *J Am Geriatr Soc*. **45**, 8–14

29. Shepherd, J., Blauw, G. J., Murphy, M. B., Bollen, E. L. E. M., Buckley, B. M., Cobbe, S. M., Ford, I., Gaw, A., Hyland, M., Jukema, J. W., Kamper, A. M., Macfarlane, P. W., Meinders, A. E., Norrie, J., Packard, C. J., Perry, I. J., Stott, D. J., Sweeney, B. J., Twomey, C., Westendorp, R. G. J., and PROSPER study group. PROspective Study of Pravastatin in the Elderly at Risk (2002) Pravastatin in elderly individuals at risk of vascular disease (PROSPER): a randomised controlled trial. *Lancet*. **360**, 1623–1630

30. MRC/BHF Heart Protection Study of cholesterol lowering with simvastatin in 20 536 high-risk individuals: a randomised placebocontrolled trial (2002) *The Lancet*. **360**, 7–22

31. Schultz, B. G., Patten, D. K., and Berlau, D. J. (2018) The role of statins in both cognitive impairment and protection against dementia: a tale of two mechanisms. *Transl Neurodegener*. 10.1186/s40035-018-0110-3

32. Simons, M., Keller, P., De Strooper, B., Beyreuther, K., Dotti, C. G., and Simons, K. (1998) Cholesterol depletion inhibits the generation of beta-amyloid in hippocampal neurons. *Proc. Natl. Acad. Sci. U.S.A.* **95**, 6460–6464

33. Kojro, E., Gimpl, G., Lammich, S., Marz, W., and Fahrenholz, F. (2001) Low cholesterol stimulates the nonamyloidogenic pathway by its effect on the alpha - secretase ADAM 10. *Proc. Natl. Acad. Sci. U.S.A.* **98**, 5815–5820

34. Ostrowski, S. M., Wilkinson, B. L., Golde, T. E., and Landreth, G. (2007) Statins Reduce Amyloid-β Production through Inhibition of Protein Isoprenylation. *J. Biol. Chem.* **282**, 26832–26844

35. Ikonen, E. (2008) Cellular cholesterol trafficking and compartmentalization. *Nat. Rev. Mol. Cell Biol.* **9**, 125–138

36. Vance, J. E., Karten, B., and Hayashi, H. (2006) Lipid dynamics in neurons. *Biochem. Soc. Trans.* **34**, 399–403

37. Wagner, E. M., Basso, F., Kim, C. S., and Amar, M. J. A. (2014) ABC lipid transporters. *Access Science*. 10.1036/1097-8542.801530

38. Mauch, D. H., Nägler, K., Schumacher, S., Göritz, C., Müller, E. C., Otto, A., and Pfrieger, F. W. (2001) CNS synaptogenesis promoted by glia-derived cholesterol. *Science*. **294**, 1354–1357

39. Walther, T. C., Chung, J., and Farese, R. V. (2017) Lipid Droplet Biogenesis. *Annual Review of Cell and Developmental Biology*. **33**, 491–510

40. O'Brien, R. J., and Wong, P. C. (2011) Amyloid Precursor Protein Processing and Alzheimer's Disease. *Annu Rev Neurosci*. **34**, 185–204

Chapter 2
Cholesterol Metabolism Is a Druggable Axis that Independently Regulates Tau and Amyloid-β in iPSC-Derived Alzheimer's Disease Neurons

Article

Cell Stem Cell

Cholesterol Metabolism Is a Druggable Axis that Independently Regulates Tau and Amyloid-β in iPSC-Derived Alzheimer's Disease Neurons

Graphical Abstract

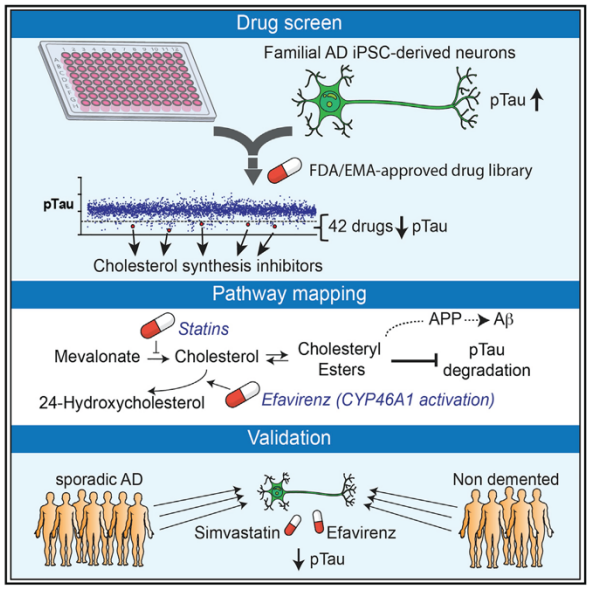

Highlights

- Drug screening identifies inhibitors of aberrant phosphorylated Tau (pTau) accumulation
- Cholesteryl esters (CE) were identified as upstream regulators of pTau proteostasis
- The effects of CE on Tau proteostasis are correlated with, but independent of, APP and Aβ
- Lead compound enhance CE-dependent pTau proteasomal turnover specifically in neurons

Authors

Rik van der Kant, Vanessa F. Langness, Cheryl M. Herrera, ..., Steven L. Wagner, Anne G. Bang, Lawrence S.B. Goldstein

Correspondence

lgoldstein@ucsd.edu

In Brief

van der Kant et al. performed a repurposing drug screen in iPSC-derived AD neurons and identified compounds that reduce aberrant accumulation of phosphorylated Tau (pTau). Reduction of cholesteryl ester levels or allosteric activation of CYP46A1 by lead compounds enhanced pTau degradation independently of APP and Aβ.

van der Kant et al., 2019, Cell Stem Cell *24*, 363–375
March 7, 2019
https://doi.org/10.1016/j.stem.2018.12.013

CellPress

Cell Stem Cell
Article

Cholesterol Metabolism Is a Druggable Axis that Independently Regulates Tau and Amyloid-β in iPSC-Derived Alzheimer's Disease Neurons

Rik van der Kant,[1,2,10] Vanessa F. Langness,[1,10] Cheryl M. Herrera,[1] Daniel A. Williams,[1,11] Lauren K. Fong,[1] Yves Leestemaker,[3] Evelyne Steenvoorden,[4] Kevin D. Rynearson,[5] Jos F. Brouwers,[6] J. Bernd Helms,[6] Huib Ovaa,[3] Martin Giera,[4] Steven L. Wagner,[5,7] Anne G. Bang,[8] and Lawrence S.B. Goldstein[1,9,12,*]

[1]Department of Cellular and Molecular Medicine, University of California, San Diego, La Jolla, CA 92093, USA
[2]Department of Functional Genomics, Center for Neurogenomics and Cognitive Research, Amsterdam Neuroscience, VU University Amsterdam de Boelelaan 1087, 1081 HV Amsterdam, the Netherlands
[3]Oncode Institute and Department of Cell and Chemical Biology, Leiden University Medical Center, Einthovenweg 20, 2333 ZC Leiden, the Netherlands
[4]Center for Proteomics and Metabolomics, Leiden University Medical Center, Albinusdreef 2, 2333 ZA Leiden, the Netherlands
[5]Department of Neurosciences, University of California, San Diego, La Jolla, CA 92093, USA
[6]Department of Biochemistry and Cell Biology, Faculty of Veterinary Medicine, Utrecht University Yalelaan 2, 3584 CM Utrecht, the Netherlands
[7]Research Biologist, VA San Diego Healthcare System, La Jolla, CA 92161, USA
[8]Conrad Prebys Center for Chemical Genomics, Sanford Burnham Prebys Medical Discovery Institute, 10901 North Torrey Pines Road, La Jolla, CA 92037, USA
[9]Sanford Consortium for Regenerative Medicine, La Jolla, CA 92037, USA
[10]These authors contributed equally
[11]Deceased
[12]Lead Contact
*Correspondence: lgoldstein@ucsd.edu
https://doi.org/10.1016/j.stem.2018.12.013

SUMMARY

Genetic, epidemiologic, and biochemical evidence suggests that predisposition to Alzheimer's disease (AD) may arise from altered cholesterol metabolism, although the molecular pathways that may link cholesterol to AD phenotypes are only partially understood. Here, we perform a phenotypic screen for pTau accumulation in AD-patient iPSC-derived neurons and identify cholesteryl esters (CE), the storage product of excess cholesterol, as upstream regulators of Tau early during AD development. Using isogenic induced pluripotent stem cell (iPSC) lines carrying mutations in the cholesterol-binding domain of APP or APP null alleles, we found that while CE also regulate Aβ secretion, the effects of CE on Tau and Aβ are mediated by independent pathways. Efficacy and toxicity screening in iPSC-derived astrocytes and neurons showed that allosteric activation of CYP46A1 lowers CE specifically in neurons and is well tolerated by astrocytes. These data reveal that CE independently regulate Tau and Aβ and identify a druggable CYP46A1-CE-Tau axis in AD.

INTRODUCTION

Pathological accumulation of phosphorylated Tau (pTau) and accumulation of amyloid-beta (Aβ) fragments are the two major biochemical hallmarks of Alzheimer's disease (AD). Effective strategies to remove Aβ in AD-patient brains have been developed but have not yet shown efficacy to slow cognitive decline in clinical trials. This finding has led to the idea that targeting Tau or combinatorial strategies that target both Tau and Aβ are required to treat AD. While Aβ generation has been studied in much detail, the processes that drive pTau accumulation in AD are poorly defined. Late stage Tau pathology, such as aggregation of accumulated Tau in neurofibrillary tangles (NFT), and subsequent neurodegeneration can be modeled in mice, or non-neuronal human cells, by (over)expression of human mutant Tau. However, Tau mutations do not occur in AD. Instead, in AD, endogenous "wild-type" pTau accumulates downstream of familial AD (FAD) mutations (in APP, PSEN1, and PSEN2 genes) or, in the case of sporadic late-onset AD (SAD), downstream of an unknown combination of genetic and environmental risk factors. How these factors drive early accumulation of pTau in AD is not understood. Recent advances in induced pluripotent stem cell (iPSC) technology (Shi et al., 2017) have made it possible to generate functional human neurons from patients and healthy controls to study early pathophysiological regulation of endogenous Tau. In iPSC-derived neurons from both FAD- and SAD-patients, pTau aberrantly accumulates at early time points (Choi et al., 2014; Israel et al., 2012; Moore et al., 2015; Muratore et al., 2014; Ochalek et al., 2017; Shi et al., 2012). Accumulation of pTau in FAD neurons can be reversed by inhibition of β-secretase, the enzyme that converts APP to β-CTF indicating a direct relationship between APP processing and Tau (Israel et al., 2012; Moore et al., 2015). Interestingly, inhibition of γ-secretase (to prevent generation of Aβ from β-CTF) did not reduce pTau, indicating that the effect of APP processing on pTau in early

AD neurons is not solely mediated by extracellular Aβ (Israel et al., 2012; Moore et al., 2015).

Identification of other cellular pathways that contribute to pTau accumulation early in FAD and SAD neurons is key to understanding Tau pathology in AD. In addition to increased Aβ and pTau levels, CE also accumulate in FAD and SAD. CE are increased in mouse models expressing human (mutant) APP (Chan et al., 2012; Tajima et al., 2013; Yang et al., 2014) and CE, as well as CE-storage organelles (lipid droplets), have been shown to accumulate in the SAD brain (Chan et al., 2012; Foley, 2010; Hamilton et al., 2015; Yang et al., 2014). CE are generated when cholesterol is converted to CE by the ER-resident Acyl-CoA cholesterol acyltransferase (ACAT) through ligation of a long-chain fatty acid to (excess) cholesterol, and CE can be converted back to cholesterol by acidic lipases in the lysosome (Ikonen, 2008; Puglielli et al., 2003). CE enhance the production of Aβ *in vivo* and *in vitro* indicating that CE can contribute to AD pathogenesis (Di Paolo and Kim, 2011; Hutter-Paier et al., 2004; Huttunen et al., 2009; Puglielli et al., 2001, 2003). CE-dependent regulation of Aβ generation is mediated by altered trafficking of APP through the early secretory pathway (Huttunen et al., 2009). Whether CE also affect Tau phosphorylation or Tau proteostasis is unknown, but inhibition of cholesterol esterification by genetic deletion of ACAT1 prevents early stage Tau pathology in Tau mutant mice through unknown mechanisms (Shibuya et al., 2015). A possible way by which CE could affect Tau pathology is through regulation of the ubiquitin-proteasome system (UPS). Cholesterol and cholesterol metabolites extensively interact with the UPS to regulate the ubiquitination and degradation of cholesterol-metabolic enzymes (Sharpe et al., 2014), and the UPS is a major regulator of pTau proteostasis. (Lee et al., 2013). Activity of the UPS is decreased in AD (Keck et al., 2003; Keller et al., 2000), and UPS (re)activation delays Tau aggregation and neurodegeneration *in vitro* and *in vivo* (Han et al., 2014; Lokireddy et al., 2015; Myeku et al., 2016).

Here, we tested a library of >1,600 compounds for their potency to inhibit pTau accumulation in cultured FAD iPSC-derived neurons and find that neuronal CE regulate the proteasome-dependent degradation of pTau. Using neurons derived from multiple AD- and non-demented control (NDC) iPSC lines, as well as isogenic CRISPR/Cas9 gene-edited lines, we demonstrate that the effect of CE on pTau is correlated with, but independent of APP processing and Aβ. Whereas the effect of CE on pTau is mediated by proteasomal upregulation, the effect of CE on Aβ secretion is mediated by a cholesterol-binding domain in APP. We identify a number of strategies to reduce pTau in a CE-dependent manner and find that allosteric activation of CYP46A1 is a neuron-specific CE-lowering strategy particularly well tolerated by human astrocytes. Collectively, our data identify a CYP46A1-CE-Tau axis as an early druggable pathway in AD.

RESULTS

A Drug Screen in iPSC-Derived Human FAD Neurons to Identify Compounds that Reduce pTau Accumulation

pThr231Tau is an early marker of AD pathology that correlates well with cognitive decline (Buerger et al., 2002; Luna-Muñoz et al., 2007). pThr231Tau accumulates in APP duplication (APP^{dp}) iPSC-derived FAD neurons (Israel et al., 2012). To identify compounds that reduce pTau accumulation in these FAD neurons, we screened a collection of 1,684 approved and preclinical drugs for their efficacy to lower neuronal pThr231Tau. For our screen, neural progenitor cells (NPCs; line APP^{dp}1-6) (Israel et al., 2012) were differentiated to neurons (Figures S1A and S1B) for 3 weeks, replated in 384 well plates, and allowed to mature for 2 weeks before treatment with compound at 5 μM for 5 days. The screen was performed in duplicate, and a ratiometric readout of pThr231Tau/total Tau (tTau) level and cell viability was determined (Figure 1A). In the primary screen, 158/1,684 compounds (9.4%) significantly reduced pThr231/tTau by a Z score <-2 in at least one of the duplicates (Figure 1B; Tables S1 and S2) and were selected for confirmation. In a repeat of the primary assay with selected compounds, 96/158 compounds were confirmed to reduce pThr231/tTau by a Z score <-2 in at least one additional replicate (Table S3). Of the 96 confirmed compounds, 42 were clearly non-toxic hits with $Z > -1$ for viability (Figure 1C). Our screen identified six microtubule-interacting compounds that reduced pThr231Tau/tTau (14% of hits) that have previously been shown to regulate pTau in other systems (Dickey et al., 2006; Merrick et al., 1996; Xie et al., 1998). Our hit-list also included four inhibitors of cholesterol synthesis; atorvastatin, simvastatin, fluvastatin, and rosuvastatin. Because cholesterol metabolism has been heavily linked to AD pathogenesis (Di Paolo and Kim, 2011) we selected these compounds for further study. We confirmed that these four statins, as well as two additional statins (lovastatin and mevastatin), reduced pThr231Tau/tTau in a dose-dependent manner with minor effects on cell viability or neuronal number (Figures 1D and S1C–S1F). Simvastatin reduced pThr231Tau in a similar dose-dependent manner in additional lines from the same patient (APP^{dp}1-2) and an independent patient APP^{dp} line (APP^{dp}2-1) (Figure S1G), indicating that the effect of statins is conserved across individual APP^{dp} lines and patients. In addition to pThr231Tau/tTau, atorvastatin also reduced pS396/S404Tau, pS202/T205Tau and levels of a pThr231 phosphorylation-dependent conformational Tau epitope (TG3) as assessed by immunofluorescence (Figure 1e). These data show that in addition to screening for Aβ (Brownjohn et al., 2017; Kondo et al., 2017), iPSC-derived AD neurons can be applied to screen for pTau modulators. In addition, these data show that statins reduce pTau levels across a number of phosphorylation epitopes and across individual FAD (APP^{dp}) patients.

The Effect of Statins on pTau Is Mediated by Cholesteryl Esters

To understand how pTau is regulated by statins, we studied the relationship between the mevalonate-cholesterol synthetic pathway and pTau levels in more detail. Statins inhibit 3-hydroxy-3-methylglutaryl-CoA reductase (HMGCR), an early rate limiting step in the cholesterol synthetic pathway that converts HMG-CoA to mevalonate (MVA) (Figure 2A). As expected, MVA supplementation rescued the effect of atorvastatin treatment on pThr231Tau/tTau indicating that the effect of statins on pTau is specific to their effects on the mevalonate pathway (Figure 2B). While atorvastatin was slightly cytotoxic at higher concentrations (Figures S2A and S2B) toxicity did not explain the effect of atorvastatin on pThr231Tau/tTau, as MVA supplementation completely rescued the effect of atorvastatin on

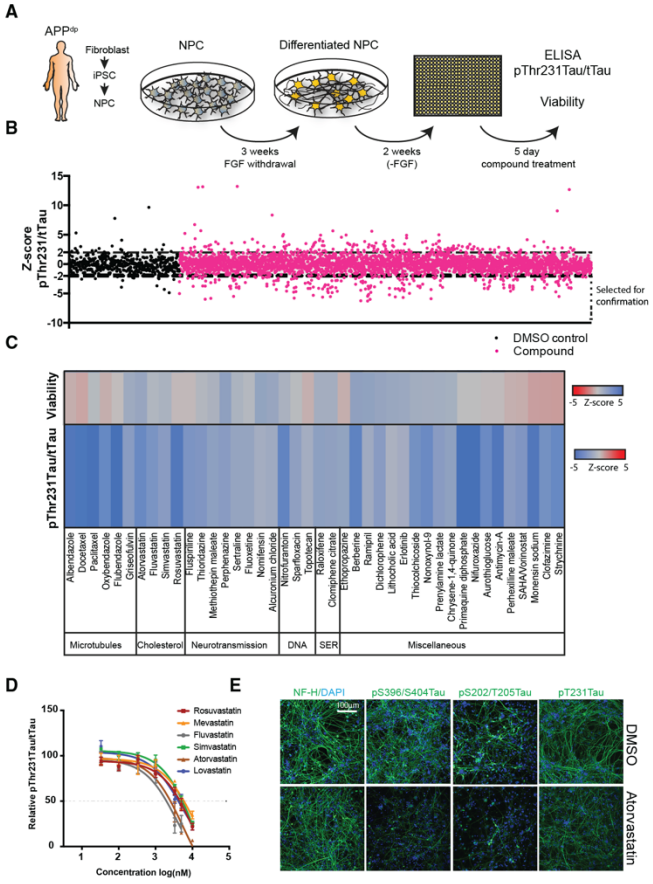

Figure 1. Identification of Compounds that Decrease pTau Levels in FAD iPSC-Derived AD Neurons

(A) Screening strategy overview: APP^{dp}1-6 NPC's were differentiated for 3 weeks, replated into 384 well plates, and after 2 weeks, treated with 5 μM of compound for 5 days; pThr231Tau/tTau ratio and cell viability was measured.

(B) 1,684 compounds (in pink) were screened in duplicate for their effect on pThr231Tau/tTau ratio as expressed by Z score. 158 compounds that decreased pThr231/tTau by $Z \leq -2$ were selected for confirmation. Vehicle alone controls (DMSO) are shown in black.

(C) 42 confirmed non-toxic hits grouped by drug category. SER, selective estrogen reuptake (n = 4).

(D) Dosage effects of different statins on pThr231Tau/tTau ratio in APP^{dp}1-6 (mean ± SEM, $n \geq 3$).

(E) APP^{dp}1-6 neurons were treated with vehicle (DMSO, upper row) or atorvastatin (10 μM, lower row) for 5 days and fixed and stained with antibodies for indicated antigens. NF-H, neurofilament H, axonal marker. The pThr231Tau antibody used is TG3, which detects a conformational epitope of pThr231Tau. Scale bar, 100 μm.

See also Figure S1.

pThr231Tau/tTau ratio without rescuing the minor effect of atorvastatin on cell viability (Figures S2A and S2B). Removal of atorvastatin after 5 days of treatment allowed recovery of pThr231Tau/Tau indicating reversible dynamic regulation (Figure S2C). Statin-treated neurons elicited a (normal) physiological response to statin treatment exemplified by upregulation of cholesterol-synthetic proteins (Figures S2D and S2E; Table S4). Statins have recently been reported to induce the degradation of mutant p53 by reduction of mevalonate-5-phosphate (MVP) (Parrales et al., 2016). The effects of statins on pTau are not mediated by MVP, as both MVP and its direct downstream metabolite, MVA-5PP, rescued the effect of statin treatment (Figure 2B). More distal of MVA-5PP, the MVA pathway branches into non-sterol isoprenoid (protein prenylation) pathways and a cholesterol synthetic pathway (Figure 2A). Inhibition of the respective non-sterol isoprenoid pathways (by geranyl- or farnesyl-transferase inhibitors GGTI-298 and FTI-227, respectively) did not significantly reduce pThr231Tau/tTau (Figures 2C, S2F, and S2G). In contrast, inhibition of the cholesterol-synthetic arm of the mevalonate pathway using a squalene synthase inhibitor (YM-53601) or Δ7-dehydrocholesterol reductase (DHCR7) inhibitor (AY-9944) did significantly decrease pThr231Tau/tTau (Figures 2C, S2F, and S2G), indicating that pTau is regulated by the cholesterol-synthetic branch of the MVA pathway. Alternative ways to reduce neuronal cholesterol such as inhibition of sterol regulatory element-binding protein (SREBP)-mediated transcriptional activation of cholesterol synthetic genes by fatostatin (Kamisuki et al., 2009) (Figures 2C, S2H, and S2I) or induction of cholesterol export by liver X receptor (LXR) agonists (Figure 2A) T0901317 and 24-hydroxycholesterol (Figures 2C, S2F, and S2G) also reduced pThr231Tau/tTau. Activation of homologous nuclear receptors such as PPARα (by GW50156) and PPARγ (by Rosiglitazone), which regulate fatty acid metabolism but not cholesterol export, did not decrease pThr231Tau/tTau (Figures 2C, S2F, and S2G). Another strategy to reduce the pool of neuronal cholesterol is the activation of cholesterol 24-hydroxylase (CYP46A1), a neuron-specific enzyme that converts cholesterol to 24-hydroxycholesterol (Anderson et al., 2016; Mast et al., 2017b; Moutinho et al., 2016). As expected, activation of CYP46A1 by efavirenz (Figures 2C, S2F, and S2G) or overexpression of CYP46A1 (Figures S2J and S2K) also reduced pThr231Tau/tTau. Together, these data show that mechanistically different cholesterol-lowering drugs all reduce pTau, strongly indicating that pTau levels are

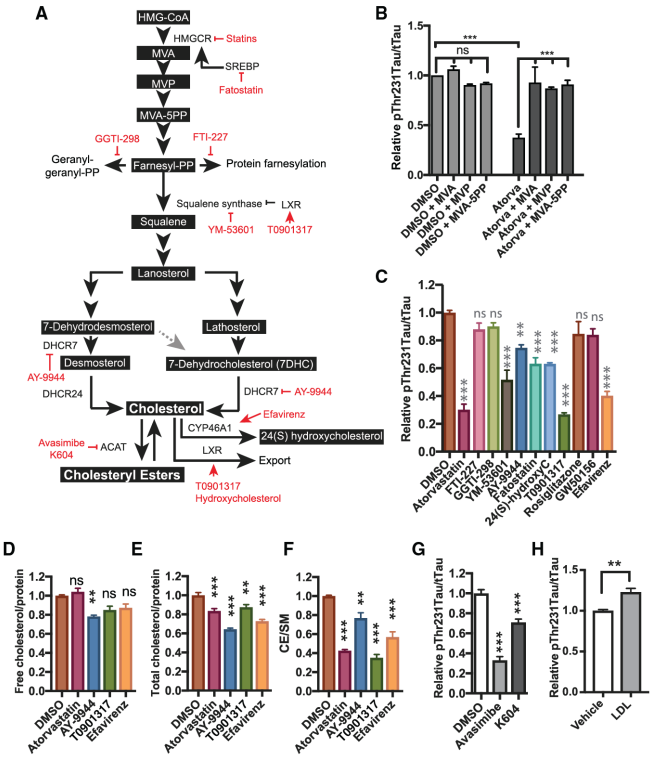

Figure 2. The Effect of Statins on pTau Is Mediated by Cholesteryl Esters

(A) Overview of the mevalonate pathway and inhibitors used in this study.

(B) APP^{dp}1-6 neurons were treated with DMSO or atorvastatin (10 μM) for 5 days. For indicated conditions, mevalonate (MVA, 0.5 mM), mevalonate-5-phosphate (MVP, 0.5 mM), or mevalonate-5-pyrophosphate (MVA-5PP, 1 mM) was added to the media at a single dose at t = 0 (mean ± SEM, n ≥ 3).

(C) APP^{dp}1-6 neurons were treated with inhibitors of specific steps in the mevalonate pathway; atorvastatin (10 μM), FTI-227 (10 μM), GGTI (10 μM), YM-53601 (20 μM), AY-9944 (10 μM), fatostatin (20 μM), 24-hydroxycholesterol (10 μM), T0901317 (10 μM), rosiglitazone (50 μM), GW501516 (10 μM), and efavirenz (10 μM). pThr231Tau/tTau levels were determined by ELISA (mean ± SEM, n ≥ 3).

(D–F) APP^{dp}1-6 neurons were treated with atorvastatin (10 μM), AY-9944 (5 μM), T0901317 (10 μM), or efavirenz (10 μM) for 3 days and lipid analysis was performed to measure (D) free cholesterol (mean ± SEM, n ≥ 8), (E) total cholesterol (mean ± SEM, n ≥ 4), and (F) CE (mean ± SEM, n ≥ 8).

(G) pThr231Tau/tTau levels after 5-day treatment of APP^{dp}1-6 neurons with avasimibe (10 μM) or K604 (25 μM) (mean ± SEM, n ≥ 3).

(H) Treatment of APP^{dp}1-6 neurons with LDL (25 μg/mL) (mean ± SEM, n ≥ 3).

See also Figure S2.

controlled by neuronal cholesterol levels or downstream cholesterol metabolites. To determine whether cholesterol itself or a cholesterol metabolite controls pTau levels, we performed extensive lipid analysis for key selected compounds from previous experiments (Figures 2D–2F and S2L–S2P; Table S5). None of the pTau-reducing drugs affected phospholipid levels (sphingomyelin [SM] and phosphatidylethanolamine [PE]) (Figure S2L). Cholesterol precursor levels were altered in accordance with the enzymatic target of the different compounds (Figures S2M–S2O); atorvastatin reduced desmosterol and lathosterol levels, AY9944 reduced desmosterol and lathosterol levels and increased 7DHC levels, and T0901317 and efavirenz had minor (slightly inhibitory) effects on precursor levels. 24-Hydroxycholesterol (a direct downstream metabolite of cholesterol) was increased in media from efavirenz-treated neurons, was decreased in AY-9944-treated samples, and was unaltered in atorvastatin- and T0901317-treated neurons (Figure S2P). Surprisingly, however, although these compounds behaved as expected, only AY-9944 (that only had minor effect on pTau, Figure 2C) reduced free cholesterol levels (Figure 2D). It is important to note that our iPSC-derived neurons are cultured in media without an exogenous source of cholesterol, and thus neuronal cholesterol levels cannot be compensated by enhanced uptake from the media. Whereas changes in free cholesterol levels were not detected for most compounds, all compounds significantly reduced the levels of total cholesterol (free + esterified cholesterol) (Figure 2E) through a strong reduction of CE (Figure 2F). This finding suggests that conversion of CE to cholesterol compensates for the loss of cholesterol through inhibition of synthesis or induction of export, and reductions in CE, not free cholesterol, mediate the effects of the different compounds on pTau. In line with this observation, direct inhibition of cholesterol esterification by the ACAT inhibitors avasimibe (aka CI-1011) (Figures 2G and S2Q–S2V) (Huttunen et al., 2009, 2010; Lee et al., 1996) or K604 (Figure 2G) also reduced pTau. Exogenous addition of cholesterol and CE (in the form of LDL) increased pThr231Tau/tTau (Figure 2H) levels. Together, our data show that CE regulate pTau levels in human FAD neurons. We investigated the mechanisms underlying CE-dependent regulation of pTau in more detail.

Regulation of pTau by CE Is Correlated with, but Independent of, APP and Aβ

APP^{dp} neurons have an extra copy of APP and increased levels of both Aβ and pTau (Israel et al., 2012; Moore et al., 2015). To understand the relationship between APP copy number, Aβ, and CE-dependent regulation of pTau in more detail, we also treated NDC neurons with the normal two copies of APP with cholesterol-targeting drugs. Simvastatin, atorvastatin, efavirenz,

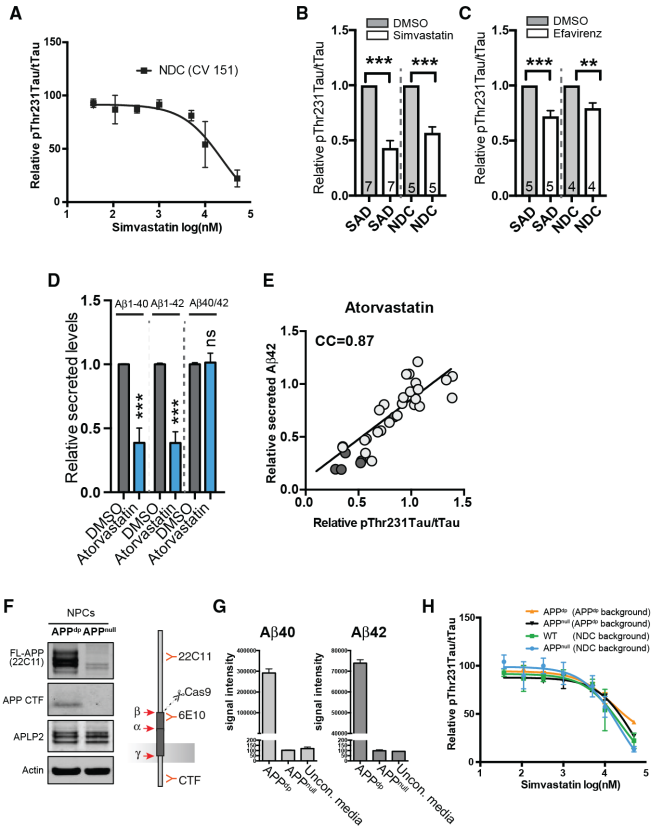

Figure 3. pTau and Aβ Are Co-regulated by CE through Separate Pathways

(A) Dosage effect of simvastatin treatment on pThr231Tau/tTau on non-demented control (NDC) neurons (CV 151 line).

(B and C) Effect of simvastatin (10 μM) (B) or efavirenz (10 μM) treatment (C) on pThr231Tau/tTau in neuronal lines from SAD and NDC subjects (mean ± SEM, number of individual patients indicated in bars).

(D) Secreted Aβ levels from APP^{dp}1-6 neurons treated with atorvastatin (10 μM) for 5 days normalized to DMSO-treated neurons (mean ± SEM, n ≥ 3).

(E) Correlation of Aβ42 and pThr231Tau/tTau levels in atorvastatin-treated neurons at different time points, dosages, and in different cell lines (light circles, APP^{dp}1-6; dark circles, APP^{dp}2-1). CC, correlation coefficient.

(F and G) Characterization of APP^{null} line. (F) Western blot with antibodies against APP in isogenic APP^{dp} (line APP^{dp} 2-1) and APP^{null} (line APP^{dp}1KO). Full-length APP (FL) and APP CTF are no longer detected in the $APP^{dp}1^{null}$ line. The FL-APP (22C11) cross reacts with APLP2 explaining the remaining signal in the FL-APP (22C11 blot). (G) ELISA analysis shows an absence of Aβ40 and Aβ42 in conditioned media from the APP^{null} line. Positive control is APP^{dp}1-2, negative control is unconditioned media. The detection antibody for the ELISA is 6E10, as indicated in (F).

(H) Dosage effect of simvastatin treatment on pThr231Tau/tTau on neurons with indicated genotypes (mean ± SEM, n ≥ 3). Isogenic knockouts used were in an APP^{dp} patient genetic background (lines APP^{dp}1-2 [^{dp}] and APP^{dp}1KO [^{null}] or non-demented control [NDC] genetic background [CV line 151 (wild-type [WT])] and IB6 [^{null}]). Mean ± SEM; n ≥ 5. See also Figure S3.

and the ACAT inhibitors avasimibe and K604 all reduced pThr231Tau/tTau in the NDC neurons (Figure S3A). For simvastatin, we further tested an extensive dose range and found that it reduced pThr231Tau/Tau in NDC neurons in a similar dose-dependent manner as in APP^{dp} neurons (Figure 3A). A single dose of statin or efavirenz also decreased pThr231Tau/tTau in sporadic AD (SAD) patient- and non-demented control (NDC) neurons (Figures 3B, 3C, S3B, and S3C). pThr231Tau/tTau was also reduced by simvastatin in cultured hippocampal mouse neurons (Figure S3D). Together, these data indicate that CE-dependent regulation of pTau is conserved across individual patients and healthy subjects (and even across species) and is not dependent on baseline APP copy number.

In addition to our findings on pTau, CE reduction has previously been reported to reduce Aβ levels (Hutter-Paier et al., 2004; Huttunen et al., 2009; Puglielli et al., 2001), and Aβ secretion from our iPSC-derived neurons was also decreased by statins (Figure 3D). We observed a strong correlation between Aβ42 secretion and pThr231Tau/tTau in response to atorvastatin treatment across time points and drug doses (Figures 3E and S3E).

To test whether the effect of CE on pTau was mediated by alterations in APP processing and/or the reduction of Aβ, we generated an isogenic APP^{null} line in an APP^{dp} patient genetic background (Figures 3F, 3G, and S3F–S3H). No APP expression or Aβ secretion was detected in the APP^{null} neurons (Figures 3F and 3G). pThr231Tau/tTau levels were reduced at baseline in the APP^{null} neurons (Figure S3I). Interestingly, in these APP^{null} neurons, simvastatin still reduced pThr231Tau/tTau in a dose-dependent manner identical to that of its isogenic control lines (Figure 3H). Similarly, simvastatin reduced pThr231Tau/tTau the same in a previously generated isogenic set of NDC (APP^{wt}) and APP^{null} neurons (CV line 151 and IB6) (Fong et al., 2018) (Figure 3H). Together, these data show that CE regulate both pTau and Aβ, but regulation of pTau by CE is APP- and Aβ-independent.

The Effect of CE on Aβ Is Mediated by a Cholesterol-Binding Domain in APP

To understand the respective pathways by which CE regulate pTau and Aβ, and to verify that these pathways are indeed

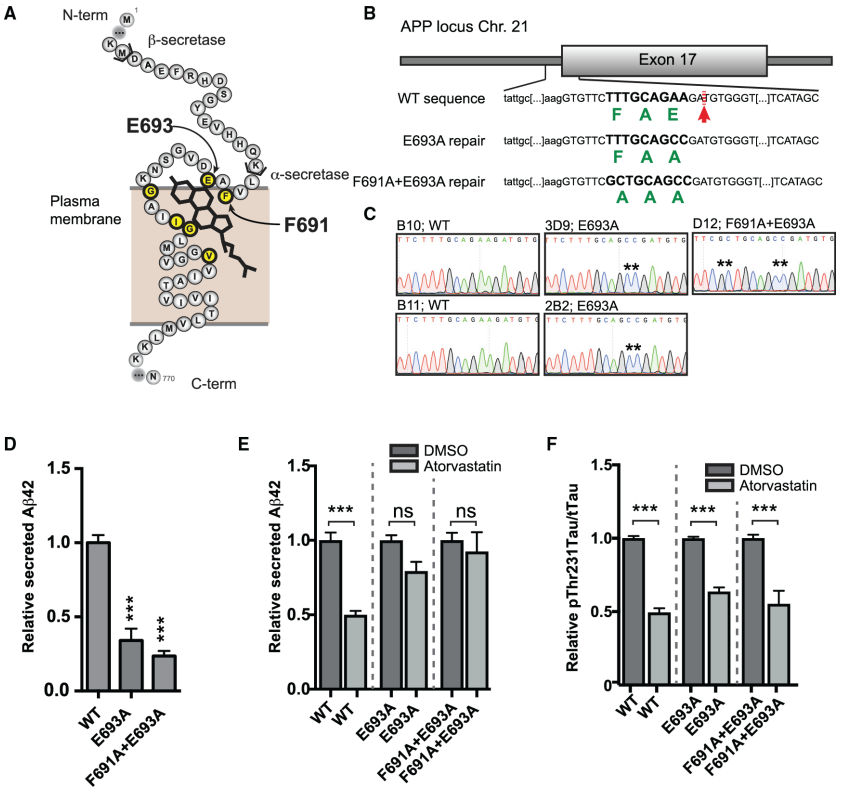

Figure 4. Regulation of Aβ by CE Is Mediated by a Cholesterol Binding Domain in APP

(A) Schematic representation of the transmembrane domain of APP with amino acids essential for cholesterol binding indicated in yellow.

(B) Schematic overview of the gene-editing strategy to generate APP-Δcholesterol lines. Green indicates amino acid sequence. Red arrow indicates CRISPR/Cas9 cut site.

(C) Sequencing results verifying correct incorporation of desired mutations in the APP-Δcholesterol lines. Two E693A (line 3D9 and 2B2) and one F691A+E693A line (line D12) were generated, as well as two non-gene-edited, but clonally expanded, WT lines (B10 and B11).

(D–F) Measurements made using APP-Δcholesterol neurons with the following genotypes: WT (average from 2 independent lines), E693A (2 independent lines), and F691A+E693A (1 line) (mean ± SEM, n ≥ 3 per line). (D) Relative secreted Aβ42 levels in conditioned media from purified $CD184^{-}$, $CD44^{-}$, and $CD24^{+}$ neurons (mean ± SEM, n ≥ 3 per line). (E) Relative secreted Aβ42 in response to atorvastatin treatment (10 μM, 3 days) (mean ± SEM, n ≥ 3 per line) (F) pThr231Tau/tTau in response to atorvastatin treatment (10 μM, 3 days) in APP-Δcholesterol neurons (mean ± SEM, n ≥ 3 per line).

See also Figure S4.

separate, we first studied the relationship between CE and Aβ secretion in more detail. We hypothesized that the effect of CE on Aβ secretion could be mediated by a recently identified cholesterol-binding domain in APP β-CTF (Barrett et al., 2012). We used CRISPR/Cas9 to mutate the cholesterol-binding domain in the endogenous APP locus (Figures 4A–4C, S4A, and S4B) and created two mutations that had previously been shown to abolish APP β-CTF-cholesterol interactions (Barrett et al., 2012), APP E693A and APP F691A+E693A. We observed that Aβ42 secretion in these isogenic APP-Δcholesterol lines was reduced under steady state conditions (Figure 4D) indicating that the cholesterol-binding domain affects APP processing and Aβ secretion. More importantly, atorvastatin treatment (Figure 4E) did not affect Aβ42 secretion in these neurons indicating that the effect of lowering CE on Aβ42 is mediated by the cholesterol-binding domain in APP. While Aβ secretion was no longer regulated by atorvastatin in these neurons, atorvastatin still decreased pT231Tau/tTau ratio (in an identical manner as in their isogenic wild-type controls) (Figure 4F), again confirming that the effect of CE on pTau and the effect of CE on Aβ are regulated through two separate pathways. We next sought to determine how CE regulate pTau.

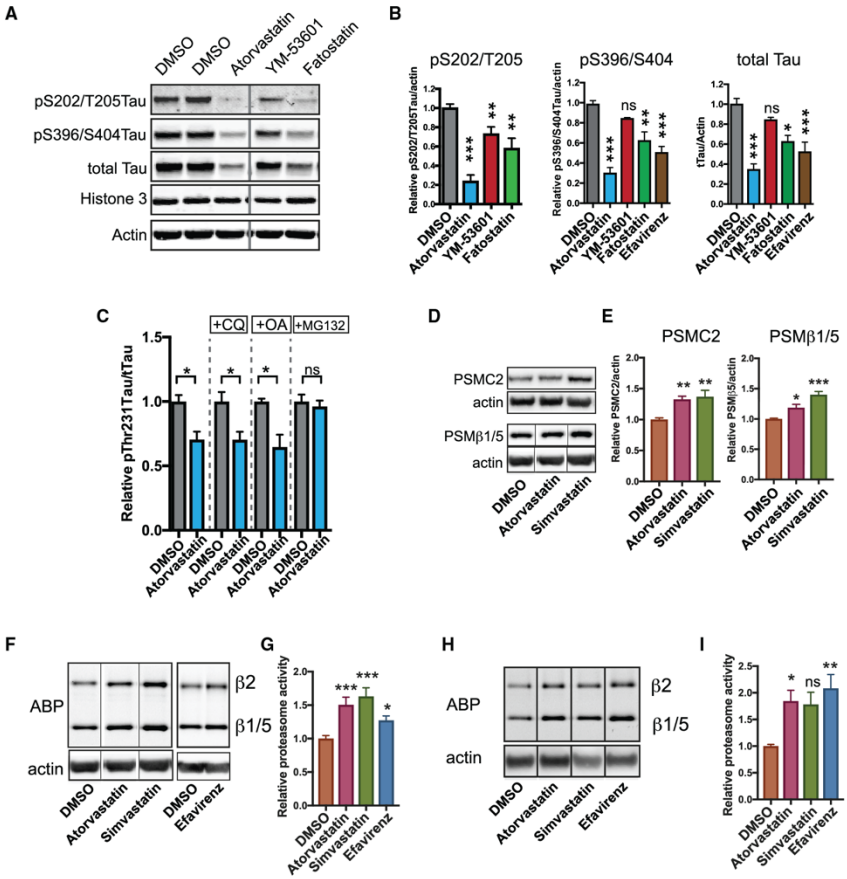

Figure 5. Regulation of pTau by CE Is Mediated by the Proteasome

(A and B) The effect of CE lowering treatments on Tau levels and Tau phosphorylation as assessed by western blot (A), quantified in (B) (mean ± SEM, n ≥ 3). Image is a composite of different loading positions on same blot, stitch is indicated by vertical line.

(C) pThr231Tau/tTau levels in APP^{dp}1-6 neurons co-treated with atorvastatin (10 μm) and a lysosomal inhibitor (chloroquine, CQ 25 μM), a phosphatase inhibitor (okadaic acid, 1.25nM) or a proteasome inhibitor (MG132, 5 μM) for 3 days as measured by ELISA (mean ± SEM, n ≥ 3).

(D and E) APP^{dp}1-6 neurons were treated for 3 days with DMSO, simvastatin (10 μM) or atorvastatin (10 μM) and levels of proteasome subunits PSMC2 and PSMβ1/5 were assessed by western blot (D). Quantified in (E) (mean ± SEM n ≥ 3). PSMβ1/5/actin image is a composite of different loading positions on same blot, stiches are indicated by vertical line.

(F–I) APP^{dp}1-6 (F and G) or NDC CV4a (H and I) neurons were treated for 3 days with DMSO, simvastatin (10 μM), atorvastatin (10 μM), or efavirenz (10 μM) and incubated with a proteasome activity binding probe (ABP) for 1 h. Cells were lysed, run on SDS-page, and ABP fluorescence from the gel was determined (mean ± SEM, n ≥ 5). (G) Quantification of the western blots from (F). (I) Quantification of western blots from (H). Images are composite of different loading positions on same blot, stiches are indicated by vertical lines.

See also Figure S5.

The Effect of CE on pTau Levels Is Mediated by the Proteasome

Previous reports indicate that accumulation of pTau in FAD neurons can be downstream of altered proteostatic regulation of (p)Tau (Moore et al., 2015). To assess whether CE affect the proteostatic regulation of pTau, we performed quantitative western blot on APP^{dp} neurons treated with different CE-targeting drugs. In addition to a reduction of pS396/S404Tau and pS202/T205Tau, CE reduction also reduced total Tau (Figures 5A, 5B, and S5A). The reduction of pTau and total Tau by our

treatments was not explained by a specific loss of neurons in the cultures (Figures S5B–S5D). The reduction of both pTau as well as tTau could indicate a proteostatic regulatory event, rather than altered Tau phosphorylation and dephosphorylation events. This was further substantiated by the finding that activity of GSK3β (a major Tau kinase) was not affected by statin-mediated CE reduction (Figure S5E). Next, we attempted to rescue the effect of CE reduction on pThr231Tau/tTau with inhibitors of phosphatase activity (okadaic acid), proteasomal (MG132), and/or or lysosomal and autophagosomal (chloroquine) degradation (Figures 5C and S5F–S5M). Only proteasomal inhibition abrogated the decrease in pThr231Tau/tTau ratio induced by atorvastatin (Figures 5C and 5N), indicating that the effect of CE on pTau is mediated by the proteasome. Interestingly, in addition to cholesterol-synthetic genes, we found that the 26S proteasome regulatory subunit 7 (PSMC2) was also upregulated after statin treatment in NDC neurons (Figure S2D; Table S2). We validated by western blot in APP^{dp} neurons that statin treatment increased the levels of proteasomal subunit PSMC2 (Figures 5D and 5E). Levels of another proteasome subunit, proteasome subunit beta type-5 (PSMβ5) in the core of the proteasome, were also increased (Figures 5D and 5E). This statin-dependent increase in proteasome levels is not mediated by transcriptional upregulation of proteasomal subunits (Figure S5N). Using a proteasome activity binding probe (Berkers et al., 2007; Leestemaker et al., 2017), we found that CE reduction through either statins or efavirenz increased total cellular proteasome activity in both APP^{dp} and NDC neurons (Figures 5F–5I). The effect of CE on proteasome function was not mediated by mechanistic target of rapamycin (mTor) (Figures S5O–S5Q). Together, our data show that reducing neuronal CE enhances proteasome levels, increases total cellular proteasome activity, and induces the proteasomal degradation of pTau indicative of a CE-proteasome-Tau axis.

CYP46A1 Activation Is a Neuron-Specific CE-Reducing Approach that Is Better Tolerated by Astrocytes Than HMGCR Inhibitors (Statins)

Our data indicate that neuronal CE are a potential therapeutic target to activate the proteasome and prevent aberrant pTau accumulation in AD. To identify possible adverse effects of candidate CE-lowering strategies on other non-neuronal brain cells, we tested the toxicity of selected compounds on iPSC-derived astrocytes. All iPSC-derived astrocytes displayed radial morphology of astrocytes and expressed the glial marker GFAP, while the neural stem cell marker SOX2 was not expressed (Figure 6A). We concentrated on two different drugs that currently have Food and Drug Administration (FDA) approval for other indications, statins (to lower cholesterol synthesis) and efavirenz (that activates the neuron-specific enzyme CYP46A1). Already, at low concentrations, simvastatin and atorvastatin induced major astrocyte cell death (Figures 6B, 6C, S6A, and S6B), whereas efavirenz did not affect astrocyte viability even at high doses (Figures 6D and S6C). 24-Hydroxycholesterol was not detected in astrocyte media before or after treatment with efavirenz. Efavirenz increased 24-hydroxycholesterol secretion from APP^{dp} and APP^{null} neurons in a dose-dependent manner that correlated well with its effect on pThr231Tau/tTau in these neurons (Figures 6D and S6D). Together, these data show that allosteric activation of CYP46A1 is a neuron-specific CE- and pTau-lowering treatment with less adverse effects on astrocytes and provides a therapeutic approach to reduce pTau accumulation in early AD-neurons.

DISCUSSION

Here, we used AD-patient iPSC-derived neurons in a phenotypic drug screen to identify compounds that reduce aberrant pTau accumulation in FAD neurons (Israel et al., 2012; Moore et al., 2015; Muratore et al., 2014; Ochalek et al., 2017). From a library of >1,600 compounds, we successfully identify 42 compounds that reduced pTau levels, including six previously reported modulators of pTau and 36 novel pTau targeting compounds (Figure 1). From the 42 identified compounds, we selected cholesterol-targeting compounds (statins) to study in more detail. Cholesterol metabolism has previously been implicated in AD (Di Paolo and Kim, 2011; Puglielli et al., 2003) and CE, the esterified storage products of cholesterol, accumulate in AD patient brains (Chan et al., 2012) and in APP-transgenic mice (Chan et al., 2012; Tajima et al., 2013; Yang et al., 2014). We show that reducing CE, through a number of mechanistically different drugs, reduces levels of pTau at multiple phosphorylation epitopes in both FAD, SAD, and NDC subject neurons. CE have previously also been shown to regulate APP processing and Aβ generation (Hutter-Paier et al., 2004; Huttunen et al., 2009; Puglielli et al., 2001), and we confirmed that CE also regulate Aβ secretion from human iPSC-derived AD patient neurons. Interestingly, we find that the effect of CE on Aβ is independent of the effect of CE on pTau (Figures 3 and 4), and pTau and Aβ are thus co-regulated by CE through independent pathways. Similar co-regulation of Aβ and Tau through independent pathways have recently been shown for ApoE (Wang et al., 2018) and the retromer complex (Young et al., 2018). These findings, together with our findings, reinforce the notion that common upstream (pathogenic) pathways in SAD, such as CE, can drive increased levels of pTau and Aβ through separate pathways (Small and Duff, 2008), rather than only through a direct linear pathway directly from Aβ to Tau.

Pathways that Mediate the Effect of CE on pTau and Aβ

We investigated the separate pathways that underlie CE-dependent regulation of pTau and Aβ, respectively, in early AD neurons. We find that the effect of CE on Aβ is mediated by a cholesterol binding-site in APP, whereas the effect of CE on pTau is mediated by the proteasome. Surprisingly, in our system, we did not observe significant differences in free cholesterol levels for the treatments that reduced CE, Aβ, and pTau. As also previously observed (Puglielli et al., 2001), these data indicate that CE mediates the effect of cholesterol-targeting drugs on Aβ. We show that the effect of CE on Aβ is mediated by a domain in APP that has previously been shown to bind cholesterol (Barrett et al., 2012), possibly suggesting that this cholesterol-binding domain can also sense CE. Alternatively, localized reductions in cholesterol in specific domains such as lipid rafts (Ehehalt et al., 2003), specific organelles, or localized changes in *de novo* synthesized cholesterol under the detection limit of our measurements could mediate the effect of statins on APP processing via the APP-cholesterol binding domain. In regard to CE-dependent regulation of pTau, we find that reduction of

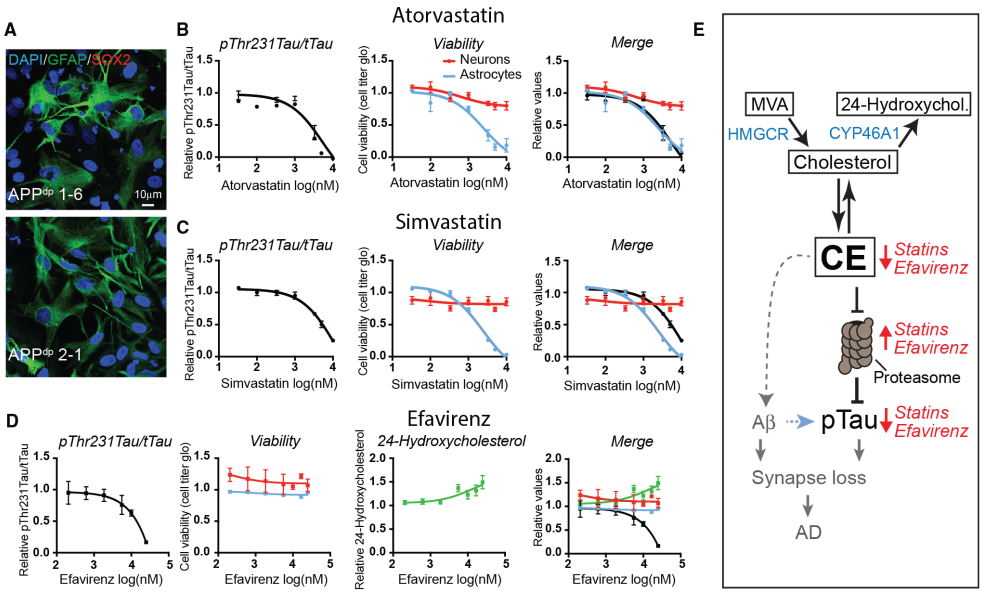

Figure 6. CYP46A1 Activation Is a Neuron-Specific CE-Reducing Approach that Is Better Tolerated by Astrocytes

(A) iPSC-derived astrocytes were fixed and stained with indicated antibodies. Scale bar, 10 μm.

(B–D) iPSC-derived APP^{dp}1-6 astrocytes were treated for 3 days with increasing concentrations of (B) atorvastatin, (C) simvastatin, and (D) efavirenz, and viability was measured (cell titer glo). Astrocytic viability (blue line) was plotted against results from Figures 1D and S1A for statins (neuronal viability and pThr231Tau/Tau ratio). For efavirenz, dose responses to measure pThr231Tau/tTau and neuronal viability were performed in APP^{dp}1-6 neurons (mean ± SEM, n ≥ 3–6).

(E) Model depicting the relationship between CE, pTau, and Aβ in early AD neurons. Statins reduce CE levels through inhibition of the cholesterol-synthetic pathway, while efavirenz enhances the turnover of cholesterol to 24-hydroxycholesterol that causes conversion of CE to cholesterol and a reduction in CE. Reduced CE cause proteasomal upregulation and degradation of pTau. In a correlated, but independent pathway, CE regulate APP processing and Aβ generation.

See also Figure S6.

CE increases the level of proteasomal subunits, overall proteasomal activity, and proteasomal degradation of pTau (see model Figure 6E). This indicates a neuronal CE-proteasome-pTau axis that regulates turnover of neuronal pTau. The effect of CE on proteasome levels is not mediated by enhanced transcription of proteasomal subunits, and the exact mechanism by which CE control proteasomal activity needs to be further determined. Interestingly, in other model systems, lipid droplets (the storage site of CE) have been shown to be active signaling organelles that regulate proteasome activity (Arrese et al., 2014; Keembiyehetty et al., 2011). The neuronal proteasome also associates with plasma membranes (Ramachandran and Margolis, 2017), offering another possible neuron-specific site of convergence between CE and the proteasome. CE-dependent regulation of the proteasome is also relevant for other neurodegenerative diseases in which altered cholesterol-homeostasis and protein aggregation occurs such as Niemann-Pick type C and Huntington disease (Karasinska and Hayden, 2011). Another open issue is why pTau is regulated by CE. Direct coupling of CE to pTau levels could indicate a pathway that coordinates the speed of Tau-regulated axonal transport or growth, with the availability of (stored) neuronal cholesterol required for membrane growth or synapse formation. Overall, our data here indicate that CE regulate pTau and Aβ by two separate pathways and suggests that CE could be an upstream driver of both Aβ secretion and pTau accumulation.

CE and AD

Our findings provide a mechanistic explanation for how changes in CE, induced by APP mutations or SAD genetic risk variants in APP (Chan et al., 2012; Tajima et al., 2013; Yang et al., 2014) could contribute to Tau pathology. Interestingly, CE production is overactive in human SAD fibroblasts (Pani et al., 2009) and APOE, the major genetic risk factor for SAD, acts as a CE transporter in brain (Liu et al., 2013; Michikawa et al., 2000; Minagawa et al., 2009). Our findings in human iPSC-derived AD neurons indicate that alterations in neuronal CE could drive pTau accumulation and are supported by previous *in vivo* observations in mouse models showing that statins reduce NFT load in animal models of tauopathy (Boimel et al., 2009), and genetic inhibition of cholesterol esterification by ACAT1 reduces tauopathy in an AD-mouse model (Shibuya et al., 2015), indicating that the

interactions between CE and Tau are conserved in the adult (mouse) brain. We describe several pharmaceutical strategies to reduce CE in early AD neurons including LXR target gene-mediated cholesterol export, conversion of cholesterol to hydroxycholesterol by CYP46A1 activators, and direct inhibition of cholesterol esterification by ACAT inhibitors. In humans, long-term statin usage has been shown to correlate with reduced AD incidence in some studies (Shepardson et al., 2011a, 2011b; Zissimopoulos et al., 2017), although the underlying mechanisms have been debated. Statins also reduce pTau levels in CSF from AD patients (Riekse et al., 2006). Here, we show that the effects of statins on pTau can be directly mediated by CE and are not merely a consequence of altered APP processing or peripheral effects of cholesterol-targeting drugs. However, our data do not indicate that statins are the best candidate drugs for targeting Tau accumulation in AD. Statins affect the levels of pTau in human neurons only at relatively high concentrations (Figure 1) unlikely reached in human brain (Björkhem-Bergman et al., 2011) and have strong adverse effects on human astrocytes at these high concentrations (Figure 6). We cannot exclude the possibility that *in vivo* statins lower neuronal CE through indirect effects on astrocytic cholesterol and/or CE production, but our data do indicate that additional potency could be gained from enhanced targeting of neuronal CE. We show that allosteric activators of CYP46A1 could provide a neuron-specific approach to reduce CE and pTau in early AD neurons. Regulation of pTau by CYP46A1 is also conserved in adult (mice) brains where genetic inhibition of CYP46A1 enhances abnormal phosphorylation of Tau (Djelti et al., 2015), and overexpression of CYP46A1 in transgenic Tau mice rescues cognitive decline (Burlot et al., 2015).

We targeted CYP46A1 through allosteric activation by the small molecule efavirenz (Anderson et al., 2016) and show that efavirenz reduces pTau in early human AD neurons without affecting astrocyte viability. Efavirenz, originally marketed as an HIV-medication (brand name Sustiva), has recently also been shown to reduce amyloid pathology in AD mice (Mast et al., 2017b) indicating that efavirenz could possibly be repurposed for AD. However, when given to HIV patients at high doses, efavirenz has significant adverse effects that include neurotoxicity (Apostolova et al., 2017). Major adverse effects were not observed in mice at lower concentrations of efavirenz that sufficed to alter brain cholesterol metabolism and reduce amyloid pathology, indicative of an appropriate therapeutic window (Mast et al., 2017b). Other allosteric activators of CYP46A1 have also recently been identified (Mast et al., 2017a). The *in vivo* data of CYP46A1 activators on inhibitors of amyloid pathology (Mast et al., 2017b), together with our findings that CYP46A1 activators reduce Tau accumulation in human AD neurons, support the development of allosteric activators of CYP46A1 as therapies for AD.

In conclusion, using high-throughput phenotypic screening, we identified >40 FDA-approved drugs with diverse biological targets that reduce pTau in early AD neurons. By pathway mapping, we identify a CYP46A1-CE-Tau axis as a druggable pathway in early AD. We find that reducing CE potently decreases neuronal pTau levels through proteasomal upregulation and degradation of pTau in an APP- and Aβ-independent manner. In a separate pathway, Aβ secretion is regulated by CE through a cholesterol-binding domain in APP. We find that allosteric activation of CYP46A1 is a neuron-specific CE-lowering strategy that is well tolerated by human astrocytes. Together, our data indicate CE as a dual upstream regulator of pTau and Aβ, and we propose CE-reduction, particularly through CYP46A1 activation, as a therapeutic approach to independently reduce accumulation of pTau and Aβ in AD patients.

STAR★METHODS

Detailed methods are provided in the online version of this paper and include the following:

- KEY RESOURCES TABLE
- CONTACT FOR REAGENT AND RESOURCE SHARING
- EXPERIMENTAL MODEL AND SUBJECT DETAILS
  - Cultured Mouse Cortical Neurons
  - Human iPSC Derived Cell lines
- METHOD DETAILS
  - Reagents
  - Phenotypic high-throughput screen
  - Aβ, pThr231Tau/total Tau, pSer9GSK3b/total Gsk3b, Phospho-4E-BP1(Thr37/46)/total 4E-BP1 ELISA Measurements
  - Cell viability
  - Mass spectrometry sample preparation and LC-MS-MS
  - Lipid measurements
  - Microscopy
  - RNA expression analysis
  - Quantitative western blot
  - Proteasomal levels and activity
  - Vectors and viral transduction
- QUANTIFICATION AND STATISTICAL ANALYSIS
  - Statistical Analysis

SUPPLEMENTAL INFORMATION

Supplemental Information includes six figures and six tables and can be found with this article online at https://doi.org/10.1016/j.stem.2018.12.013.

ACKNOWLEDGMENTS

We would like to acknowledge Majid Ghassemian and the UCSD Biomolecular and Proteomic Mass Spectrometry Facility for assistance with the generation of the mass spectrometry data. We would like to acknowledge Eline Kompanje, Ruben Ruiz, and Robbert Zalm for experimental support; Somasish Dastidar for help with the mice neuronal cultures; and Matthijs Verhage, Vivi Heine, and Charlotte Teunissen for generously sharing reagents and equipment. We would like to acknowledge Elsa Rodrigues (University of Lisbon) for the generous sharing of CYP46A1 plasmids. R.v.d.K. was supported by an Alzheimer Netherlands Fellowship (WE.15-2013-01) and an ERC Marie Curie International Outgoing fellowship (622444, APPtoTau). V.F.L. was supported by an NIH T32 training grant (5T32AG000216-24). This work is supported by NIA 1RF1AG048083-01 and CIRM RB5-07011 grants to L.S.G. We would like to dedicate this paper to our friend and colleague, Daniel Williams.

AUTHOR CONTRIBUTIONS

R.v.d.K. and V.F.L. designed and performed the experiments and wrote the paper together with L.S.B.G. C.M.H., D.A.W., and A.G.B. performed the drug screen. L.K.F. generated the APP knockout lines. Y.L. and H.O.

performed the experiments with proteasome binding probe. E.S. and M.G. performed lipid measurements for figures in the manuscript. J.F.B. and J.B.H. performed pilot measurements for cholesterol precursors. S.L.W. and K.D.R. were involved in screen design and compound identification.

DECLARATION OF INTERESTS

The authors declare no competing interests.

Received: March 9, 2018
Revised: September 26, 2018
Accepted: December 17, 2018
Published: January 24, 2019

REFERENCES

Anderson, K.W., Mast, N., Hudgens, J.W., Lin, J.B., Turko, I.V., and Pikuleva, I.A. (2016). Mapping of the allosteric site in cholesterol hydroxylase CYP46A1 for efavirenz, a drug that stimulates enzyme activity. J. Biol. Chem. *291*, 11876–11886.

Apostolova, N., Blas-Garcia, A., Galindo, M.J., and Esplugues, J.V. (2017). Efavirenz: what is known about the cellular mechanisms responsible for its adverse effects. Eur. J. Pharmacol. *812*, 163–173.

Arrese, E.L., Saudale, F.Z., and Soulages, J.L. (2014). Lipid droplets as signaling platforms linking metabolic and cellular functions. Lipid Insights *7*, 7–16.

Barrett, P.J., Song, Y., Van Horn, W.D., Hustedt, E.J., Schafer, J.M., Hadziselimovic, A., Beel, A.J., and Sanders, C.R. (2012). The amyloid precursor protein has a flexible transmembrane domain and binds cholesterol. Science *336*, 1168–1171.

Berkers, C.R., van Leeuwen, F.W.B., Groothuis, T.A., Peperzak, V., van Tilburg, E.W., Borst, J., Neefjes, J.J., and Ovaa, H. (2007). Profiling proteasome activity in tissue with fluorescent probes. Mol. Pharm. *4*, 739–748.

Björkhem-Bergman, L., Lindh, J.D., and Bergman, P. (2011). What is a relevant statin concentration in cell experiments claiming pleiotropic effects? Br. J. Clin. Pharmacol. *72*, 164–165.

Boimel, M., Grigoriadis, N., Lourbopoulos, A., Touloumi, O., Rosenmann, D., Abramsky, O., and Rosenmann, H. (2009). Statins reduce the neurofibrillary tangle burden in a mouse model of tauopathy. J. Neuropathol. Exp. Neurol. *68*, 314–325.

Brownjohn, P.W., Smith, J., Portelius, E., Serneels, L., Kvartsberg, H., De Strooper, B., Blennow, K., Zetterberg, H., and Livesey, F.J. (2017). Phenotypic screening identifies modulators of amyloid precursor protein processing in human stem cell models of Alzheimer's disease. Stem Cell Reports *8*, 870–882.

Buerger, K., Teipel, S.J., Zinkowski, R., Blennow, K., Arai, H., Engel, R., Hofmann-Kiefer, K., McCulloch, C., Ptok, U., Heun, R., et al. (2002). CSF tau protein phosphorylated at threonine 231 correlates with cognitive decline in MCI subjects. Neurology *59*, 627–629.

Burlot, M.-A., Braudeau, J., Michaelsen-Preusse, K., Potier, B., Ayciriex, S., Varin, J., Gautier, B., Djelti, F., Audrain, M., Dauphinot, L., et al. (2015). Cholesterol 24-hydroxylase defect is implicated in memory impairments associated with Alzheimer-like Tau pathology. Hum. Mol. Genet. *24*, 5965–5976.

Chan, R.B., Oliveira, T.G., Cortes, E.P., Honig, L.S., Duff, K.E., Small, S.A., Wenk, M.R., Shui, G., and Di Paolo, G. (2012). Comparative lipidomic analysis of mouse and human brain with Alzheimer disease. J. Biol. Chem. *287*, 2678–2688.

Choi, S.H., Kim, Y.H., Hebisch, M., Sliwinski, C., Lee, S., D'Avanzo, C., Chen, H., Hooli, B., Asselin, C., Muffat, J., et al. (2014). A three-dimensional human neural cell culture model of Alzheimer's disease. Nature *515*, 274–278.

D'Antonio, M., Woodruff, G., Nathanson, J.L., D'Antonio-Chronowska, A., Arias, A., Matsui, H., Williams, R., Herrera, C., Reyna, S.M., Yeo, G.W., et al. (2017). High-throughput and cost-effective characterization of induced pluripotent stem cells. Stem Cell Reports *8*, 1101–1111.

de Jong, A., Schuurman, K.G., Rodenko, B., Ovaa, H., and Berkers, C.R. (2012). Fluorescence-based proteasome activity profiling. Methods Mol. Biol. *803*, 183–204.

Di Paolo, G., and Kim, T.-W. (2011). Linking lipids to Alzheimer's disease: cholesterol and beyond. Nat. Rev. Neurosci. *12*, 284–296.

Dickey, C.A., Ash, P., Klosak, N., Lee, W.C., Petrucelli, L., Hutton, M., and Eckman, C.B. (2006). Pharmacologic reductions of total tau levels; implications for the role of microtubule dynamics in regulating tau expression. Mol. Neurodegener. *1*, 6.

Djelti, F., Braudeau, J., Hudry, E., Dhenain, M., Varin, J., Bièche, I., Marquer, C., Chali, F., Ayciriex, S., Auzeil, N., et al. (2015). CYP46A1 inhibition, brain cholesterol accumulation and neurodegeneration pave the way for Alzheimer's disease. Brain *138*, 2383–2398.

Ehehalt, R., Keller, P., Haass, C., Thiele, C., and Simons, K. (2003). Amyloidogenic processing of the Alzheimer beta-amyloid precursor protein depends on lipid rafts. J. Cell Biol. *160*, 113–123.

Foley, P. (2010). Lipids in Alzheimer's disease: a century-old story. Biochim. Biophys. Acta *1801*, 750–753.

Fong, L.K., Yang, M.M., Dos Santos Chaves, R., Reyna, S.M., Langness, V.F., Woodruff, G., Roberts, E.A., Young, J.E., and Goldstein, L.S.B. (2018). Full-length amyloid precursor protein regulates lipoprotein metabolism and amyloid-β clearance in human astrocytes. J. Biol. Chem. *293*, 11341–11357.

Giera, M., Plössl, F., and Bracher, F. (2007). Fast and easy in vitro screening assay for cholesterol biosynthesis inhibitors in the post-squalene pathway. Steroids *72*, 633–642.

Gore, A., Li, Z., Fung, H.-L., Young, J.E., Agarwal, S., Antosiewicz-Bourget, J., Canto, I., Giorgetti, A., Israel, M.A., Kiskinis, E., et al. (2011). Somatic coding mutations in human induced pluripotent stem cells. Nature *471*, 63–67.

Hamilton, L.K., Dufresne, M., Joppé, S.E., Petryszyn, S., Aumont, A., Calon, F., Barnabé-Heider, F., Furtos, A., Parent, M., Chaurand, P., and Fernandes, K.J.L. (2015). Aberrant lipid metabolism in the forebrain niche suppresses adult neural stem cell proliferation in an animal model of Alzheimer's disease. Cell Stem Cell *17*, 397–411.

Han, D.H., Na, H.-K., Choi, W.H., Lee, J.H., Kim, Y.K., Won, C., Lee, S.-H., Kim, K.P., Kuret, J., Min, D.-H., and Lee, M.J. (2014). Direct cellular delivery of human proteasomes to delay tau aggregation. Nat. Commun. *5*, 5633.

Hutter-Paier, B., Huttunen, H.J., Puglielli, L., Eckman, C.B., Kim, D.Y., Hofmeister, A., Moir, R.D., Domnitz, S.B., Frosch, M.P., Windisch, M., and Kovacs, D.M. (2004). The ACAT inhibitor CP-113,818 markedly reduces amyloid pathology in a mouse model of Alzheimer's disease. Neuron *44*, 227–238.

Huttunen, H.J., Peach, C., Bhattacharyya, R., Barren, C., Pettingell, W., Hutter-Paier, B., Windisch, M., Berezovska, O., and Kovacs, D.M. (2009). Inhibition of acyl-coenzyme A: cholesterol acyl transferase modulates amyloid precursor protein trafficking in the early secretory pathway. FASEB J. *23*, 3819–3828.

Huttunen, H.J., Havas, D., Peach, C., Barren, C., Duller, S., Xia, W., Frosch, M.P., Hutter-Paier, B., Windisch, M., and Kovacs, D.M. (2010). The acyl-coenzyme A: cholesterol acyltransferase inhibitor Cl-1011 reverses diffuse brain amyloid pathology in aged amyloid precursor protein transgenic mice. J. Neuropathol. Exp. Neurol. *69*, 777–788.

Ikonen, E. (2008). Cellular cholesterol trafficking and compartmentalization. Nat. Rev. Mol. Cell Biol. *9*, 125–138.

Israel, M.A., Yuan, S.H., Bardy, C., Reyna, S.M., Mu, Y., Herrera, C., Hefferan, M.P., Van Gorp, S., Nazor, K.L., Boscolo, F.S., et al. (2012). Probing sporadic and familial Alzheimer's disease using induced pluripotent stem cells. Nature *482*, 216–220.

Kamisuki, S., Mao, Q., Abu-Elheiga, L., Gu, Z., Kugimiya, A., Kwon, Y., Shinohara, T., Kawazoe, Y., Sato, S., Asakura, K., et al. (2009). A small molecule that blocks fat synthesis by inhibiting the activation of SREBP. Chem. Biol. *16*, 882–892.

Karasinska, J.M., and Hayden, M.R. (2011). Cholesterol metabolism in Huntington disease. Nat. Rev. Neurol. *7*, 561–572.

Keck, S., Nitsch, R., Grune, T., and Ullrich, O. (2003). Proteasome inhibition by paired helical filament-tau in brains of patients with Alzheimer's disease. J. Neurochem. *85*, 115–122.

Keembiyehetty, C.N., Krzeslak, A., Love, D.C., and Hanover, J.A. (2011). A lipid-droplet-targeted O-GlcNAcase isoform is a key regulator of the proteasome. J. Cell Sci. *124*, 2851–2860.

Keller, J.N., Hanni, K.B., and Markesbery, W.R. (2000). Impaired proteasome function in Alzheimer's disease. J. Neurochem. *75*, 436–439.

Kondo, T., Imamura, K., Funayama, M., Tsukita, K., Miyake, M., Ohta, A., Woltjen, K., Nakagawa, M., Asada, T., Arai, T., et al. (2017). iPSC-based compound screening and in vitro trials identify a synergistic anti-amyloid β combination for Alzheimer's disease. Cell Rep. *21*, 2304–2312.

Lee, H.T., Sliskovic, D.R., Picard, J.A., Roth, B.D., Wierenga, W., Hicks, J.L., Bousley, R.F., Hamelehle, K.L., Homan, R., Speyer, C., et al. (1996). Inhibitors of acyl-CoA: cholesterol O-acyl transferase (ACAT) as hypocholesterolemic agents. CI-1011: an acyl sulfamate with unique cholesterol-lowering activity in animals fed noncholesterol-supplemented diets. J. Med. Chem. *39*, 5031–5034.

Lee, M.J., Lee, J.H., and Rubinsztein, D.C. (2013). Tau degradation: the ubiquitin-proteasome system versus the autophagy-lysosome system. Prog. Neurobiol. *105*, 49–59.

Leestemaker, Y., de Jong, A., Witting, K.F., Penning, R., Schuurman, K., Rodenko, B., Zaal, E.A., van de Kooij, B., Laufer, S., Heck, A.J.R., et al. (2017). Proteasome activation by small molecules. Cell Chem. Biol. *24*, 725–736.

Liu, C.-C., Liu, C.-C., Kanekiyo, T., Xu, H., and Bu, G. (2013). Apolipoprotein E and Alzheimer disease: risk, mechanisms and therapy. Nat. Rev. Neurol. *9*, 106–118.

Lokireddy, S., Kukushkin, N.V., and Goldberg, A.L. (2015). cAMP-induced phosphorylation of 26S proteasomes on Rpn6/PSMD11 enhances their activity and the degradation of misfolded proteins. Proc. Natl. Acad. Sci. USA *112*, E7176–E7185.

Luna-Muñoz, J., Chávez-Macías, L., García-Sierra, F., and Mena, R. (2007). Earliest stages of tau conformational changes are related to the appearance of a sequence of specific phospho-dependent tau epitopes in Alzheimer's disease. J. Alzheimers Dis. *12*, 365–375.

Mast, N., Anderson, K.W., Johnson, K.M., Phan, T.T.N., Guengerich, F.P., and Pikuleva, I.A. (2017a). *In vitro* cytochrome P450 46A1 (CYP46A1) activation by neuroactive compounds. J. Biol. Chem. *292*, 12934–12946.

Mast, N., Saadane, A., Valencia-Olvera, A., Constans, J., Maxfield, E., Arakawa, H., Li, Y., Landreth, G., and Pikuleva, I.A. (2017b). Cholesterol-metabolizing enzyme cytochrome P450 46A1 as a pharmacologic target for Alzheimer's disease. Neuropharmacology *123*, 465–476.

Merrick, S.E., Demoise, D.C., and Lee, V.M. (1996). Site-specific dephosphorylation of tau protein at Ser202/Thr205 in response to microtubule depolymerization in cultured human neurons involves protein phosphatase 2A. J. Biol. Chem. *271*, 5589–5594.

Michikawa, M., Fan, Q.W., Isobe, I., and Yanagisawa, K. (2000). Apolipoprotein E exhibits isoform-specific promotion of lipid efflux from astrocytes and neurons in culture. J. Neurochem. *74*, 1008–1016.

Minagawa, H., Gong, J.-S., Jung, C.-G., Watanabe, A., Lund-Katz, S., Phillips, M.C., Saito, H., and Michikawa, M. (2009). Mechanism underlying apolipoprotein E (ApoE) isoform-dependent lipid efflux from neural cells in culture. J. Neurosci. Res. *87*, 2498–2508.

Moore, S., Evans, L.D.B., Andersson, T., Portelius, E., Smith, J., Dias, T.B., Saurat, N., McGlade, A., Kirwan, P., Blennow, K., et al. (2015). APP metabolism regulates tau proteostasis in human cerebral cortex neurons. Cell Rep. *11*, 689–696.

Moutinho, M., Nunes, M.J., and Rodrigues, E. (2016). Cholesterol 24-hydroxylase: brain cholesterol metabolism and beyond. Biochim. Biophys. Acta *1861* (12 Pt A), 1911–1920.

Müller, C., Binder, U., Bracher, F., and Giera, M. (2017). Antifungal drug testing by combining minimal inhibitory concentration testing with target identification by gas chromatography-mass spectrometry. Nat. Protoc. *12*, 947–963.

Muratore, C.R., Rice, H.C., Srikanth, P., Callahan, D.G., Shin, T., Benjamin, L.N.P., Walsh, D.M., Selkoe, D.J., and Young-Pearse, T.L. (2014). The familial Alzheimer's disease APPV717I mutation alters APP processing and Tau expression in iPSC-derived neurons. Hum. Mol. Genet. *23*, 3523–3536.

Myeku, N., Clelland, C.L., Emrani, S., Kukushkin, N.V., Yu, W.H., Goldberg, A.L., and Duff, K.E. (2016). Tau-driven 26S proteasome impairment and cognitive dysfunction can be prevented early in disease by activating cAMP-PKA signaling. Nat. Med. *22*, 46–53.

Naldini, L., Blömer, U., Gallay, P., Ory, D., Mulligan, R., Gage, F.H., Verma, I.M., and Trono, D. (1996). In vivo gene delivery and stable transduction of nondividing cells by a lentiviral vector. Science *272*, 263–267.

Ochalek, A., Mihalik, B., Avci, H.X., Chandrasekaran, A., Téglási, A., Bock, I., Giudice, M.L., Táncos, Z., Molnár, K., László, L., et al. (2017). Neurons derived from sporadic Alzheimer's disease iPSCs reveal elevated TAU hyperphosphorylation, increased amyloid levels, and GSK3B activation. Alzheimers Res. Ther. *9*, 90.

Pani, A., Dessì, S., Diaz, G., La Colla, P., Abete, C., Mulas, C., Angius, F., Cannas, M.D., Orru, C.D., Cocco, P.L., et al. (2009). Altered cholesterol ester cycle in skin fibroblasts from patients with Alzheimer's disease. J. Alzheimers Dis. *18*, 829–841.

Parrales, A., Ranjan, A., Iyer, S.V., Padhye, S., Weir, S.J., Roy, A., and Iwakuma, T. (2016). DNAJA1 controls the fate of misfolded mutant p53 through the mevalonate pathway. Nat. Cell Biol. *18*, 1233–1243.

Puglielli, L., Konopka, G., Pack-Chung, E., Ingano, L.A., Berezovska, O., Hyman, B.T., Chang, T.Y., Tanzi, R.E., and Kovacs, D.M. (2001). Acyl-coenzyme A: cholesterol acyltransferase modulates the generation of the amyloid beta-peptide. Nat. Cell Biol. *3*, 905–912.

Puglielli, L., Tanzi, R.E., and Kovacs, D.M. (2003). Alzheimer's disease: the cholesterol connection. Nat. Neurosci. *6*, 345–351.

Ramachandran, K.V., and Margolis, S.S. (2017). A mammalian nervous-system-specific plasma membrane proteasome complex that modulates neuronal function. Nat. Struct. Mol. Biol. *24*, 419–430.

Riekse, R.G., Li, G., Petrie, E.C., Leverenz, J.B., Vavrek, D., Vuletic, S., Albers, J.J., Montine, T.J., Lee, V.M.-Y., Lee, M., et al. (2006). Effect of statins on Alzheimer's disease biomarkers in cerebrospinal fluid. J. Alzheimers Dis. *10*, 399–406.

Sharpe, L.J., Cook, E.C.L., Zelcer, N., and Brown, A.J. (2014). The UPS and downs of cholesterol homeostasis. Trends Biochem. Sci. *39*, 527–535.

Shepardson, N.E., Shankar, G.M., and Selkoe, D.J. (2011a). Cholesterol level and statin use in Alzheimer disease: II. Review of human trials and recommendations. Arch. Neurol. *68*, 1385–1392.

Shepardson, N.E., Shankar, G.M., and Selkoe, D.J. (2011b). Cholesterol level and statin use in Alzheimer disease: I. Review of epidemiological and preclinical studies. Arch. Neurol. *68*, 1239–1244.

Shi, Y., Kirwan, P., Smith, J., MacLean, G., Orkin, S.H., and Livesey, F.J. (2012). A human stem cell model of early Alzheimer's disease pathology in Down syndrome. Sci. Transl. Med. *4*, 124ra29.

Shi, Y., Inoue, H., Wu, J.C., and Yamanaka, S. (2017). Induced pluripotent stem cell technology: a decade of progress. Nat. Rev. Drug Discov. *16*, 115–130.

Shibuya, Y., Niu, Z., Bryleva, E.Y., Harris, B.T., Murphy, S.R., Kheirollah, A., Bowen, Z.D., Chang, C.C.Y., and Chang, T.-Y. (2015). Acyl-coenzyme A:cholesterol acyltransferase 1 blockage enhances autophagy in the neurons of triple transgenic Alzheimer's disease mouse and reduces human P301L-tau content at the presymptomatic stage. Neurobiol. Aging *36*, 2248–2259.

Small, S.A., and Duff, K. (2008). Linking Abeta and tau in late-onset Alzheimer's disease: a dual pathway hypothesis. Neuron *60*, 534–542.

Tajima, Y., Ishikawa, M., Maekawa, K., Murayama, M., Senoo, Y., Nishimaki-Mogami, T., Nakanishi, H., Ikeda, K., Arita, M., Taguchi, R., et al. (2013). Lipidomic analysis of brain tissues and plasma in a mouse model expressing mutated human amyloid precursor protein/tau for Alzheimer's disease. Lipids Health Dis. *12*, 68.

Wang, C., Najm, R., Xu, Q., Jeong, D.-E., Walker, D., Balestra, M.E., Yoon, S.Y., Yuan, H., Li, G., Miller, Z.A., et al. (2018). Gain of toxic apolipoprotein

E4 effects in human iPSC-derived neurons is ameliorated by a small-molecule structure corrector. Nat. Med. *24*, 647–657.

Xie, H., Litersky, J.M., Hartigan, J.A., Jope, R.S., and Johnson, G.V. (1998). The interrelationship between selective tau phosphorylation and microtubule association. Brain Res. *798*, 173–183.

Yang, D.-S., Stavrides, P., Saito, M., Kumar, A., Rodriguez-Navarro, J.A., Pawlik, M., Huo, C., Walkley, S.U., Saito, M., Cuervo, A.M., and Nixon, R.A. (2014). Defective macroautophagic turnover of brain lipids in the TgCRND8 Alzheimer mouse model: prevention by correcting lysosomal proteolytic deficits. Brain *137*, 3300–3318.

Young, J.E., Boulanger-Weill, J., Williams, D.A., Woodruff, G., Buen, F., Revilla, A.C., Herrera, C., Israel, M.A., Yuan, S.H., Edland, S.D., and Goldstein, L.S.B. (2015). Elucidating molecular phenotypes caused by the SORL1 Alzheimer's disease genetic risk factor using human induced pluripotent stem cells. Cell Stem Cell *16*, 373–385.

Young, J.E., Fong, L.K., Frankowski, H., Petsko, G.A., Small, S.A., and Goldstein, L.S.B. (2018). Stabilizing the retromer complex in a human stem cell model of Alzheimer's disease reduces TAU phosphorylation independently of amyloid precursor protein. Stem Cell Reports *10*, 1046–1058.

Yuan, S.H., Martin, J., Elia, J., Flippin, J., Paramban, R.I., Hefferan, M.P., Vidal, J.G., Mu, Y., Killian, R.L., Israel, M.A., et al. (2011). Cell-surface marker signatures for the isolation of neural stem cells, glia and neurons derived from human pluripotent stem cells. PLoS ONE *6*, e17540.

Zissimopoulos, J.M., Barthold, D., Brinton, R.D., and Joyce, G. (2017). Sex and race differences in the association between statin use and the incidence of Alzheimer disease. JAMA Neurol. *74*, 225–232.

STAR★METHODS

KEY RESOURCES TABLE

REAGENT or RESOURCE	SOURCE	IDENTIFIER
Antibodies		
anti-total Tau clone 7 (IF 1:100, WB 1:1000)	EMD Millipore	MAB2239 RRID:AB_1587549
anti-pS202/T205 Tau (IF 1:50, WB 1:500)	Peter Davies	CP13 RRID:AB_2314223
anti-pS396/S404 Tau (IF 1:50, WB 1:500)	Peter Davies	PHF1 RRID:AB_2315150
anti-pThr231 conformational (IF 1:50)	Peter Davies	TG3 RRID:AB_2716726
anti-MAP2 (IF 1:1000)	Abcam	ab5392 RRID:AB_2138153
anti-neurofilament 131/132 (IF 1:5000)	Covance	SMI31 RRID:AB_2314901
anti-Actin clone C4 (WB 1:50,000)	EMD Millipore	MAB1501 RRID:AB_2223041
anti-APLP2 (WB 1:1000)	Calbiochem/Millipore	171617 RRID:AB_565357
anti-APP A4 clone 22C11 (WB 1:1000)	EMD Millipore	MAB348 RRID:AB_94882
anti-APP C-Terminal (WB 1:500)	EMD Millipore	171610 RRID:AB_211444
anti-total Tau (WB 1:1000)	Sigma	T6402 RRID:AB_261728
anti-histone 3 clone (WB 1:1000)	Upstate/Millipore	06-755 RRID:AB_11211742
anti-LC3b (WB 1:1000)	Novus biologicals	NB600-1384 RRID:AB_669581
anti-ubiquitin (WB 1:250)	EMD Millipore	MAB1510 RRID:AB_2180556
anti-Phospho-4E-BP1 (Thr37/46) (WB 1:1000)	Cell Signaling	Antibody #9459 RRID:AB_330985
anti-p70 S6 Kinase Antibody (WB 1:1000)	Cell Signaling	Antibody #9202 RRID:AB_331676
anti-4E-BP1 Antibody (WB 1:1000)	Cell Signaling	Antibody #9452 RRID:AB_331692
anti-Phospho-p70 S6 Kinase (Thr389) (WB 1:1000)	Cell Signaling	108D2, Antibody RRID:AB_2269803
Anti-PSMC2 (D5T1T)) (WB 1:1000)	Cell Signaling	#14395 RRID:AB_2752224
anti-PSMB5 (WB 1:1000)	Enzo Lifesciences	Cat# BML-PW8895 RRID: AB_10540901
anti-GAPDH (WB 1:1000)	Life Technologies	AM4300 RRID: AB_2536381
anti-Nestin Clone 25/NESTIN (RUO) (1:500)	BD	611658 RRID:AB_399176
anti-S100b (1:500)	Proteintech	15146-1-AP RRID:AB_2254244
anti-Vamp2 (aka synaptobrevin 2) (1:1000)	synaptic systems	104 211 RRID:AB_887811
anti- Syntaxin 1 (1:5000)	Gift from the Thomas Sudhof lab	polyclonal #I379
anti-Synaptotagmin (1:2000	Gift from the Thomas Sudhof lab	polyclonal #W855
Tra-181-647	BD	560124 RRID:AB_1645449
CD184-APC (FC 1:10)	BD	555976 RRID:AB_398616
CD44-PE (FC 1:10)	BD	555479 RRID:AB_395871
CD24-PECy7 (FC 1:40)	BD	561646 RRID:AB_10892826
CD271-PE	BD	557196 RRID:AB_396599
Chemicals, Peptides, and Recombinant Proteins		
T0901317	Sigma	T2320
GW501516	Enzo life sciences	89150-762
Rosiglitazone	Sigma	R2408
Atorvastatin calcium salt	Sigma	PZ001
Simvastatin	Sigma	S6196
Rosuvastatin	Sigma	SML1264
Fluvastatin	Sigma	SML0038
Mevastatin	Tocris	1526
Lovastatin	Sigma	PHR1285
Mevalonolactone (Mevalonic Acid)	Sigma	M4777

(*Continued on next page*)

Continued

REAGENT or RESOURCE	SOURCE	IDENTIFIER
(R)-Mevalonic acid 5-pyrophosphoate tetralithium salt	Sigma	77631
Mevalonic acid 5-phosphate thrilithium salt hydrate	Sigma	79849
Methyl-β-cyclodextrin	Sigma	C4555
YM-53601	Cayman Chemicals	18113
AY 9944 dihydrochloride	Tocris	1639
FTI-227 trifluoroacetate salt	Sigma	F9803
GGTI-298 trifluoracetate salt hydrate	Sigma	G5169
Fatostatin hydrobromide	Sigma	F8932
24(S)-hydroxycholesterol	Cayman Chemicals	10009931
chloroquine diphosphate salt	Sigma	C6628
MG-132 (InSolution)	Calbiochem	37391
Cholestane	Sigma-Aldrich	C8003
N-Methyl-*N*-(trimethylsilyl)trifluoroacetamide (MSTFA)	ThermoFisher	TS48910
dry pyridine	Sigma-Aldrich	270970
sodium hydroxide solution 10M (BioUltra)	Sigma Aldrich	72068
Ri, Y-27632 dihydrochloride	Abcam	ab120129
SB431542	Stemgent	4-0010
Noggin	R&D	3344-NG
Proteasome activity probe 1	Berkers et al., 2007; de Jong et al., 2012	N/A
SCR7	Excess Bioscience	M60082-2
L-755,507	Sigma	SML1362
K-604	Sigma	SML1837
Critical Commercial Assays		
Phospho(Thr231)/Total Tau Kit	MSD	K15121D-3
V-PLEX Ab Peptide Panel 1 (6E10) Kit (25 Plate)	MSD	K15200E-4
24(S)-Hydroxycholesterol ELISA kit	Enzo	ADI-900-210-0001
CellTiter-Glo® Luminescent Cell Viability Assay	Promega	G7571
CellTiter 96® AQueous One Solution Cell Proliferation Assay	Promega	G3580
Pierce LDH Cytotoxicity Assay Kit	Thermo Fisher Scientific	88954
Amplex Red Cholesterol Assay Kit	ThermoFisher Scientific	A12216
Lipidyzer	Sciex	N/A
Experimental Models: Cell Lines		
CV (NPC)	Gore et al., 2011	RRID:CVCL_1N86
151 (CV WT) (iPSC, NPC)	Fong et al., 2018	RRID: CVCL_UI49
IB6 (APP^{null} in CV background) (iPSC, NPC)	Fong et al., 2018	RRID:CVCL_UI22
B10 (CV Wt) (iPSC, NPC)	This Paper	RRID:CVCL_VR50
B11 (CV Wt) (iPSC, NPC)	This Paper	RRID:CVCL_VR51
3d9 (CV APP E693A) (iPSC, NPC)	This Paper	RRID:CVCL_VR53
2b2 (CV APP E693A) (iPSC, NPC)	This Paper	RRID:CVCL_VR52
D12 (CV APP E693A+F691A) (iPSC, NPC)	This Paper	RRID:CVCL_VR54
APP^{dp}1.2 (iPSC, NPC)	Israel et al., 2012	RRID:CVCL_EJ97
APP^{dp} 1.6 (iPSC, NPC)	Israel et al., 2012	RRID:CVCL_EJ96
APP^{dp} 2.1 (iPSC, NPC)	Israel et al., 2012	RRID:CVCL_EJ99
APP 1KO (APP^{null} in APP^{dp}1.2 background) (iPSC, NPC)	This Paper	RRID: CVCL_UI23
NDC1 (M) NPC	Israel et al., 2012; Young et al. 2015	RRID:CVCL_EJ84
NDC2 (M) NPC	Israel et al., 2012; Young et al., 2015	RRID:CVCL_EJ87

(*Continued on next page*)

Continued

REAGENT or RESOURCE	SOURCE	IDENTIFIER
NDC3 (M) NPC	Young et al., 2015	RRID: CVCL_UB88
NDC4 (M) NPC	Young et al., 2015	RRID: CVCL_UB89
NDC5 (M) NPC	Young et al., 2015	RRID: CVCL_UB90
SAD1 (F) NPC	Israel et al., 2012; Young et al., 2015	RRID: CVCL_EJ90
SAD2 (M) NPC	Israel et al., 2012; Young et al., 2015	RRID: CVCL_EJ93
SAD3 (M) NPC	Young et. al. 2015	RRID: CVCL_UB91
SAD4 (F) NPC	Young et. al. 2015	RRID: CVCL_UB92
SAD5 (F) NPC	Young et. al. 2015	RRID: CVCL_UB93
SAD6 (M) NPC	Young et. al. 2015	RRID: CVCL_UB94
SAD7 (M) NPC	Young et. al. 2015	RRID: CVCL_UB95
Experimental Models: Organisms/Strains		
C57BL/6J Mice	Jackson Laboratory	000664
Oligonucleotides		
Repair Oligos used to make CRISPR mutant lines See Table S6	This Paper	N/A
Primers for amplification of APP Cholesterol Binding region See Table S6	This Paper	N/A
APP Cholesterol binding region genomic DNA Sequencing Primer See Table S6	This Paper	N/A
qPCR Primers See Table S6	This Paper	N/A
Recombinant DNA		
G7A: TOPO guide RNA plasmid for Generating cholesterol-mutant lines with target sequence: 5′GTGTTCTTTGCAGAAGATGTGGG3′	This Paper	N/A
Guide RNA plasmid for generating APP^{null} line in APP^{dp}-patient background with target sequence: 5′GGAGATCTCTGAAGTGAAGATGG3′	This Paper	N/A
CMV::Cas9-2A-eGFP	Sigma-Aldrich	CAS9GFPP-1EA
CYP46A1-pDESTlentiFGA1.0.	This Paper	N/A
GFP-only plasmid-pDESTlentiFGA1.0. (pSyn(pr)EGFPLL3.7)	This Paper	N/A

CONTACT FOR REAGENT AND RESOURCE SHARING

Further information and requests for resources and reagents should be directed to and will be fulfilled by the Lead Contact, Larry Goldstein (lgoldstein@ucsd.edu).

All cell line requests will require a material transfer agreement (MTA).

EXPERIMENTAL MODEL AND SUBJECT DETAILS

Cultured Mouse Cortical Neurons

Primary cortical neurons were cultured from postnatal day zero C57BL/6J pups. Briefly, pups were decapitated into Hanks' medium without Ca^{2+} and Mg^{2+}, and cortices were dissected in Neurobasal-A medium supplemented with 10 mm HEPES. After dissection, cortices were trypsinized for 25 min at 37°C and dissociated. Neurons were plated in Neurobasal-A with B27 supplement and drug-treatment was performed after 2 weeks.

Human iPSC Derived Cell lines

Cell lines

Novel NPC lines were generated from previously established iPSC lines. The APP^{dp} AD-patient NPC lines used in this study are; APP^{dp}1-6 (derived from iPSC-line APP^{dp}1.1 in Israel et al. [2012]), APP^{dp}1-2 (derived from iPSC-line APP^{dp}1.2 in Israel et al. [2012]) and APP^{dp}2-1 (derived from iPSC-line APP^{dp}2.3 in Israel et al. [2012]). See Israel et al. (2012) for generation and

characterization of these APP^{dp} iPSC lines and patient details. SAD and NDC NPC lines used are CV4a, SAD1, SAD2, SAD5, SAD5, SAD7, NDC1, NDC2, NDC4 and NDC5 described in Young et al. (2015);

To generate isogenic APP knockout iPSCs in an APP^{dp} patient 1 background, iPSC-line APP^{dp}1-2 was gene edited to generate the iPSC and NPC-line APP^{dp}1KO. To generate isogenic APP knockout lines in wild-type (Craig Venter, CV) background, iPSC-line CVB (Gore et al., 2011) was gene edited to generate IPSC and NPC-line IB6 (CV APP^{null}) and 151 (CV wt) (Fong et al., 2018). To generate isogenic Δcholesterol APP mutants the iPSC-line CVB (Gore et al., 2011) was gene edited to generate iPSC and NPC-lines B10 (wt), B11 (wt), 3D9 (homozygous E693A), 2B2b (homozygous E693A) and D12 (homozygous F691A+E693A).

iPSC genome editing

Generation of isogenic APP knockout lines in a wild-type (CV iPSC) background, IB6 (APP knockout) and 151 (wt) was described previously (Fong et al., 2018). For gene-editing, iPSCs were pretreated with 10uM Rock inhibitor (Ri, Y-27632 dihydrochloride, Abcam) 2 hours prior to nucleofection. iPSC's were dissociated with Accutase and filtered through 100uM filter and spun down at 1000rpm for 5 minutes. Two million cells were nucleofected according to manufacturer instructions using the Amaxa Human Stem Cell Nucleofector Kit 1 (Lonza).

To generate an isogenic APP^{null} line in an APP^{dp}-patient background, the iPSC-line APP^{dp}1.2 was nucleofected with 6 μg CMV::Cas9-2A-eGFP vector and 3 μg U6::gRNA vector. To target the CRISPR/Cas9 we used the gRNA target sequence: 5′-GGA GATCTCTGAAGTGAAGATGG-3′ (see Table S6 for all oligos used). Nucleofected iPSCs were replated into a 6 well of MEF feeder cells in the presence of Ri and allowed to recover for 72 hours, 1 × 10^4 GFP$^+$ iPSCs were FACS sorted (FACS Aria IIu, BD Biosciences) and (sparsely) plated on 10 cm MEF-feeder plates in the presence of Ri. After 7 days, individual colonies were manually picked and cultured in individual wells of a 96-well plate. Cells were split and DNA was isolated from individuals wells (quickextract kit, Epicenter), PCR amplified using the primers (APPex16-F: CCC GTA AGC CAA GCC AAC AT, APPex16-R: CAT GCA CGA ACT TTG CTG CC**)** and sequenced using the primer AGGCAGCAGAAGCCTT and aligned against the APP wild-type sequence. Amplified PCR-fragments from non-wild-type colonies were selected, cloned using the Zero Blunt TOPO PCR Cloning Kit (Invitrogen) and sequenced to analyze the (edited) genomic DNA sequence on both alleles. One confirmed APP^{null} line was expanded and differentiated to neural progenitor cells and characterized as detailed in Figure S3. To generate isogenic APPΔcholesterol lines in a CV background, the CV iPSC-line was nucleofected with 3.4 μg of a CMV::Cas9-2A-eGFP vector, 1.6 μg of a TOPO blunt II::gRNA vector, and 50nmol (4ng) repair single-stranded oligonucleotide. To target the CRISPR/Cas9 we used the gRNA target sequence: 5′-GTGTTCTTTGCAGAA GATGTGGG-3′. Repair oligo's to generate E693A and F691+E693A respectively were 5′-Tattgcatttagaaattaaaattcttttttcttaatt tgttttcaaggtgttctttgcagccgatgtgggttcaaacaaaggtgcaatcattggactcatggtgggcggtgttgtcatagc-3′ and E693A+F691A Repair Oligo Sequence: 5′-ttatattgcatttagaaattaaaattcttttttcttaatttgttttcaaggtgttcgctgcagccgatgtgggttcaaacaaaggtgcaatcattggactcatggtggg cggtgttgtcat-3′ respectively.

Nucleofected iPSCs were re-plated into a 6 well of MEF feeder cells in the presence of Ri and and 1 μM SCR7 (Excess Bioscience, M60082-2) and/or 5 μM L-755,507 (Sigma, SML1362).

Cells were then allowed to recover for 48 hours after which, live, GFP+ iPSCs were FACS sorted (FACS Aria IIu, BD Biosciences) and plated at 10,000 cells per 10 cm MEF-feeder plates in the presence of Ri. After 7-14 days, individual colonies were manually picked and cultured in individual wells of 96-well plates. 96 well plates were split and DNA was isolated from each well of one of the plates (quickextract kit, Epicenter). The region of interest was PCR amplified using Forward Primer: 5′-CTTCCTCGAACTGGG GAAGC-3′ and Reverse Primer: 5′-TCACGGTAAGTTGCAATGAATGA-3. Coincidentally, mutation of the wild-type sequence to the sequence corresponding to the E693A mutation generates a novel BbvI restriction motif, whereas introduction of the F691A mutation creates a PstI restriction enzyme motif. Therefore, initial screening was performed by performing a restriction digest on the PCR-amplified fragment by incubating the PCR amplicon with BbvI (for E693A) or PstI (F691A+E693A). These fragments were run on a DNA-gel and samples in which full restriction had occurred (homozygous for the desired mutation) were confirmed by sequencing of the amplicon using the primer: 5′-CCAACCAGTTGGGCAGAGAA-3′ Once confirmed, two individual IPSC lines containing the homozygous E693A mutation (3D9, 2B2), one line containing the homozygous F691A+E693A mutation (D12) and two unedited controls lines (B10, B11) that underwent the same clonal expansion process were expanded and differentiated to neural progenitor cells.

Additional Cell Line Information

The Craig Venter Cell line (CV) as well as all gene edited isogenic lines generated from this line are male. The CV line was previously reported and characterized in Gore et al. (2011). Cell lines generated in this background include the isogenic knockout lines IB6 (APP knockout) and 151 (wt), and the Δcholesterol mutant lines 3D9 and 2B2 (APP E693A), D12 (F691A+E693A), and B10 and B11 (WT controls). All APP^{dp}1 (patient 1) derived lines are male, all APP^{dp}2 (patient 2) derived lines are female (Israel et al., 2012).

The lines NDC1, NDC2, NDC3, NDC4, NDC5, SAD2, SAD3, SAD6, and SAD7 are male. The lines SAD1, SAD4, and SAD5 are female. The NDC and SAD lines were previously reported and characterized in Israel et al. (2012) and Young et al. (2015). Analyses of the influence of sex was not evaluated in this study. Rather the effect of drug-treatment on individual cell-lines before and after treatment was compared or between isogenic gene-edited lines.

Copy number determination

200 ng of DNA was hybridized to Illumina HumanCore arrays (Illumina), and stained per Illumina's standard protocol. Copy Number Variation (CNV) calling was carried out in Nexus CN (version 7.5) and manually inspected, visualizing the B-allele frequencies (proportion of A and B alleles at each genotype) and log R ratios (ratio of observed to expected intensities) for each sample, as described in D'Antonio et al. (2017).

Generation of neural progenitor cells

NPC's were generated from iPSCs as described previously (Yuan et al., 2011). In short, 2 × 10^5 FACS-purified iPSC TRA1-81$^+$ cells were seeded onto two 10 cm plates that were seeded the previous day with 5 × 10^5 PA6 cells and were cultured in PA6 differentiation media (450ml Glasgow DMEM, 50ml KO Serum Replacer, 5ml sodium pyruvate, 5ml Nonessential Amino Acids) + 10um SB431542+ 0.5ug/ml Noggin. After 6 days in culture, media was changed to PA6 differentiation media without SB431542 and Noggin. At day 11, cells were dissociated with Accutase and ~5 × 10^5 CD184$^+$CD24$^+$CD44$^-$CD271$^-$ NPCs were FACS-purified and plated onto poly-L-ornithine/laminin-coated plates and cultured with NPCbase + 20ng/ml bFGF (Millipore). Of note, while iPSC are grown in lipid containing media, the derived NPC after sorting (and for neuronal differentiation) are always grown in medium that does not contain an exogenous source of lipids.

Cell culture, generation of neurons and astrocytes

iPSCs were cultured on a MEF feeder layer in HUES medium (KO DMEM, knockout serum, plasmanate, pen-strep, non-essential amino acids, glutamax and β-mercaptoethanol) + 20ng/ml bFGF (Millipore) as described previously (Israel et al., 2012) on a MEF feeder layer and passaged with Accutase (Innovative Cell Technologies). NPCs were cultured on poly-L-ornithine (0.02 mg/ml) and laminin (5 ug/ml) (Sigma)-coated plates in DMEM:F12 + Glutamax, 0.5x N2, 0.5x B27, Pen/Strep (all Life Technologies), and 20 ng/ml FGF, and passaged with Accutase. For neuronal differentiation, NPCs were expanded to confluence, after which FGF was withdrawn from the culture medium and the medium was changed twice weekly. For all experiments, unless stated otherwise, neurons after 3 weeks of differentiation were replated into 96 wells (2 × 10^5 living cells/well) for 2 weeks in 200 ul NPC base + BDNF/GDNF/cAMP. After 2 weeks media was removed and fresh media (200 ul NPC base + BDNF/GDNF/cAMP) containing the tested compounds was added. At indicated time points, the conditioned culture media was harvested from cells and cells were lysed in 70 μL MSD lysis buffer (MSD) with protease (Calbiochem) and phosphatase inhibitors (Halt). For Figures 4E and 4F (cholesterol mutants) 3-week differentiated neurons were plated for 2 weeks and treated with DMSO and Atorvastatin respectively for 2 days. On day 3 a full media change was performed (containing DMSO or Atorvastatin) and 24 hours later the media was collected for Aβ measurements. For experiments in Figure 5C, MG132 was added fresh to the media every day. For astrocytic differentiation, a confluent 10 cm plate of NPCs was scraped in NPC medium, and transferred to 3 wells of a 6 well plate placed on a 90 RPM orbital shaker in the incubator to promote neurosphere formation. 24 hours later, 5 μM RI was supplemented to the medium for 48 hours. After 48 hours the neurospheres were grown in NPC medium (withouth FGF) that was replaced every 2 to 3 days. One week after scraping, media was changed to Astrocyte Growth Medium (AGM) containing 3% FBS, ascorbic acid, rhEGF, GA-1000, insulin, and L-glutamine (Lonza) and cell were cultured for an additional two weeks. After two weeks, the neurospheres were plated on a poly-L-ornithine/laminin-coated 10 cm plate. After seven days the astrocytes emerging from the neurospheres were passaged with Accutase, cultured in AGM, and maintained with the neurospheres.

Neuron FACS sort

For Aβ measurements in purified Δcholesterol mutant neurons (Figure 4D) and tau measurements in the APPdp and APP^{null} cells (Figure S3I), neurons were purified to compare steady state Aβ measurement within different lines. After three weeks of neuronal differentiation in NPCbase media without FGF; CD184$^-$, CD44$^-$, CD24$^+$ (antibodies from BD Bioscience) neurons were purified by FACS (BD Biosciences) and were plated onto poly-L-ornithine/laminin-coated coated plates. Sorted neurons were cultured in NPCbase media + 0.5mM dbCAMP, 20ng/mL BDNF, and 20ng/mL GDNF for 5-7 days before experiments.

METHOD DETAILS

Reagents

Compounds used are T0901317 (Sigma, T2320) GW501516 (Enzo life sciences, 89150-762), Rosiglitazone (Sigma, R2408), Atorvastatin calcium salt (Sigma, PZ001), Simvastatin (Sigma, S6196), Rosuvastatin (Sigma, SML1264), Fluvastatin (Sigma, SML0038), Mevastatin (Tocris, 1526) Lovastatin (Sigma, PHR1285), Mevalonolactone (Mevalonic Acid) (Sigma, M4777), (R)-Mevalonic acid 5-pyrophosphoate tetralithium salt (Sigma, 77631), Mevalonic acid 5-phosphate thrilithium salt hydrate (Sigma, 79849), Methyl-β-cyclodextrin (Sigma, C4555), YM-53601 (Cayman Chemicals, 18113), AY 9944 dihydrochloride (Tocris), FTI-227 trifluoroacetate salt (Sigma, F9803), GGTI-298 trifluoracetate salt hydrate (Sigma, G5169), Fatostatin hydrobromide (Sigma, F8932), 24(S)-hydroxycholesterol (Cayman Chemicals, 10009931), K-604 (Sigma-Aldrich, SML1837), chloroquine diphosphate salt (Sigma, C6628), MG-132 (InSolution, Calbiochem, 37391), Cholestane (Sigma-Aldrich C8003) *N*-Methyl-*N*-(trimethylsilyl)trifluoroacetamide (MSTFA, ThermoFisher TS48910), 1 μL of dry pyridine (Sigma-Aldrich, 270970) and sodium hydroxide solution 10M (BioUltra, Sigma Aldrich, 72068).

The compound collection for the screen consisted of 1684 FDA and EMA approved drugs, as well as drugs that had been tested in clinical trials. This collection was assembled from multiple commercially available libraries, including the Prestwick Chemical Library (Prestwick Chemical), Microsource US and International Drug Collections (Microsource Discovery Systems, Inc.), and NIH clinical collection libraries (http://www.nihclinicalcollection.com). An overview of all compounds in the screen can be found in Table S1.

Phenotypic high-throughput screen

After thawing, APP^{dp}1-6 NPC's (passage 13) were expanded to confluence on 10cm dishes and differentiated at passage 16 (p16) by withdrawal of bFGF. After 3 weeks, differentiated NPC's were washed with PBS and dissociated using Accutase:Accumax

(Innovative Cell Technologies) (1:1). Cells were resuspended in sort buffer (NPCbase Media+ 1% FBS (Mediatech 35-011-CV)+2.5mM EDTA) and filtered through a sterile cell strainer (100um, Fisher scientific, Cat no. 22363549) to remove clumps. Cells were spun down (5 min at 1000RPM) and resuspended in NPCbase + 20 ng/μl BDNF, 20 ng/μl GDNF (Peprotech) and 0.5 mM dbcAMP (Sigma).

Cells were plated in 384 well poly-L-ornithine/laminin-coated plates at 5 × 10^4 live cells/well in 50 μL and were allowed to further mature for 2 weeks. After 1 week, 25 μL media was aspirated and replaced with fresh media (NPC base + BDNF/GDNF/cAMP). 1 week later (in total 2 weeks on the 384 well plate) 15 μL of media was aspirated (leaving 35 μL in the well) and 35 μL media + 2x compound (NPC base + 2x BDNF/GDNF/cAMP and 10 μM of compound) was added to generate a final concentration of 5 μM compound/well or vehicle (DMSO, 16 wells per 384 well plate) in duplicate. After five days of treatment, media was aspirated and cells were lysed in 70 μL Mesoscale discovery lysis buffer (MSD R60TX-3) with protease (Calbiochem) and phosphatase inhibitors (Halt) and lysates were stored at −80 awaiting analysis. From the lysates viability was measured using CellTiter-Glo® Luminescent Cell Viability Assay (Promega) according to manufacturer instructions with a modified ratio of lysate to CeLLTiterGlo reagent (1:1) and pThr231/tTau levels were determined using Phospho(Thr231)/Total Tau kit (K15121D, Meso Scale Discovery). For each 384 well plate, Z-scores were determined for each data point, as the number of standard deviations from the mean of the control, vehicle-treated (DMSO) wells. Compounds that decreased pThr231Tau/tTau by $Z < -2$ in one of the duplicates were selected for confirmational screening (repeat of the methods described for the primary screen). Compounds that decreased pThr231Tau/tTau in an additional replicate ($Z < -2$) in the secondary screen were defined as hits.

Aβ, pThr231Tau/total Tau, pSer9GSK3b/total Gsk3b, Phospho-4E-BP1(Thr37/46)/total 4E-BP1 ELISA Measurements

For Aβ measurements, 25 μL of the culture media was run on a V-PLEX Aβ Peptide Panel 1 (6E10) (K150SKE) kit, for pThr231Tau/tTau lysate was run on a Phospho (Thr231)/Total Tau Kit (K15121D), for pSer9GSK3β/total Gsk3β lysate was run on pSer9GSK3β /total Gsk3β Kit (K15109D). For Phospho-4E-BP1(Thr37/46)/total 4E-BP1 lysates were run separately on a Phospho-4E-BP1(Thr37/46) kit (K150KHD) and a total 4E-BP1 kit (K151OLD) and ratio was determined by combining these two measures from the same lysates. All kits from Mesoscale discovery. Measurements were performed on Mesoscale discovery sector imager 600. For Figure 4D (cholesterol mutants) purified neurons were replated after FACS and media was collected after 5 days.

Cell viability

From the lysates viability was measured using CellTiter-Glo® Luminescent Cell Viability Assay (Promega) according to manufacturer instructions with a modified ratio of lysate to CeLLTiterGlo reagent (1:1). CellTiter 96® AQueous One Solution Cell Proliferation Assay (Promega) and Pierce LDH Cytotoxicity Assay Kit (Thermo Fisher Scientific) were performed in 96-well plates in accordance with manufacturer instructions.

Mass spectrometry sample preparation and LC-MS-MS

The frozen cell pellet was resuspended in an equal volume of water and then vortexed to thaw the sample. We added 100 ul of cell suspension to 500μl of 6 Molar Guanidine solution followed by vortexing. The sample was then boiled for 5 minutes followed by 5 minutes cooling at room temperature, this step was repeated 3 times. The proteins were precipitated with addition of methanol followed by vortex and centrifugation at 14000 rpm for 10 minutes. The soluble fraction was removed. The pellet was resuspended in 600ul of 8 M Urea made in 100mM Tris pH 8.0 and by vortexing for 5-10 minutes. TCEP was added to final concentration of 10 mM. The sample was then frozen overnight at −20C. Next day the solution was thawed and vortexed for another 5 minutes until the solution became clear. Chloro-acetamide solution was added to final concentration of 40 mM and vortexed for 5 minutes. Equal volume of 50mM Tris pH 8.0 was added to the sample to reduce the urea concentration to 4 M. Lys C was added in 1:500 ratio of LysC to protein content and incubated at 37C in a rotating incubator for 4-6 hours. Equal volume of 50mM Tris pH 8.0 was added to the sample to reduce the urea concentration to 2 M. Trypsin was added in 1:50 ratio of trypsin to protein content. Next day the solution was acidified using TFA (0.5% TFA final concentration) and vortexed for 5 minutes. The sample was centrifuged at 15, 700 g for 5 min to obtain aqueous and organic phases. The lower aqueous phase was collected and desalted using 100 mg C18-StageTips as described by the manufacturer protocol. The peptide concentration of sample was measured using BCA after resuspension in sample loading buffer and the total of 2 ug is injected for each label free quantification run. Trypsin-digested peptides were analyzed by ultra high pressure liquid chromatography (UPLC) coupled with tandem mass spectroscopy (LC-MS/MS) using nano-spray ionization. The nanospray ionization experiments were performed using a Orbitrap fusion Lumos hybrid mass spectrometer (Thermo) interfaced with nano-scale reversed-phase UPLC (Thermo Dionex UltiMate 3000 RSLC nano System) using a 25 cm, 75-micron ID glass capillary packed with 1.7-μm C18 (130) BEH™ beads (Waters corporation). Peptides were eluted from the C18 column into the mass spectrometer using a linear gradient (5%–80%) of ACN (Acetonitrile) at a flow rate of 375 μl/min for 1h. The buffers used to create the ACN gradient were: Buffer A (98% H_2O, 2% ACN, 0.1% formic acid) and Buffer B (100% ACN, 0.1% formic acid). Mass spectrometer parameters are as follows; an MS1 survey scan using the orbitrap detector (mass range (m/z): 400-1500 (using quadrupole isolation), 120000 resolution setting, spray voltage of 2200 V, Ion transfer tube temperature of 275 C, AGC target of 400000, and maximum injection time of 50 ms) was followed by data dependent scans (top speed for most intense ions, with charge state set to only include +2-5 ions, and 5 s exclusion time, while selecting ions with minimal intensities of 50000 at in which the collision event was carried out in the high energy collision cell (HCD Collision Energy of 30%), and the fragment masses where analyzed in the ion trap mass analyzer (With ion trap scan rate of turbo, first mass m/z was 100, AGC Target 5000 and maximum

injection time of 35ms). Protein identification and label free quantification was carried out using Peaks Studio 8.5 (Bioinformatics solutions Inc.)

Lipid measurements

For the analysis of cholesterol and its precursors by means of gas chromatography mass spectrometry (GC-MS), treated neurons were pelleted by centrifugation and resuspended in 50 μL water. 600 μL MTBE and 160 μL methanol was added and samples were vortexed and shaken at room temperature for 30 minutes. For phase separation 200 μL water was added. Samples were spun at 16.100 g for 5 minutes and the organic (soluble) extract (350 μL) was separated from the pelleted protein. Extraction was repeated by the addition of 100 μL methanol, 100 μL water and 300 μL MTBE. After centrifugation the organic extracts were combined (650 μL) and split into two fresh glass vials (one for the total cholesterol fraction (200μL) and one for free cholesterol fraction (450μL)). Samples were dried under a gentle stream of nitrogen. For free cholesterol analysis, 10 μL of an internal standard solution (IS) containing 10 μg/mL cholestane in MTBE, 50 μL of *N*-Methyl-*N*-(trimethylsilyl)trifluoroacetamide (MSTFA), 1 μL of dry pyridine and 39 μL of MTBE were added to the dried extract. The samples were kept at room temperature for 30 minutes in order to complete derivatization before injection. For total cholesterol analysis, 10 μL IS solution, 400 μL LC-MS grade water and 100 μL 10M NaOH were added and samples were heated to 60°C for one hour. After samples had cooled to room temperature sterols were extracted twice using 750 μL MTBE. The combined organic extracts were dried under a gentle stream of nitrogen and dissolved in 50 μL of MSTFA, 1 μL of dry pyridine and 49 μL of MTBE. Samples were kept at room temperature for 30 minutes before injection. GC-MS analysis was carried out on a ScionTQ GC-MS system (Bruker Daltonics). Helium (99.9990%) was used as carrier gas on an Agilent VF-5ms column (5% phenyl-methyl; 25 m × 0.25 mm internal diameter; 0.25 μm film thickness). The injector was kept at 280°C and 1 μL was injected split-less. The oven program started at 50°C, held for 1 minute, followed by a ramp of 50°C/min to 260°C, continued to ramp with 4°C/min to 310°C, held for 0.3 minutes. Sterols were identified based on their relative retention time and comparison of electron ionization mass spectra (Giera et al., 2007; Müller et al., 2017). For quantification of free and total cholesterol an external calibration line from 0-500 μg/mL cholesterol was constructed. Total ion current chromatograms were integrated and quantified by the use of the external calibration lines. Pelleted protein was resuspended in 2% SDS and quantified according to the manufacturers instructions using the Pierce BCA Protein Assay Kit (cat. no. 23225).

Quantitative cholesterol ester and phospholipid analysis was carried out using a commercial platform (The Lipidyzer, Sciex, Redwood, CA, USA). In brief, treated neurons were pelleted by centrifugation and resuspended in 100 μL water and 100 μL internal standard mixture in methyl-tert.-butyl ether (MTBE). An additional 500 μL MTBE and 160 μL methanol was added and samples were vortexed and shaken at room temperature for 30 minutes. For phase separation 200 μL LC-MS grade water was added and samples were spun for 3 minutes at 16.100 × g. The upper organic layer was transferred to a glass vial. The extraction was repeated after the addition of 300 μL MTBE, 100 μL methanol and 100 μL water. The combined organic extracts were dried under a gentle stream of nitrogen and 250 μL running buffer was added. The analysis was carried out using the commercial flow-injection based quantitative lipidomics platform (The Lipidyzer). For analysis of relative cholesterol ester levels the cumulative concentrations of all cholesterol esters detected was normalized over the cumulative concentration of all sphingomyelins detected.

Microscopy

After differentiation, neurons were directly fixed or replated on 96-well imaging plates at a density of 2×10^5 living cells per well. Cells were imaged either 1 week (APPΔcholesterol mutants, supplemental 4b) or 2 weeks + 5 days drug treatment (APP^{dp}1-6 lines, Figure 1C) after replating. Cells were fixed with 4% PFA + 4% sucrose for 15 minutes at room temperature, washed 3 times with PBS, permeabilized with 0.1% Triton X-100, blocked with 0.5% BSA/PBS for 30 minutes and incubated with primary antibodies in 0.5% BSA/PBS for 1 hour at room temperature. Cells were subsequently washed 3 times with PBS, incubated with secondary antibodies in 0.5% BSA/PBS for 45 minutes and washed 3 more times with PBS (with the first wash containing 1:1000 DAPI). After 3 washes 100 μL PBS was added to each well and samples were imaged. The antibodies used for immunofluorescence experiments were anti-total Tau clone 7 (MAB2239, 1:100, EMD Millipore), anti-pS202/T205 Tau (CP13, 1:50 Peter Davies), anti-pS396/S404 Tau (PFH1, 1:50 Peter Davies), anti-pThr231 conformational (TG3, 1:50 Peter Davies), anti-MAP2 ab5392 (1:1000, Abcam) and anti-neurofilament 131/132 (SMI31) (1:5000, Covance). Anti-Nestin (BD biosciences, Clone 25/NESTIN (RUO), 611658)

S100b (Proteintech, 15146-1-AP) Secondary antibodies were Alexa Fluor anti-mouse, anti-rabbit and anti-chick (Invitrogen) and used at 1:200. Images for Figures 1E, 6A, S1F, and S4A were acquired on a Leica TCS SPE confocal microscope, images for Figures S1A, S1B, and S5A were acquired on a Nikon A1 confocal microscope.

RNA expression analysis

For mRNA expression analysis, RNA was isolated using the RNeasy Mini Kit (QIAGEN) and DNase-treated using TURBO DNase (Ambion) for one hour at 37°C. cDNA was generated from RNA primed with oligo(dT) using the SuperScript First-Strand Synthesis System (Invitrogen). We performed RT-qPCR using FastStart SYBR Green (Roche) using an Applied Biosystems 7300 RT-PCR system. Data was analyzed using the delta-Ct method and target genes were normalized to the geometric mean of a housekeeping gene (RPL27). The following primers were used: *HMGCR-F*: CGT GGA ATG GCA ATT TTA GGT CC, *HMGCR-R*: ATT TCA AGC TGA CGT ACC CCT, *LDLR-F*: GTC TTG GCA CTG GAA CTC GT, *LDLR-R*: CTG GAA ATT GCG CTG GAC, PSMB5 FW: GCTACCGGT

GAACCAGCG, PSMB5 RV: CAACTATGACTCCATGGCGGA, PSMC2 FW: TGAGAGTGGGCGTGGATAGA, PSMC2 RV: GTACCGGGTGGACCAAAGAG, *RPL27-F*: AAA CCG CAG TTT CTG GAA GA, *RPL27-R*: TGG ATA TCC CCT TGG ACA AA.

Quantitative western blot

NPCs were differentiated in 6 wells for 3 weeks and treated for 5 days with compound after which cells were lysed in RIPA Lysis Buffer (Millipore) with protease (Calbiochem) and phosphatase inhibitors (Halt). Protein concentrations were determined (Pierce BCA Protein Assay Kit, Thermo Fisher) and normalized. 4x LDS Sample buffer (novex) + β-mercaptoethanol was added to the lysate to generate a final concentration of 1x sample buffer + 5% β-mercaptoethanol. Samples were boiled (100°C) for 5 minutes. Equal amounts of lysates were run on NuPAGE 4%–12% Bis-Tris gels (Invitrogen), transferred to nitrocellulose or PVDF membranes, and blocked for one hour at room temperature using Odyssey Blocking Buffer (LI-COR). Blots were probed overnight at 4°C using the corresponding primary antibodies followed by IRDye secondary antibodies (LI-COR) at 1:5,000 and images were acquired by LICOR Odyssey imager. Bands were quantified using ImageJ software. Western blot images within one panel showing a composition of bands of interest for a particular immunogen are always from the same image (identical blot and exposure), but cropped and grouped together for clarity. Stiches are indicated by vertical lines. Antibodies used were: anti-Actin (1:50,000; EMD Millipore), anti-APLP2 (1:1,000; Calbiochem), anti-APP A4 clone 22C11 (1:1,000; EMD Millipore), anti-APP C-Terminal (1:500; EMD Millipore), anti-pS202/T205 Tau (CP13, 1:500 Peter Davies), anti-pS396/S404 Tau (PHF1, 1:500 Peter Davies), anti-total Tau T6402 (1:1000, Sigma), anti-total Tau clone 7 (MAB2239, 1:1000, EMD Millipore), anti-histone 3 clone 06-755 (1:1000, Upstate), anti-LC3b (NB600-1384, 1:1000, Novus biologicals), anti-ubiquitin (MAB1510, 1:250, EMD Millipore), Phospho-4E-BP1 (Thr37/46) (Antibody #9459, 1:1000 Cell Signaling), p70 S6 Kinase Antibody (Antibody #9202, 1:1000 Cell Signaling), 4E-BP1 Antibody (Antibody #9452, 1:1000 Cell Signaling) and Phospho-p70 S6 Kinase (Thr389) (108D2, Antibody #9452, 1:1000 Cell Signaling). Vamp2 (aka synaptobrevin 2) (synaptic systems 104 211) Syntaxin 1 (polyclonal #I379, gift from the Thomas Sudhof lab to the CNCR FGA department), Synaptotagmin (polyclonal #W855, gift from the Thomas Sudhof lab to the CNCR FGA department), Munc18/STXBP1 (BD biosciences, Clone 31/Munc-18 (RUO), 610337)

Proteasomal levels and activity

After treatment of neurons with the indicated drugs for three days, neurons were incubated with Proteasome activity probe 1 (Berkers et al., 2007; de Jong et al., 2012) for two hours (250 nM in media). After labeling, cells were harvested and resuspended in HR buffer (50 mM Tris, 5 mM MgCl2, 250 mM sucrose, 1 mM DTT and 2 mM ATP, pH = 7.4). Cell lysis was achieved by sonication (Bioruptor Pico, Diagenode, high intensity for 5 minutes with an ON/OFF cycle of 30 s) at 4°C. After a centrifugation step (21.100 g for 15 minutes) to remove cell debris, protein concentration of the supernatant was determined by a NanoDrop spectrophotometer (Thermo Fisher Scientific) by measuring the absorbance at 280 nm. Equal amounts of protein were denatured by boiling in LDS (lithium dodecyl sulfate) sample buffer (Invitrogen Life Technologies, Carlsbad, CA, USA) containing 2.5% β-mercaptoethanol. Polypeptides were resolved by 12% SDS-PAGE using the NuPAGE system and MOPS running buffer (Invitrogen Life Technologies, Carlsbad, CA, USA). Wet gel slabs were imaged with a resolution of 50 μm, using the Typhoon FLA9800 imaging system (GE), with appropriate filter settings (λ(ex/em) = 480/530 nm). For Western Blot analysis, proteins were transferred onto PVDF membrane using the Trans-Blot Turbo Transfer System (Bio-Rad). Membranes were blocked with 5% BSA solution and subsequently incubated with primary antibody overnight at 4°C. After washing with PBS-Tween 20 (0.2%) membranes were incubated with secondary antibody and signals visualized by using an Amersham Imager 600 RGB (GE) imager or Odyssey Fc (Li-Cor). Western blot images within one panel showing a composition of bands of interest for a particular immunogen are always from the same image (identical blot and exposure), but cropped and grouped together for clarity. Stiches are indicated by vertical lines. Immunoblotting with an antibody against GADPH or actin was used to verify equal protein loading. Antibodies used were: anti-Actin (1:50,000; EMD Millipore), anti-PSMD7 (1:1000 PSMC2 (D5T1T) Rabbit mAb #14395), anti-PSMB5 (1:1,000; Enzo Lifesciences, AB_105409012), anti-GAPDH (1:1000; Life Technologies, AB_2536381). Secondary antibodies used (1:5000) were HRP-conjugated polyclonal swine anti-rabbit (DAKO Cat# P0217) and HRP-conjugated polyclonal rabbit anti-mouse (DAKO Cat# P0161).

Vectors and viral transduction

pCMV10-CYP46A1-flag vector was a kind gift from Dr. Rodrigues Elsa, University of Lisbon. CYP46A1-Flag was amplified by primers gtacaaaaaagcaggcttaaatggactacaaagaccatgacgg and GTACAAGAAAGCTGGGTAGCggatccTCAGCAGGGGGGTGGT and subcloned into the gateway entry vector pENTRrz1 and subsequently recombined into the destination vector pDESTlentiFGA1.0. Viral particles containing the CYP46A1 plasmid, or an GFP-only plasmid (pSyn(pr)EGFPLL3.7) were produced as described previously (Naldini et al., 1996). In short HEK293T cells were transfected with viral packing plasmids ENV plasmid p.MDG2:PACK plasmid pCMVΔR8.2 together with the transgene vector carrying GFP or CYP46A1. After 24 hours the medium is replaced, and after 48 hours the medium is harvested and concentrated using amicon filters with 100kDA cutoff (UFC910024, Millipore). The concentrated virus is then filtered through a 0.2 micron filter, aliquoted and frozen at −80 degrees. For use, virus is thawed directly prior to vial transduction. For experiments, three week differentiated NPC's (APPdp1-6) were replated on 96-well plates (2×10^5 living cells/well) and left to mature for another two weeks, after which they were infected with virus for 24 hours. After 24 hours, and again after 6 days media was replaced with fresh 200 μl NPC base + BDNF/GDNF/cAMP. 13 days after viral transduction the media was collected for 24-hydroxycholesterol measurements and cells were lysed for pThr231Tau/tTau analysis.

QUANTIFICATION AND STATISTICAL ANALYSIS

Statistical Analysis

The correlation coefficient (CC) for Figure 3E was calculated in excel using the formula

$$Correl(X,Y) = \frac{\sum (x-\bar{x})(y-\bar{y})}{\sqrt{\sum (x-\bar{x})^2 \sum (y-\bar{y})^2}}$$

All other data was analyzed using GraphPad Prism Software (GraphPad Software). Statistical analysis comparing multiple groups was performed using a one-way Anova with a Tukey's multiple comparison test. Statistical analysis comparing two groups (treated versus untreated groups within the same genotype were calculated using multiple t tests. Data are depicted with bar graphs of the mean ± SEM of all values. Significance was defined as $p < 0.05$(*** $p < 0.001$, ** $p < 0.01$, *$p < 0.05$). n indicates independent measures from independent wells.

Cell Stem Cell, Volume *24*

Supplemental Information

Cholesterol Metabolism Is a Druggable Axis that Independently Regulates Tau and Amyloid-β in iPSC-Derived Alzheimer's Disease Neurons

Rik van der Kant, Vanessa F. Langness, Cheryl M. Herrera, Daniel A. Williams, Lauren K. Fong, Yves Leestemaker, Evelyne Steenvoorden, Kevin D. Rynearson, Jos F. Brouwers, J. Bernd Helms, Huib Ovaa, Martin Giera, Steven L. Wagner, Anne G. Bang, and Lawrence S.B. Goldstein

Supplemental Figure 1. Characterization of neuronal cultures and statin effects on pTau and viability, Related to Figure 1.

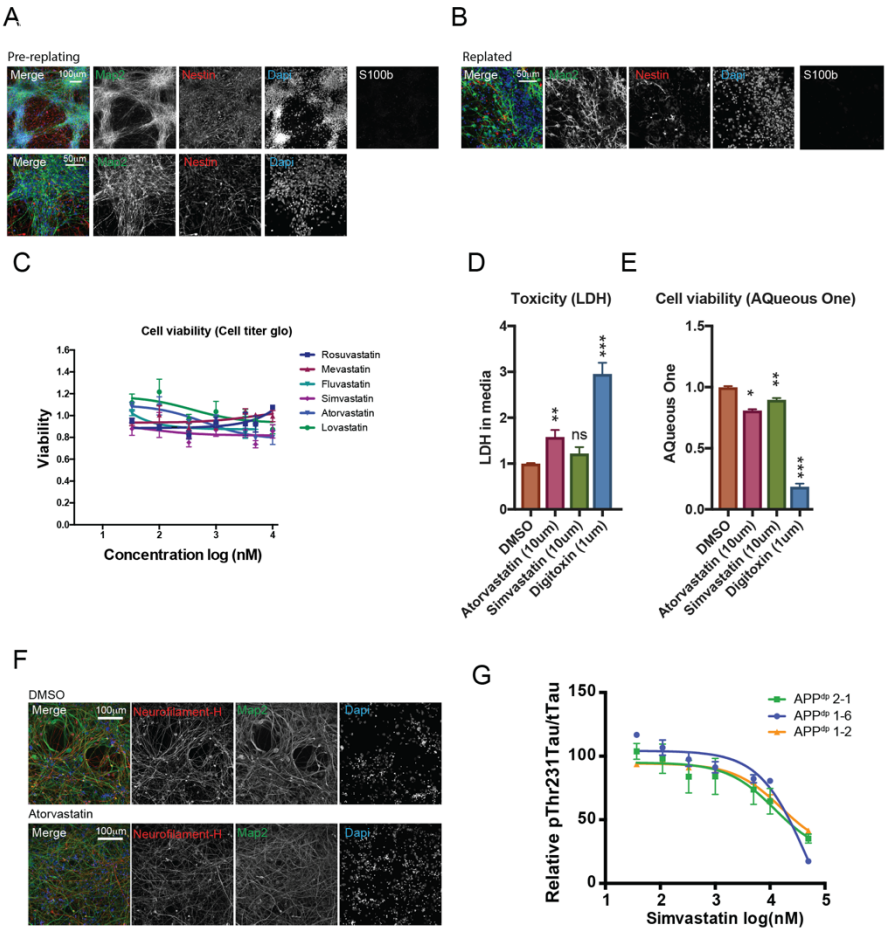

(**A-B**) Three week differentiated neuronal cultures (**A**) and differentiated neurons at point of screening (three weeks of differentiation, replating and two additional weeks of maturation) Scale bar represents 100µm. (**B**). Cultures were fixed and stained with antibodies for mature neurons (MAP2), neuronal progenitor cells (Nestin) and astrocytes (S100b). In keeping with previous observations at these time points the majority of cells are MAP2 neurons with a smaller group of nestin-positive neuronal precursor cells and absence/very low abundance of

astrocytic cells (Yuan et al., 2011). Scale bar represents 100μm. (**C**) Dosage effects of statins (five day treatment) on neuronal viability as measured by CeLLTiter-Glo luminescent cell viability assay. (**D-E**) Effects of a single dose of statins and a known toxic agent (Digitoxin) (five day treatment) on toxicity (**D**) determined by lactate dehydrogenase (LDH) released into the media (mean±SEM, n≥3) and (**E**) cell viability (mean±SEM, n≤3) determined by AQueous one cell viability assay (mean±SEM, n≥3). **(F)** Neuronal cultures (differentiated for three weeks, replated, matured for two more weeks) were treated with atorvastatin or DMSO for five days and stained for MAP2 and Neurofilament-H. Scale bar represents 100μm. **(G)** Dosage effects of simvastatin on pThr231Tau/tTau ratio in an additional FAD line from patient 1 (APP^{dp}1-2) and in an independent FAD APP^{dp} patient line (APP^{dp}2-1) (mean±SEM, n≥3). Dosage effects are compared to the effect of simvastatin on APP^{dp}1-6 from figure 1d. *** $p<0.001$, ** $p<0.01$, * $p<0.05$.

Supplemental Figure 2. Effect of cholesterol-metabolism targeting compounds on neuronal viability and cholesterol metabolism, Related to Figure 2.

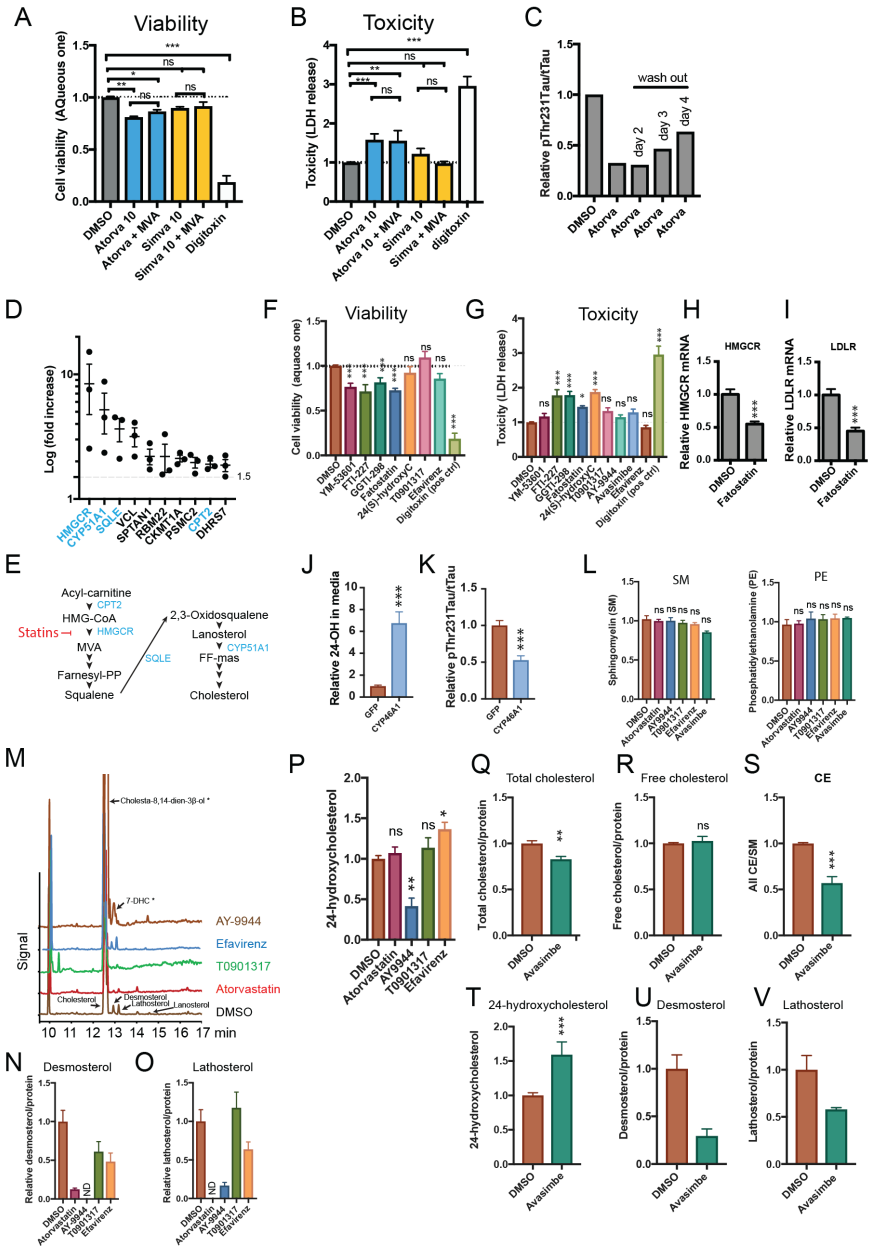

Effects of indicated compounds at same concentrations as in Figure 2 and a known toxic agent (Digitoxin) (five day treatment) on cell viability determined by (**A**) AQueous one cell viability assay (mean±SEM, n≥3). (**B**) lactate dehydrogenase (LDH) released into the media (mean±SEM, n≥3). (**C**) Effect of atorvastatin and atorvastatin washout on pThr231Tau/tTau ratio in APP^{dp}1-6. Neurons were treated for 5 days with DMSO or Atorvastatin and directly harvested, or after 5 days atorvastatin was washed-out and cells were harvested 2-4 days after wash out. (**D**) Purified neurons (NDC line B11 and B10) were treated for three days with atorvastatin or DMSO and harvested for quantitative mass spectrometry. In total three runs from three independent experiments were performed (two different experiments with B11 and one experiment with B10). All proteins that were increased >1.5 fold in all three runs were selected as hits and plotted by their effect on fold change (mean±sem). For complete dataset see Table S4. Proteins with a role in cholesterol synthesis are indicated in blue. HMGCR, 3-Hydroxy-3-Methylglutaryl-CoA Reductase; CYP51A1, Cytochrome P450 Family 51 Subfamily A Member 1 aka Lanosterol 14α-demethylase; SQLE, Squalene Epoxidase; VCL, Vinculin; SPTAN1, spectrin alpha, non-erythrocytic 1; RBM22, RNA Binding Motif Protein 22; CKMT1A, Creatine Kinase, Mitochondrial 1A; PSMC2, 26S proteasome regulatory subunit 7; CPT2, carnitine palmitoyltransferase 2; DHRS7, Dehydrogenase/Reductase 7. **(E)** Schematic depicting the identified hits in (D) with a role in cholesterol synthesis. **(F)** Cell viability (AQueous one) and **(G)** compound toxicity (LDH release) of conditions in Figure 2c. Digitoxin was used as a positive control for cell death (mean±SEM, n≥3). **(H-I)** APP^{dp}1-6 Neurons were treated for 5 days with 20μM fatostatin and mRNA levels of SREBP-target genes (3-hydroxy-3-methylglutaryl-coenzyme A reductase, HMGCR **(H)** and Low-Density Lipoprotein Receptor, LDLR **(I)**) were determined by quantitative real-time polymerase chain reaction (RT-qPCR) and normalized over housekeeping genes (RPLP27) (mean±SEM, n≥12). (**J-K**) Differentiated neurons were transduced with lentivirus carrying CYP46A1 or GFP expression vectors. After

13 days 24-hydroxycholesterol in media (**J**) and neuronal pThr231Tau/tTau ratio was determined (**K**). (**L**) APP^{dp}1-6 neurons were treated with Atorvastatin (10 μM), AY-9944 (10 μM), T0901317 (10μM), Efavirenz (10μM) and Avasimibe (10μM) and lipid analysis was performed to measure the proportion of sphingomyelin (SM) and Phosphatidylethanolamine (PE) (mean±SEM, n≥3). (**M-O**) APP^{dp}1-6 neurons were treated with Atorvastatin (10 μM), AY-9944 (5 μM), T0901317 (10μM) and Efavirenz (10μM) for three days and lipid analysis was performed to measure cholesterol precursors. **(M)** Typical traces from lipid GM-MS showing detected cholesterol precursors in neuronal cultures treated with indicated inhibitors (zoomed-in to show precursor peaks). **(N-O**) Overall precursor levels were low abundant and could be quantified only for desmosterol (**N**) and lathosterol (**O**) (mean±SEM). Efavirenz had previously been shown to increase precursor levels, but in our cultures did not increase (rather modestly decrease) precursor levels. *In the AY-9944 treated neurons 7DHC and Cholesta-8,14-dien-3β-o accumulated as previously reported (Giera et al., 2007). N≥4 for all treatments, expect for desmosterol levels in atorvastatin treated samples, which were below detection in two out of four samples. ND=not detected. (**P**) 24-hydroxycholesterol (five day treatment) levels in media from APP^{dp}1-6 neuronal cultures treated with indicated compounds (mean±SEM, n≥3). (**Q-V**) APP^{dp}1-6 neurons were treated with avasimibe (5μM) and lipid analysis was performed to measure (**Q**) total cholesterol (mean±sem, N≥8), three day treatment, (**R**) free cholesterol (mean±SEM, n≥4), three day treatment (**S**) CE (mean±SEM, n≥8) three day treatment (**T**) 24-hydroxycholesterol in media (mean±SEM, n≥4) (five day treatment) and (**U**) desmosterol and (**V**) lathosterol both (mean±SEM, n≥3) three day treatment. *** $p<0.001$, **$p<0.01$, *$p<0.05$.

Supplemental Figure 3. The effect of CE-reducing drugs on pTau in neurons with different genetic backgrounds, Related to Figure 3.

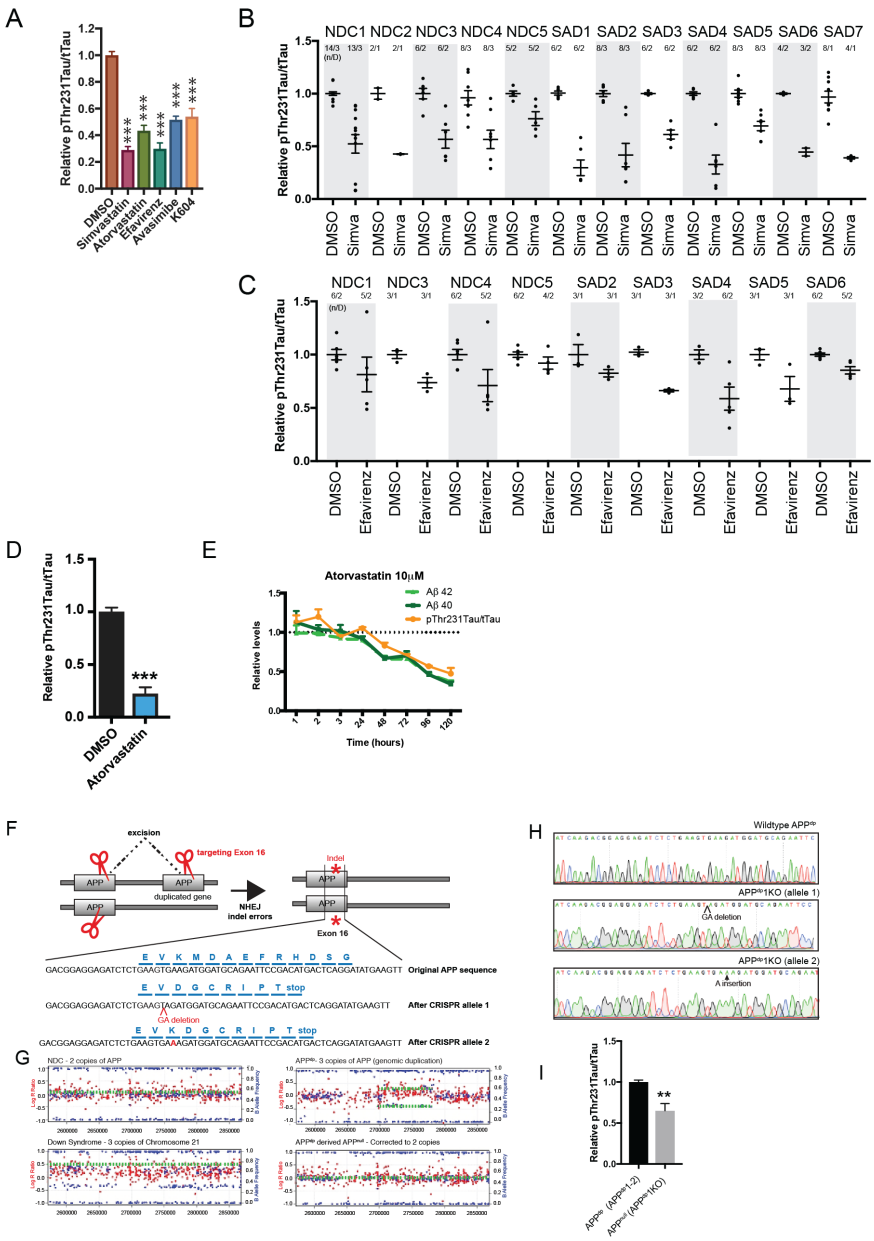

(A) NDC CV4a neurons were treated with indicated compounds; Simvastatin (10 μM), Atorvastatin (10 μM), Efavirenz (25μM), Avasimibe (10μM) and K604 (50μM) pThr231Tau/tTau levels were determined by ELISA (mean±SEM, n≥3). **(B)** Effect of simvastatin (10μm) (**B**) or Efavirenz (10μm) (**C**) treatment on pThr231Tau/tTau in neuronal lines from indicated NDC and SAD subject iPSC-derived neurons (mean±SEM). Same as in main figure 3b-c but here plotted for individual lines. Indicated (n/D) are number of measurements (n) and number of independent differentiations (D). **(D**) Effect of atorvastatin (10μm) treatment on *in vitro* cultured mouse cortical neurons (mean±SEM, n≥3)**. (E**) APP^{dp} 1-6 neurons were treated for indicated time points with atorvastatin. Cell lysates and media were analyzed by ELISA for pThr231Tau/ tTau and Aβ levels. (**F**) Schematic overview of the gene-editing strategy to generate an isogenic APP^{null} line in APP^{dp}-genetic background. The original patient has a duplication of APP (three copies of the gene for APP). Cutting by CRISPR/Cas9 at indicated sites (red scissors) causes the excision of the duplication site between cut-sites and correction of copy number. Non-homologues end-joining (NHEJ) insertion/deletion errors (indel) generated during the repair introduce respective premature stop-codons in the two remaining alleles as indicated. (**G**) Copy number analysis (digital karyotyping) of the region with APP duplication for a non-demented control genome, Down syndrome genome (duplication of the entire chromosome 21) and APP^{dp} line before (3 copies of APP) and after ("corrected to 2 copies of APP") gene editing showing copy number correction. **(H)** Sequencing results from TOPO-cloning of the individual alleles verifying a "GA" deletion on one allele and an "A" insertion in the other allele, compared to wildtype sequence (APPdp) (upper box) generating a premature stop. (**I**) pThr231Tau/tTau ratio in isogenic purified APP^{dp} (APP^{dp}1-2) and APP^{null} (APPdp1KO) neurons (five days after sort) (mean±SEM, n≥3). *** $p<0.001$, **$p<0.01$, *$p<0.05$.

Supplemental Figure 4. Characterization of APP-Δcholesterol neurons, Related to Figure 4.

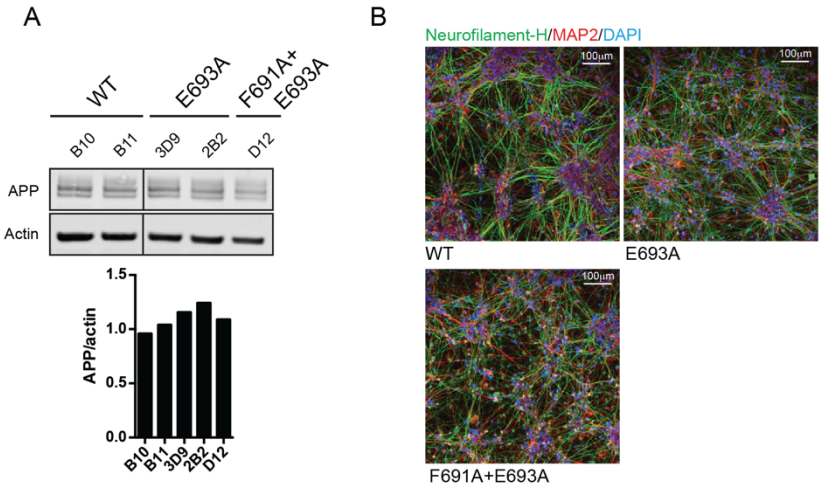

(**A**) Analysis of APP-protein level in control and mutant lines, showing normal expression of full-length APP. Image is a composite of different loading positions on same blot, stich is indicated by vertical line. (**B**) Immunofluorescence staining of wild type and indicated APP-Δcholesterol neurons showing neuronal morphology and polarization. Scale bar represents 100μm.

Supplemental Figure 5. Characterization of drug-treatment effects on neuronal cultures and pTau-mediated turnover by the proteasome, Related to Figure 5.

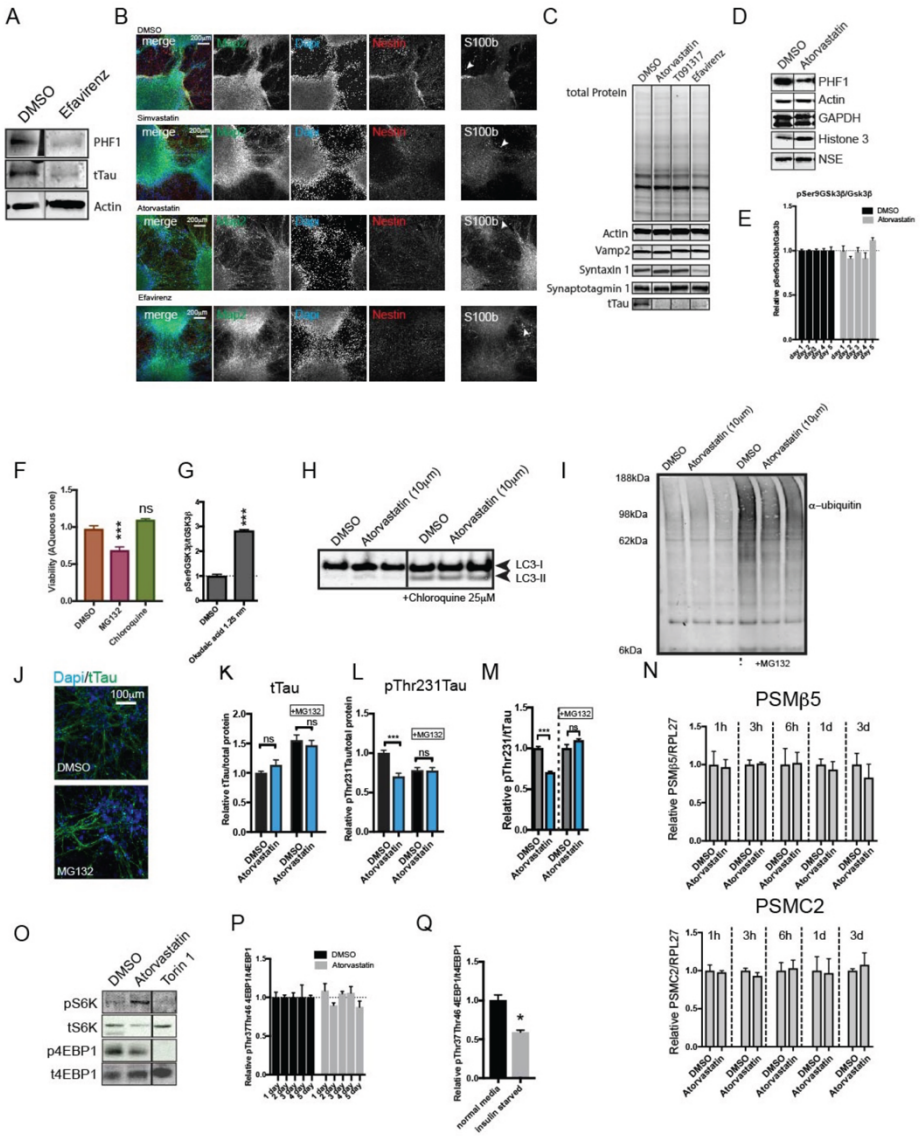

(**A**) The effect of Efavirenz (five day treatment, 10μM, APP^{dp}1-6 neurons) on Tau levels and Tau phosphorylation as assessed by western blot (see quantification in main figure 5B). Image

is a composite of different loading positions on same blot, stich is indicated by vertical line. (**B**) Neuronal (MAP2), precursor (Nestin) and astrocyte (S100b) staining of three-week differentiated non-replated neurons (conditions used for western blot) after five day treatment with DMSO, Simvastatin (10µm), Atorvastatin (10µm) or Efavirenz (25µm) in CV4a neurons. High non-specific background staining for S100b was observed in this line, arrows indicate examples of low abundant above-background S100b positive cells. Scale bar represents 200µm. (**C**) Western blot analysis of indicated synaptic proteins after treatment with DMSO, Atorvastatin (10µm), T0901317 (10µm) Efavirenz (25µm) (five day treatment, APP^{dp}1-6 neurons). Image is a composite of different loading positions on same blot, stiches are indicated by vertical lines. (**D**) Western blot analysis of housekeeping genes and neuron-specific enolase (NSE) after treatment with DMSO or Atorvastatin (10µm) (five day treatment, APP^{dp}1-6 neurons). Image is a composite of different loading positions on same blot, stiches are indicated by vertical lines. (**E**) APP^{dp}1-6 neurons were treated for indicated time points with atorvastatin. Cell lysates were analyzed by ELISA for pSer9GSK3b/ tGsk3b (mean±SEM, n≥3). **(F)** APP^{dp}1-6 neurons were treated for 3 days with 25µM chloroquine (inhibitor of lysosomal acidification and autophagosomal degradation) or 5µM MG-132 (proteasomal inhibitor) and cell viability was determined (mean±sem, N≥3). **(G)** APP^{dp}1-6 neurons were treated for 3 days with 1.25nM okadaic acid (phosphatase inhibitor) and pGSK3b/GSK3b levels were determined by ELISA as a measure of phosphatase inhibition (mean±sem, N≥3). **(H-I)** APP^{dp}1-6 neurons were treated for 3 days with 10µM atorvastatin in the presence of 25µM chloroquine (**H**) or 5µM MG-132 (**I**). Lysates were collected and assessed by western blot staining with antibodies against (**H**) microtubule-associated protein 1A/1B-light chain 3 (LC3) to show inhibition of autophagic flux by chloroquine and staining with antibodies for (**I**) ubiquitin to show accumulation of ubiquitinated proteins in MG-132 treated samples. (**J**) APP^{dp}1-6 neurons were treated for 3 days with 5µM MG-132, fixed and stained with a total Tau antibody. (**K**) tTau/total protein levels

and **(L)** pThr231Tau/total protein in APP^{dp} neurons co-treated with atorvastatin (10µm) and the proteasome inhibitor (MG132, 5µM) for 3 days as measured by ELISA. Results are averages from two independent APP^{dp} lines (APP^{dp} 1-6 and 2-1) (mean±SEM, n≥3 per line). (**M**) pThr231Tau/tTau levels in WT neurons co-treated with atorvastatin (10µm) and a proteasome inhibitor (MG132, 5µM) for 3 days as measured by ELISA. Results are averages from two independent WT lines (CV4a and line 151) (mean±sem, N≥3 per line). MG-132 is unstable in solution and was therefore added fresh every day in all experiments. (**N**) APP^{dp}1-6 Neurons were treated for indicated time points with 10µM atorvastatin and mRNA levels of proteasomal subunits PSMβ5 and PSMC2 were determined by quantitative real-time polymerase chain reaction (RT-qPCR) and normalized over housekeeping genes (RPLP27) (mean±SEM, n≥3). (**O**) APP^{dp}1-6 neurons were treated for 5 days with DMSO, 10µM atorvastatin or Torin1 (an mTor inhibitor) and phosphorylation status of mTor target proteins was determined by western blot. Image is a composite of different loading positions on same blot, stiches are indicated by vertical lines. (**P**) APP^{dp}1-6 neurons were treated for indicated time points with DMSO or 10µM atorvastatin and phosphorylation status of the mTor target 4EBP1 was determined by ELISA (mean±SEM, n≥3) (**Q**) Positive control for 4EBP ELISA. APP^{dp}1-6 neurons were treated for three days with insulin containing media or insulin-free media and phosphorylation status of the mTor target 4EBP1 was determined by ELISA (mean±SEM, n≥3). *** $p<0.001$, ** $p<0.01$, * $p<0.05$.

Supplemental Figure 6. Astrocytic and neuronal viability in response to statins and efavirenz, Related to Figure 6.

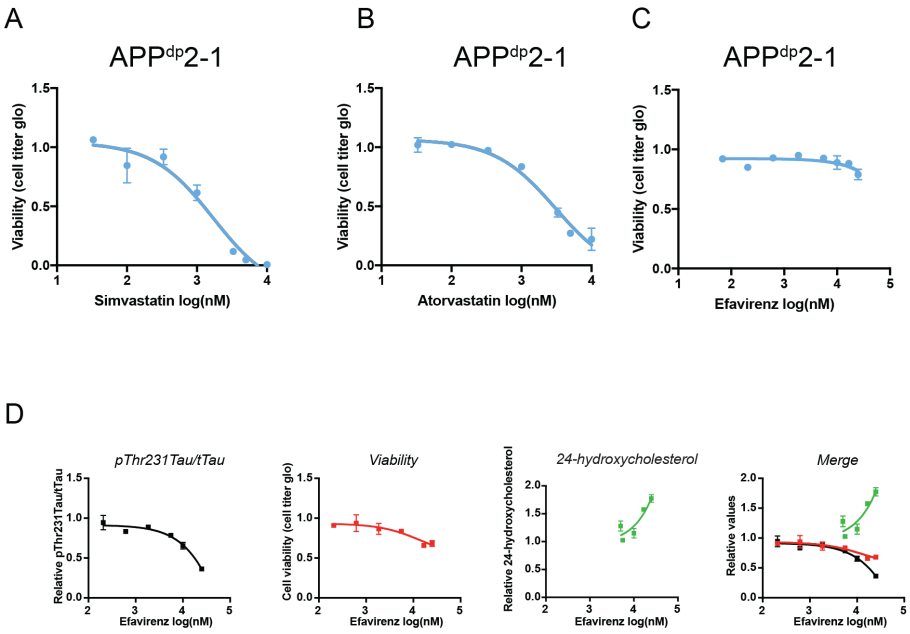

iPSC-derived APP^{dp}2-1astrocytes were treated for three days with increasing concentrations of **(A)** simvastatin, **(B)** atorvastatin and **(C)** efavirenz and viability was determined (cell titer glo). **(D)** APP^{null} (APPdp1KO) neurons were treated for five days with increasing concentrations efavirenz and pThr231Tau/Tau levels, 24-hydroxycholesterol levels and viability was measured (mean±SEM, n≥3).

Supplemental Table 2. Coefficient of variation for screening campaign, Related to Figure 1.

	ptau/total tau ratio			Cell Titer Glo		
plate #	ave	std dev	cv	ave	std dev	cv
1	4.89	1.05	0.21	427566	87006	0.20
2	4.38	0.76	0.17	439798	105410	0.24
3	4.80	0.68	0.14	417468	46284	0.11
4	4.42	0.71	0.16	413676	65711	0.16
5	6.05	0.72	0.12	540691	134415	0.25
6	6.88	0.60	0.09	538648	128503	0.24
7	5.87	1.64	0.28	252201	42936	0.17
8	5.79	1.69	0.29	237674	55155	0.23
9	5.03	1.12	0.22	193892	56904	0.29
10	5.30	1.14	0.21	276671	43889	0.16
11	4.36	1.01	0.23	202913	60936	0.30
12	5.18	1.15	0.22	215490	47718	0.22
13	5.15	1.23	0.24	221407	75762	0.34
14	4.30	0.65	0.15	224197	41101	0.18
15	6.07	1.47	0.24	233372	57994	0.25
16	7.76	0.69	0.09	534782	49171	0.09
17	6.57	1.30	0.20	377836	67072	0.18
18	4.38	1.04	0.24	333269	51268	0.15
19	4.99	1.35	0.27	336305	76970	0.23
20	5.09	0.94	0.19	421618	90686	0.22
			AVERAGE CV			AVERAGECV
			0.20			**0.21**

Coefficient of variation (CV) for pThr231Tau/tTau and cell titer glo in DMSO-treated samples for each of the 20 384 well plates used for the screening campaign (primary screen, conformation, dose response experiments)

Supplemental Table 5. Absolute levels of cholesterol, Related to Figure 2.

	free cholesterol ng/ug protein		total cholesterol ng/ug protein	
	mean	stdev	mean	stdev
DMSO	85.9	1.6	119.1	10.1
Atorvastatin	89.5	6.3	99.4	8.3
AY-9944	67.2	2.5	76.6	4.5
T0901317	73.0	6.9	104.2	8.2
Efavirenz	75.1	6.6	88.1	4.5
Avasimibe	88.2	8.4	98.7	9.8

Table depicts the absolute levels of free cholesterol (N=8) and total cholesterol (N=4) over protein corresponding to the relative levels plotted in figure 2d and e.

Supplemental Table 6. Oligonucleotides used in this study, Related to STAR methods.

Oligonucleotides	Source	Identifier
5'tattgcatttagaaattaaaattcttttttcttaatttgttttcaaggtgttctttgcagccgatgtgggttcaaacaaaggtgcaatcattggactcatggtggcggtgttgtcatagc3'	This Paper	E693A Repair Oligo
5'ttatattgcatttagaaattaaaattcttttttcttaatttgttttcaaggtgttcgctgcagccgatgtgggttcaaacaaaggtgcaatcattggactcatggtgggcggtgttgtcat3'	This Paper	E693A+F691A Repair Oligo
5'CTTCCTCGAACTGGGGAAGC3'	This Paper	APP Chol mut region forward primer
5'TCACGGTAAGTTGCAATGAATGA3'	This Paper	APP Chol mut region reverse primer
5'CCAACCAGTTGGGCAGAGAA3'	This Paper	APP Chol mut genomic DNA Sequencing Primer
5'CGTGGAATGGCAATTTTAGGTCC3'	This Paper	HMGCR-F (qPCR)
HMGCR-R (qPCR): 5'ATTTCAAGCTGACGTACCCCT3'	This Paper	*HMGCR-R (qPCR)*
LDLR-F (qPCR): 5'GTCTTGGCACTGGAACTCGT3'	This Paper	*LDLR-F (qPCR)*
LDLR-R (qPCR): 5'CTGGAAATTGCGCTGGAC3'	This Paper	LDLR-R (qPCR)
5'GCTACCGGTGAACCAGCG3'	This Paper	PSMB5 FW (qPCR)
5'CAACTATGACTCCATGGCGGA3'	This Paper	PSMB5 RV (qPCR)
5'TGAGAGTGGGCGTGGATAGA3'	This Paper	PSMC2 FW (qPCR)
5'GTACCGGGTGGACCAAAGAG3'	This Paper	PSMC2 RV (qPCR)
5'AAACCGCAGTTTCTGGAAGA3'	This Paper	RPL27-F (qPCR)
5'TGGATATCCCCTTGGACAAA3'	This Paper	RPL27-R (qPCR)
5'gtacaaaaaagcaggcttaaatggactacaaagaccatgacgg3'	This paper	CYP46A1 PCR primer 1
5'GTACAAGAAAGCTGGGTAGCggatccTCAGCAGGGGGGTGGT3'	This paper	CYP46A1 PCR primer 2

ACKNOWLEDGEMENTS

Chapter 2, in full, is a reprint of the material as it appears in Cell Stem Cell 2019. Kant, R. van der, Langness, V. F., Herrera, C. M., Williams, D. A., Fong, L. K., Leestemaker, Y., Steenvoorden, E., Rynearson, K. D., Brouwers, J. F., Helms, J. B., Ovaa, H., Giera, M., Wagner, S. L., Bang, A. G., and Goldstein, L. S. B. (2019) The dissertation author was the co-first author on this paper.

Chapter 3
Cholesterol Lowering Drugs Reduce APP Processing to Aβ by Inducing APP Dimerization

Vanessa F. Langness[1,3], Rik van der Kant, Utpal Das[2], Louie Wang[1,3],

Rodrigo Chaves[1,3], Lawrence SB. Goldstein[1,2,3]

From the

[1]Department of Cellular and Molecular Medicine, University of California, San Diego, La Jolla, CA 92093, USA.

[2]Department of Neurosciences, University of California, San Diego, La Jolla, CA 92093, USA.

[3]Sanford Consortium for Regenerative Medicine, University of California, San Diego, La Jolla, CA 92093, USA.

Abstract

Amyloid beta (Aβ) is a major component of amyloid plaques which are a key pathological hallmark found in brains of Alzheimer's Disease (AD) patients. Aβ is derived from Amyloid Precursor Protein (APP) through sequential proteolytic cleavage by BACE1 and y-secretase. Previous studies show that cholesterol metabolism regulates APP processing to Aβ. However, the mechanism is not well understood. We used transfected HEK cells and iPSC derived neurons to elucidate how statins influence APP processing. We show that statins alter APP fragmentation in a Tau independent pathway. APP fragmentation changes induced by atorvastatin are indicative of reduced processing by BACE1 and y-secretase. We used a fluorescence complementation assay to show that atorvastatin increases full length APP (flAPP) dimerization and reduces full length APP interaction with BACE1. In contrast, atorvastatin treatment caused a decrease in βCTF dimerization and a decrease in βCTF interaction with y-secretase catalytic subunits. We use inhibitors of various steps in the mevalonate pathway to show that cholesteryl esters are important regulators of Aβ production. Additionally, we show that statins are effective at lowering Aβ in iPSC derived neurons from multiple individuals including non-demented controls (NDC), and subjects with familial AD (FAD), and sporadic AD (SAD). These data reveal that cholesterol lowering drugs reduce APP processing to Aβ by decreasing BACE1 interaction with flAPP and by decreasing y-secretase interaction with βCTF and suggest that these changes may be mediated by alterations in flAPP and βCTF dimerization.

Introduction

The brains of patients with Alzheimer's disease (AD) exhibit two key characteristic pathological hallmarks: accumulation of extracellular plaques primarily composed of amyloid beta peptide (Aβ) and accumulation of intracellular hyperphosphorylated Tau protein (pTau) (1). The amyloid cascade hypothesis, a dominant hypothesis in the AD field, proposes that Aβ is the causative agent in AD and that changes in Aβ cause downstream accumulation of pTau which can lead to the neurodegeneration that occurs in AD (2–7). Thus, understanding the mechanism of Aβ generation is a major area of interest to AD researchers.

Aβ is derived from sequential proteolytic cleavage of Amyloid Precursor Protein (APP). APP can be cleaved in two major pathways. In the amyloidogenic pathway, APP is first cleaved by the β-secretase BACE1 to generate two protein fragments: soluble APP β (sAPPβ) and a β C-terminal fragment (βCTF). sAPPβ is released into the extracellular space. βCTF is cleaved by y-secretase which releases the APP intracellular domain (AICD) into the cytosol and generates Aβ peptides of various lengths. Aβ40, a 40 amino acid peptide is the major species generated. Aβ42, a slightly longer and more hydrophobic peptide is produced in smaller quantities but is a major component found in amyloid plaques and is thought to be more prone to oligomerization into toxic Aβ species.(1)

In the alternative, non-amyloidogenic pathway, APP is first cleaved by α-secretase to generate soluble APP α (sAPPα) and α C-terminal fragment (αCTF). sAPPα is released into the extracellular space. αCTF is cleaved by y-secretase which

releases the AICD into the cytosol and generates a small fragment called p3. y-secretase is a multi-subunit complex consisting of at least four proteins: presenilin (PS), nicastrin, Aph-I, and Pen-2. Presenilin is the catalytic subunit of y-secretase. Presenilin has two isoforms Presenilin-1 (PS1) and Presenilin-2 (PS2), either one of which can be incorporated into the y-secretase complex (1).

A large body of genetic, epidemiological, and biochemical evidence supports a link between cholesterol and AD. Statins inhibit cholesterol biosynthesis and epidemiology studies have shown that statin users are at a decreased risk for AD (10–15). Randomized clinical trials have failed to show a beneficial effect(16–20). The randomized clinical trials have known limitations such as insufficient follow-up times, exclusion of hyper-lipidemic patients, and short treatment time frames which could explain the lack of beneficial findings (21). It is well established that statins can alter APP processing and reduce Aβ levels (22–24) however, the mechanism is unclear.

Several studies have shown that APP can form dimers (25–27) which in turn can influence APP processing. The glycine-XXX-glycine (GXXXG) amino acid sequence is a common motif in transmembrane helices that can mediate helix-helix interactions and dimerization of proteins (28, 29). APP contains three of these GXXXG motifs in the juxtamembrane and transmembrane region which are thought to mediate β-CTF dimerization and in part mediate flAPP dimerization (30–35). The APP ectodomain can also contribute to dimerization of flAPP (35). The role that dimerization plays in regulating APP processing is controversial. One set of studies showed that disrupting APP dimerization modulates APP processivity by y-secretase leading to a

decrease in processing to Aβ42 (34, 36). These results indicate that βCTF dimerization may promote APP processing to Aβ42. However, these claims have been refuted by two studies which instead of disrupting APP dimerization, induced or enriched for βCTF dimers. These studies showed that βCTF dimers are less susceptible to processing by y-secretase (37, 38). Another study showed that inducing dimerization of flAPP caused an increase in flAPP and a mild decrease in sAPPβ (37, 39), suggesting that dimerization may additionally inhibit processing of flAPP by BACE1. Researchers have hypothesized that cholesterol levels may have an inverse relationship with APP dimerization (40). This suggestion is supported by biochemical evidence (41) but has not been shown in live cells. More work is needed to understand the relationship between cholesterol levels, APP dimerization, and APP processing.

We used transfected HEK cells and iPSC derived neurons to study the effects of statins and cholesterol/CE lowering drugs on APP dimerization and processing. We used a Bimolecular Fluorescence Complementation (BiFC) split Venus based approach to show that atorvastatin treatment causes increased flAPP dimerization. This is accompanied by a concurrent decrease in flAPP interaction with BACE1. Atorvastatin treatment additionally caused a decrease in βCTF dimerization along with a decrease in βCTF interaction with PS1 and PS2. These changes are accompanied by alterations in APP fragmentation that suggest a decrease in processing of APP by BACE1 and y-secretase leading to a reduction in Aβ levels. Collectively, our data elucidates a pathway by which reductions in cholesterol/CE can reduce APP processing to Aβ by reducing APP interaction with the secretases. Reduced interaction

with the secretases after statin treatment is tightly correlated with increased flAPP dimerization and decreased βCTF dimerization.

Results

Atorvastatin causes a reduction of secreted Aβ42 and Aβ40 in transfected cells

We probed for the effects of cholesterol lowering drugs on APP fragmentation, APP dimerization and APP-secretase interactions by modifying a bimolecular fluorescence complementation (BiFC) assay described in (42). BiFC is an established tool to study protein-protein interactions (43). This approach involves transfecting cells with plasmids encoding two potentially interacting proteins, one tagged with the Venus fluorophore N-terminus (vn) and the other tagged with the Venus fluorophore C-terminus (vc). When the two proteins come together to interact, the two halves of the Venus fluorophore reconstitute into a fully fluorescent molecule and give off a Venus signal. This Venus signal can be measured using microscopy or flow cytometry as a metric of relative levels of interaction of the two tagged proteins. We used previously published constructs BACE1vc and wtAPPvn to study APP-BACE1 interaction. We also made constructs that we could co-transfect with wtAPPvn to study flAPP dimerization (wtAPPvc). We made βCTFvn and βCTFvc constructs to study the effects of atorvastatin on βCTF dimerization. We also made two constructs that we can co-transfect with βCTFvn to study βCTF-presenilin interaction (PS1vc and PS2vc).

We first wanted to determine if transfected APP can be processed by endogenous secretases. To test this, we compared levels of APP fragmentation in

untransfected cells and in transfected cells and additionally tested whether secretase inhibitors changed APP fragmentation in transfected cells. Prior to transfection, we pretreated HEK cells with DMSO or the indicated treatment for 24 hours. Conditioned media and cell lysates were harvested 24 hours post transfection. Meso Scale Discovery electrochemiluminescence (MSD-ECL) based measurements of Aβ42 (Fig. 1A), Aβ40 (Fig. 1B), sAPPβ (Fig. 1C) and sAPPα (Fig. 1D) from media of wtAPPvc transfected cells were much higher than that detected in untransfected cells, indicating that most of the measured fragments are derived from processing of the transfected construct rather than from endogenous APP. Treatment with a y-secretase inhibitor (compound E) and a BACE1 inhibitor (BIV) both reduced Aβ42 (Fig. 1A), and Aβ40 (Fig. 1B) measured in conditioned media from transfected cells. Treatment with a BACE1 inhibitor (BIV) reduced sAPPβ (Fig. 1C) and did not significantly change sAPPα (Fig. 1D). These data show that transfected APP can be processed by endogenous BACE1 and y-secretase.

Next, we wanted to determine whether cells transfected with wtAPPvc can recapitulate statin induced reduction of Aβ42 and Aβ40 that we previously observed in hiPSC derived neurons(44). MSD-ECL based measurements revealed that atorvastatin treatment reduced both Aβ42 (Fig. 1A), Aβ40 (Fig. 1B) in the transfected cells. This shows that APP transfected HEK cells recapitulate atorvastatin induced phenotypes that we originally observed in hiPSC derived neurons. Treatment of the untransfected cells with atorvastatin trended toward reduced Aβ42 (Fig. 1A), and Aβ40 (Fig. 1B) production, however these changes were not significant. Together, these data

show that atorvastatin treatment reduces processing of exogenous APP and that we can use HEK cells transfected with split Venus tagged constructs to model changes in APP processing that occur after treatment with drugs like statins.

To explore how atorvastatin alters APP processing in the split Venus system, we characterized how atorvastatin treatment affected levels of sAPPβ, sAPPα, and flAPP. Atorvastatin treatment of wtAPPvc transfected cells caused a reduction in levels of the BACE1 cleavage product sAPPβ (Fig. 1C) and the α-secretase cleavage product sAPPα (Fig. 1D) suggesting that atorvastatin may block α-and β-secretase cleavage of transfected APP. In line with this, atorvastatin treatment caused an increase in levels of full length wtAPPvc (visualized with an anti-GFP antibody) in the transfected HEK cells. (Fig. 1E). This suggests that full length APP is accumulating, and processing is reduced. Together, we see that atorvastatin treatment reduces the products of α- and β- secretase cleavage (sAPPα and sAPPβ respectively) and reduces Aβ40 and Aβ42 while concurrently increasing levels of flAPP. Together, these data suggest that atorvastatin treatment reduces BACE1 mediated processing of APP leading to an accumulation of flAPP.

Atorvastatin increases APP dimerization

Previous studies have suggested that full length APP dimerization can alter APP processing by BACE1(45, 46). We hypothesized that atorvastatin may reduce APP processing by altering levels of APP dimerization. To determine whether atorvastatin alters dimerization, we made use of the split Venus BiFC assay. BiFC has been used

to study APP dimerization in previous studies (47–49). We transfected HEK cells with two APP constructs, one tagged with the Venus N-terminus (wtAPPvn) and one tagged with the Venus C-terminus (wtAPPvc) as well as a soluble mCherry construct for cell selection. When split Venus tagged proteins dimerize, we can detect a Venus signal and measure relative levels of APP dimerization (Fig. 2A).

To robustly quantify Venus signal (APP dimerization) we developed a flow cytometry assay that quantitatively measures thousands of cells from many samples. Fig. S1 A-E shows an example of the gating scheme used for this experiment as well as all of the split Venus flow cytometry assays discussed below. After gating out cell debris (Fig. S1B), and doublets (Fig. S1C&D), an untransfected control (Fig. S2A) was used to set a gate to discriminate transfected cells from untransfected cells. Venus median fluorescence intensity (dimerization) was measured in the transfected cell population. Untransfected cells were excluded from this measurement. Representative compensation controls are shown in (Fig. S2 A,B,&C) and include the untransfected control (Fig. S2A), a control transfected with only mCherry (Fig. S2B), and a control transfected with a split Venus pair without mCherry (Fig. S2C). These were used to ensure there was no bleed through from one channel to another. None of the split Venus tagged constructs expressed on their own generated Venus signal (Fig. S4 A&B). Additionally, when wtAPPvn is co-transfected with a plasmid expressing just the VC fragment and when wtAPPvc is co-transfected with a plasmid expressing just the VN fragment, we see very little signal compared to when wtAPPvn and wtAPPvc are

co-transfected together. (Fig. S4 C&D). Together, these control experiments show that the Venus signal is specific to dimerization.

We used this split Venus assay to measure the effects of atorvastatin on APP dimerization. Figure 2B shows the flow cytometry histograms generated for transfected cells. One set was treated with DMSO (shown in black) and the other set was treated with atorvastatin (shown in grey). After atorvastatin treatment, we observed a clear shift in the histogram population toward a higher Venus median fluorescence intensity. This shift is quantified in Figure 2C and shows that atorvastatin treatment causes a significant increase in APP dimerization by approximately 25%. Figure S3 A&B shows that atorvastatin treatment did not significantly affect the transfection efficiency as measured by the percentage of transfected singlets. These results indicate that atorvastatin treatment increases APP dimerization in transfected HEK cells.

We additionally tested the effects of atorvastatin on APP dimerization in transfected hiPSC derived neurons using microscopy. We pre-treated WT hiPSC derived neurons with DMSO or atorvastatin for 5 days. We then co-transfected with wtAPPvn and wtAPPvc and a soluble mCherry construct to assist with selection of transfected cells. On the next day, cells were fixed, permeabilized and stained for MAP2 which we used as a marker for neurons. Imaging and image processing were performed blind. We observed that atorvastatin treatment increased APP dimerization in the transfected neurons. (Fig. 2D) Together our results show that atorvastatin treatment induces APP dimerization in transfected HEK cells and in hiPSC derived neurons.

Mutations in the APP GXXXG motifs reveal residues that mediate dimerization but decrease Aβ42 and Aβ40 in a dimerization independent manner

To determine whether residues in the GXXXG motif mediate APP dimerization, we used site directed mutagenesis to induce point mutations in each of the dimerization split Venus pairs (wtAPPvn and wtAPPvc). We generated mutant split Venus pairs containing a glycine(G) to isoleucine(I) substitution for each of the four glycines in the three tandem GXXXG domains. This gave us G25I, G29I, G33I, and G37I split Venus pairs (Aβ numbering). We transfected HEK cells with each of these split Venus pairs and measured the effects of the mutations on APP dimerization using the split Venus dimerization assay described above. Supplemental figure 5A shows the flow cytometry histograms generated for WT, G25I, G29I, G33I, and G37I split Venus pair transfected cells. Venus median fluorescence intensity was quantified for each condition. G33I mutations caused a significant decrease in APP dimerization (Venus median fluorescence intensity) while G25I, G29I, and G37I did not significantly affect APP dimerization (Fig. S5A,B). These data indicate that the G33 amino acid residue is crucial to mediating APP dimerization. This result is in partial agreement with a previous study which showed that the G33I mutation in βCTF but not flAPP can abolish dimerization. (34) Our mutations were made in the flAPP sequence. However, we showed above that in our system, transfected APP is processed by endogenous secretases and thus it is possible that the reduction in dimerization we observe is arising from CTFs derived from processing of the full-length split Venus tagged

constructs. We conclude that G33 is an important residue in the GXXXG motif that regulates flAPP and/or βCTF dimerization.

To determine whether mutations in the GXXXG motif influence APP processing, we measured Aβ42 and Aβ40 in conditioned media from HEK cells transfected with the WT, G25I, G29I, G33I, and G37I split Venus pairs. We observed that all four mutations caused a reduction in Aβ42 (Fig. S5C). All mutations except for G25I caused a reduction in Aβ40 (Fig. S5D). These results show that mutations in the GXXXG motif cause reductions in APP processing to Aβ that are independent of APP dimerization. These results confirm previous studies that show that mutations within the Aβ sequence influence APP processing by interfering with secretase cleavage independently of dimerization (30, 37). More recent work that studies the effects of APP dimerization using systems that do not exclusively rely on intra-APP mutations shows that APP dimers are resistant to y-secretase cleavage. (37, 38) Our results support these claims and show that mutations within the APP sequence are not appropriate to study the effects of dimerization on APP processing.

Atorvastatin decreases APP-BACE1 interaction

To test the hypothesis that atorvastatin causes alterations in APP processing by changing levels of APP-BACE1 interaction, we made use of the split Venus BiFC system. We co-transfected HEK cells with two constructs, BACE1 tagged with the Venus C-terminus (BACE1vc) and APP tagged with the Venus N-terminus (wtAPPvn) as well as a soluble mCherry construct for cell selection. When split Venus tagged APP

and BACE1 interact, we can detect a Venus signal and use this as a measure of APP-BACE1 interaction (Fig. 3A). Cells were gated in the same way as described above. Analysis of Venus median fluorescence intensity (APP-BACE1 interaction) was performed only on transfected cells.

We performed several control experiments to determine whether the Venus signal in this assay is specific to APP-BACE1 interaction rather than non-specific reconstitution of the Venus signal. None of the individually expressed split Venus tagged constructs generated Venus signal (Fig. S6 A&B). When BACE1 is co-transfected with a truncated APP which lacks most of the C-terminal region (stop40APPvn) which is suspected to mediate APP-BACE1 interactions (42, 50), we see essentially no Venus signal (Fig. S6 A&B). Additionally, when wtAPPvn is co-transfected with a plasmid expressing just the vc fragment and when BACE1vc is co-transfected with a plasmid expressing just the vn fragment, we see very little signal compared to when wtAPPvn and BACE1vc are co-transfected together (Fig. S6 C&D). These control experiments show that the Venus signal in this assay is specific to APP-BACE1 interaction.

We used this split Venus assay to measure the effects of atorvastatin on APP-BACE1 interaction. Figure 3B shows flow cytometry histograms for BACE1vc and wtAPPvn transfected cells, one set was treated with DMSO (shown in black) and the other with atorvastatin (shown in grey). After atorvastatin treatment, we observed a clear shift in the histogram population toward a lower Venus median fluorescence intensity. This shift is quantified in Figure 3C and shows that atorvastatin treatment

causes a decrease in APP-BACE1 interaction by approximately 25% (Fig. 3B,C). Atorvastatin treatment did not significantly affect the transfection efficiency as measured by the percentage of transfected singlets (Fig. S3C&D). These data show that statin treatment reduces APP-BACE1 interaction in transfected HEK cells.

We additionally tested the effects of atorvastatin on APP-BACE1 interaction in transfected hiPSC derived neurons using microscopy. We pre-treated WT hiPSC derived neurons with DMSO or atorvastatin for 5 days. We then co-transfected with wtAPPvn and BACE1vc and a soluble mCherry construct to assist with selection of transfected cells. On the next day, cells were fixed, permeabilized and stained for MAP2 which we used as a marker for neurons. Imaging and image processing were performed blind. We observed that atorvastatin treatment decreased BACE1 interaction with APP in the transfected neurons. (Fig. 3D) Together our results show that atorvastatin treatment reduces APP-BACE1 interaction in transfected HEK cells and in hiPSC derived neurons.

Atorvastatin decreases βCTF dimerization

To determine whether atorvastatin treatment influences dimerization of βCTF, we used the split Venus BiFC system. We co-transfected HEK cells with two constructs, βCTF tagged with the Venus C-terminus (βCTFvc) and βCTF tagged with the Venus N-terminus (βCTFvn) as well as a soluble mCherry construct for cell selection. When βCTF dimerizes we can detect a Venus signal and use this as a measure of βCTF dimerization (Fig. 4A). Cells were gated in the same way as

described above. Analysis of Venus median fluorescence intensity (βCTF dimerization) was performed only on transfected cells.

We performed a control experiment to determine whether the Venus signal in this assay is specific to βCTF dimerization rather than non-specific reconstitution of the Venus signal. When βCTFvn is co-transfected with a plasmid expressing just the vc fragment and when βCTFvc is co-transfected with a plasmid expressing just the vn fragment, we see very little signal compared to when βCTFvn and βCTFvc are co-transfected together (Fig. S7 A&B). This experiment shows that the Venus signal in this assay is specific to βCTF dimerization.

We used this split Venus assay to measure the effects of atorvastatin on βCTF dimerization. Figure 4B shows flow cytometry histogram data for βCTFvc and βCTFvn transfected cells, one set was treated with DMSO (shown in black) and the other with atorvastatin (shown in grey). After atorvastatin treatment, we observed a shift in the histogram population toward a lower Venus median fluorescence intensity. This shift is quantified in Figure 4C and shows that atorvastatin treatment causes a small decrease in βCTF dimerization (Fig. 4B&C).

Atorvastatin decreases βCTF-PS1 and βCTF-PS2 interaction

To determine whether atorvastatin treatment influences interaction of βCTF with the y-secretase catalytic subunits PS1 or PS2, we again used the split Venus BiFC system. We co-transfected HEK cells with two constructs, PS1 or PS2 tagged with the Venus C-terminus (PS1vc or PS2vc) and βCTF tagged with the Venus N-terminus (βCTFvn) as well as a soluble mCherry construct for cell selection. When βCTFvn and

PS1vc or PS2vc interact, we can detect a Venus signal and use this to quantify βCTF-PS1 or βCTF-PS2 interaction (Fig. 5A). Cells were gated in the same way as described above. Analysis of Venus median fluorescence intensity (βCTF-PS1 or βCTF-PS2 interaction) was performed only on transfected cells.

We performed several control experiments to determine whether the Venus signal in this assay is specific to APP-PS1 or APP-PS2 interaction rather than non-specific reconstitution of the Venus signal. None of the individually expressed split Venus tagged constructs generated Venus signal. (Fig. S8 A&B). Additionally, when wtAPPvn is co-transfected with a plasmid expressing just the vc fragment and when PS1vc or PS2vc is co-transfected with a plasmid expressing just the vn fragment, we see very little signal compared to when wtAPPvn and PS1vc or PS2vc are co-transfected together (Fig. S8 C-F). Together, these control experiments show that the Venus signal in this assay is specific to βCTF-PS1 and βCTF-PS2 interaction.

We used this split Venus assay to measure the effects of atorvastatin on βCTF-PS1 and βCTF-PS2 interaction. Figure 5B shows flow cytometry histogram data for PS1vc or PS2vc and βCTFvn transfected cells, one set was treated with DMSO (shown in black) and the other with atorvastatin (shown in grey). After atorvastatin treatment, we observed a shift in the histogram population toward a lower Venus median fluorescence intensity. This shift is quantified in Figure 5C and shows that atorvastatin treatment causes an approximately 20-25% decrease in both βCTF-PS1 and βCTF-PS2 interaction (Fig. 5B&C). Atorvastatin treatment did not significantly affect the

transfection efficiency as measured by the percentage of transfected singlets (Fig. S3E&F).

Atorvastatin causes accumulation of flAPP and a reduction of sAPPβ and sAPPα but no change in BACE1 levels in iPSC derived neurons

To determine whether the mechanism by which atorvastatin reduces APP processing to Aβ is the same in our transfected HEK cell system and in human iPSC derived neurons, we characterized the effects of atorvastatin on APP fragments in WT hiPSC derived neurons. We observed a decrease in both sAPPβ (Fig. 6A) and sAPPα (Fig. 6B) in conditioned media from WT neurons after atorvastatin treatment. This observation suggests that atorvastatin treatment interferes with APP processing by α-secretase and BACE1. If this is true, then atorvastatin treatment would cause less cleavage of flAPP to sAPPβ by BACE1 and less cleavage of flAPP to sAPPα by α-secretase and we would expect to see an accumulation of flAPP. (Fig. 9B) In agreement with this view, we see an increase in flAPP levels in WT neuron lysates after atorvastatin treatment. (Fig. 6C&D). The changes in APP fragmentation that we observe in hiPSC derived neurons match the changes we see in transfected HEK cells after atorvastatin treatment. Our data supports the conclusion that the changes modeled in the transfected HEK cells are similar to human neurons. Our results indicate that in both of our model systems, atorvastatin treatment reduces processing of flAPP, thus leading to accumulation of flAPP and a reduction in its cleavage products.

To test the hypothesis that the reduction in BACE1 processing is a result of reduced levels of BACE1 protein, we performed a western blot on atorvastatin treated WT hiPSC derived neuron lysates. The two WT lines we used had slightly different baseline expression levels of BACE1, however, both WT lines responded the same to atorvastatin. We observed that atorvastatin treatment caused no change in BACE1 levels in either of the two WT lines tested. (Fig. 6E&F) This indicates that atorvastatin does not directly affect BACE1 protein levels. Thus, the effect of atorvastatin on APP processing by BACE1 appears to occur independently of BACE1 expression levels.

Atorvastatin treatment causes accumulation of αCTF and no change in βCTF

When flAPP is cleaved by BACE1 to generate sAPPβ and βCTF they are produced in equimolar quantities (Fig. 9A). Since we observed atorvastatin induced decreases in sAPPβ levels, we hypothesized that we would also observe a decrease in βCTF levels after atorvastatin treatment. Surprisingly, there was no significant change in βCTF levels after atorvastatin treatment when normalized to actin. (Fig. 7A&B) This suggests that atorvastatin may also inhibit the second step in APP processing which involves cleavage of βCTF to Aβ by y-secretase.

When flAPP is cleaved by α-secretase to generate sAPPα and αCTF, they are produced in equimolar quantities (Fig. 9A). Since we observe a reduction in sAPPα after atorvastatin treatment, indicating a reduction in α-secretase processing, we hypothesized that we would observe a decrease in αCTF levels after atorvastatin treatment. Interestingly, α-CTF levels were significantly increased after atorvastatin

treatment when normalized to actin. (Fig. 7A&C) This suggests that atorvastatin may also inhibit cleavage of αCTF by y-secretase.

Because we observed fragmentation changes that suggest a decrease in y-secretase processing, we tested for a decrease in protein levels of presenilin, which forms the catalytic subunit of y-secretase. We performed western blots for two different isoforms of presenilin: presenilin 1 (PS1) and presenilin 2 (PS2). We see that atorvastatin treatment does not cause a significant change in PS1 protein levels in the WT neuron lysates. (Fig. 7D&E) We observed that atorvastatin causes a small but significant decrease in PS2 protein levels in the WT neurons. (Fig. 7D&F) This small but significant reduction in PS2 levels is unlikely to completely explain the reduction in Aβ that we observe after atorvastatin treatment but may contribute to some extent.

Statins reduce Aβ42 and Aβ40 secretion in both WT and Tau KO human iPSC derived neurons

Previously, we showed that statins reduce pTau in iPSC derived neurons. We showed that the effects of statins on pTau occur independently of their effects on Aβ and APP (51). Here, we invert the question and ask whether the effects of statins on Aβ are dependent on Tau. We treated both WT and Tau KO iPSC derived neurons with DMSO, atorvastatin or simvastatin and measured the effects on Aβ levels. Simvastatin and atorvastatin reduced Aβ42 (Fig. S9A) and Aβ40 (Fig. S9B) levels in both WT and Tau KO neurons to a similar extent. These results show that the effects of statins on APP processing to Aβ occur independently of their effects on Tau.

Additionally, these results show that the effects of statins on Aβ42 and Aβ40 are not limited to atorvastatin. Simvastatin is also effective at lowering Aβ42 and Aβ40 in hiPSC derived neurons.

Cholesterol/CE lowering drugs cause a reduction of secreted Aβ42 and Aβ40 in hiPSC derived neurons

We tested the hypothesis that Aβ levels are regulated by cholesterol metabolism. We treated hiPSC derived neurons from an individual with familial AD caused by an APP duplication with various inhibitors of the mevalonate pathway. The mevalonate pathway is the primary pathway responsible for cholesterol biosynthesis. Statins inhibit 3-hydroxy-3-methylglutaryl-CoA reductase (HMGCR) which catalyzes conversion of HMG-CoA to mevalonate (MVA)(Fig. 8A) (52). This is an early, rate limiting step in cholesterol biosynthesis. Atorvastatin and simvastatin both significantly reduce Aβ42 (Fig. 8B) and Aβ40 (Fig. 8C) secretion showing that statins can lower Aβ secretion in neurons from individuals with familial AD. Supplementation with MVA rescued the effect of simvastatin treatment on both Aβ42 (Fig. 8B) and Aβ40 (Fig. 8C) levels indicating that the effects of statins on Aβ are due to their effects on the mevalonate pathway. After synthesis of farnesyl-pyrophosphate (farnesyl-PP), the mevalonate pathway branches off into several pathways leading to synthesis of various end products, one of which is cholesterol. Squalene synthase catalyzes the first step of the pathway that is committed exclusively to cholesterol biosynthesis (Fig. 8A)(52). Inhibition of the cholesterol biosynthetic specific arm of the mevalonate pathway using

the squalene synthase inhibitor (YM-53601) significantly reduced both Aβ42 (Fig. 8B) and Aβ40 (Fig. 8C) secretion. This shows that levels of secreted Aβ42 and Aβ40 are regulated specifically by the cholesterol-biosynthetic arm of the mevalonate pathway. We previously showed that statin treatment does not lower free cholesterol levels but that it does significantly reduce the levels of total cholesterol (free+esterified cholesterol) by way of a strong reduction of CE. This likely occurs because conversion of CE to cholesterol can compensate for a reduction in cholesterol synthesis due to inhibitor treatment. This suggests that reductions in CE, but not free cholesterol mediate the effects of statins on Aβ secretion. To test this hypothesis, we inhibited cholesterol esterification in hiPSC derived neurons with the Acyl-CoA cholesterol acyltransferase (ACAT) inhibitor avasimibe. ACAT catalyzes conversion of Cholesterol to CE. Avasimibe treatment, which we previously showed reduces CE levels without affecting cholesterol levels, led to a reduction of both Aβ42 (Fig. 8B) and Aβ40 (Fig. 8C). Together, these data indicate that CE regulate levels of Aβ in human iPSC derived neurons.

Simvastatin reduces secreted Aβ42 and Aβ40 from neurons derived from NDC and SAD subjects

We showed that atorvastatin and simvastatin can lower Aβ secretion in transfected HEK cells, WT neurons, and in neurons from a subject with FAD, but we wanted to determine if statins would be effective in neurons derived from SAD or NDC subjects. We treated hiPSC derived neurons from four NDC individuals and from five

individuals with SAD with simvastatin and measured the effects on Aβ42 and Aβ40. Simvastatin treatment reduced both Aβ42 (Fig. 8D) and Aβ40 (Fig. 8E) levels in neurons derived from all four NDC subjects and all five SAD subjects tested. These results indicate that simvastatin induced reduction of Aβ secretion is conserved across neurons derived from individual SAD and NDC subjects.

Discussion

Here, we probed the mechanisms of how statins regulate APP processing to Aβ. We made three principal observations: Simvastatin reduces Aβ secretion in SAD and FAD patient derived neurons. Statins reduce APP processing to Aβ by reducing APP interaction with the secretases and by altering APP dimerization. And, cholesteryl esters reduce Aβ levels through a Tau independent mechanism.

Statins reduce APP processing to Aβ by reducing APP interaction with secretases and altering APP dimerization

Together, the APP fragmentation changes along with the decreases in APP-secretase interaction that we observe after atorvastatin treatment suggests that atorvastatin reduces APP processing to Aβ42 and Aβ40 by reducing APP interaction with BACE1 and y-secretase. These changes are tightly correlated with atorvastatin induced increases in flAPP dimerization and atorvastatin induced decreases in βCTF dimerization. We propose a model in which atorvastatin treatment inhibits processing

by BACE1 and y-secretase by inducing flAPP dimerization and inhibiting βCTF dimerization (Fig. 9B)

βCTF dimerization has previously been shown to exert effects on APP processing by y-secretase. When we reduce βCTF dimerization with statins, we see reductions in Aβ secretion and reductions in βCTF interaction with PS1 and PS2. This can be interpreted in two ways. First, statins may have a direct effect on βCTF dimerization, and the reduced dimerization may cause reduced processing by y-secretase. Alternatively, statins may have a direct negative effect on βCTF processing by y-secretase and reduced dimerization may occur as part of a feedback mechanism. While studies using mutations in the GXXXG motif to disrupt dimerization show that reduced dimerization reduces Aβ secretion. We showed that mutations within the GXXXG motif are not appropriate to study the effects of dimerization on APP processing due to dimerization independent effects of the mutations on APP processing. Elegant studies which avoid the use of intra-APP mutations to assess how dimerization influences processing show that dimerization reduces βCTF processing by y-secretase (38, 53). In light of these studies, our data may suggest that reduced dimerization of βCTF in response to statins occurs as a feedback mechanism in an attempt of the cell to balance out atorvastatin induced decreases in y-secretase processing. However, more work is needed to parse out exactly how βCTF dimerization influences y-secretase mediated processing.

We showed that atorvastatin treatment induces flAPP dimerization and reduces APP processing by BACE1. Very few studies have looked at the effects of flAPP

dimerization on APP processing by BACE1(45, 46). The most direct study of the effects of flAPP dimerization on processing showed that inducing dimerization of flAPP using a chimeric APP-FKBP protein which can be induced to dimerize by addition of an FKBP binding drug led to an increase in flAPP and a mild reduction in sAPPβ suggesting that flAPP dimerization may decreases flAPP processing by BACE1 (53). Combining this with our observations, we propose that atorvastatin treatment first induces dimerization and thus inhibits APP processing by BACE1, contributing to statin induced reductions of Aβ secretion.

The mechanism by which APP dimerization alters interaction with the secretases has not been fully elucidated. One possibility is that the induction of flAPP dimerization that we observe after statin treatment makes APP impervious to BACE1 interaction. It is plausible that dimerization could obscure amino acids involved in APP-secretase interactions or obscure APP cleavage sites. Another possibility is that dimerization could affect intracellular trafficking of APP, leading to altered interaction with secretases. One recent paper showed that APP dimerization changes its trafficking (39). Trafficking of APP through various compartments is thought to play a major role in regulation of APP interaction with these secretases and thus its processing. More work will be needed to elucidate whether statins and other Cholesterol/CE lowering drugs alter APP interaction with these secretases by altering APP or secretase intracellular localization.

Cholesteryl esters reduce Aβ through a Tau independent mechanism

Many previous studies have investigated the effect of statins on APP processing and Aβ levels. Most of these studies show that statins reduce Aβ levels, however, there doesn't appear to be a consensus on one pathway by which statins reduce Aβ levels. (42, 43)

Statins have pleiotropic effects on several pathways that may influence Aβ levels due to the fact that they inhibit an early step in the mevalonate pathway and thus block production of precursors used in multiple important pathways (54, 55). Several studies have shown that statins can alter APP processing by interfering with isoprenoid synthesis and thus can block protein prenylation (24, 55). Our data contradict this conclusion. We use various inhibitors of crucial steps in the mevalonate pathway to show that APP processing to Aβ is regulated by the cholesterol biosynthetic arm of the mevalonate pathway. We previously published that statins reduce CE levels (the storage form of cholesterol) but do not actually cause a decrease in free cholesterol (51). Here, we show that an ACAT inhibitor which blocks conversion of cholesterol to CE leads to reduced APP processing to Aβ in human iPSC derived neurons. This confirms the results of previous studies performed in mouse and tissue culture models which show that ACAT inhibitors can reduce Aβ production (56–59).

One possible explanation for the differences in reported mechanisms is that the effects of statins are likely going to be different depending on the model system used. For example, cholesterol metabolism may differ significantly in an actively dividing cancer cell line compared to a post-mitotic cell such as a neuron. Additionally,

differences in cell culture conditions such as whether an exogenous source of cholesterol such as from serum is supplemented into the culture media may greatly change the effects of statins on APP processing. Furthermore, mice and humans exhibit crucial differences in lipid metabolism that could affect the ability to translate statin research done in mice to humans. Mice do not express functional cholesterol ester transfer protein (CETP)(60, 61) which plays a role in regulating cholesterol/CE metabolism in the human brain. (62) Careful choice of which model system to use and validation of results in more than one system may be crucial in studying the effects of cholesterol metabolism on AD biology.

We provide a mechanism for how atorvastatin influences APP processing by first testing in HEK cells and then validating our results in human iPSC derived neurons thus overcoming some of these limitations. While hiPSC derived neurons have some advantages over other model systems, they lack the complexity of an in vivo system. Neuronal cholesterol metabolism in the brain is heavily dependent on uptake of cholesterol containing lipoproteins secreted by astrocytes. In the future, co-culture studies with both astrocytes and neurons may help to elucidate non-cell autonomous effects of statins and cholesterol/CE levels on APP processing.

Previously, we published that pharmacologic reduction of CE causes a reduction in pTau levels that is independent of APP and Aβ (51). We show here that CE also causes a reduction of Aβ levels that is independent of Tau by showing that simvastatin reduces Aβ in both WT and Tau KO neurons. This suggests that in addition to previously defined pathways in which Aβ and Tau can work together in the same

pathway, Aβ and pTau levels can both be closely co-regulated by changes in CE but through separate independent pathways. Finding drugs that target early pathogenic changes that occur upstream of Tau and AD pathology may be key to treating the disease.

Several studies have shown that Cholesterol esters (CE) (the storage form of cholesterol) are enriched in AD patient brains and in transgenic AD mouse models (63–65). Additionally FAD causing mutations have been associated with altered cholesterol homeostasis (66). Elevated LDL cholesterol has been associated with early onset AD (67). Furthermore, APOEe4, the major genetic risk factor for SAD is a major component of lipoproteins which regulate cholesterol and cholesterol ester homeostasis in the brain. APP and its fragments have been shown to play roles in regulating cholesterol homeostasis (68–72). Conversely, cholesterol metabolism has been shown to play a role in regulating APP processing (22, 23, 73–75).Together with our data, these studies suggest that changes in cholesterol homeostasis that are driven by FAD or SAD genetic risk factors could influence downstream Aβ pathology. Statins, ACAT inhibitors and other cholesterol lowering drugs are promising targets that need to be investigated further for their potential therapeutic benefit. More work is needed to gain an understanding of whether genetic and environmental AD risk factors may lead to alterations in brain cholesterol homeostasis which act as upstream regulators of amyloid and Tau pathology.

Simvastatin reduces Aβ secretion in patient derived neurons

We used iPSC derived neurons from multiple NDC, SAD, and FAD patients to show that statins are effective at lowering Aβ in multiple different individuals from a variety of genetic backgrounds. This data provides mechanistic evidence in multiple patient lines that compliments epidemiological studies showing an association between statin use and reduced AD incidence(10–12). Randomized clinical trials have failed to find a benefit of statins on cognitive function in AD patients. We provide molecular evidence that statins or other CE/cholesterol lowering drugs should be investigated further for their potential therapeutic benefit. One possible explanation for the failure of statins in randomized clinical trials is that they tend to enroll older people who already have signs of cognitive dysfunction, meaning the disease course is already in full swing. It is likely that if statins or other cholesterol lowering drugs are to be used in the treatment of AD they will need to be used as a preventative therapeutic, or they will need to be combined with earlier diagnostic methods. This could explain why epidemiological studies, which include patients that have been taking statins long term and before the first signs of cognitive dysfunction, consistently find a lowered risk of AD in statin users. Often when a patient gets their first cognitive symptoms of AD, AD pathology has been accumulating for years and by that point the disease is extremely difficult to halt or reverse. We previously showed that statins also reduce pTau levels in hiPSC derived neurons derived from multiple FAD, SAD, and NDC subjects.(51) Together these studies suggest the need for clinical trials that test the

effects preventative use of statins or other cholesterol lowering drugs on younger patients over longer treatment periods.

General Conclusions

Several failed clinical trials for Aβ reducing drugs have led researchers to question whether reducing Aβ will be an effective way to treat or prevent AD. Whether Aβ is a causative agent in AD or whether its accumulation is an epiphenomenon that results from pathways that become dysregulated earlier in the disease process, gaining an understanding of the upstream pathways which regulate Aβ may lead us to a better understanding of APP function, AD pathogenesis, and ultimately to better drug targets. More studies will be needed to elucidate whether SAD and FAD genetic risk factors can contribute to amyloid and tau pathology through alterations in brain cholesterol homeostasis. Additionally, well designed, long term clinical trials are needed to determine whether statins, ACAT inhibitors, or other drugs that target brain cholesterol metabolism will be useful in AD treatment and prevention.

Experimental procedures

Human iPSC Derived Cell lines

The WT iPSC lines used in this study includes the control lines WT1(B10) (RRID:CVCL_VR50) and WT2(B11) (RRID:CVCL_VR51) which are two unedited control lines derived from the CVB iPSC line (RRID:CVCL_1N86) which was generated and characterized in (76). WT1(B10) and WT2(B11) were generated and characterized in (51).

SAD and NDC iPSC lines used are SAD2 (RRID: CVCL_EJ93), SAD3 (RRID: CVCL_UB91), SAD4 (RRID: CVCL_UB92), SAD5 (RRID: CVCL_UB93), SAD6 (RRID: CVCL_UB94), NDC1 (RRID:CVCL_EJ84), NDC3 (RRID: CVCL_UB88), NDC4 (RRID: CVCL_UB89), and NDC5 (RRID: CVCL_UB90) described and characterized in (77)

The APP^{dp} AD-patient iPSC lines used here are; APP^{dp}1-6 (derived from iPSC-line APP^{dp}1.1 (RRID:CVCL_EJ96) in (78)) , APP^{dp}1-2 (derived from iPSC-line APP^{dp}1.2 (RRID:CVCL_EJ97) in (78)) and APP^{dp}2-1 (derived from iPSC-line APP^{dp}2.3 (CVCL_1N92) in (78)). See (78) for characterization of these cell lines and for patient details.

To generate isogenic Tau KO cell lines, the iPSC line CVB (76) was gene edited using CRISPR/Cas9.

Generation of neural progenitor cells (NPCs)

NPCs were generated from iPSCs as described in (79) Briefly, 2×10^5 FACS-purified iPSC TRA1-81$^+$ cells were seeded onto two 10 cm plates that were seeded the previous day with 5×10^5 PA6 cells and were cultured in PA6 differentiation media (450ml Glasgow DMEM, 50ml KO Serum Replacer, 5ml sodium pyruvate, 5ml Nonessential Amino Acids) + 10um SB431542+ 0.5ug/ml Noggin. On the 11th day, cells were dissociated with Accutase and $\sim 5 \times 10^5$ CD184$^+$CD24$^+$CD44$^-$CD271$^-$ NPCs were FACS-purified and plated onto poly-L-ornithine/laminin-coated plates and cultured with NPCbase + 20ng/ml bFGF (Millipore). From here, cells were expanded and frozen down for use in future experiments.

Cell culture and generation of neurons

iPSCs were cultured on a MEF feeder layer in HUES medium: (400ml KO DMEM (Gibco 10829) + 50ml Knockout serum (Thermo Fisher 10828028) + 50ml plasmanate (Chapin) + 5ml pen-strep (Gibco 15140-122) + 5ml non-essential amino acids (Gibco 11140-050) + 5ml glutamax (Gibco 35050-061) + 1ml β-mercaptoethanol(Gibco 21985-023))+20ng/ml FGF (R&D Systems 233-FB-1) as described in (78) iPSCs were passaged with Accutase (Innovative Cell Technologies).

MEFS were plated in MEF media (450ml DMEM High glucose(Gibco 11965) +50ml FBS (Mediatech 35-011-CV) + 5ml Pen-Strep (Gibco 15140-122)+5ml Glutamine (Gibco 250303)) on plates coated with 0.1% gelatin.

NPCs were cultures on poly-L-ornithine (0.02 mg/ml) and laminin (5 ug/ml) (Sigma)-coated plates in NPC base media (DMEM:F12 + Glutamax, 0.5x N2, 0.5x B27, Pen/Strep (all Gibco)) + 20 ng/ml FGF. Culture medium was changed three times weekly. NPCs were passaged with Accutase.

To differentiate NPCs to Neurons, NPCs were grown to confluence, after which FGF was withdrawn from the NPC base culture media. Media was changed twice weekly for differentiation NPCs.

HEK Cell Culture

HEK293T cells were obtained from ATCC (ATCC, CRL-3216). HEK cells were expanded on uncoated 10 cm plates in MEF media. HEK cells were passaged with

trypsin. HEK cell transfections were performed with Effectene Transfection Reagent kit using the manufacturer instructions (Qiagen 301425)

Drug treatments

Compounds used are: Atorvastatin calcium salt (Sigma, PZ001), Simvastatin (Sigma, S6196), Mevalonolactone (Mevalonic Acid) (Sigma, M4777), YM-53601 (Cayman Chemicals, 18113), Avasimibe (Sigma, PZ0190-5MG). Compound E (Calbiochem CAS 209986-17-4), BACE1 inhibitor (BIV) (Calbiochem CAS 797035-11-1)

Aβ, sAPPβ, and sAPPα MSD-ECL measurements

For MSD-ECL measurements of conditioned media from iPSC derived neurons, neurons were replated after 3 weeks of differentiation into 96 wells (2×10^5 living cells/well). Replated neurons were cultured for 2 weeks in 200 ul NPC base + BDNF/GDNF/cAMP. After 2 weeks, media was removed and fresh media (200 ul NPC base + BDNF/GDNF/cAMP) containing the tested compounds was added. The conditioned culture media was harvested from cells at indicated time points.

For MSD-ECL measurements of conditioned media from HEK cells, HEK cells were plated on 12 well plates coated with Poly-L-Lysine (2×10^5 living cells/well) in the indicated drug treatment. On the second day, media was removed, the cells were washed once with PBS and media was replaced with fresh dilutions of the indicated treatment and cells were transfected. Media was harvested for analysis at indicated time points (typically 16-24 hours post-transfection)

For all Aβ measurements, 25 µL of the culture media was run on a V-PLEX Aβ Peptide Panel 1 (6E10) (K150SKE) kit. For all sAPP measurements, 25ul of the culture media was run on a MULTI-SPOT sAPPα/sAPPβ plate (K15120E) All kits are from Mesoscale discovery. Measurements were performed on the MSD imager MESO QuickPlex SQ 120.

Microscopy

Replated CV4a neurons (Derived from WT CVB iPSCs) on MatTek glass bottom dishes were treated with 10 μM Atorvastatin and DMSO for 5 days. Following treatment, cells were transfected with either APPvn/APPvc/sol. mCherry or APPvn/BACE1vc/sol. mCherry plasmids using Lipofectamine 2000 for 16-18 h. Cells were fixed in 4 % PFA and permeabilized using Triton-X100. Immunostaining was performed using the MAP2 antibody.

Imaging and subsequent data analyses were done blinded. Images were acquired using an Olympus IX81 inverted epifluorescence microscope. *Z*-stack images were captured using a 100× objective (imaging parameters: 0.4 µm *z*-step, 400-800 ms exposure, and 1×1 binning). Neurons - double-positive for MAP2 and sol. mCherry were selected for imaging. Captured images were deconvolved and subjected to a maximum intensity projection using Metamorph Software (Molecular Devices). Region of interest (ROI) was placed around the cell body using MAP2 as a marker. The venus punta were thresholded to the same scale on the processed ROIs.

Western blots

For Western blots of iPSC derived neurons, neurons were replated after 3 weeks of differentiation onto 24 well plates ($2x10^6$ live cells/well). Replated neurons were cultured for 2 weeks in 200 ul NPC base + BDNF/GDNF/cAMP. After 2 weeks, half of the media was removed and fresh media (500 ul NPC base + BDNF/GDNF/cAMP) containing the tested compounds was added. The cells were harvested for western blot at indicated time points.

For western blots of HEK cell lysates, HEK cells were plated on 12 well plates coated with Poly-L-Lysine (2×10^5 living cells/well) in the indicated drug treatment. On the second day, media was removed, the cells were washed once with PBS and media was replaced with fresh dilutions of the indicated treatment and cells were transfected. Cells were harvested for western blot at indicated time points (typically 16-24 hours post-transfection)

Cells were lysed in RIPA Lysis Buffer (Millipore) with protease inhibitors (Halt) and phosphatase inhibitors (Halt 1861277). Protein concentrations were measured using a Pierce BCA Protein Assay Kit (Thermo Fisher) and samples were diluted to equal protein concentrations. 4x LDS Sample buffer (Invitrogen NP0007) + β-mercaptoethanol was added to the lysate to generate a final concentration of 1x sample buffer + 5% β-mercaptoethanol. Samples were boiled at 100°C for 5 minutes.

Equal sample volumes were run on NuPAGE 4%–12% Bis-Tris gels (Invitrogen). Gels were transferred to PVDF membranes then blocked for one hour at room temperature in Odyssey Blocking Buffer (LI-COR). Blots were probed overnight

at 4°C using the indicated primary antibody. The next day, blots were probed with IRDye secondary antibodies (LI-COR) at 1:5,000. Images were acquired using a LICOR Odyssey imager. Bands were quantified using LICOR Image Studio Lite software.

Antibodies used were: anti-Actin (1:10,000; EMD Millipore), anti-BACE1 EPR3956 (1:1000; Abcam ab108394), anti-PS1 263-378 (1:500; Millipore MAB5232), anti-PS2 EP1515Y (1:1000; Abcam ab51249), anti-APP C-Terminal 751-770 (1:500; Millipore 171610)

Flow Cytometry Bimolecular Fluorescence Complementation Assay

For flow cytometry analysis of transfected HEK cells, HEK cells were plated on 12 well plates coated with Poly-L-Lysine (2×10^5 living cells/well) in the indicated drug treatment. On the second day, media was removed, the cells were washed once with PBS and media was replaced with fresh dilutions of the indicated treatment and cells were transfected. Cells were harvested for flow cytometry at indicated time points (typically 16-24 hours post-transfection).

To harvest cells for flow cytometry analysis, HEK cells were washed once in PBS, then incubated with trypsin to dissociate cells. Trypsinized cells were washed with FACS wash buffer () and filtered through 100um filters. Cells were centrifuged to pellet cells. Cell pellets were resuspended in FACS wash buffer and filtered through 70um filters.

Cells were analyzed on a BD FACSAria II flow cytometer.

Plasmids

APPvn, BACE1vc, and APPStop40vn plasmids were reported in Das et al., 2016 (42). C99 fragment was PCR amplified using human full-length APP as a template, and subsequently subcloned to generate C99vc. Plasmids carrying human PS1 and PS2 were generously gifted by Dr. Wim Annaert and Dr. Ragna Sannerud and were used to PCR amplify and subclone to generate PS1vc and PS2vc. All the plasmids were sequence verified.

Statistical Analysis

Statistical analyses were performed using Graphpad Prism software. Statistical analyses comparing multiple groups were performed using a one-way ANOVA with a Tukey's multiple comparison test. Statistical analysis comparing two groups were calculated using two-tailed unpaired t-tests. Data are depicted with bar graphs of the mean ± SEM of all values. Significance was defined as $p < 0.05$(**** $p < 0.0001$,*** $p < 0.001$, ** $p < 0.01$, $^{*}p < 0.05$). n indicates measurements from independent wells.

ACKNOWLEDGEMENTS

We would like to thank Wim Annaert and Ragna Sannerud for generously providing us with PS1 and PS2 plasmids.

We thank Cody Fine and Jesus Olvera at the Sanford Consortium Stem Cell Core for helpful advice on flow cytometry data analysis.

R.v.d.K. was supported by an Alzheimer Netherlands Fellowship (WE.15-2013-01) and an ERC Marie Curie International Outgoing fellowship (622444, APPtoTau). V.F.L. was supported by an NIH T32 training grant (5T32AG000216-24).

This work is supported by NIA 1RF1AG048083-01 and CIRM RB5-07011 grants to L.S.G.

Chapter 3, in full, is currently being prepared for submission for publication of the material. Langness, V. F., Kant, R. van der, Das, U., Wang, L., Chaves, R., Young, J., Goldstein, L. S. B. The dissertation author was the primary investigator and author of this material.

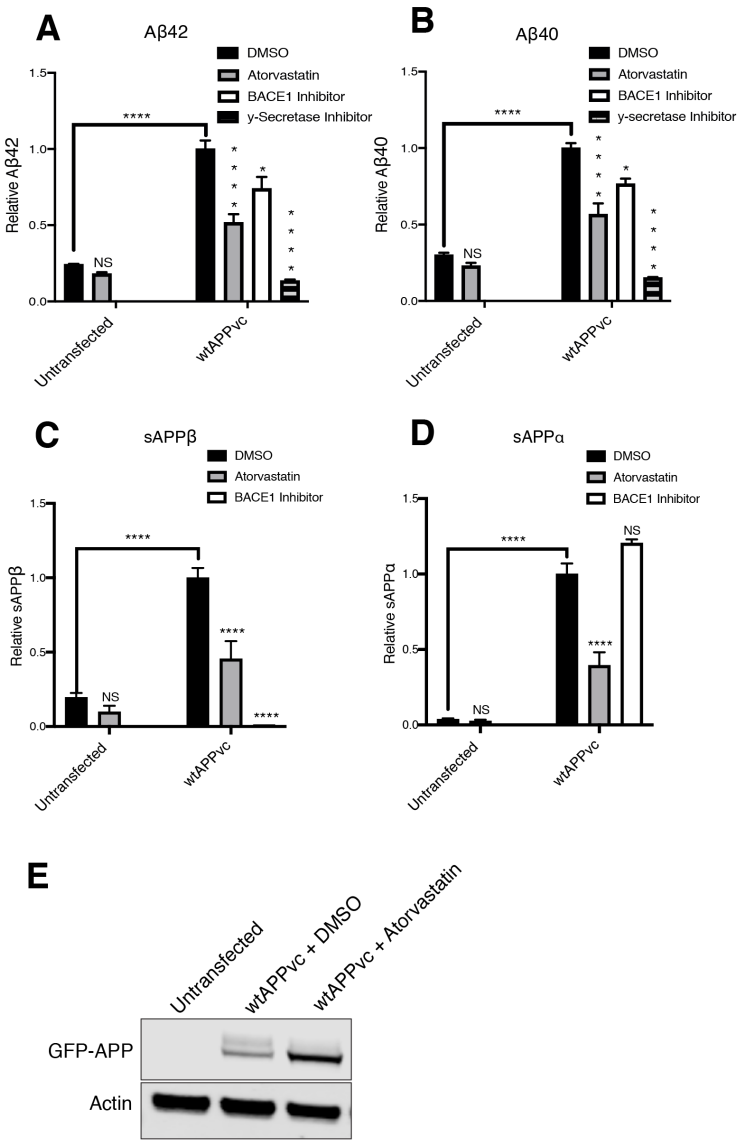

Figure 3.1: Atorvastatin reduces processing of transfected APP in HEK cells (A-E) HEK cells were plated in DMSO, 10 μM atorvastatin, 4 μM BACE1 inhibitor (BIV), or 200 nM y-secretase inhibitor (Compound E) and then transiently transfected 24 hours later. Cells and conditioned media were collected 16 hours after transfection. (A) Aβ42 levels (B) Aβ40 levels (C) sAPPβ levels and (D) sAPPα levels from conditioned media were determined by MSD-ECL. (mean ± SEM, n ≥ 3) (E) Levels of flAPP were determined by western blot.

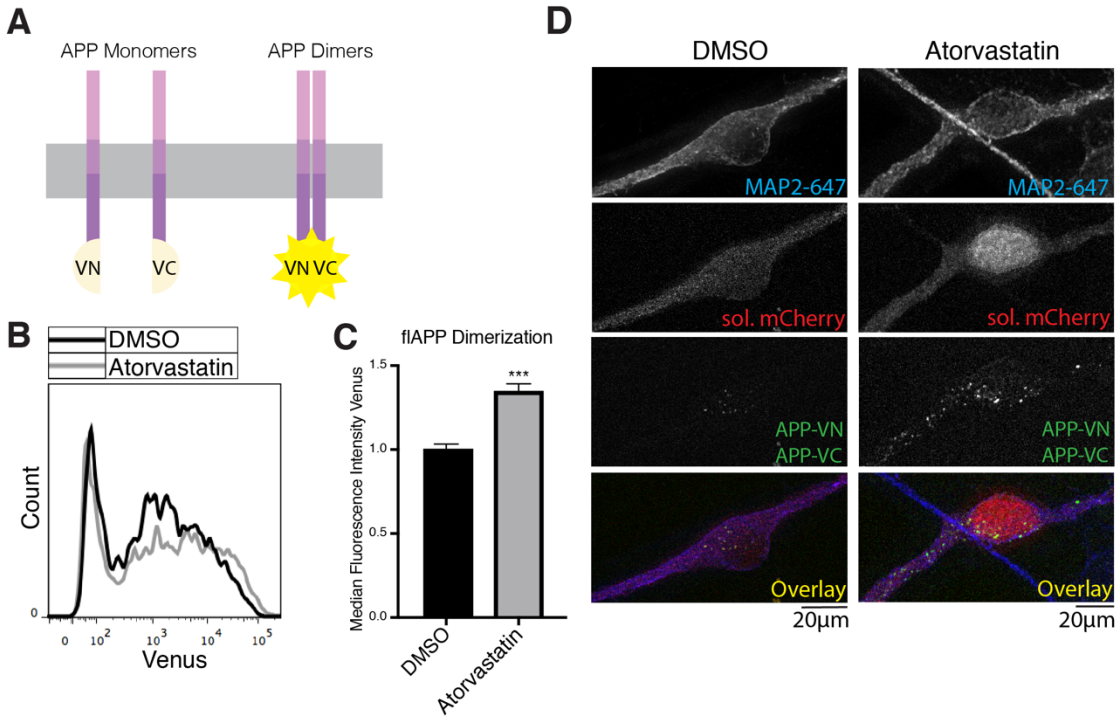

Figure 3.2: Atorvastatin increases flAPP dimerization (A) Two flAPP constructs were tagged to complementary n-terminus (vn) or c-terminus (vc) fragments of Venus fluorescent protein (VFP). Dimerization of APP gives rise to Venus fluorescence. (B-C) HEK cells were plated in DMSO or 10 µM atorvastatin and then transiently transfected with wtAPPvn, wtAPPvc, and mCherry 24 hours later. Cells were analyzed 16 hours after transfection. (B) Histograms showing flow cytometry analysis of dimerization (Venus median fluorescence intensity) (C) Quantification of flow cytometry analysis of APP dimerization (Venus median fluorescence intensity) (mean ± SEM, n ≥ 3) (D) iPSC derived WT neurons were plated in DMSO or 10 µM atorvastatin. Four days later, neurons were transiently transfected with wtAPPvn, wtAPPvc, and mCherry. Cells were fixed, permeabilized, and stained with MAP2 16 hours after transfection. Imaging and image processing were performed blind.

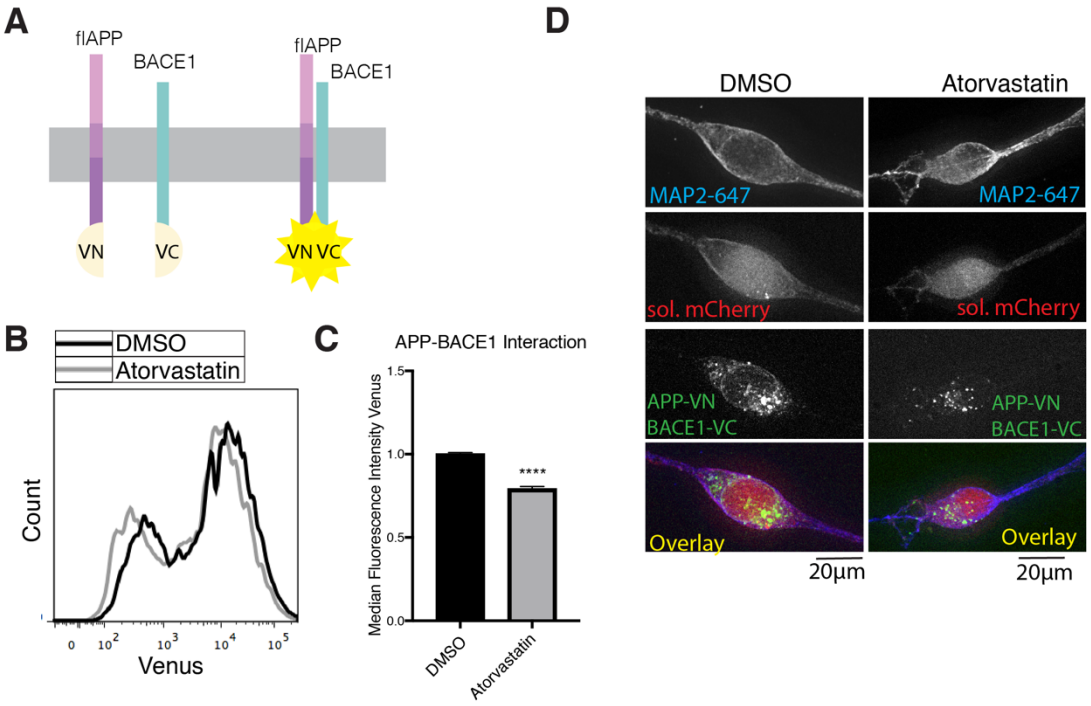

Figure 3.3: Atorvastatin decreases flAPP-BACE1 interaction (A) A BACE1 construct was tagged to the c-terminus (vc) fragment of Venus fluorescent protein (VFP) and co-transfected with an APPvn plasmid. BACE1-flAPP interaction gives rise to Venus fluorescence. (B&C) HEK cells were plated in DMSO or 10 µM Atorvastatin and then transiently transfected 24 hours later. Cells were analyzed 16 hours after transfection. (B) Histograms showing flow cytometry analysis of BACE1-flAPP interaction (Venus median fluorescence intensity). (C) Quantification of flow cytometry analysis of BACE1-flAPP interaction (Venus median fluorescence intensity) (mean ± SEM, n ≥ 3). (D) iPSC derived WT neurons were plated in DMSO or 10 µM atorvastatin. Four days later, neurons were transiently transfected with wtAPPvn, BACE1vc, and mCherry. Cells were fixed, permeabilized, and stained with MAP2 16 hours post transfection. Imaging and image processing were performed blind.

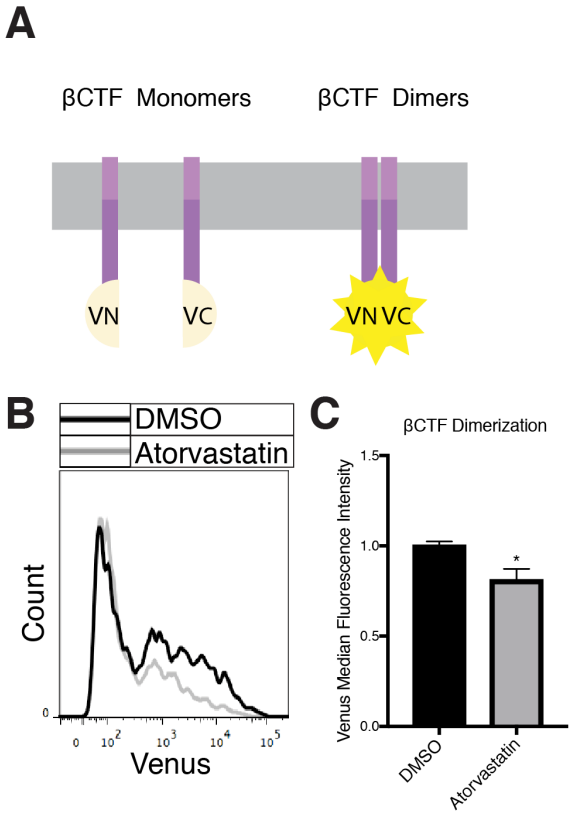

Figure 3.4: Atorvastatin decreases βCTF dimerization (A) Two βCTF constructs were tagged to complementary n-terminus (vn) or c-terminus (vc) fragments of Venus fluorescent protein (VFP). Dimerization of βCTF gives rise to Venus fluorescence. (B-C) HEK cells were plated in DMSO or 10 μM atorvastatin. 24 hours later, cells were transiently transfected with βCTFvn, βCTFvc, and mCherry. Cells were analyzed 16 hours after transfection. (B) Histograms showing flow cytometry analysis of dimerization (Venus median fluorescence intensity) (C) Quantification of flow cytometry analysis of βCTF dimerization (Venus median fluorescence intensity) (mean ± SEM, n ≥ 3).

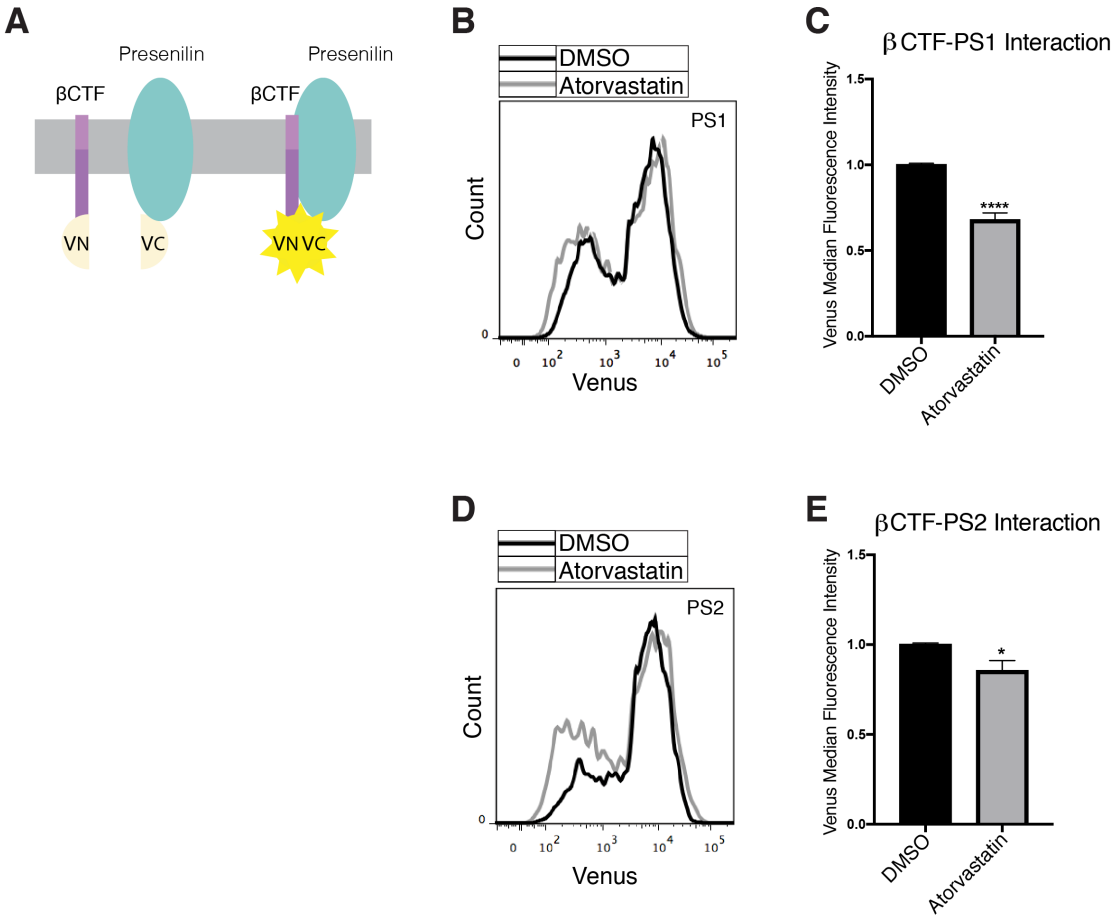

Figure 3.5: Atorvastatin decreases βCTF-PS1 and βCTF-PS2 interaction (A) PS1 and a PS2 constructs were each tagged to the c-terminus (vc) fragment of Venus fluorescent protein (VFP). A βCTF plasmid was tagged to the complementary Venus n-terminus (vn). PS1vc or PS2vc was co-transfected with βCTFvn. PS1-βCTF and PS2-βCTF interaction gives rise to Venus fluorescence. (B-E) HEK cells were plated in DMSO or 10 μM Atorvastatin and then transiently transfected 24 hours later. Cells were analyzed 16 hours after transfection. (B) Histograms showing flow cytometry analysis of PS1- βCTF interaction (Venus median fluorescence intensity). (C) Quantification of flow cytometry analysis of PS1-βCTF interaction (Venus median fluorescence intensity). (mean ± SEM, n ≥ 3) (D) Histograms showing flow cytometry analysis of PS2-βCTF interaction (Venus median fluorescence intensity). (E) Quantification of flow cytometry analysis of PS2-βCTF interaction (Venus median fluorescence intensity) (mean ± SEM, n ≥ 3).

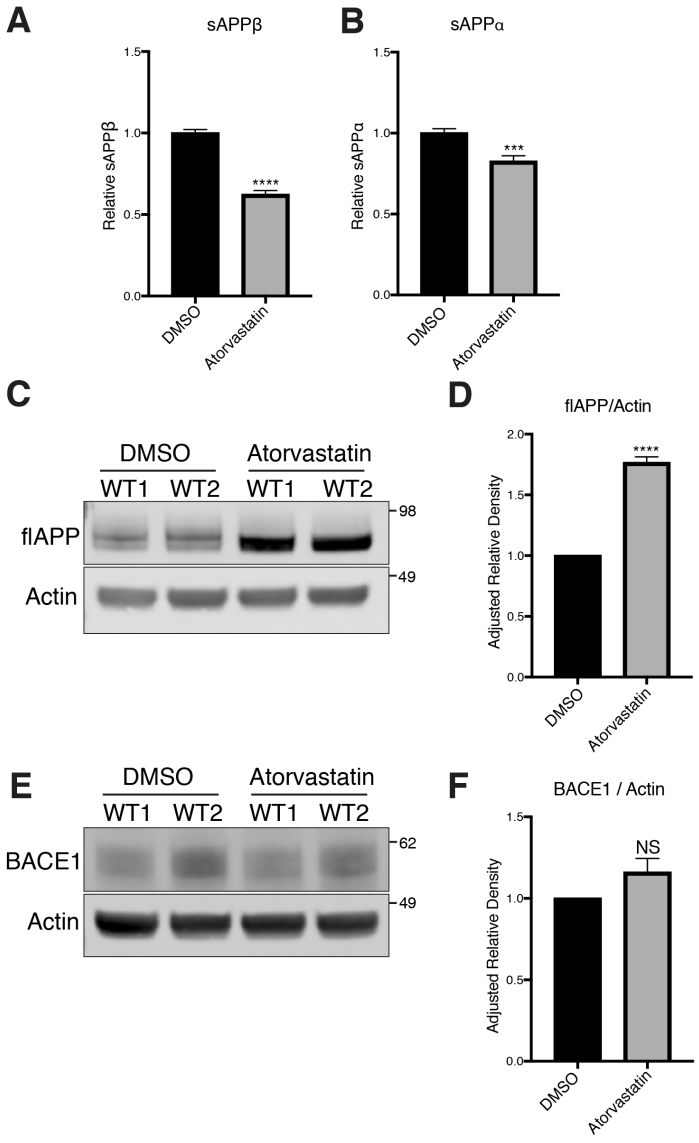

Figure 3.6: Atorvastatin treatment causes a reduction of sAPPβ and sAPPα, accumulation of flAPP and but no change in BACE1 levels (A-F) WT neurons were treated with DMSO or 10 μM Atorvastatin for 5 days. Levels of (A) sAPPβ and (B) sAPPα were determined by MSD-ECL. Levels of (C) flAPP were determined by western blot and quantified in (D) Levels of (E) BACE1 were determined by western blot and quantifed in (F) (mean ± SEM, n ≥ 3).

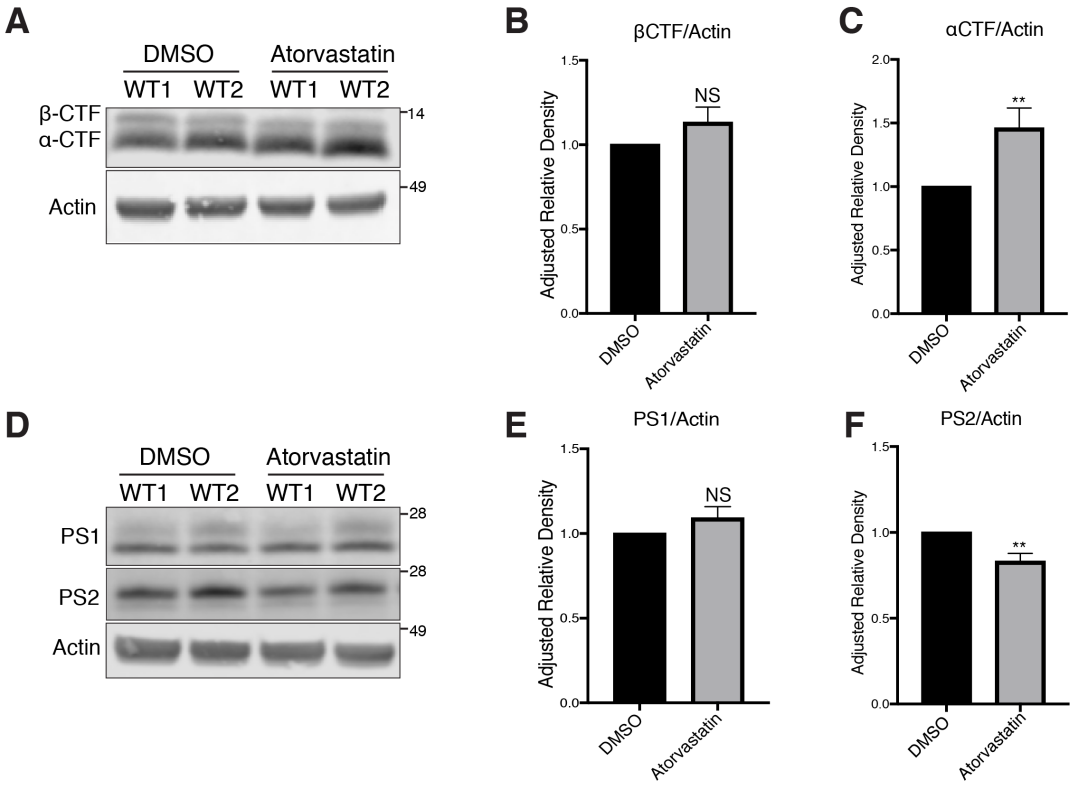

Figure 3.7: Atorvastatin treatment causes accumulation of αCTF and no change in βCTF (A-E) WT neurons were treated with DMSO or 10 μM Atorvastatin for 5 days. (A) Levels of αCTF and βCTF were determined by western blot (B) quantification of βCTF (C) quantification of αCTF (D) Levels of PS1 and PS2 were determined by western blot (E) quantification of PS1 (F) quantification of PS2 (mean ± SEM, n ≥ 3).

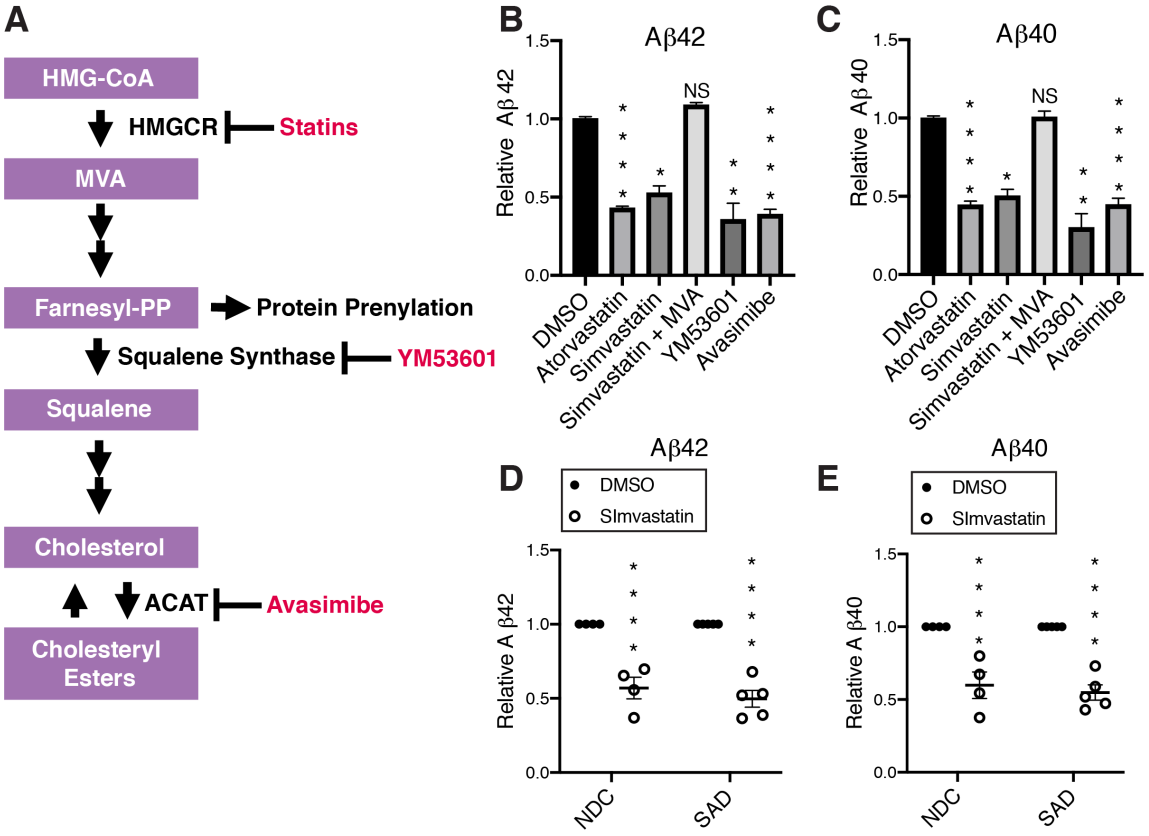

Figure 3.8: Cholesteryl ester lowering drugs cause a reduction of secreted Aβ42 and Aβ40 (A) Diagram of the mevalonate pathway and compounds used in this study (B&C) APP^{dp}1-6 mixed culture neurons were treated with inhibitors of specific steps in the mevalonate pathway; atorvastatin (10 μM), simvastatin (10 μM), YM-53601 (10 μM), avasimibe (10 μM) for 5 days. For indicated conditions, mevalonate (MVA, 0.5mM) was added to the media at t=0. (B) Aβ42 levels and (C) Aβ40 levels were determined by MSD-ECL (mean ± SEM, n ≥ 3). (D-E) Effect of 5 day simvastatin (10 μM) treatment on (D) Aβ42 levels (E) Aβ40 levels in iPSC derived neurons from SAD (sporadic AD) and NDC (non-demented control) subjects. Each dot represents an average of n ≥ 3 measurements from one individual (NDC n=4 individuals, SAD n=5 individuals) (mean ± SEM)

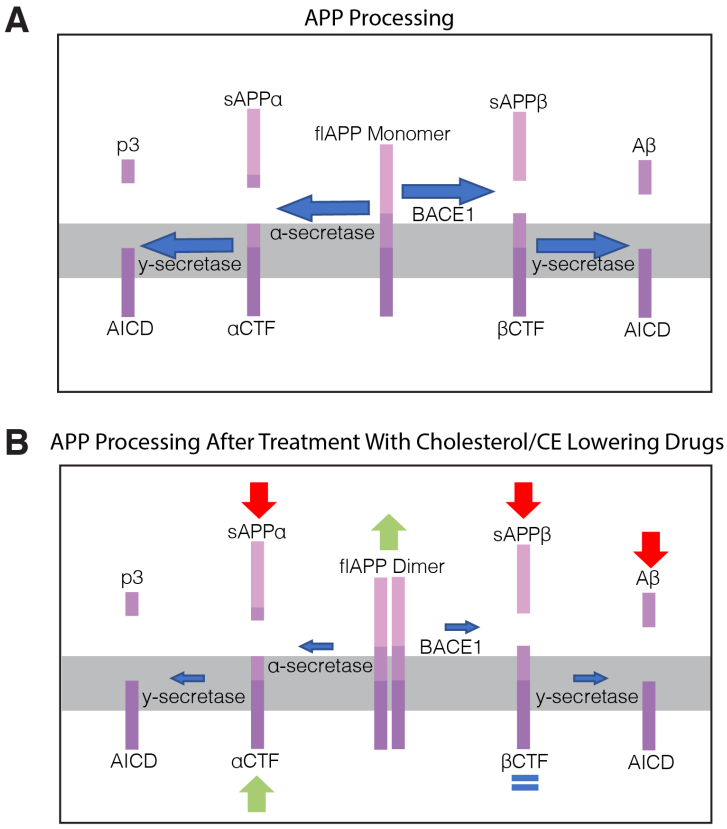

Figure 3.9: Model: Cholesterol/CE lowering drugs block APP processing by promoting dimerization (A) Diagram showing canonical APP processing pathways (B) Diagram summarizing APP processing changes observed after statin treatment. flAPP dimerizes and accumulates while sAPPα and sAPPβ decrease. These changes are accompanied by reduced APP-BACE1 interaction, suggesting reduced β-secretase cleavage. αCTF accumulates and βCTF remains unchanged while Aβ secretion is reduced. These changes are accompanied by reduced PS1-βCTF and PS2-βCTF interaction suggesting reduced y-secretase processing.

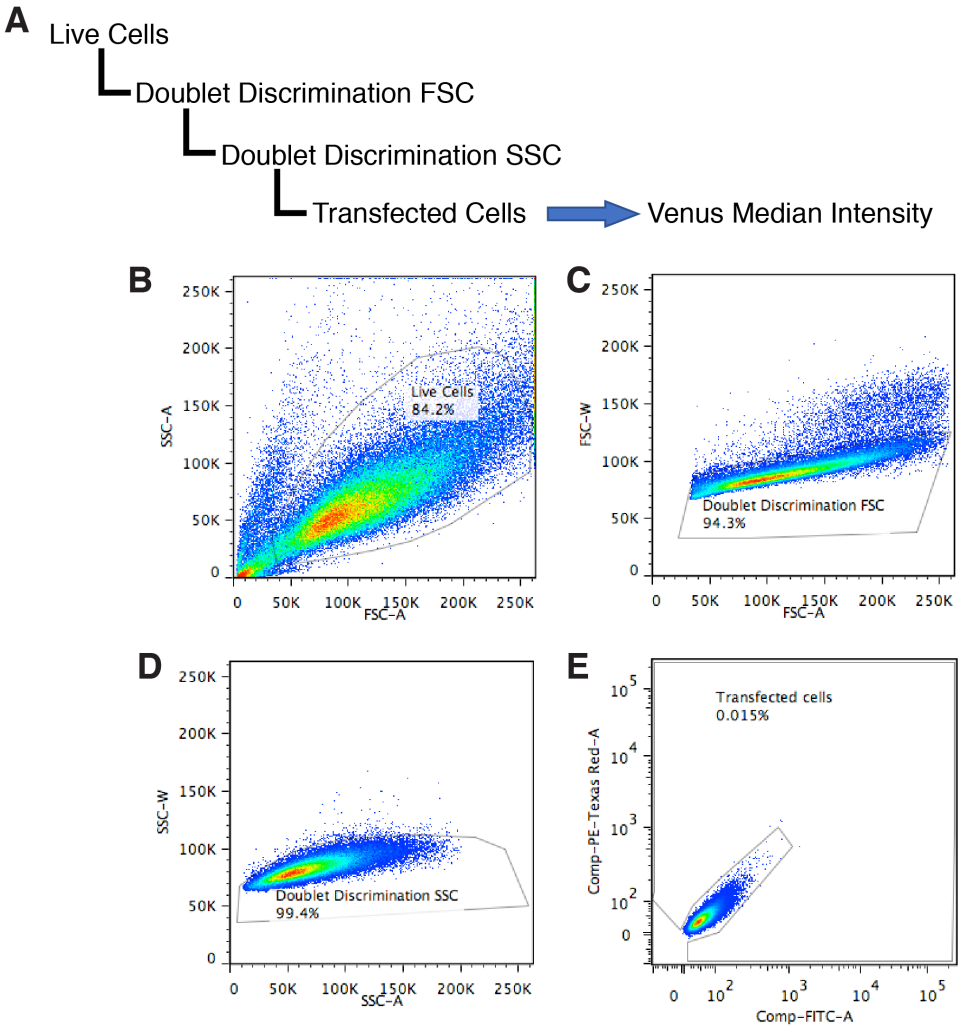

Supplemental Figure 3.1: Representative flow cytometry gating scheme (A) Hierarchy showing the gating scheme used for analysis of all flow cytometry data in this manuscript. (B) Representative live cell discrimination gate (C) Representative FSC doublet discrimination gate (D) Representative SSC doublet discrimination gate (E) Representative untransfected control sample which is used to set the transfected cell gate.

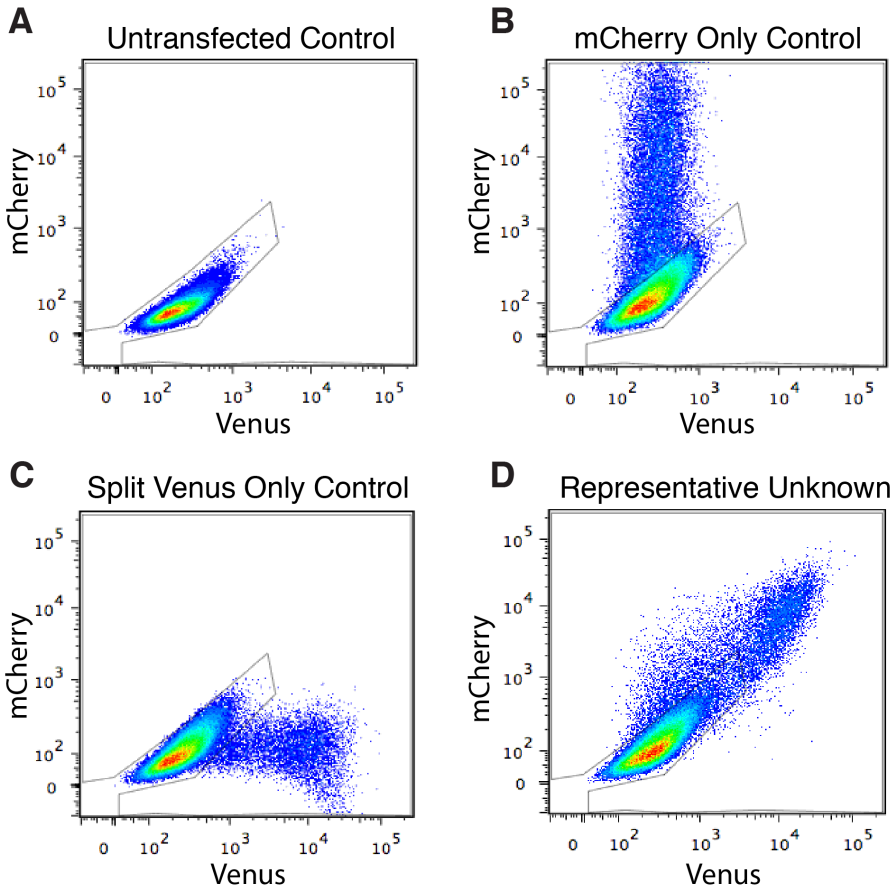

Supplemental Figure 3.2: Flow cytometry compensation controls (A-C) All flow cytometry experiments were run with compensation controls. The compensation controls were used to set up compensation in such a way that cells expressing only Venus showed signal only on the Venus axis and cells expressing only mCherry showed signal only on the mCherry axis. The unstained control was used to gate out untransfected cells. Compensation controls are all shown as dot plots along with the transfected cell gate. (A) Representative untransfected control (B) Representative mCherry only control (C) Representative Venus only control (transfected with a split Venus pair) (D) Representative unknown sample transfected with both mCherry and a split Venus pair.

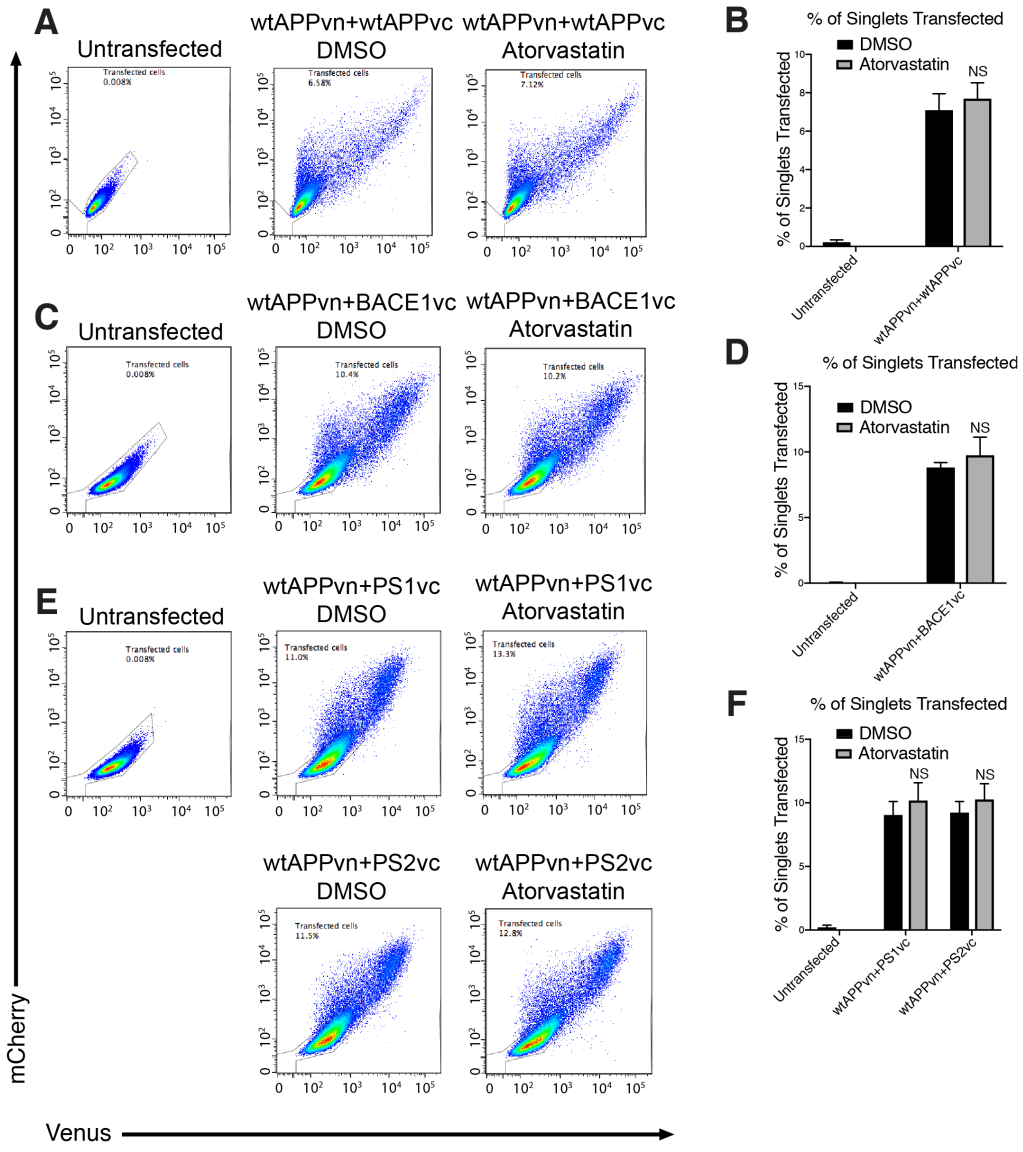

Supplemental Figure 3.3: Atorvastatin does not affect transfection efficiency HEK cells were plated in DMSO or 10 µM atorvastatin and then transiently transfected 24 hours later. Cells were analyzed 16 hours after transfection. (A,C,E) Dot plots showing (A) Untransfected controls and wtAPPvc+wtAPPvn+mCherry transfected cells treated with DMSO or atorvastatin (C) Untransfected controls, and BACE1vc+wtAPPvn+mCherry transfected cells treated with DMSO or Atorvastatin) (D) Untransfected controls, and PS1vc or PS2vc +wtAPPvn+mCherry transfected cells treated with DMSO or Atorvastatin (as indicated in the figure). Each plot shows the transfected cell gate. (B,D,F) Quantification of the percentage of transfected singlets as a measure of transfection efficiency for each condition.

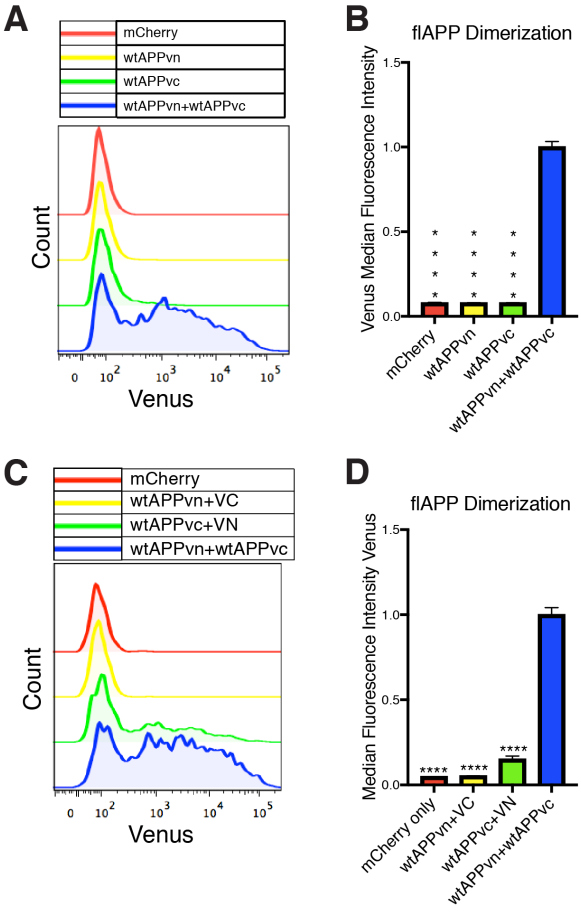

Supplemental Figure 3.4: Validation of APP dimerization split Venus assay
(A-D) HEK cells were plated in DMSO and then transiently transfected 24 hours later. Cells were analyzed 16 hours after transfection. (A&B) HEK cells were transfected with mCherry in addition to the indicated construct to determine whether each half of the split Venus dimer pairs fluoresce on their own (C&D) HEK cells were transfected with mCherry in addition to the indicated constructs to determine whether each split Venus dimer pair non-specifically interacts with co-transfected VN or VC protein. (A&C) Histograms showing flow cytometry analysis of dimerization (Venus median fluorescence intensity). (B&D) Quantification of flow cytometry analysis of APP dimerization (Venus median fluorescence intensity).

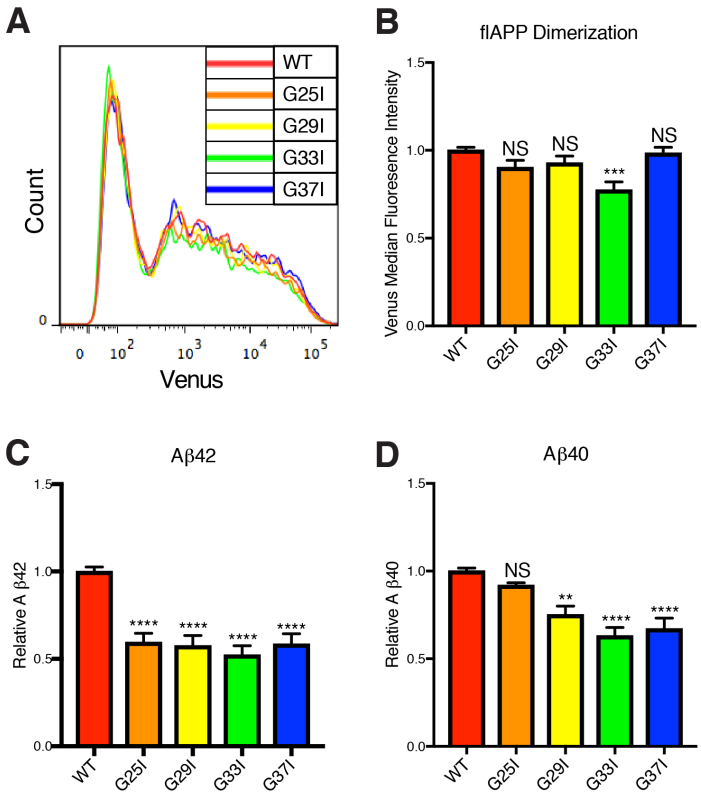

Supplemental Figure 3.5: Mutations in the APP GXXXG motifs reveal amino acids that mediate dimerization. Mutations in this region decrease Aβ42 and Aβ40 in a dimerization independent manner. (A-D) Site directed mutagenesis was used to mutate each of the wtAPPvn and wtAPPvc plasmids within each of the GXXXG motifs. HEK cells were co-transfected with an APPvn +APPvc split Venus pair which both encode the indicated mutation along with mCherry for cell selection. Cells and conditioned media were harvested for analysis 16 hours post transfection (A) Histograms showing flow cytometry analysis of dimerization (Venus median fluorescence intensity) (B) Quantification of flow cytometry analysis of APP dimerization (Venus median fluorescence intensity) (mean ± SEM, n ≥ 3) (C) Aβ42 levels and (D) Aβ40 levels from conditioned media were determined by MSD-ECL (mean ± SEM, n ≥ 3).

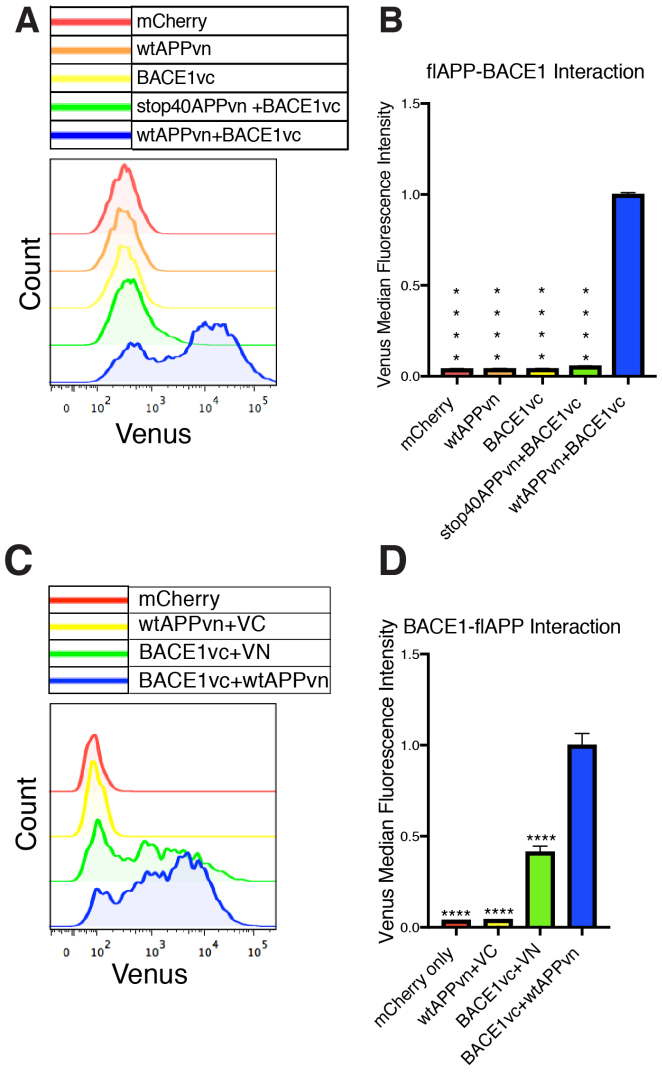

Supplemental Figure 3.6: Validation of flAPP-BACE1 split Venus interaction assay(A-D) HEK cells were plated in DMSO and then transiently transfected 24 hours later. Cells were analyzed 16 hours after transfection. (A&B) HEK cells were transfected with mCherry in addition to the indicated construct to determine whether each half of the split Venus APP-BACE1 pair fluoresce on their own (C&D) HEK cells were transfected with mCherry in addition to the indicated constructs to determine whether each split Venus APP-BACE1 pair non-specifically interacts with co-transfected VN or VC protein. (A&C) Histograms showing flow cytometry analysis of APP-BACE1 interaction (Venus median fluorescence intensity). (B&D) Quantification of flow cytometry analysis of APP-BACE1 interaction (Venus median fluorescence intensity) (mean ± SEM, n ≥ 3).

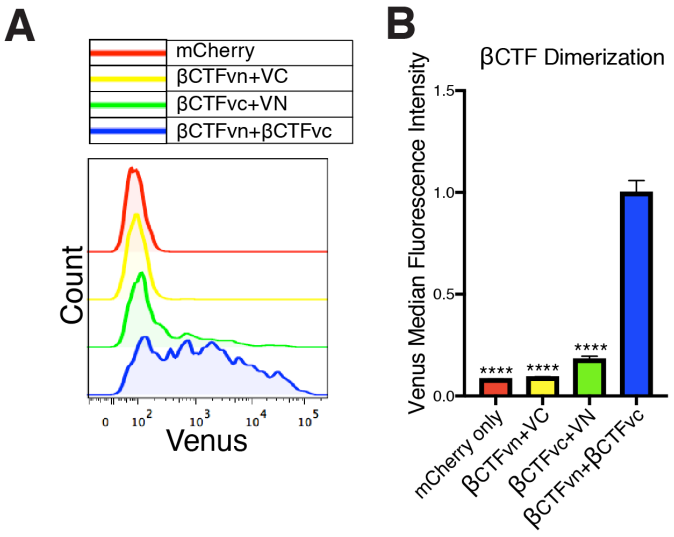

Supplemental Figure 3.7: Validation of βCTF **dimerization split Venus assay**
(A&B) HEK cells were plated in DMSO and then transiently transfected 24 hours later. Cells were analyzed 16 hours after transfection. HEK cells were transfected with mCherry in addition to the indicated constructs to determine whether each split Venus βCTF dimer pair non-specifically interacts with co-transfected VN or VC protein. (A) Histograms showing flow cytometry analysis of βCTF dimerization (Venus median fluorescence intensity). (B) Quantification of flow cytometry analysis of βCTF dimerization (Venus median fluorescence intensity) (mean ± SEM, n ≥ 3).

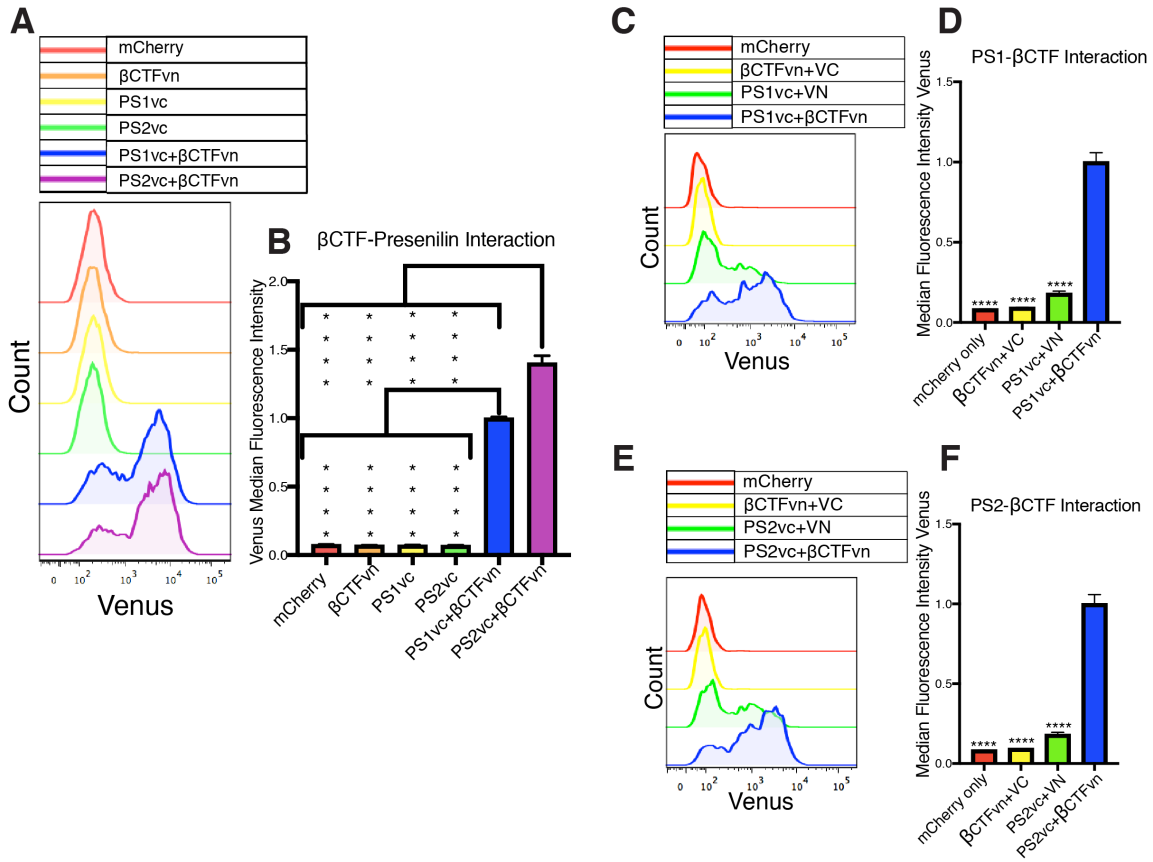

Supplemental Figure 3.8: Validation of βCTF-PS1 and βCTF-PS2 split Venus interaction assay (A-F) HEK cells were plated in DMSO and then transiently transfected 24 hours later. Cells were analyzed 16 hours after transfection. (A&B) HEK cells were transfected with mCherry in addition to the indicated construct to determine whether each half of the split Venus APP-PS1 or APP-PS2 pair fluoresce on their own (C-F) HEK cells were transfected with mCherry in addition to the indicated constructs to determine whether each split Venus pair non-specifically interacts with co-transfected VN or VC protein. (A,C,E) Histograms showing flow cytometry analysis of PS1-βCTF or PS2-βCTF interaction (Venus median fluorescence intensity). (B,D,F) Quantification of flow cytometry analysis of PS1-βCTF or PS2-βCTF interaction (Venus median fluorescence intensity) (mean ± SEM, n ≥ 3).

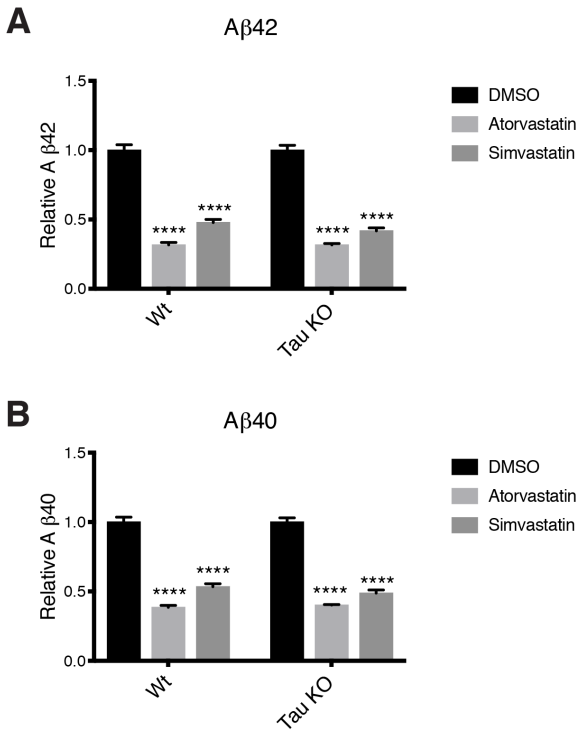

Supplemental Figure 3.9: Statins reduce Aβ42 and Aβ40 secretion in both WT and Tau KO human iPSC derived neurons WT or Tau KO neurons were treated with DMSO or 10 μM Atorvastatin for 5 days._(A) Aβ42 levels and (B) Aβ40 levels were determined by MSD-ECL (mean ± SEM, n ≥ 3).

REFERENCES

1. O'Brien, R. J., and Wong, P. C. (2011) Amyloid Precursor Protein Processing and Alzheimer's Disease. *Annu Rev Neurosci*. **34**, 185–204

2. Hardy, J. A., and Higgins, G. A. (1992) Alzheimer's disease: the amyloid cascade hypothesis. *Science*. **256**, 184–185

3. Hardy, J., and Allsop, D. (1991) Amyloid deposition as the central event in the aetiology of Alzheimer's disease. *Trends Pharmacol. Sci.* **12**, 383–388

4. Hardy, J., and Selkoe, D. J. (2002) The amyloid hypothesis of Alzheimer's disease: progress and problems on the road to therapeutics. *Science*. **297**, 353–356

5. Selkoe, D. J. (1991) The molecular pathology of Alzheimer's disease. *Neuron*. **6**, 487–498

6. Beyreuther, K., and Masters, C. L. (1991) Amyloid precursor protein (APP) and beta A4 amyloid in the etiology of Alzheimer's disease: precursor-product relationships in the derangement of neuronal function. *Brain Pathol.* **1**, 241–251

7. Karran, E., and De Strooper, B. (2016) The amyloid cascade hypothesis: are we poised for success or failure? *J. Neurochem.* **139 Suppl 2**, 237–252

8. Bergmans, B. A., and De Strooper, B. (2010) γ-secretases: from cell biology to therapeutic strategies. *The Lancet Neurology*. **9**, 215–226

9. Sannerud, R., Esselens, C., Ejsmont, P., Mattera, R., Rochin, L., Tharkeshwar, A. K., De Baets, G., De Wever, V., Habets, R., Baert, V., Vermeire, W., Michiels, C., Groot, A. J., Wouters, R., Dillen, K., Vints, K., Baatsen, P., Munck, S., Derua, R., Waelkens, E., Basi, G. S., Mercken, M., Vooijs, M., Bollen, M., Schymkowitz, J., Rousseau, F., Bonifacino, J. S., Van Niel, G., De Strooper, B., and Annaert, W. (2016) Restricted Location of PSEN2/γ-Secretase Determines Substrate Specificity and Generates an Intracellular Aβ Pool. *Cell*. **166**, 193–208

10. Wolozin, B., Kellman, W., Ruosseau, P., Celesia, G. G., and Siegel, G. (2000) Decreased prevalence of Alzheimer disease associated with 3-hydroxy-3-methyglutaryl coenzyme A reductase inhibitors. *Arch. Neurol.* **57**, 1439–1443

11. Jick, H., Zornberg, G. L., Jick, S. S., Seshadri, S., and Drachman, D. A. (2000) Statins and the risk of dementia. *Lancet*. **356**, 1627–1631

12. Zissimopoulos, J. M., Barthold, D., Brinton, R. D., and Joyce, G. (2017) Sex and Race Differences in the Association Between Statin Use and the Incidence of Alzheimer Disease. *JAMA Neurol*. **74**, 225–232

13. Haag, M. D. M., Hofman, A., Koudstaal, P. J., Stricker, B. H. C., and Breteler, M. M. B. (2009) Statins are associated with a reduced risk of Alzheimer disease regardless of lipophilicity. The Rotterdam Study. *J. Neurol. Neurosurg. Psychiatry*. **80**, 13–17

14. Li, G., Shofer, J. B., Rhew, I. C., Kukull, W. A., Peskind, E. R., McCormick, W., Bowen, J. D., Schellenberg, G. D., Crane, P. K., Breitner, J. C. S., and Larson, E. B. (2010) Age-varying association between statin use and incident Alzheimer's disease. *J Am Geriatr Soc*. **58**, 1311–1317

15. Lin, F.-C., Chuang, Y.-S., Hsieh, H.-M., Lee, T.-C., Chiu, K.-F., Liu, C.-K., and Wu, M.-T. (2015) Early Statin Use and the Progression of Alzheimer Disease. *Medicine (Baltimore)*. 10.1097/MD.0000000000002143

16. Feldman, H. H., Doody, R. S., Kivipelto, M., Sparks, D. L., Waters, D. D., Jones, R. W., Schwam, E., Schindler, R., Hey-Hadavi, J., DeMicco, D. A., Breazna, A., and LEADe Investigators (2010) Randomized controlled trial of atorvastatin in mild to moderate Alzheimer disease: LEADe. *Neurology*. **74**, 956–964

17. Sano, M., Bell, K. L., Galasko, D., Galvin, J. E., Thomas, R. G., van Dyck, C. H., and Aisen, P. S. (2011) A randomized, double-blind, placebo-controlled trial of simvastatin to treat Alzheimer disease. *Neurology*. **77**, 556–563

18. Santanello, N. C., Barber, B. L., Applegate, W. B., Elam, J., Curtis, C., Hunninghake, D. B., and Gordon, D. J. (1997) Effect of pharmacologic lipid lowering on health-related quality of life in older persons: results from the Cholesterol Reduction in Seniors Program (CRISP) Pilot Study. *J Am Geriatr Soc*. **45**, 8–14

19. Shepherd, J., Blauw, G. J., Murphy, M. B., Bollen, E. L. E. M., Buckley, B. M., Cobbe, S. M., Ford, I., Gaw, A., Hyland, M., Jukema, J. W., Kamper, A. M., Macfarlane, P. W., Meinders, A. E., Norrie, J., Packard, C. J., Perry, I. J., Stott, D. J., Sweeney, B. J., Twomey, C., Westendorp, R. G. J., and PROSPER study group. PROspective Study of Pravastatin in the Elderly at Risk (2002) Pravastatin in elderly individuals at risk of vascular disease (PROSPER): a randomised controlled trial. *Lancet*. **360**, 1623–1630

20. MRC/BHF Heart Protection Study of cholesterol lowering with simvastatin in 20 536 high-risk individuals: a randomised placebocontrolled trial (2002) *The Lancet*. **360**, 7–22

21. Schultz, B. G., Patten, D. K., and Berlau, D. J. (2018) The role of statins in both cognitive impairment and protection against dementia: a tale of two mechanisms. *Transl Neurodegener*. 10.1186/s40035-018-0110-3

22. Simons, M., Keller, P., De Strooper, B., Beyreuther, K., Dotti, C. G., and Simons, K. (1998) Cholesterol depletion inhibits the generation of beta-amyloid in hippocampal neurons. *Proc. Natl. Acad. Sci. U.S.A.* **95**, 6460–6464

23. Kojro, E., Gimpl, G., Lammich, S., Marz, W., and Fahrenholz, F. (2001) Low cholesterol stimulates the nonamyloidogenic pathway by its effect on the alpha - secretase ADAM 10. *Proc. Natl. Acad. Sci. U.S.A.* **98**, 5815–5820

24. Ostrowski, S. M., Wilkinson, B. L., Golde, T. E., and Landreth, G. (2007) Statins Reduce Amyloid-β Production through Inhibition of Protein Isoprenylation. *J. Biol. Chem.* **282**, 26832–26844

25. Rossjohn, J., Cappai, R., Feil, S. C., Henry, A., McKinstry, W. J., Galatis, D., Hesse, L., Multhaup, G., Beyreuther, K., Masters, C. L., and Parker, M. W. (1999) Crystal structure of the N-terminal, growth factor-like domain of Alzheimer amyloid precursor protein. *Nat Struct Mol Biol*. **6**, 327–331

26. Scheuermann, S., Hambsch, B., Hesse, L., Stumm, J., Schmidt, C., Beher, D., Bayer, T. A., Beyreuther, K., and Multhaup, G. (2001) Homodimerization of Amyloid Precursor Protein and Its Implication in the Amyloidogenic Pathway of Alzheimer's Disease. *J. Biol. Chem.* **276**, 33923–33929

27. Beher, D., Hesse, L., Masters, C. L., and Multhaup, G. Regulation of Amyloid Protein Precursor (APP) Binding to Collagen and Mapping of the Binding Sites on APP and Collagen Type I. *Journal of Biological Chemistry*. 10.1074/jbc.271.3.1613

28. Russ, W. P., and Engelman, D. M. (2000) The GxxxG motif: A framework for transmembrane helix-helix association11Edited by G. von Heijne. *Journal of Molecular Biology*. **296**, 911–919

29. Kleiger, G., Grothe, R., Mallick, P., and Eisenberg, D. (2002) GXXXG and AXXXA: Common α-Helical Interaction Motifs in Proteins, Particularly in Extremophiles. *Biochemistry*. **41**, 5990–5997

30. Higashide, H., Ishihara, S., Nobuhara, M., Ihara, Y., and Funamoto, S. (2017) Alanine substitutions in the GXXXG motif alter C99 cleavage by γ-secretase but not its dimerization. *Journal of Neurochemistry*. **140**, 955–962

31. Kienlen-Campard, P., Tasiaux, B., Hees, J. V., Li, M., Huysseune, S., Sato, T., Fei, J. Z., Aimoto, S., Courtoy, P. J., Smith, S. O., Constantinescu, S. N., and Octave, J.-N. (2008) Amyloidogenic Processing but Not Amyloid Precursor Protein (APP) Intracellular C-terminal Domain Production Requires a Precisely Oriented APP Dimer Assembled by Transmembrane GXXXG Motifs. *J. Biol. Chem.* **283**, 7733–7744

32. Decock, M., El Haylani, L., Stanga, S., Dewachter, I., Octave, J.-N., Smith, S. O., Constantinescu, S. N., and Kienlen-Campard, P. (2015) Analysis by a highly sensitive split luciferase assay of the regions involved in APP dimerization and its impact on processing. *FEBS Open Bio*. **5**, 763–773

33. Decock, M., Stanga, S., Octave, J.-N., Dewachter, I., Smith, S. O., Constantinescu, S. N., and Kienlen-Campard, P. (2016) Glycines from the APP GXXXG/GXXXA Transmembrane Motifs Promote Formation of Pathogenic Aβ Oligomers in Cells. *Front Aging Neurosci*. 10.3389/fnagi.2016.00107

34. Munter, L.-M., Voigt, P., Harmeier, A., Kaden, D., Gottschalk, K. E., Weise, C., Pipkorn, R., Schaefer, M., Langosch, D., and Multhaup, G. (2007) GxxxG motifs within the amyloid precursor protein transmembrane sequence are critical for the etiology of Aβ42. *EMBO J*. **26**, 1702–1712

35. Khalifa, N. B., Van Hees, J., Tasiaux, B., Huysseune, S., Smith, S. O., Constantinescu, S. N., Octave, J.-N., and Kienlen-Campard, P. (2010) What is the role of amyloid precursor protein dimerization? *Cell Adh Migr*. **4**, 268–272

36. Richter, L., Munter, L.-M., Ness, J., Hildebrand, P. W., Dasari, M., Unterreitmeier, S., Bulic, B., Beyermann, M., Gust, R., Reif, B., Weggen, S., Langosch, D., and Multhaup, G. (2010) Amyloid beta 42 peptide (Aβ42)-lowering compounds directly bind to Aβ and interfere with amyloid precursor protein (APP) transmembrane dimerization. *PNAS*. **107**, 14597–14602

37. Eggert, S., Midthune, B., Cottrell, B., and Koo, E. H. (2009) Induced Dimerization of the Amyloid Precursor Protein Leads to Decreased Amyloid-β Protein Production. *J Biol Chem*. **284**, 28943–28952

38. Jung, J. I., Premraj, S., Cruz, P. E., Ladd, T. B., Kwak, Y., Koo, E. H., Felsenstein, K. M., Golde, T. E., and Ran, Y. (2014) Independent Relationship between Amyloid Precursor Protein (APP) Dimerization and γ-Secretase Processivity. *PLoS One*. 10.1371/journal.pone.0111553

39. Eggert, S., Gonzalez, A. C., Thomas, C., Schilling, S., Schwarz, S. M., Tischer, C., Adam, V., Strecker, P., Schmidt, V., Willnow, T. E., Hermey, G., Pietrzik, C. U., Koo, E. H., and Kins, S. (2018) Dimerization leads to changes in APP (amyloid precursor protein) trafficking mediated by LRP1 and SorLA. *Cell. Mol. Life Sci.* **75**, 301–322

40. Beel, A. J., Sakakura, M., Barrett, P. J., and Sanders, C. R. (2010) Direct Binding of Cholesterol to the Amyloid Precursor Protein: An Important Interaction in Lipid-Alzheimer's Disease Relationships? *Biochim Biophys Acta*. **1801**, 975–982

41. Song, Y., Hustedt, E. J., Brandon, S., and Sanders, C. R. (2013) Competition Between Homodimerization and Cholesterol Binding to the C99 Domain of the Amyloid Precursor Protein. *Biochemistry*. **52**, 5051–5064

42. Das, U., Wang, L., Ganguly, A., Saikia, J. M., Wagner, S. L., Koo, E. H., and Roy, S. (2016) Visualization of APP and BACE-1 approximation in neurons: new insights into the amyloidogenic pathway. *Nat Neurosci*. **19**, 55–64

43. Kerppola, T. K. (2006) Design and Implementation of Bimolecular Fluorescence Complementation (BiFC) Assays for the Visualization of Protein Interactions in Living Cells. *Nat Protoc*. **1**, 1278–1286

44. van der Kant, R., Langness, V. F., Herrera, C. M., Williams, D. A., Fong, L. K., Leestemaker, Y., Steenvoorden, E., Rynearson, K. D., Brouwers, J. F., Helms, J. B., Ovaa, H., Giera, M., Wagner, S. L., Bang, A. G., and Goldstein, L. S. B. (2019) Cholesterol Metabolism Is a Druggable Axis that Independently Regulates Tau and Amyloid-β in iPSC-Derived Alzheimer's Disease Neurons. *Cell Stem Cell*. **24**, 363-375.e9

45. Kaden, D., Munter, L.-M., Joshi, M., Treiber, C., Weise, C., Bethge, T., Voigt, P., Schaefer, M., Beyermann, M., Reif, B., and Multhaup, G. (2008) Homophilic Interactions of the Amyloid Precursor Protein (APP) Ectodomain Are Regulated by the Loop Region and Affect β-Secretase Cleavage of APP. *J. Biol. Chem.* **283**, 7271–7279

46. Bhattacharyya, R., Fenn, R. H., Barren, C., Tanzi, R. E., and Kovacs, D. M. (2016) Palmitoylated APP Forms Dimers, Cleaved by BACE1. *PLOS ONE*. **11**, e0166400

47. Ben Khalifa, N., Tyteca, D., Marinangeli, C., Depuydt, M., Collet, J.-F., Courtoy, P. J., Renauld, J.-C., Constantinescu, S., Octave, J.-N., and Kienlen-Campard, P. (2011) Structural features of the KPI domain control APP dimerization, trafficking, and processing. *The FASEB Journal*. **26**, 855–867

48. So, P. P., Khodr, C. E., Chen, C.-D., and Abraham, C. R. (2013) Comparable dimerization found in wildtype and familial Alzheimer's disease amyloid precursor protein mutants. *Am J Neurodegener Dis*. **2**, 15–28

49. Chen, C.-D., Oh, S.-Y., Hinman, J. D., and Abraham, C. R. (2006) Visualization of APP dimerization and APP-Notch2 heterodimerization in living cells using bimolecular fluorescence complementation. *Journal of Neurochemistry*. **97**, 30–43

50. Citron, M., Teplow, D. B., and Selkoe, D. J. (1995) Generation of amyloid beta protein from its precursor is sequence specific. *Neuron*. **14**, 661–670

51. Kant, R. van der, Langness, V. F., Herrera, C. M., Williams, D. A., Fong, L. K., Leestemaker, Y., Steenvoorden, E., Rynearson, K. D., Brouwers, J. F., Helms, J. B., Ovaa, H., Giera, M., Wagner, S. L., Bang, A. G., and Goldstein, L. S. B. (2019) Cholesterol Metabolism Is a Druggable Axis that Independently Regulates Tau and Amyloid-β in iPSC-Derived Alzheimer's Disease Neurons. *Cell Stem Cell*. **24**, 363-375.e9

52. Buhaescu, I., and Izzedine, H. (2007) Mevalonate pathway: A review of clinical and therapeutical implications. *Clinical Biochemistry*. **40**, 575–584

53. Eggert, S., Midthune, B., Cottrell, B., and Koo, E. H. (2009) Induced Dimerization of the Amyloid Precursor Protein Leads to Decreased Amyloid-β Protein Production. *J Biol Chem*. **284**, 28943–28952

54. Liao, J. K., and Laufs, U. (2005) PLEIOTROPIC EFFECTS OF STATINS. *Annu Rev Pharmacol Toxicol*. **45**, 89–118

55. Cole, S. L., Grudzien, A., Manhart, I. O., Kelly, B. L., Oakley, H., and Vassar, R. (2005) Statins Cause Intracellular Accumulation of Amyloid Precursor Protein, β-Secretase-cleaved Fragments, and Amyloid β-Peptide via an Isoprenoid-dependent Mechanism. *J. Biol. Chem.* **280**, 18755–18770

56. Hutter-Paier, B., Huttunen, H. J., Puglielli, L., Eckman, C. B., Kim, D. Y., Hofmeister, A., Moir, R. D., Domnitz, S. B., Frosch, M. P., Windisch, M., and Kovacs, D. M. (2004) The ACAT inhibitor CP-113,818 markedly reduces amyloid pathology in a mouse model of Alzheimer's disease. *Neuron*. **44**, 227–238

57. Huttunen, H. J., Peach, C., Bhattacharyya, R., Barren, C., Pettingell, W., Hutter-Paier, B., Windisch, M., Berezovska, O., and Kovacs, D. M. (2009) Inhibition of acyl-coenzyme A: cholesterol acyl transferase modulates amyloid precursor protein trafficking in the early secretory pathway. *FASEB J.* **23**, 3819–3828

58. Huttunen, H. J., Havas, D., Peach, C., Barren, C., Duller, S., Xia, W., Frosch, M. P., Hutter-Paier, B., Windisch, M., and Kovacs, D. M. (2010) The Acyl-Coenzyme A:Cholesterol Acyltransferase Inhibitor CI-1011 Reverses Diffuse Brain Amyloid Pathology in Aged Amyloid Precursor Protein Transgenic Mice. *J Neuropathol Exp Neurol*. **69**, 777–788

59. Puglielli, L., Konopka, G., Pack-Chung, E., Ingano, L. A. M., Berezovska, O., Hyman, B. T., Chang, T. Y., Tanzi, R. E., and Kovacs, D. M. (2001) Acyl-coenzyme A: cholesterol acyltransferase modulates the generation of the amyloid β-peptide. *Nat Cell Biol*. **3**, 905–912

60. Hogarth, C. A., Roy, A., and Ebert, D. L. (2003) Genomic evidence for the absence of a functional cholesteryl ester transfer protein gene in mice and rats. *Comp. Biochem. Physiol. B, Biochem. Mol. Biol.* **135**, 219–229

61. Guyard-Dangremont, V., Desrumaux, C., Gambert, P., Lallemant, C., and Lagrost, L. (1998) Phospholipid and cholesteryl ester transfer activities in plasma from 14 vertebrate species. Relation to atherogenesis susceptibility. *Comp. Biochem. Physiol. B, Biochem. Mol. Biol.* **120**, 517–525

62. Albers, J. J., Tollefson, J. H., Wolfbauer, G., and Albright, R. E. (1992) Cholesteryl ester transfer protein in human brain. *Int. J. Clin. Lab. Res.* **21**, 264–266

63. Chan, R. B., Oliveira, T. G., Cortes, E. P., Honig, L. S., Duff, K. E., Small, S. A., Wenk, M. R., Shui, G., and Di Paolo, G. (2012) Comparative Lipidomic Analysis of Mouse and Human Brain with Alzheimer Disease. *J Biol Chem*. **287**, 2678–2688

64. Tajima, Y., Ishikawa, M., Maekawa, K., Murayama, M., Senoo, Y., Nishimaki-Mogami, T., Nakanishi, H., Ikeda, K., Arita, M., Taguchi, R., Okuno, A., Mikawa, R., Niida, S., Takikawa, O., and Saito, Y. (2013) Lipidomic analysis of brain tissues and plasma in a mouse model expressing mutated human amyloid precursor protein/tau for Alzheimer's disease. *Lipids Health Dis*. **12**, 68

65. Yang, D.-S., Stavrides, P., Saito, M., Kumar, A., Rodriguez-Navarro, J. A., Pawlik, M., Huo, C., Walkley, S. U., Saito, M., Cuervo, A. M., and Nixon, R. A. (2014) Defective macroautophagic turnover of brain lipids in the TgCRND8 Alzheimer mouse model: prevention by correcting lysosomal proteolytic deficits. *Brain*. **137**, 3300–3318

66. Cho, Y. Y., Kwon, O.-H., Park, M. K., Kim, T.-W., and Chung, S. (2019) Elevated cellular cholesterol in Familial Alzheimer's presenilin 1 mutation is associated with lipid raft localization of β-amyloid precursor protein. *PLoS ONE*. **14**, e0210535

67. Wingo, T. S., Cutler, D. J., Wingo, A. P., Le, N.-A., Rabinovici, G. D., Miller, B. L., Lah, J. J., and Levey, A. I. (2019) Association of Early-Onset Alzheimer Disease With Elevated Low-Density Lipoprotein Cholesterol Levels and Rare Genetic Coding Variants of APOB. *JAMA Neurol*. **76**, 809–817

68. Cao, X., and Südhof, T. C. (2001) A transcriptionally [correction of transcriptively] active complex of APP with Fe65 and histone acetyltransferase Tip60. *Science*. **293**, 115–120

69. Pierrot, N., Tyteca, D., D'auria, L., Dewachter, I., Gailly, P., Hendrickx, A., Tasiaux, B., Haylani, L. E., Muls, N., N'kuli, F., Laquerrière, A., Demoulin, J.-B., Campion, D., Brion, J.-P., Courtoy, P. J., Kienlen-Campard, P., and Octave, J.-N. (2013) Amyloid precursor protein controls cholesterol turnover needed for neuronal activity. *EMBO Mol Med*. **5**, 608–625

70. Liu, Q., Zerbinatti, C. V., Zhang, J., Hoe, H.-S., Wang, B., Cole, S. L., Herz, J., Muglia, L., and Bu, G. (2007) Amyloid precursor protein regulates brain apolipoprotein E and cholesterol metabolism through lipoprotein receptor LRP1. *Neuron*. **56**, 66–78

71. Wang, W., Mutka, A.-L., Zmrzljak, U. P., Rozman, D., Tanila, H., Gylling, H., Remes, A. M., Huttunen, H. J., and Ikonen, E. (2014) Amyloid precursor protein α- and β-cleaved ectodomains exert opposing control of cholesterol homeostasis via SREBP2. *FASEB J.* **28**, 849–860

72. Grimm, M. O. W., Grimm, H. S., Pätzold, A. J., Zinser, E. G., Halonen, R., Duering, M., Tschäpe, J. A., De Strooper, B., Müller, U., Shen, J., and Hartmann, T. (2005) Regulation of cholesterol and sphingomyelin metabolism by amyloid-beta and presenilin. *Nat. Cell Biol.* **7**, 1118–1123

73. Xiong, H., Callaghan, D., Jones, A., Walker, D. G., Lue, L.-F., Beach, T. G., Sue, L. I., Woulfe, J., Xu, H., Stanimirovic, D. B., and Zhang, W. (2008) Cholesterol retention in Alzheimer's brain is responsible for high beta- and gamma-secretase activities and Abeta production. *Neurobiol. Dis.* **29**, 422–437

74. Wahrle, S., Das, P., Nyborg, A. C., McLendon, C., Shoji, M., Kawarabayashi, T., Younkin, L. H., Younkin, S. G., and Golde, T. E. (2002) Cholesterol-Dependent γ-Secretase Activity in Buoyant Cholesterol-Rich Membrane Microdomains. *Neurobiology of Disease*. **9**, 11–23

75. Cossec, J.-C., Simon, A., Marquer, C., Moldrich, R. X., Leterrier, C., Rossier, J., Duyckaerts, C., Lenkei, Z., and Potier, M.-C. (2010) Clathrin-dependent APP endocytosis and Abeta secretion are highly sensitive to the level of plasma membrane cholesterol. *Biochim. Biophys. Acta*. **1801**, 846–852

76. Gore, A., Li, Z., Fung, H.-L., Young, J., Agarwal, S., Antosiewicz-Bourget, J., Canto, I., Giorgetti, A., Israel, M., Kiskinis, E., Lee, J.-H., Loh, Y.-H., Manos, P. D., Montserrat, N., Panopoulos, A. D., Ruiz, S., Wilbert, M., Yu, J., Kirkness, E. F., Belmonte, J. C. I., Rossi, D. J., Thomson, J., Eggan, K., Daley, G. Q., Goldstein, L. S. B., and Zhang, K. (2011) Somatic coding mutations in human induced pluripotent stem cells. *Nature*. **471**, 63–67

77. Young, J. E., Boulanger-Weill, J., Williams, D. A., Woodruff, G., Buen, F., Revilla, A. C., Herrera, C., Israel, M. A., Yuan, S. H., Edland, S. D., and Goldstein, L. S. B. (2015) Elucidating molecular phenotypes caused by the SORL1 Alzheimer's disease genetic risk factor using human induced pluripotent stem cells. *Cell Stem Cell*. **16**, 373–385

78. Israel, M. A., Yuan, S. H., Bardy, C., Reyna, S. M., Mu, Y., Herrera, C., Hefferan, M. P., Van Gorp, S., Nazor, K. L., Boscolo, F. S., Carson, C. T., Laurent, L. C., Marsala, M., Gage, F. H., Remes, A. M., Koo, E. H., and Goldstein, L. S. B. (2012) Probing sporadic and familial Alzheimer's disease using induced pluripotent stem cells. *Nature*. **482**, 216–220

79. Yuan, S. H., Martin, J., Elia, J., Flippin, J., Paramban, R. I., Hefferan, M. P., Vidal, J. G., Mu, Y., Killian, R. L., Israel, M. A., Emre, N., Marsala, S., Marsala, M., Gage, F. H., Goldstein, L. S. B., and Carson, C. T. (2011) Cell-Surface Marker Signatures for the Isolation of Neural Stem Cells, Glia and Neurons Derived from Human Pluripotent Stem Cells. *PLOS ONE*. **6**, e17540

Chapter 4
Full-length Amyloid Precursor Protein Regulates Lipoprotein Metabolism and Amyloid-β Clearance in Human Astrocytes

JBC ARTICLE

Full-length amyloid precursor protein regulates lipoprotein metabolism and amyloid-β clearance in human astrocytes

Received for publication, October 14, 2017, and in revised form, May 11, 2018 Published, Papers in Press, June 1, 2018, DOI 10.1074/jbc.RA117.000441

Lauren K. Fong[‡§], Max M. Yang[‡§], Rodrigo dos Santos Chaves[‡§], Sol M. Reyna[‡§], Vanessa F. Langness[‡§], Grace Woodruff[‡§], Elizabeth A. Roberts[‡§], Jessica E. Young[‡¶], and Lawrence S. B. Goldstein[‡§‖1]

From the Departments of [‡]Cellular and Molecular Medicine and [‖]Neurosciences, University of California at San Diego, La Jolla, California 92093, the [¶]Department of Pathology and Institute of Stem Cell and Regenerative Medicine, University of Washington, Seattle, Washington 98195, and the [§]Sanford Consortium for Regenerative Medicine, La Jolla, California 92093

Edited by Paul E. Fraser

Mounting evidence suggests that alterations in cholesterol homeostasis are involved in Alzheimer's disease (AD) pathogenesis. Amyloid precursor protein (APP) or multiple fragments generated by proteolytic processing of APP have previously been implicated in the regulation of cholesterol metabolism. However, the physiological function of APP in regulating lipoprotein homeostasis in astrocytes, which are responsible for *de novo* cholesterol biosynthesis and regulation in the brain, remains unclear. To address this, here we used CRISPR/Cas9 genome editing to generate isogenic APP-knockout (KO) human induced pluripotent stem cells (hiPSCs) and differentiated them into human astrocytes. We found that APP-KO astrocytes have reduced cholesterol and elevated levels of sterol regulatory element-binding protein (SREBP) target gene transcripts and proteins, which were both downstream consequences of reduced lipoprotein endocytosis. To elucidate which APP fragments regulate cholesterol homeostasis and to examine whether familial AD mutations in APP affect lipoprotein metabolism, we analyzed an isogenic allelic series harboring the APP Swedish and APP V717F variants. Only astrocytes homozygous for the APP Swedish ($APP^{Swe/Swe}$) mutation, which had reduced full-length APP (FL APP) due to increased β-secretase cleavage, recapitulated the APP-KO phenotypes. Astrocytic internalization of β-amyloid (Aβ), another ligand for low-density lipoprotein (LDL) receptors, was also impaired in APP-KO and $APP^{Swe/Swe}$ astrocytes. Finally, impairing cleavage of FL APP through β-secretase inhibition in $APP^{Swe/Swe}$ astrocytes reversed the LDL and Aβ endocytosis defects. In conclusion, FL APP is involved in the endocytosis of LDL receptor ligands and is required for proper cholesterol homeostasis and Aβ clearance in human astrocytes.

Alzheimer's disease (AD)[2] is a progressive and irreversible neurodegenerative disease that is the most common form of dementia in the elderly (1). Genetically, AD can be subdivided into two subgroups: early onset, familial Alzheimer's disease (FAD) and late onset, sporadic Alzheimer's disease (SAD) (2). Although FAD can be attributed to rare and highly penetrant mutations in amyloid precursor protein (APP), presenilin-1 or presenilin-2, the precise etiology of SAD is unknown (3). Recently, several lines of evidence have implicated cholesterol metabolism as a common biological pathway involved in FAD and SAD. The ϵ4 allele of APOE, the major cholesterol carrier of the brain, is the strongest known genetic risk factor in AD (4, 5). Genome-wide association studies have identified additional mutations in lipid metabolism–related proteins like APOJ/Clusterin and ABCA7 as other highly-associated risk factors (6). Finally, retrospective studies, although controversial, have suggested that use of the cholesterol-lowering statins lowers the risk for AD (7–9).

APP is a ubiquitously expressed, single-pass, type I transmembrane protein that is thought to have multiple putative biological functions (10). The functional heterogeneity of APP may stem from its multiple proteolytic fragments, which are generated by two major pathways: nonamyloidogenic cleavage via sequential proteolysis by α- and then γ-secretase or amyloidogenic cleavage by β- and then γ-secretase. APP or various proteolytic fragments of APP have recently been implicated in the control of brain cholesterol metabolism via regulation of LDL receptor-family mRNA and protein (11–15). Normally, low intracellular cholesterol levels induce cholesterol biosynthesis via intricate transcriptional and posttranslational mechanisms involving increased proteolytic processing of SREBPs, which result in up-regulated cholesterol biosynthesis enzymes and increased internalization of extracellular cholesterol via

This work was supported in whole or part by National Institutes of Health Predoctoral Training Grant T32 GM008666; Fundação de Amparo à Pesquisa do Estado de São Paulo (FAPESP) Grant 2013/18028-9, and National Institutes of Health Grants RF1 AG048083-01 and 2P50 AG005131-31 from NIA. The authors declare that they have no conflicts of interest with the contents of this article. The content is solely the responsibility of the authors and does not necessarily represent the official views of the National Institutes of Health.

[1] To whom correspondence should be addressed: Depts. of Cellular and Molecular Medicine and of Neurosciences, University of California, San Diego, and Sanford Consortium for Regenerative Medicine, La Jolla, CA 92093. Tel.: 858-534-9702; Fax: 858-246-0162l; E-mail: lgoldstein@ucsd.edu.

[2] The abbreviations used are: AD, Alzheimer's disease; APP, amyloid precursor protein; CTF, C-terminal fragment; Aβ, amyloid-β; KO, knockout; hiPSC, human induced pluripotent stem cell; iPSC, induced pluripotent stem cells LDL, low density lipoprotein; LDLR, low density lipoprotein receptor; SREBP, sterol-regulatory element-binding protein; BBR, berberine; SREBP, sterol regulatory element-binding protein; qRT-PCR, quantitative RT-PCR; NPC, neural precursor cell; HMGCR, HMG-CoA reductase; sAPP, soluble APP; FL, full length; Tfn, transferrin; SAD, sporadic Alzheimer's disease; FAD, familial Alzheimer's disease; BSI, β-secretase inhibitor; DMEM, Dulbecco's modified Eagle's medium; RI, ROCK inhibitor; FBS, fetal bovine serum; Bis-Tris, 2-[bis(2-hydroxyethyl)amino]-2-(hydroxymethyl)propane-1,3-diol; MEF, mouse embryonic fibroblast.

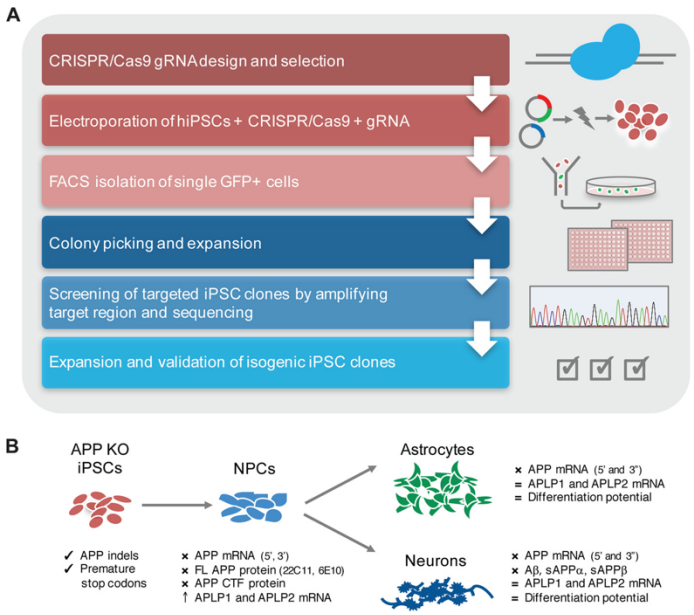

Figure 1. Generation of APP-KO hiPSCs using CRISPR/Cas9-targeted genome editing. *A*, diagram of CRISPR/Cas9 workflow to generate isogenic hiPSCs. *B*, summary diagram of the validation of isogenic APP-KO hiPSCs, astrocytes, and neurons.

LDL receptors. In contrast, high-intracellular cholesterol levels inhibit the proteolytic processing of SREBP and thus turn off cholesterol biosynthesis and uptake (16). Regulation of LDL receptor mRNA and protein is also relevant to mechanisms of Aβ clearance in the brain because LDL receptors like low-density lipoprotein receptor (LDLR) and lipoprotein receptor-related protein 1 (LRP1) mediate the internalization of Aβ by binding to Aβ directly or via apoE (17–21).

Despite our understanding of the sensitive and complex mechanisms regulating intracellular cholesterol, there is little consensus as to how APP regulates this pathway in the brain. Multiple studies on these subjects have yielded mixed results, likely due to the use of nonendogenous APP levels, the study of nonneural cell types, or the use of whole brain tissue, which masks the unique phenotypes of individual cell types. To begin to address these issues, we utilized CRISPR/Cas9 genome editing to generate an isogenic series of APP-KO and FAD mutant hiPSCs. We further differentiated these hiPSCs into astrocytes, the cell type primarily responsible for the brain's *de novo* cholesterol synthesis and regulation. Using APP-KO, APP Swedish, and APP V717F astrocytes, we identify a role for FL APP in the uptake of LDL receptor ligands and demonstrate that proper levels of FL APP in human astrocytes are essential for lipoprotein regulation and Aβ clearance. Our data shed light onto the elusive function of FL APP, establish a linkage between APP and biological pathways implicated in SAD, and finally highlight the utility of using hiPSC technology to study the physiological function of endogenous proteins in specific cell types.

Results

Generation of isogenic APP-knockout hiPSCs using CRISPR/Cas9

To study the role of endogenous human amyloid precursor protein (APP) in regulating astrocytic cholesterol metabolism, we utilized CRISPR/Cas9 genome editing to knock out (KO) APP in hiPSC (Fig. 1). To induce gene disruption, we utilized a guide RNA targeting exon 16 of APP. In both APP-KO clones used in our experiments, the CRISPR/Cas9 – guide RNA complexes generated unique indels at the predicted cut site in each allele. All of these indels were predicted to generate premature stop codons in either exon 16 or exon 17 of APP (Fig. 2*A*). For analysis, we compared these APP-KO hiPSCs to WT, unedited subclones of the original hiPSC line that also underwent the genome editing process but were not modified.

To test whether premature stop codon formation had induced nonsense-mediated decay of *APP* mRNA and thus loss of APP protein, we first examined APP transcript using primer sets targeting regions upstream and downstream of the CRISPR/Cas9 cut site. There was little detectable *APP* mRNA in APP-KO neural precursor cells (NPCs), neurons, and astrocytes (Fig. 2, *B–D*). Consistent with these results, two N-terminal full-length APP (FL APP) antibodies, which recognized epitopes either upstream (22C11) or downstream (6E10) of the CRISPR/Cas9 cut site, and one C-terminal APP antibody (APP CTF) failed to detect any APP protein in APP-KO NPCs (Figs. 2*E* and Fig. S1). Furthermore, the medium from APP-KO neurons contained no detectable cleaved APP fragments like Aβ or the secreted soluble APP (sAPP) fragments (data not shown).

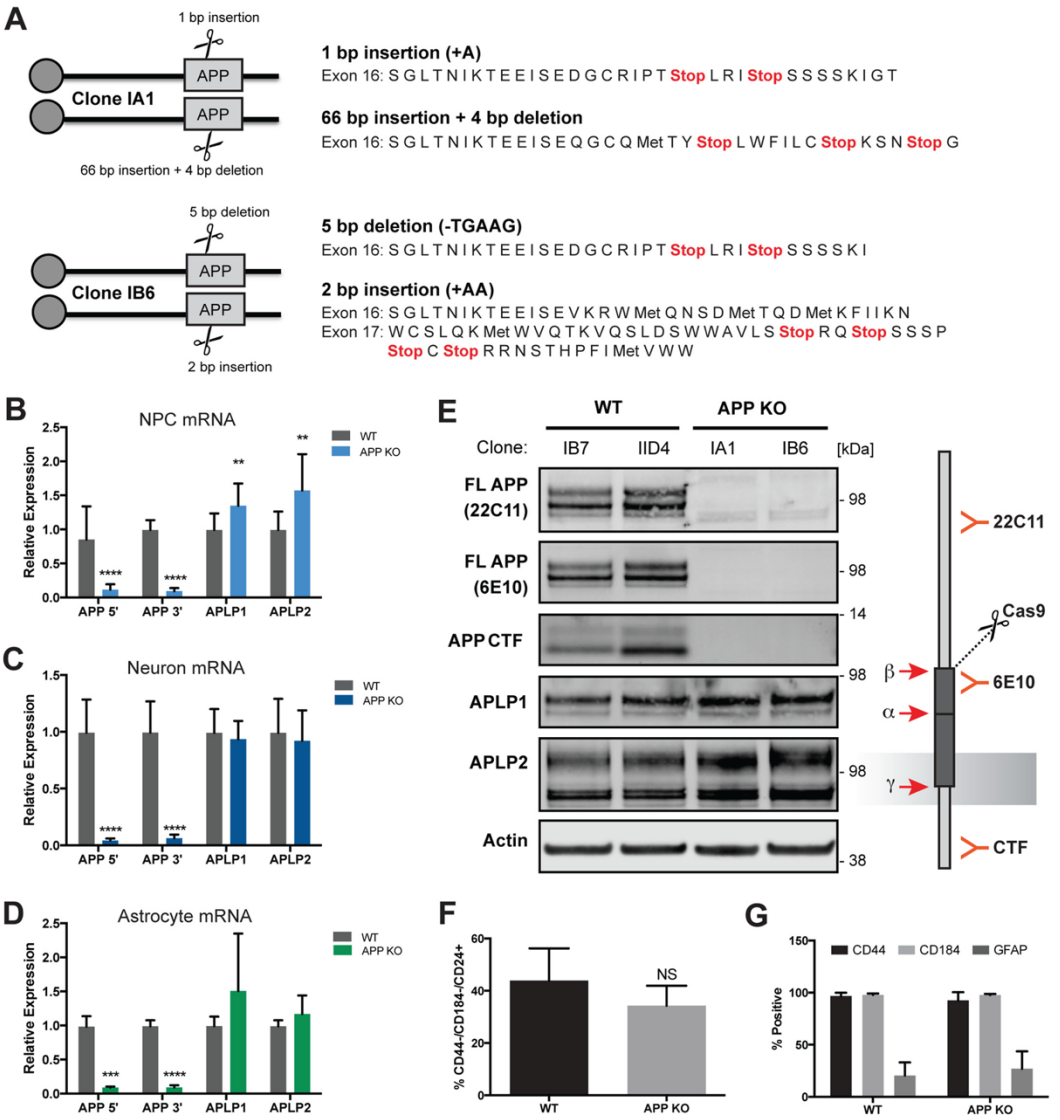

Figure 2. Characterization of APP-KO isogenic cells. *A*, insertions or deletions induce premature stop codon formation in both alleles of two independently derived APP-KO hiPSC clones, IA1 and IB6. The qRT-PCR analysis of *APP*, *APLP1*, and *APLP2* mRNA levels in NPCs ($n \geq 8$ from three independent experiments) (*B*), purified neurons ($n \geq 8$ from two independent experiments) (*C*), and astrocytes ($n \geq 6$ from at least two independent experiments) (*D*) shows little detectable *APP* mRNA (***, $p < 0.001$; ****, $p < 0.0001$) and no significant differences in *APLP1* or *APLP2* mRNA levels in neurons or astrocytes. There was a significant increase in *APLP1* (**, $p = 0.0082$) and *APLP2* (**, $p = 0.0035$) mRNA in NPCs. All qRT-PCR data were normalized to *RPL13A*, *RPL27*, and *TBP*. *E*, representative Western blots from WT and APP-KO NPCs using antibodies for APP and APP family members, APLP1 and APLP2, show no detectable APP protein but a slight elevation in APLP1 and APLP2. *F*, percentage of neurons identified by flow cytometry using a CD44−/CD184−/CD24+ cell–surface signature after 3 weeks of neural differentiation shows that loss of APP does not affect neuronal differentiation ($n \geq 7$ from four independent experiments). *G*, percentage of astrocytes positive for CD44, CD184, and GFAP by flow cytometry is not different between WT and APP-KO astrocytes ($n = 12$ from three independent experiments). Data are depicted with *bar graphs* of the mean ± S.D. *NS* is nonsignificant.

Together, these data suggested that CRISPR/Cas9-induced nonsense-mediated decay of *APP* transcripts prevented translation of APP protein in APP-KO NPCs, neurons, and astrocytes.

We also examined the expression of APP family members, amyloid precursor-like protein 1 and 2 (APLP1 and APLP2), which have been shown to exert some functional redundancy

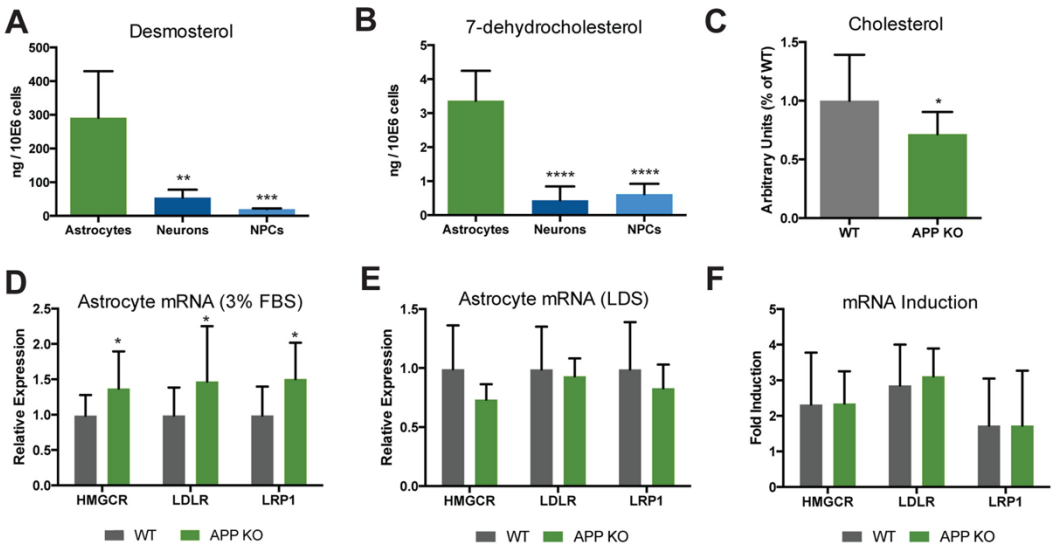

Figure 3. APP-KO astrocytes have altered cholesterol metabolism. *A,* lipidomics MS quantification of the cholesterol precursors: desmosterol (**, $p = 0.0025$; ***, $p = 0.0003$; $n \geq 4$); *B,* 7-dehydrocholesterol (****, $p < 0.0001$; $n \geq 4$) in astrocytes, neurons, and NPCs shows much higher levels of cholesterol precursors in astrocytes. *C,* quantification of total cellular cholesterol levels by Amplex Red cholesterol assay kit shows decreased cholesterol in APP-KO astrocytes (*, $p = 0.0226$; $n \geq 13$ from three independent experiments). *D,* qRT-PCR analysis of mRNA levels from astrocytes grown in medium containing 3% FBS shows up-regulated *HMGCR* (*, $p = 0.0382$), *LDLR* (*, $p = 0.0427$), and *LRP1* (*, $p = 0.0157$) gene expression in APP-KO astrocytes ($n \geq 10$ from at least two independent experiments). *E,* qRT-PCR analysis of *HMGCR*, *LDLR*, and *LRP1* mRNA levels from astrocytes grown with lipoprotein-depleted serum (*LDS*) shows no significant differences in expression between WT and APP-KO astrocytes ($n \geq 8$ from at least two independent experiments). *F,* quantification of mRNA induction of *HMGCR*, *LDLR*, and *LRP1* mRNA by qRT-PCR 24 h after changing growth medium from 3% FBS-containing medium to lipoprotein-depleted medium shows no significant differences in the fold induction of SREBP-target genes in WT and APP-KO astrocytes ($n \geq 4$ from at least two independent experiments). Data are depicted with *bar graphs* of the mean ± S.D.

with APP. Interestingly, in APP-KO NPCs, we saw a modest up-regulation of *APLP1* and *APLP2* mRNA levels (Fig. 2*B*) and protein (Fig. 2*E*). However, when these APP-KO NPCs were further differentiated to neurons (Fig. 2*C*) or astrocytes (Fig. 2*D*), this up-regulation of *APLP1* and *APLP2* mRNA was no longer detected. These data indicated that there were no off-target effects on homologous APP family members, and any phenotypes observed in APP-KO neurons or astrocytes were not due to loss or overexpression of APLP1 or APLP2.

Because APP is a key protein in neural development (22), we next tested whether the loss of APP influenced the capability of APP-KO NPCs to differentiate into neurons or astrocytes. Using flow cytometry for a neuronal cell-surface signature of CD184−, CD44−, and CD24+ (23), we found no difference in the percentage of neurons generated from WT or APP-KO NPCs following multiple rounds of neuronal differentiation (Fig. 2*F*). Similarly, using the glial markers, CD44, CD184, and GFAP, we found no difference in the differentiation capability of WT or APP-KO NPCs to generate astrocytes (Fig. 2*G*).

hiPSC-derived astrocytes produce high levels of de novo synthesized cholesterol in vitro

Given the relative isolation of the brain from the periphery because of the blood-brain barrier, cholesterol is synthesized locally in the brain (24). Previous studies examining sterol synthesis in brain-specific cell types have identified astrocytes as the brain's primary source of cholesterol (25). To test whether our hiPSC-derived system recapitulated this essential function of astrocytes *in vivo*, we performed a comprehensive analysis of free sterols in astrocytes, neurons, and NPCs using LC-MS. We found that, relative to neurons and NPCs, astrocytes had significantly elevated levels of the immediate cholesterol precursors, desmosterol (Fig. 3*A*) and 7-dehydrocholesterol (Fig. 3*B*). Consistent with previous work reporting that astrocytes predominantly contain sterols from the Bloch pathway of cholesterol biosynthesis (26), we observed higher concentrations of astrocyte-derived desmosterol relative to 7-dehydrocholesterol. These data suggest that hiPSC-derived astrocytes recapitulate the ability to synthesize cholesterol, similar to their native function *in vivo*.

APP-KO astrocytes have altered cholesterol metabolism

We next sought to determine whether loss of APP affected cholesterol levels in hiPSC-derived astrocytes. Compared with WT, APP-KO astrocytes had decreased cholesterol (Fig. 3*C*). Given that levels of intracellular cholesterol regulate the activity of the sterol regulatory element-binding protein (SREBP) family of transcription factors (27, 28), we next analyzed SREBP-target genes. These included HMG-CoA reductase (*HMGCR*), the rate-limiting enzyme in cholesterol biosynthesis, and the low-density lipoprotein receptor (*LDLR*). We also analyzed expression of low-density lipoprotein receptor–related protein 1 (*LRP1*), another highly expressed lipoprotein receptor in human astrocytes (29), whose expression has been reported to be regulated by the APP

intracellular domain (12) in addition to SREBP (30). mRNA expression of *HMGCR*, *LDLR*, and *LRP1* was up-regulated in APP-KO astrocytes when grown in normal growth medium with 3% serum (Fig. 3*D*). To test whether this result in APP-KO astrocytes was a consequence of low intracellular cholesterol and not simply aberrant SREBP function, we examined whether APP-KO astrocytes could further up-regulate transcript in response to prolonged lipoprotein depletion. Indeed, after culture under lipoprotein-free conditions, differences in SREBP-target gene expression were no longer observed between WT and APP-KO astrocytes (Fig. 3*E*). Furthermore, there was no difference between WT and APP-KO astrocytes in the fold induction of either *HMGCR*, *LDLR*, or *LRP1* mRNA after 24 h of cholesterol withdrawal (Fig. 3*F*). These data suggested that because APP-KO astrocytes could still modulate SREBP-target gene expression, low intracellular cholesterol resulted in up-regulation of cholesterol synthesis and internalization genes.

APP-KO astrocytes have decreased lipoprotein endocytosis but are not defective in bulk endocytosis, bulk receptor recycling, or expression of LDL receptors at the cell surface

Because APP-KO astrocytes exhibited a cholesterol starvation phenotype, but did not demonstrate impaired SREBP signaling in response to cholesterol withdrawal, we hypothesized that APP-KO astrocytes had reduced endocytosis of extracellular lipoproteins from the culture media. To test this, WT and APP-KO cells were treated with fluorescently-labeled LDL (Fig. 4*A*). After 1 h of continuous LDL treatment, APP-KO astrocytes demonstrated a modest but significant reduction in lipoprotein endocytosis as reflected by a reduction in intensity of intracellular LDL fluorescence. To test whether this reduction in lipoprotein endocytosis was a result of reduced bulk endocytosis, we treated cells with fluorescently-labeled dextran (Fig. 4*B*). We found no difference in dextran internalization between WT and APP-KO astrocytes, suggesting that impaired endocytosis was specific for lipoproteins.

Next, to understand the mechanism of reduced lipoprotein endocytosis in APP-KO astrocytes, we also tested bulk receptor recycling by flow cytometry using fluorescently-labeled transferrin (Tfn). Tfn marks recycled cargo and allows for characterization of recycling compartments (31), and APP is known to recycle back to the cell surface in Tfn receptor–positive vesicles. To test the endocytic recycling of receptors at the cell surface, astrocytes were incubated with Tfn at 37 °C for 10 min to allow Tfn uptake. Cells were then acid-washed to remove surface-bound Tfn before being chased with growth medium at fixed time points to allow Tfn to be recycled back to the cell surface. We observed no difference in the rate of Tfn recycling between WT and APP-KO astrocytes over time (Fig. 4*C*), suggesting that general recycling of receptors in endosomes, which normally contain APP, was not impaired in APP-KO astrocytes.

Given that both bulk endocytosis and Tfn receptor-marked recycling pathways were not defective in APP-KO astrocytes, we next examined whether newly synthesized lipoprotein receptors could be shuttled to the cell surface via the secretory pathway. To do this, we measured cell-surface LDLR by flow cytometry after treatment with berberine (BBR), which stimulates LDLR mRNA expression and up-regulates cell-surface LDLR (32). Although BBR treatment up-regulated surface LDLR levels compared with DMSO-treated astrocytes (Fig. 4*D*), there were no differences in cell-surface LDLR between WT or APP-KO astrocytes in either condition. To further verify that the loss of APP does not affect cell-surface LDL receptor levels, we used a cell-surface biotinylation assay to label plasma membrane-bound proteins with a cleavable biotin and then used streptavidin beads to pull down surface proteins. This allowed us to measure cell surface (pulldown fraction), total (input fraction), and intracellular (supernatant fraction) LDLR and LRP1 levels via Western blotting (Fig. 4, *E–P*). Confirming our previous results, we saw no difference in the amount of cell-surface LDLR or LRP1 protein (Fig. 4, *E–H*). However, in line with up-regulated *LDLR* and *LRP1* transcript in APP-KO astrocytes, we observed increased total LDLR and LRP1 protein (Fig. 4, *I–L*). Consistent with these results, intracellular LDLR and LRP1 protein were also elevated (Fig. 4, *M–P*). Finally, examination of APP-KO astrocytes by immunofluorescence revealed the presence of enlarged LRP1 puncta (Fig. 4*Q*).

Together, these data revealed no defects in regulation of transcription, Tfn-receptor recycling pathways, or the shuttling of newly synthesized receptors to the cell surface via the secretory pathway in APP-KO astrocytes. These data suggest that the loss of APP attenuated lipoprotein endocytosis and contributed to decreased cholesterol and increases in *SREBP*-target genes.

FAD astrocytes exhibit alterations in APP processing

In light of previous work implicating multiple APP fragments in the regulation of cholesterol homeostasis, we aimed to determine which APP fragments are required for proper lipoprotein metabolism. We also sought to examine whether FAD mutations in APP affect cholesterol homeostasis in human astrocytes. To do this, we analyzed an isogenic allelic series of astrocytes either heterozygous or homozygous for the APP Swedish mutation ($APP^{Swe/WT}$ and $APP^{Swe/Swe}$) or APP V717F mutation ($APP^{V717F/WT}$ and $APP^{V717F/V717F}$) (33). The Swedish and V717F mutations are thought to have different defects in APP processing, which would allow us to make distinct predictions about which APP fragments are relevant for lipoprotein regulation (34, 35).

To characterize the APP processing alterations in FAD mutant astrocytes, we quantified protein levels of FL APP (Fig. 5*A*). Of all FAD genotypes, only $APP^{Swe/Swe}$ astrocytes exhibited a reduction of FL APP (Fig. 5*B*). However, given that β-secretase processing of FL APP is favored in the APP Swedish mutation (36, 37), we hypothesized that this loss of FL APP in $APP^{Swe/Swe}$ astrocytes would coincide with increases in Aβ and soluble APP (sAPP) β along with a decrease in sAPPα. As predicted, APP Swedish astrocytes secreted high levels of Aβ40, Aβ42, and Aβ38 (Fig. 5, *F–H*), with no change in the Aβ42/Aβ40 ratio compared with WT (Fig. 5*E*). Additionally, APP Swedish astrocytes exhibited decreases in sAPPα (Fig. 5*I*), little detectable WT sAPPβ (Fig. 5*J*), and increased Swedish sAPPβ (Fig. 5*K*), which was recognized by an antibody specific for the APP Swedish mutation and only detectable in APP Swedish astrocytes. To detect APP C-terminal fragments (APP CTFs),

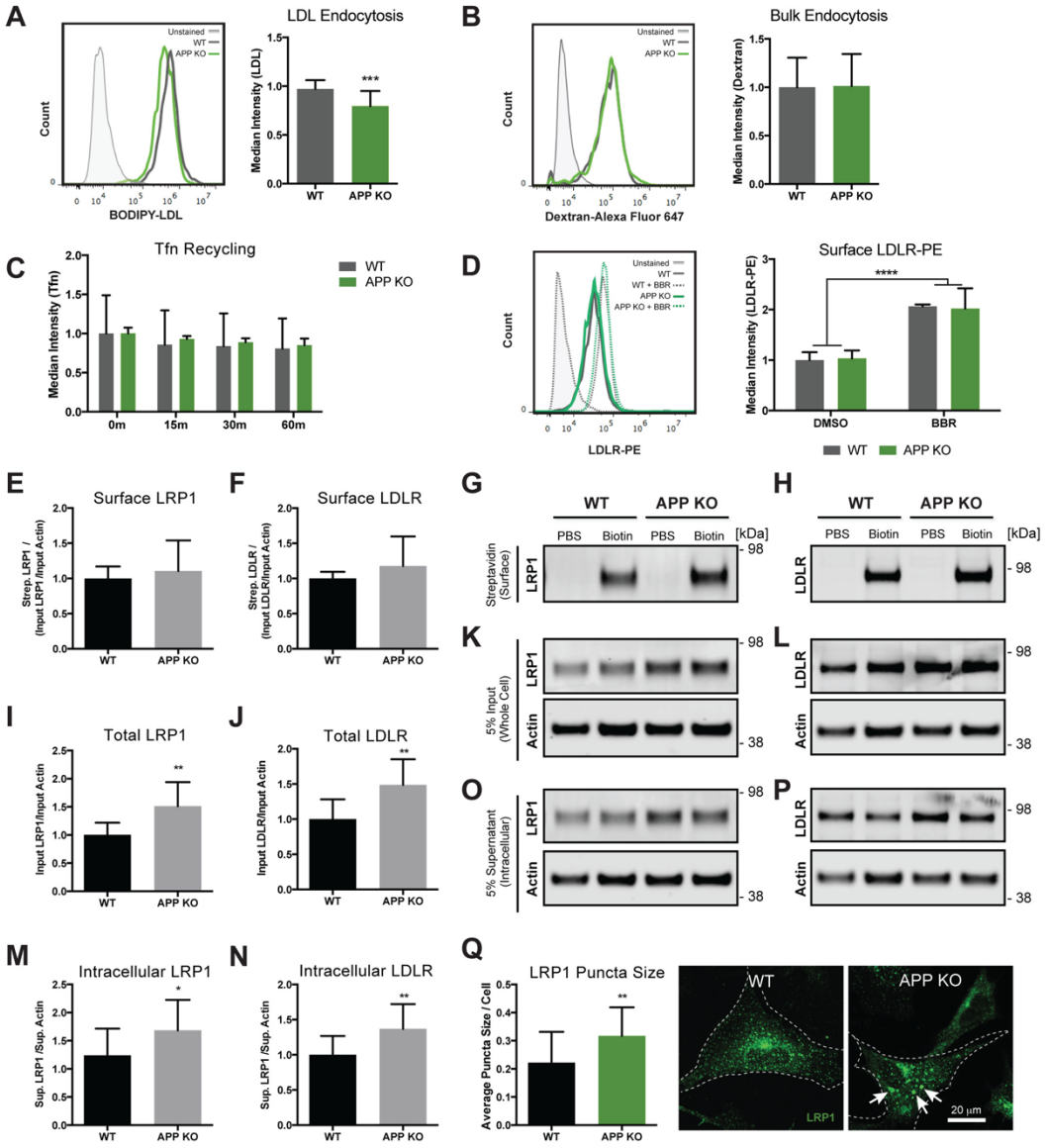

Figure 4. APP-KO astrocytes have impaired lipoprotein endocytosis. *A*, quantification of LDL endocytosis by flow cytometry shows reduced lipoprotein endocytosis in APP-KO astrocytes (***, $p = 0.0001$; $n = 24$ from four independent experiments). *B*, quantification of bulk endocytosis of dextran by flow cytometry shows no significant differences between WT and APP-KO astrocytes ($n = 24$ from four independent experiments). *C*, quantification of transferrin recycling over time by flow cytometry shows no difference in the rate of recycling between WT and APP-KO astrocytes ($n \geq 10$ from three independent experiments). *D*, quantification of cell-surface LDLR protein of WT and APP-KO astrocytes upon DMSO or berberine (*BBR*) treatment by flow cytometry. Although BBR treatment did up-regulate cell-surface LDLR (****, $p < 0.0001$), there were no significant differences between WT and APP astrocytes ($n \geq 2$ from two independent experiments). *E–H*, cell-surface biotinylation and Western blot analysis of biotinylated LRP1 (*G*) or LDLR (*H*) at the cell surface (50% pulldown), quantified in *E* and *F* in WT or APP-KO astrocytes, show no significant differences in surface receptor levels between WT and APP-KO astrocytes ($n = 6$ from three independent experiments). *I–L*, Western blot analysis of 5% input LRP1 or LDLR shows elevated total LRP1 (**, $p = 0.0013$) and LDLR (**, $p = 0.0013$) protein levels in APP-KO astrocytes ($n = 12$ from three independent experiments). *M–P*, Western blot analysis and quantification of 5% supernatant or intracellular lipoprotein receptor levels showed elevated intracellular LRP1 (*, $p = 0.0452$) and LDLR (**, $p = 0.0083$; $n = 12$ from three independent experiments). *Q*, immunofluorescence images of enlarged LRP1 puncta in APP-KO astrocytes compared with WT (**, $p = 0.0050$; $n \geq 19$ from two independent experiments). Data are depicted with *bar graphs* of the mean ± S.D.

astrocytes were treated with a γ-secretase inhibitor for 48 h. Only APP Swedish astrocytes exhibited increased APP β-CTF fragments (Fig. 5*D*) and reductions in the APP α-CTF fragment (Fig. 5*C*). In APP V717F astrocytes, by contrast, we observed a dose-dependent increase in the Aβ42/Aβ40 ratio (Fig. 5*E*) as a result of increased Aβ42 (Fig. 5*G*) and no significant change in the amount of APP CTFs compared with WT after 48 h of γ-secretase inhibitor treatment (Fig. 5, *C* and *D*). APP V717F astrocytes also showed no changes in the levels of the soluble fragments, sAPPα (Fig. 5*I*) or sAPPβ (Fig. 5*J*). Collectively, these data are consistent with previous data reporting that the APP Swedish mutation enhances β-secretase cleavage of APP (36, 37), and the APP V717F mutation promotes an increased Aβ42/Aβ40 ratio (38, 39). We hypothesized that these distinct alterations in APP processing could help us elucidate which APP fragment is most important in regulating lipoprotein metabolism in FAD astrocytes.

APP$^{Swe/Swe}$ astrocytes recapitulate APP-KO phenotypes of impaired lipoprotein endocytosis and altered cholesterol metabolism

To examine cholesterol homeostasis in APP mutant FAD astrocytes, we tested lipoprotein endocytosis in which we had previously observed a defect in APP-KO astrocytes. Of all APP mutant genotypes, only APP$^{Swe/Swe}$ astrocytes phenocopied APP-KO astrocytes in reduced lipoprotein endocytosis (Fig. 6*A*) without a concomitant reduction in bulk endocytosis (Fig. 6*B*). APP-KO, APP$^{Swe/WT}$, and APP$^{Swe/Swe}$ astrocytes all exhibited reductions in the APP fragments generated by α-secretase cleavage (Fig. 5, *C* and *I*). However, given that only APP$^{Swe/Swe}$, but not APP$^{Swe/WT}$, astrocytes mimicked APP-KO phenotypes, we hypothesized that FL APP might be crucial in regulating lipoprotein metabolism.

To determine whether reduced lipoprotein endocytosis in FAD astrocytes with reduced FL APP levels also led to downstream alterations in cholesterol metabolism, we looked at the expression of multiple proteins involved in lipoprotein regulation (Fig. 6*C*). We first examined the transcription factor SREBP1, which regulates intracellular cholesterol levels. SREBP function is controlled by multiple mechanisms, including self-regulation by transcriptional positive feedback and activation via sequential proteolysis and translocation of its mature, cleaved fragment to the nucleus. Protein levels of both full-length (Fig. 6*D*) and cleaved SREBP1 (Fig. 6*E*) were elevated in APP-KO and APP$^{Swe/Swe}$ astrocytes. In response to attenuated lipoprotein endocytosis, we observed that the ratio of cleaved/FL-SREBP protein was also significantly increased in APP-KO and APP$^{Swe/Swe}$ astrocytes (Fig. 6*F*). Because mature SREBP also up-regulates lipoprotein receptor-mediated uptake of extracellular lipoproteins, we further examined LDLR protein in FAD astrocytes. As observed previously in APP-KO astrocytes, LDLR protein was elevated in APP$^{Swe/Swe}$ astrocytes (Fig. 6*G*). Together, these data suggest that both APP-KO and APP$^{Swe/Swe}$ astrocytes have impaired lipoprotein endocytosis and exhibit downstream biochemical changes expected in cholesterol-deficient cells.

APP-KO astrocytes and APP$^{Swe/Swe}$ astrocytes also have impaired uptake of Aβ, another LDL-receptor ligand

Given that reduction of FL APP coincided with impaired lipoprotein endocytosis and cholesterol homeostasis, we speculated that FL APP might also be required for other astrocyte-specific functions related to lipoprotein receptor function. We hypothesized that astrocytes with reduced FL APP would also be defective in lipoprotein receptor–mediated internalization of the Aβ peptide.

To determine whether our hiPSC-derived astrocytes could internalize Aβ, WT astrocytes were treated with FITC-conjugated Aβ for 15 min, washed, and given fresh medium (Fig. 7*A*). Over the course of 72 h, we examined the presence of Aβ-FITC, early endosome marker EEA1, and M6PR, which tags vesicles destined for transport to the lysosome. Although the amount of EEA1 and M6PR puncta remained constant, the number of Aβ-FITC puncta decreased over time (Fig. 7*B*). Further analysis demonstrated that Aβ colocalization with M6PR increased over time (Fig. 7*C*), suggesting that Aβ was being targeted for lysosomal degradation. We further verified this observation using flow cytometry of WT astrocytes treated with the pH-sensitive Aβ-FITC or the pH-insensitive Aβ-HiLyte Fluor 647 (Fig. 7*D*). Both probes were utilized because a pH-sensitive signal will decrease in fluorescence intensity when it reaches a more acidic compartment like the lysosome (40). Over the course of 48 h, the intensity of both Aβ-FITC and Aβ-HiLyte Fluor 647 increased over time. However, at 72 h we observed a reduction in the pH-sensitive Aβ-FITC, but not Aβ-HiLyte Fluor 647, suggesting that Aβ was being targeted to an acidic compartment following internalization. To exclude the possibility that the reduction of Aβ-FITC simply reflected an inability to detect the probe, but not actual Aβ degradation, we supplemented astrocyte culture medium with Aβ for 24 h and measured the concentration of Aβ in astrocytes over time (Fig. 7*E*). Over the course of 48 h, we observed a 90% reduction in Aβ. Together, these data indicate that WT hiPSC–astrocytes could both internalize and degrade Aβ. To test whether APP-KO and APP$^{Swe/Swe}$ astrocytes are defective in Aβ internalization in addition to lipoprotein endocytosis, we treated astrocytes with Aβ-HiLyte Fluor 647 for 24 h of continuous uptake (Fig. 7*F*). We observed reduced internalization of Aβ in both APP-KO and APP$^{Swe/Swe}$ astrocytes but not in APP V717F astrocytes, indicating that normal levels of FL APP are required for proper LDL receptor function in the endocytosis of both extracellular lipoproteins and Aβ.

β-Secretase inhibitor treatment reverses impairments in lipoprotein and Aβ endocytosis in APP$^{Swe/Swe}$ astrocytes

Because APP$^{Swe/Swe}$ astrocytes recapitulated defects observed in APP-KO cells, we hypothesized that this was a consequence of increased cleavage and loss of FL APP protein by β-secretase. Because FL APP is transported away from the plasma membrane in an endocytic compartment for β-secretase cleavage (41, 42), we predicted that APP$^{Swe/Swe}$ astrocytes also had reduced APP at the cell surface. Using cell-surface biotinylation and streptavidin beads to pull down surface proteins (Fig. 8*A*), we find that ~10% of total cellular APP is present at the cell

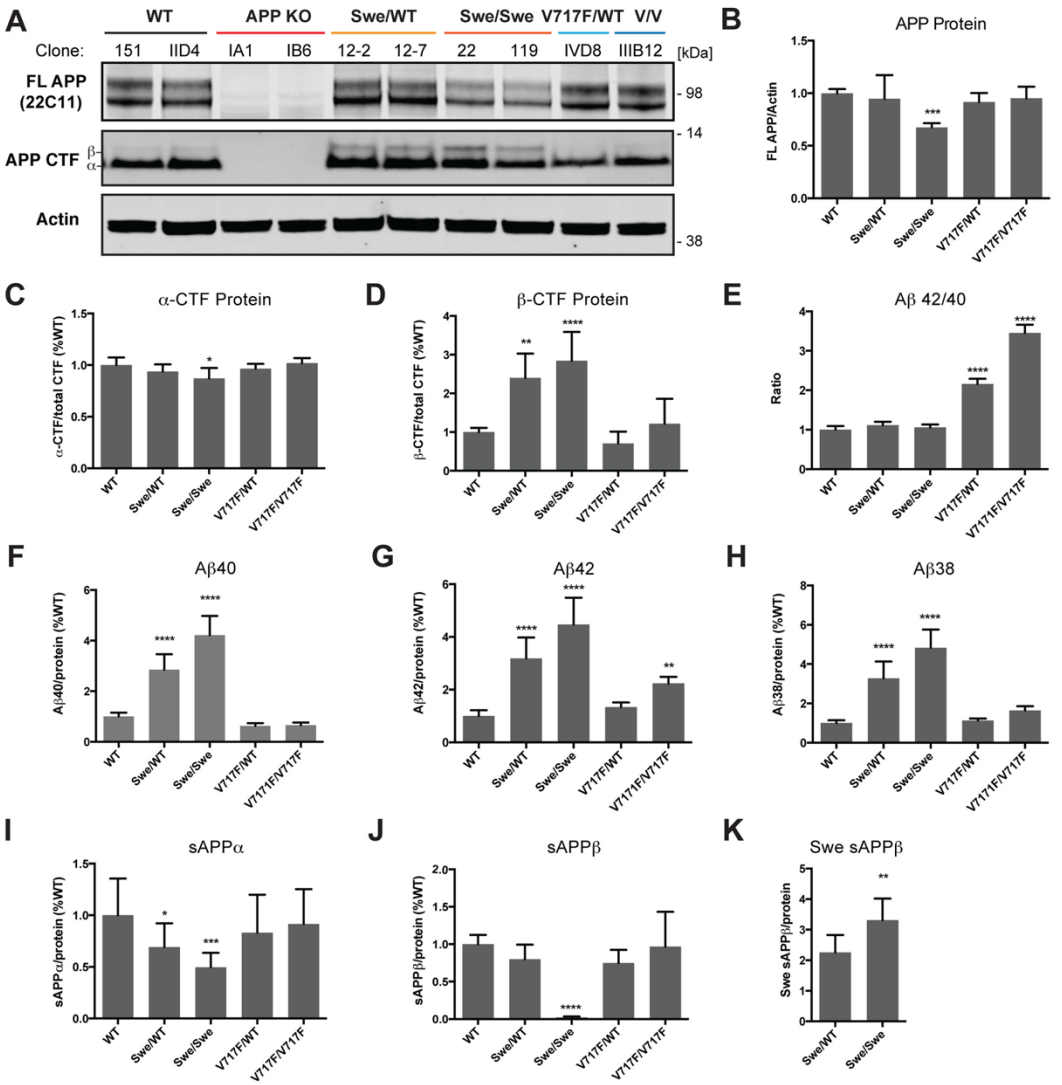

Figure 5. FAD astrocytes exhibit alterations in APP processing. *A–C*, FL APP (22C11), APP CTF, and actin protein levels in astrocytes by Western blotting. *B*, quantification of FL APP protein normalized to actin shows a 30% reduction in FL APP in $APP^{Swe/Swe}$ astrocytes (***, $p = 0.0007$; $n \geq 3$ from at least three independent experiments). *C*, quantification of APP α-CTF protein in astrocytes normalized to total CTF protein after 48 h of 200 nM compound E treatment (*, $p = 0.0306$; $n \geq 3$ from at least three independent experiments). *D*, quantification of APP β-CTF protein in astrocytes normalized to total CTF protein after 48 h of 200 nM compound E treatment (**, $p = 0.0012$; ****, $p < 0.0001$; $n \geq 3$ from at least three independent experiments). *E*, quantification of the Aβ42/Aβ40 ratio after measuring secreted Aβ peptides from astrocytes by MSD immunoassay (****, $p < 0.0001$; $n \geq 6$ from three independent experiments). *F*, secreted Aβ40 from astrocytes (****, $p < 0.0001$; $n \geq 6$ from three independent experiments). *G*, secreted Aβ42 from astrocytes (****, $p < 0.0001$; **, $p = 0.0012$; $n \geq 6$ from three independent experiments). *H*, secreted Aβ38 from astrocytes (****, $p < 0.0001$; $n \geq 6$ from three independent experiments). *I*, secreted sAPPα from astrocytes (*, $p = 0.0362$; ***, $p < 0.0002$; $n \geq 5$ from three independent experiments). *J*, secreted sAPPβ from astrocytes (****, $p < 0.0001$; $n \geq 5$ from three independent experiments). *K*, secreted Swedish sAPPβ from astrocytes (**, $p = 0.0052$; $n = 8$ from two independent experiments). Data are depicted with *bar graphs* of the mean ± S.D.

surface in WT astrocytes (Fig. 8*B*). However, in $APP^{Swe/Swe}$ astrocytes, we observed a 50% reduction of cell-surface APP compared with WT.

To test our hypothesis that normal levels of FL APP are required for proper lipoprotein metabolism and Aβ clearance, we utilized a β-secretase inhibitor (BSI) to inhibit β-cleavage in

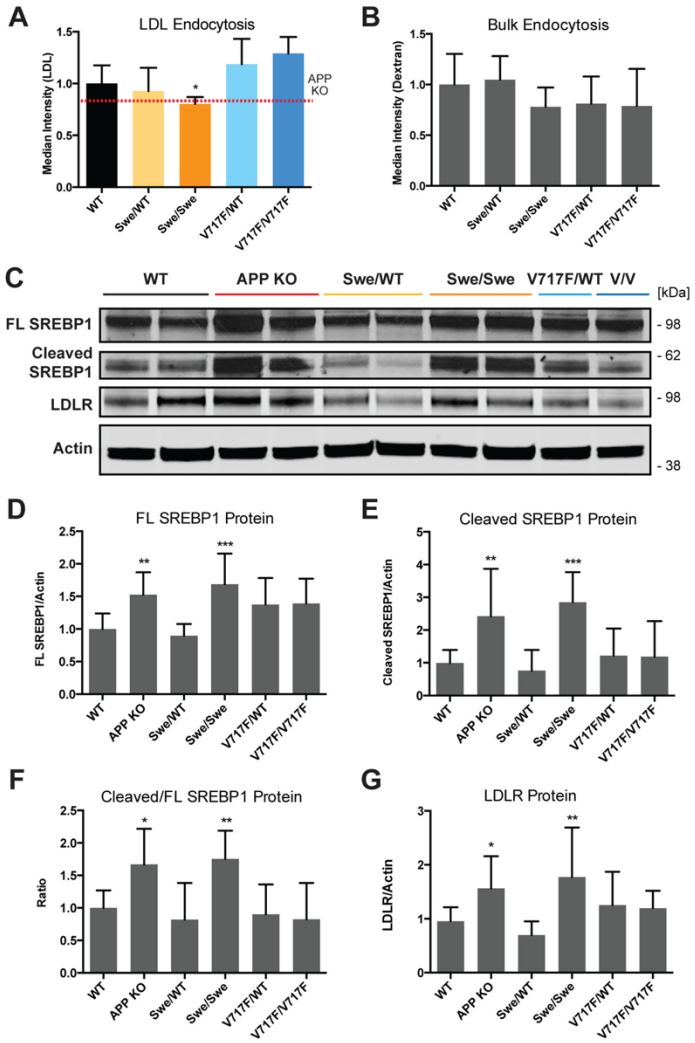

Figure 6. APP$^{Swe/Swe}$ astrocytes recapitulate APP-KO phenotypes. *A*, quantification of LDL endocytosis in FAD astrocytes by flow cytometry demonstrates that APP$^{Swe/Swe}$ astrocytes also exhibit reduced lipoprotein endocytosis ($p = 0.0242$; $n \geq 4$ from three independent experiments). *B*, quantification of bulk endocytosis in FAD astrocytes by flow cytometry for fluorescently-tagged dextran shows no significant differences between WT and all genotypes ($n \geq 6$ from three independent experiments). *C–F*, Western blot analysis of full-length SREBP1 protein, cleaved or mature SREBP1 protein, LDLR, and actin show increased levels of FL SREBP1 protein (**, $p = 0.0071$; ***; $p = 0.0004$; $n \geq 4$ from four independent experiments) (*D*), cleaved SREBP1 protein (**, $p = 0.0077$; ***, $p = 0.0005$; $n \geq 4$ from four independent experiments) (*E*), and an increased ratio of cleaved/FL SREBP1 protein (*, $p = 0.0204$; **, $p = 0.0052$; $n \geq 4$ from four independent experiments) (*F*) in APP-KO and APP$^{Swe/Swe}$ astrocytes. *G*, APP-KO and APP$^{Swe/Swe}$ astrocytes also demonstrate increased total LDLR protein (*, $p = 0.0326$; **, $p = 0.0022$; $n \geq 5$ from five independent experiments). Data are depicted with *bar graphs* of the mean ± S.D.

APP$^{Swe/Swe}$ astrocytes. Because BSIs are sometimes reported to have low potency in cells expressing the APP Swedish mutation (43), we measured whether 24 h of BSI treatment could reduce Aβ secretion in WT and APP$^{Swe/Swe}$ astrocytes. We observed decreased Aβ40 peptides in BSI-treated WT astrocytes and a marked reduction of Aβ40 in BSI-treated APP$^{Swe/Swe}$ astrocytes near WT levels (Fig. 8*C*). To test whether BSI treatment could rescue the defects we observed in APP$^{Swe/Swe}$ astrocytes, we treated WT, APP-KO, and APP$^{Swe/Swe}$ astrocytes with a BSI for 24 h and measured LDL and Aβ endocytosis. Upon pharmacological inhibition of β-secretase in APP$^{Swe/Swe}$ astrocytes, we observed a reversal of defects in both LDL endocytosis (Fig. 8*D*) and Aβ endocytosis (Fig. 8*E*). Significant increases in LDL or Aβ endocytosis were not observed in the absence of APP,

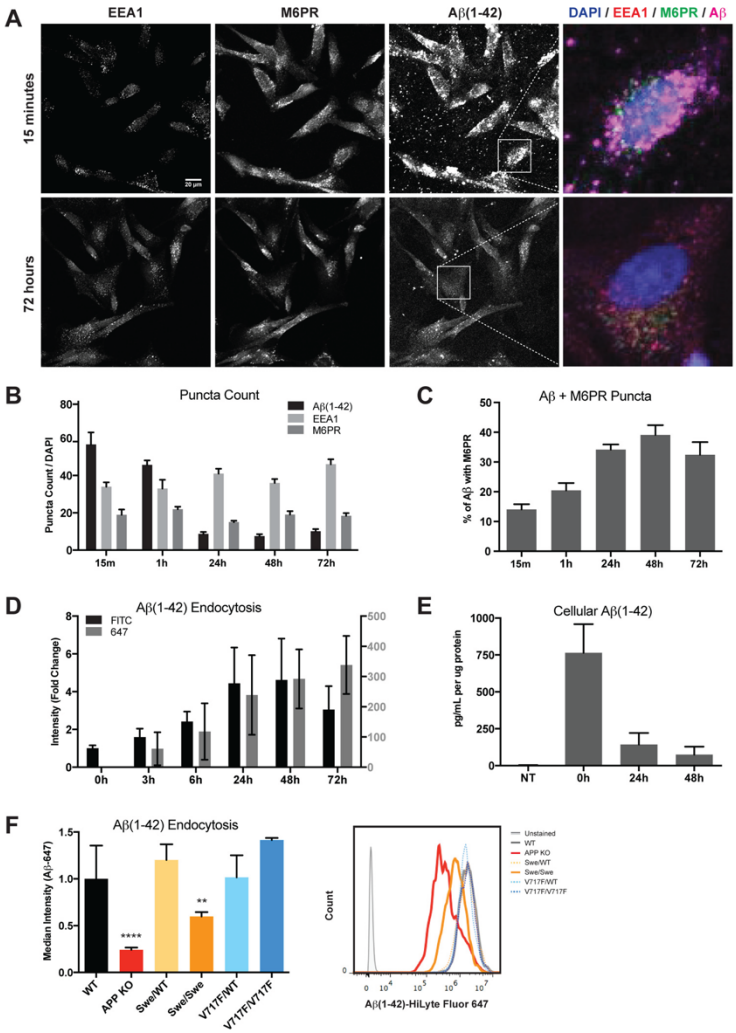

Figure 7. APP-KO and APP$^{Swe/Swe}$ astrocytes have impaired Aβ internalization. *A,* representative immunofluorescence images of WT astrocytes treated with Aβ-FITC for 15 min, harvested at different time points, and stained for EEA1, M6PR, and Aβ. *B,* quantification of puncta count shows relatively equal numbers of EEA1 and M6PR over time, but decreased Aβ-FITC puncta in WT astrocytes over 72 h. *C,* Colocalization analysis shows that the percent of Aβ with M6PR increased over time, but with a slight reduction from 48 to 72 h. Data are representative of two independent experiments. *D,* flow cytometry analysis of continuous Aβ internalization in WT astrocytes treated with Aβ-FITC or Aβ-HiLyte Fluor 647 shows increased Aβ over the course of 48 h, but a reduction of intracellular Aβ between 48 and 72 h in astrocytes treated with the pH-sensitive Aβ-FITC, but not pH-insensitive Aβ-HiLyte Fluor 647 ($n \geq 10$ from two independent experiments). *E,* quantification of cellular Aβ42 by MSD immunoassay in WT astrocytes over time after pre-treatment with Aβ42 for 24 h ($n = 6$ from two independent experiments). *F,* quantification of Aβ internalization in APP-KO and FAD astrocytes by flow cytometry demonstrates that APP-KO (****, $p < 0.0001$) and APP$^{Swe/Swe}$ (**, $p = 0.0012$) astrocytes have impaired Aβ uptake ($n \geq 6$ from two independent experiments). Data are depicted with *bar graphs* of the mean ± S.D.

indicating that rescue of impaired endocytosis relied on impairing β-secretase cleavage of FL APP.

Discussion

APP is a transmembrane protein that is highly expressed in the central nervous system. It has been shown to have many varied biological functions, likely due to multilayered mechanisms of regulation resulting in multiple proteolytic products and alternatively spliced isoforms. To determine whether APP or any of its proteolytic cleavage products are involved in lipoprotein regulation, we employed CRISPR/Cas9-genome editing to generate APP-KO, APP Swedish, and APP V717F hiPSCs

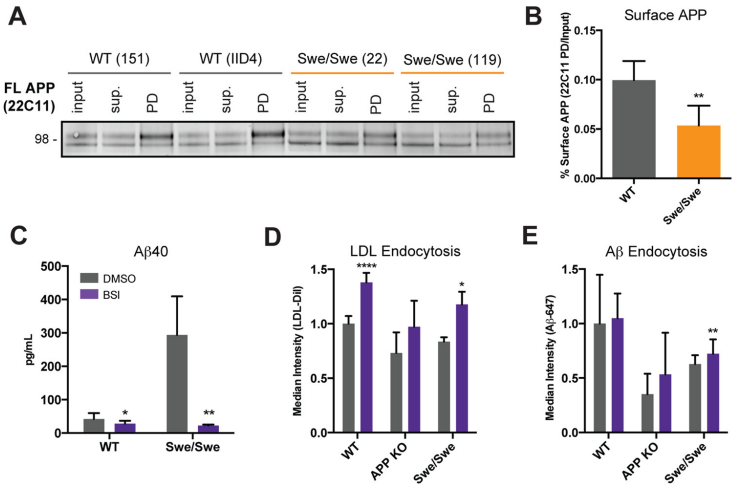

Figure 8. Pharmacological inhibition of β-secretase reverses LDL and Aβ endocytosis defects in APP$^{Swe/Swe}$ astrocytes. *A* and *B*, quantification of cell-surface biotinylation experiments shows that APP$^{Swe/Swe}$ astrocytes have reduced cell-surface APP levels, identified in the pulldown (*PD*) lanes, compared with WT astrocytes (**, $p = 0.0016$). Western blots were run with 5% of input, 5% of supernatant (*sup.*), and 50% of pulldown ($n \geq 5$ from three independent experiments). *C*, secreted Aβ40 peptide levels, measured by MSD immunoassay, in WT and APP$^{Swe/Swe}$ astrocytes after 24 h of treatment ± a β-secretase inhibitor (*BSI*) exhibit significant reductions in secreted Aβ40 peptides upon β-secretase inhibitor treatment (*, $p = 0.0154$; **, $p = 0.0020$; $n = 6$ from two independent experiments). *D* and *E*, flow cytometry analysis of LDL ($n \geq 4$ from two independent experiments) (*D*) and Aβ endocytosis (*E*) ($n \geq 4$ from two independent experiments) in WT and APP$^{Swe/Swe}$ astrocytes ± β-secretase inhibitor treatment shows that β-secretase inhibition reverses defects in APP$^{Swe/Swe}$ (LDL, $p = 0.0120$; Aβ, $p = 0.0092$) but not APP-KO astrocytes. ****, $p \leq 0.0001$. Data are depicted with *bar graphs* of the mean ± S.D.

and differentiated them into human astrocytes, the source of *de novo* cholesterol in the brain. Here, we show that FL APP regulates LDL receptor function. Loss of FL APP resulted in impaired lipoprotein and Aβ endocytosis, reduced intracellular cholesterol, and aberrant elevations of transcripts and proteins related to cholesterol synthesis and internalization. Finally, we show that inhibiting cleavage of FL APP by β-secretase can reverse LDL and Aβ endocytosis defects, but only in the presence of APP. Thus, in addition to having a critical role in mammalian brain development (44), normal levels of FL APP are also critical in the maintenance of homeostatic brain functions. We propose that pathological alterations of FL APP levels could contribute to glial dysfunction in multiple neurodegenerative disorders.

Mechanistically, we attribute defective lipoprotein and Aβ endocytosis in APP-KO and APP$^{Swe/Swe}$ astrocytes to the loss of FL APP in each of these genotypes. APP isoforms containing the KPI domain have been shown to bind to LRP1 at the N terminus (45, 46). Intracellularly, the cytoplasmic adaptor protein FE65 has been shown to link the C-terminal NPXY endocytosis motifs of APP and multiple LDL receptors (47–49). Thus, astrocytic APP isoforms, which include the KPI domain, may have a dual linkage with LDL receptors at both the N and C termini. In light of this prior work demonstrating interactions between APP and LDL receptors, it is possible that FL APP acts as a coreceptor for LDL receptor ligands in human astrocytes. A further explanation for dysregulated cholesterol metabolism in APP-KO and Swedish astrocytes is that these genotypes also have a high rate of ligand-independent receptor endocytosis. It is feasible that both decreased endocytosis of lipoproteins and increased ligand-independent endocytosis of the LDL receptors combine in an additive manner to produce the results we observed. Overall, it is consistent with our data that without proper FL APP levels the function of LDL receptors is impaired. This dovetails nicely with previous studies demonstrating that APP interacts with diverse binding partners, including APOE (50), kinesin (51, 52), SORLA (53), and cholesterol (54). Interestingly, all of these interacting partners modulate APP metabolism, and alterations in these interactions are hypothesized to contribute to AD pathology.

FL APP regulates brain cholesterol metabolism

In human astrocytes, we find that normal levels of FL APP are essential for proper regulation of cholesterol homeostasis. Loss of FL APP led to impairments in lipoprotein endocytosis (Fig. 4*A*), resulting in decreased intracellular cholesterol (Fig. 3*C*) and activation of SREBP-target gene transcripts and protein (Figs. 3*D* and 4, *I–L*) in both APP-KO and Swedish astrocytes. Interestingly, we did not observe a dose-dependent effect of FL-APP levels in our LDL endocytosis experiments as we did in the Aβ endocytosis experiments. Although both APP-KO and Swedish astrocytes exhibited differential handling of lipoproteins compared with WT astrocytes, it is possible that more subtle changes in lipoprotein endocytosis correlating with FL APP levels are below the level of detection in the assay.

Previous work done by our lab using the same isogenic FAD hiPSC lines to study human neurons revealed that accumulation of a different APP fragment, β-CTF, caused impairments in lipoprotein endocytosis and a neuron-specific transcytotic trafficking pathway via defects in recycling (33). Although we cannot rule out that the overabundance of APP β-CTF in

$APP^{Swe/Swe}$ astrocytes outcompetes FL APP for binding to LDL receptors and thus impairs recycling of LDL receptors to the surface, CTFs were difficult to detect in our hiPSC-derived astrocytes without γ-secretase inhibition. This suggests that steady-state levels of the rapidly processed or degraded β-CTF might be quite low relative to FL APP or Aβ in $APP^{Swe/Swe}$ astrocytes. Given the low levels of astrocytic β-CTF we observed, we hypothesize that we might not observe cholesterol phenotypes in FAD astrocytes that are characterized by accumulation of β-CTF protein, like presenilin mutant astrocytes. By contrast, in mutant astrocytes characterized by increased APP expression (*e.g.* APP duplication or Down syndrome), we hypothesize that there will be alterations in cholesterol metabolism. Altering APP gene dosage in astrocytes is likely to alter its normal physiological processing as well as the processing of other proteins, like LRP1, with which APP may be competitive substrate. Collectively, these data shed light on the importance of studying the role of endogenous proteins in specific cell types as we find that alterations in APP processing can affect either astrocyte or neuron-specific functions via different mechanisms. Increased β-CTF in human neurons and loss of FL APP in human astrocytes may impair lipoprotein endocytosis independently in a cell-specific context. Additional work comparing astrocytes and neurons from different FAD mutations would be revealing.

In this study, we demonstrate a linkage between FL APP levels and lipoprotein endocytosis. However, further study of how FL APP levels in astrocytes influence lipoprotein export and thus neuronal health is also needed, given the reliance of neurons on astrocyte-derived lipoproteins (25, 56). Future work to investigate how aberrant lipoprotein metabolism in astrocytes contributes to AD phenotypes could provide mechanistic insight into the development of new AD therapeutics.

FL APP regulates Aβ clearance

Here, we report that loss of FL APP in APP-KO and $APP^{Swe/Swe}$ astrocytes impairs Aβ internalization (Fig. 7*F*). Interestingly, we do not observe Aβ clearance defects in the other FAD mutations. This not only reflects the high degree of clinical and pathological heterogeneity within AD, but also heterogeneity within subgroups of FAD patients harboring different FAD mutations (57, 58). Although it is possible that some FAD mutant astrocytes could have small alterations in FL APP levels that are also below our level of detection, these phenotypic differences are also in agreement with the notion that the accumulation of Aβ in FAD is primarily due to neuronal overproduction of Aβ. In line with this idea, FAD mutations in APP are often considered to be gain-of-function mutations due to the generation and accumulation of some toxic proteolytic product (3). However, here we find in $APP^{Swe/Swe}$ astrocytes that the mutation confers a loss-of-function phenotype associated with the loss of FL APP to β-secretase cleavage. We postulate that the impairment in Aβ clearance in $APP^{Swe/Swe}$ astrocytes could also contribute to the greatly increased Aβ plaque load observed in mouse models overexpressing the APP Swedish mutation (59–61).

In light of data suggesting that the increased deposition of Aβ in SAD is primarily a result of impaired Aβ clearance rather than increased Aβ generation (62), further work in this system could examine whether astrocytes derived from SAD patients are defective in Aβ clearance. Also, given the observation that both reactive astrocytes and cells undergoing a cellular stress response alter APP expression and APP processing (63–65), it would be revealing to study how FL APP levels under these pathological conditions affect Aβ clearance mechanisms.

Linking APP to mechanisms of glial dysfunction in SAD

In this study, we find that loss of FL APP impairs LDL receptor function. We provide a novel linkage between FL APP levels and two potential mechanisms of glial dysfunction in AD: dysregulation of cholesterol metabolism and Aβ clearance. Although several studies have addressed the effect of the loss of LDL receptors on APP processing (66–69), little has been done to elucidate how the loss of APP affects LDL receptor function. The concept that FL APP levels directly affect the ability of LDL receptors to endocytose lipoproteins or Aβ is in agreement with the known stoichiometry of the LRP1–FE65–APP trimeric complex (47). Loss or overproduction of any member of this multimeric complex could alter the various functions of the LDL receptors by abrogating complex formation. Together, using endogenous protein levels in an isogenic series of iPSC-derived human astrocytes, our data shed light on the novel function of FL APP in controlling LDL receptor–mediated cholesterol metabolism and Aβ clearance in human astrocytes. These findings suggest that FL APP may have a more central role in the etiology of AD than previously suspected.

Experimental procedures

Cell culture

IPSCs were cultured as described previously (70–72) on a MEF feeder layer in HUES medium: knockout DMEM, 10% knockout serum replacement, 10% plasmanate (Grifols Therapeutics, Inc.), 1× nonessential amino acids, 1× Glutamax, 1× penicillin/streptomycin, and 0.1 mM β-mercaptoethanol (all Invitrogen) with 20 ng/ml FGF-2 (Millipore). The iPSCs were passaged with Accutase (Innovative Cell Technologies) and supplemented with 10 μM ROCK inhibitor (RI, Y-27632 dihydrochloride, Abcam) after passaging only. The iPSCs were differentiated into NPCs, as described previously (23), by seeding iPSCs on a PA6 stromal cell layer in PA6 differentiation medium: Glasgow DMEM, 10% knockout serum replacement, 1 mM sodium pyruvate, 0.1 mM nonessential amino acids, and 0.1 mM β-mercaptoethanol (all Invitrogen), in the presence of 500 ng/ml Noggin (R&D Systems) and 10 mM SB431542 (Stemgent) for 6 days. Following 12–14 days of differentiation, NPCs were FACS-purified using a CD184-APC+, CD271-PE−, CD44-PE−, CD24−PECy7+ (BD Biosciences) cell-surface signature on a BD FACSAria II flow cytometer. NPCs were cultured on 20 mg/ml poly-L-ornithine and 5 mg/ml laminin (Sigma)-coated plates in NPC medium: DMEM/F-12 + Glutamax, 0.5× N2, 0.5× B27, penicillin/streptomycin (all Life Technologies, Inc.), and 20 ng/ml FGF-2, and passaged with Accutase. For neuronal differentiation, NPCs were expanded to confluent 10-cm plates, after which FGF-2 was withdrawn from the culture medium, and the medium was changed twice a week. After 3 weeks, neurons were FACS-purified using a CD184-APC−, CD44-PE−, CD24−PECy7+ (BD Biosciences) cell-surface sig-

nature, plated on poly-L-ornithine/laminin-coated plates in NPC medium supplemented with 20 ng/μl BDNF, 20 ng/μl glial cell line-derived neurotrophic factor (both from Peprotech), and 0.5 mM dibutyryl cAMP (Sigma). NPCs were differentiated to astrocytes using the following protocol. Briefly, a confluent 10-cm plate of NPCs was scraped in NPC medium, transferred to three wells of a 6-well plate, and placed on a 90 rpm orbital shaker in the incubator to promote neurosphere formation. After 24 h, 5 μM RI was supplemented to the medium. Following 48 h with RI, the neurospheres were grown in NPC medium without FGF-2, and the medium was changed every 2–3 days. One week after scraping, neurosphere medium was changed to Astrocyte Growth Medium (AGM) containing 3% FBS, ascorbic acid, recombinant human EGF, GA-1000, insulin, and L-glutamine (Lonza) and cultured for 2 weeks. Next, the neurospheres were plated on a poly-L-ornithine/laminin-coated 10-cm plate. One week later, after which astrocytes emerged from the neurospheres, the cells were passaged with Accutase, cultured in AGM, and maintained with the neurospheres. To make lipoprotein-free astrocyte medium, FBS was replaced with lipoprotein-deficient serum (Sigma). For experimental use, neurospheres were not included. In every experiment, each genotype is represented by the following number of independently differentiated hiPSC subclones/astrocyte lines: WT (2 or 3 clones: 151, IB7, and IID4), APP-KO (2 clones: IA1 and IB6), $APP^{Swe/WT}$ (2 clones: 12-2 and 12-7), $APP^{Swe/Swe}$ (2 clones: 22 and 119), $APP^{V717F/WT}$ (1 clone: IVD8), $APP^{V717F/V717F}$ (1 clone: IIIB12).

Genome editing

All isogenic iPSCs were derived using CRISPR/Cas9 as described previously from the CVB iPSC line (33, 71) derived from J. Craig Venter (73), whose diploid genome sequence is publicly available (74). In brief, iPSCs were pretreated with 10 μM RI prior to nucleofection. To obtain single cells, iPSCs were dissociated with Accutase and filtered twice through 100-μm filters. To generate APP-KO and APP V717F clones, 2×10^6 iPSC were nucleofected using the Amaxa Human Stem Cell Nucleofector Kit I (Lonza) with 6 μg of CMV::Cas9 –2A-eGFP vector and 3 μg of U6::gRNA vector, which was generated using the gRNA synthesis protocol as described previously (75). For APP Swedish clones, 8×10^5 iPSC were nucleofected with 5 μg of pSpCas9(BB)-2A-GFP (PX458) vector, which was generated as described previously (76). The following guide RNA sequences were used, targeting exon 16 for APP-KO and APP Swedish: GGA GAT CTC TGA AGT GAA GAT GG, and exon 17 for APP V717F: GAC AGT GAT CGT CAT CAC CTT GG. To introduce the APP Swedish or APP V717F point mutations in our WT CVB hiPSC line using CRISPR/Cas9-mediated homology directed repair, 100 μM single-stranded DNA oligonucleotides were also included during nucleofection. After culturing the iPSCs in the presence of RI for 48–72 h, 1×10^4 GFP+ iPSCs were FACS sorted (FACS Aria IIu, BD Biosciences) and plated on 10-cm MEF feeder plates in the presence of RI. After 1 week, single colonies were manually picked, cultured in 96-well plates, and expanded. DNA from single clones was harvested using QuickExtract DNA Extraction Solution (Epicenter) and PCR-amplified using the following PCR primers: *APPex16-F*, CCC GTA AGC CAA GCC AAC AT, and *APPex16-R*, CAT GCA CGA ACT TTG CTG CC; or *APPex17-F*, TGT TCC ACC TGT CAA AGG GT, and *APPex17-R*, AGT TGA GAT AAC AAC ACA CAC TCT. PCR products were purified using the QIAquick PCR purification kit (Qiagen) or ExoSAP-IT PCR Product Cleanup Reagent (ThermoFisher Scientific) as directed by the manufacturer and Sanger sequenced. Clones in which disruptions at the predicted gRNA/Cas9 cut site were observed were further sequenced after cloning using the Zero Blunt TOPO PCR cloning kit (Invitrogen). All previously unpublished isogenic iPSCs were digitally karyotyped by hybridization to the Infinium CoreExome-24 BeadChip (Illumina) as described previously (77) and determined to be euploid.

RNA expression

For mRNA expression analysis, RNA was isolated using the RNeasy mini kit (Qiagen) and DNase-treated using TURBO DNase (Ambion) for 1 h at 37 °C. cDNA was synthesized from RNA primed with oligo(dT) using the SuperScript First-Strand synthesis system (Invitrogen). qRT-PCR was performed using FastStart SYBR Green (Roche Applied Science), and samples were run in triplicate on an Applied Biosystems 7300 RT-PCR system. Data were analyzed using the $\Delta\Delta Ct$ method, and target genes were normalized to the geometric mean of three housekeeping genes: *RPL13A*, *RPL27*, and *TBP*. The following primers were used: 3′-*APP-F*, ATC ATG GTG TGG TGG AGG TT, and 3′-*APP-R*, ACA CCG ATG GGT AGT GAA GC; 5′-*APP-F*, GAA GCA GCC AAT GAG AGA CAG, and 5′-*APP-R*, TCA AAA TGC TTT AGG GTG TGC; *APLP1-F*, CTT CCC ACA GCC AGT AGA TGA, and *APLP1-R*, CCA GGC ATG CCA AAG TAA ATA; *APLP2-F*, CCA TGG CAC TGA ATA TGT GTG, and *APLP2-R*, CCT CAT CAT CCT CAT CCA CAG; *HMGCR-F*, TCC CTG GGA AGT CAT AGT GG, and *HMGCR-R*, AGG ATG GCT ATG CAT CGT GT; *LDLR-F*, CTG GAA ATT GCG CTG GAC, and *LDLR-R*, GTC TTG GCA CTG GAA CTC GT; *LRP1-F*, CCA GCC CTT TGA GAT ACA GG, and *LRP1-R*, CTG CTC TCA GCT CTG GTC G; *RPL13A-F*, GGA CCT CTG TGT ATT TGT CAA, and *RPL13A-R*, GCT GGA AGT ACC AGG CAG TG; *RPL27-F*, AAA CCG CAG TTT CTG GAA GA, and *RPL27-R*, TGG ATA TCC CCT TGG ACA AA; *SREBF2-F*, GAG ACC ATG GAG ACC CTC AC, and *SREBF2-R*, TCA GGG AAC TCT CCC ACT TG; *TBP-F*, TGC TTC ATA AAT TTC TGC TCT G, and *TBP-R*, TAG AAG GCC TTG TGC TCA CC.

Protein expression

Cells were lysed in RIPA Lysis Buffer (Millipore) with protease (Calbiochem) and phosphatase inhibitors (Halt). Protein concentrations were determined using the Pierce BCA protein assay kit (ThermoFisher Scientific). Equal amounts of protein lysates were run on NuPAGE 4–12% BisTris gels (Invitrogen), transferred to nitrocellulose or polyvinylidene difluoride membranes, and blocked for 1 h at room temperature using either 5% milk or Odyssey Blocking Buffer (LI-COR). Blots were probed overnight at 4 °C using the corresponding primary antibodies followed by HRP-conjugated (Vector Laboratories) or IRDye secondary antibodies (LI-COR) at 1:5000. Bands were quantified using ImageJ software or the Odyssey Imaging System follow-

ing the manufacturer's instructions. The following antibodies were used: anti-actin (1:50,000; EMD Millipore MAB1501); anti-APLP1 (1:1000; Calbiochem 171615); anti-APLP2 (1:1000; Calbiochem 171616/7); anti-APP A4 clone 22C11 (1:1000; EMD Millipore MAB348); anti-APP C terminus (1:500; EMD Millipore 171610); anti-β-amyloid, 6E10 (1:1000, BioLegend 803015); anti-LDLR (1:1000; Abcam AB14056); anti-LRP1 (1:1000; Abcam AB92544); and anti-SREBP1 (1:500; Proteintech 14088-1-AP).

Sterol analysis

For free sterol analysis, 1×10^6 cells were pelleted and stored at −80 °C before sterols were extracted and analyzed as described previously at the UCSD Lipidomics Core (55, 78). Briefly, sterols were extracted by dichloromethane/methanol (50:50; v/v), hydrolyzed, and separated using reverse-phase LC using a 1.7-μm 2.1 × 150-mm Kinetex C18 column (Phenomenex) on an ACQUITY UPLC system (Waters) followed by analysis on QTRAP 6500 mass spectrometer (Ab Sciex). A mixture of deuterated standards (Avanti Polar Lipids) was used for internal standards. For intracellular cholesterol measurements, 1×10^6 subconfluent astrocytes were pelleted and stored at −80 °C. Cells were resuspended in PBS, mixed with chloroform/methanol (2:1 v/v), vortexed, and rotated. Following centrifugation, the chloroform and lipid-containing layer was transferred to a new tube, vacuum-dried, and resuspended in Reaction Buffer E from the Amplex Red Cholesterol Assay (Invitrogen). Cholesterol was measured from the chloroform/methanol-extracted samples using the Amplex Red Cholesterol Assay as directed by the manufacturer.

Cell-surface biotinylation

For surface biotinylation of lipoprotein receptors, astrocytes were seeded in a 10-cm plate at a density of 2×10^6 cells per plate in duplicate. After 48 h, sub-confluent astrocytes were washed three times with ice-cold PBS and then incubated with either PBS or 2 mM EZ-Link Sulfo-NHS-SS-Biotin (ThermoFisher Scientific) for 30 min at 4 °C. Cells were washed three times with TBS, pH 7.4, and lysed in RIPA buffer with protease and phosphatase inhibitors. For streptavidin pulldown, 250 μg of protein lysate at 0.5 μg/μl was incubated with 100 μl of pre-washed PureProteome Streptavidin Magnetic Beads (EMD Millipore) by rotating overnight at 4 °C. The next day, beads were immobilized, and a sample of supernatant was saved to measure nonbiotinylated intracellular protein. The beads were washed five times in cold PBS containing 1% Triton X-100, and biotinylated proteins were released from the streptavidin beads by boiling the samples in 2× NuPAGE LDS Sample Buffer (Invitrogen) at 100 °C. Western blots were run with 5% of input, 5% of supernatant, and 50% of pulldown.

Preparation of Aβ peptide

Lyophilized FITC-labeled β-amyloid(1–42) (American Peptide) or β-amyloid(1–42) HiLyte Fluor 647 (Anaspec) was solubilized following the manufacturer's instructions using a minimal amount of alkaline 1.0% NH_4OH immediately followed by 1× PBS to a working concentration of 100 μM. Small aliquots were immediately stored at −80 °C and only used once to eliminate variability due to freeze-thawing.

Flow cytometry

For lipoprotein and bulk endocytosis assays, astrocytes were seeded in a 24-well plate at a density of 8×10^4 cells per well. Two days later, cells were treated with 20 μg/ml BODIPY FL LDL or DiI LDL for 1 h at 37 °C or 50 μg/ml dextran-fluorescein or dextran-Alexa Fluor 647 (Life Technologies, Inc.). Following incubation with labeled substrates, cells were washed with cold PBS and dissociated with trypsin (Invitrogen) for 5–10 min at 37 °C to remove any ligand bound to the cell surface. For the transferrin recycling assay, astrocytes were seeded in a 24-well plate at a density of 8×10^4 cells per well. Two days later, cells were treated with 100 μg/ml transferrin-Alexa Fluor 647 (Life Technologies, Inc.) for 10 min at 37 °C. Following the 10-min incubation, cells were washed with cold PBS and cold acid wash buffer to remove transferrin bound to the cell surface. Cells at the "0" time point were dissociated using Accutase, filtered, and stored on ice until analysis. The remaining conditions were "chased" with culture medium and harvested at the indicated time points. For analysis of cell-surface LDLR protein, astrocytes were seeded in a 24-well plate at a density of 8×10^4 cells per well. After 24 h, astrocytes were treated with either DMSO or berberine (10 μg/ml, Selleck Chemicals) for 24 h. Next, cells were washed with PBS and dissociated using an EDTA dissociation buffer (50 mM HEPES, pH 7.4, 1 mM EDTA, 5 mM glucose, 5 mM KCl, 125 mM NaCl, and 2 mg/ml BSA) for 10 min at 37 °C. Cells were then incubated with (*R*)-phycoerythrin mouse anti-human LDLR (BD Biosciences 565653) at a final concentration of 8 μg/ml on ice for 30 min. For continuous Aβ uptake assays, astrocytes were incubated with 500 nM FITC-labeled β-amyloid(1–42) (American Peptide) or 500 nM β-amyloid(1–42) HiLyte Fluor 647 (Anaspec). At the indicated time points, cells were harvested by trypsinization to remove any surface-bound ligand and fixed with 4% paraformaldehyde at room temperature for 15 min. Fixed cells were stored in PBS at 4 °C until analysis. All experiments were analyzed on an Accuri C6 flow cytometer (BD Biosciences). 10,000–20,000 events were recorded per sample, and the median fluorescence intensity was quantified.

Immunofluorescence

Astrocytes were seeded in 8-well chamber slides at a density of 3×10^4 cells per chamber and fixed 2–3 days after plating. Briefly, cells were fixed with 4% paraformaldehyde for 15 min at room temperature, permeabilized with 0.1% Triton X-100, and blocked in serum. The antibodies used for immunofluorescence experiments were anti-EEA1 (1:100; BD Biosciences 610456/7), anti-LRP1 (1:200; Abcam AB92544), and anti-M6PR (1:1,000, Abcam AB12894). Secondary antibodies were Alexa Fluor anti-mouse and anti-rabbit IgG (Invitrogen) and used at 1:200. Images were acquired on a Zeiss or Leica confocal microscope

Aβ and sAPP measurements

For secreted Aβ and sAPP measurements, astrocytes were seeded at 2.5×10^5 cells per well of a 24-well plate. The follow-

ing day, the medium was changed. After 5 days in culture, medium was harvested and run on a V-PLEX Aβ Peptide Panel 1 (6E10) kit, sAPPα/sAPPβ kit, and/or Swedish sAPPβ kit (Meso Scale Discovery). For cellular Aβ measurements, 500 nM Aβ(1–42) (American Peptide) was supplemented to astrocyte culture medium. After 24 h, cells were washed with PBS, and fresh medium was added. At the indicated times, cell lysates were harvested using MSD Lysis Buffer with protease and phosphatase inhibitors and stored at −80 °C until they were run on a V-PLEX Aβ Peptide Panel 1 (6E10) kit (Meso Scale Discovery). These measurements were normalized to protein content using the Pierce BCA Protein Assay kit (ThermoFisher Scientific). γ-Secretase inhibitor treatment was performed using 200 nM Compound E (EMD Chemicals) for 48 h. β-Secretase inhibitor treatment was performed using 4 μM β-Secretase Inhibitor IV (Calbiochem) for 24 h.

Statistics

All data were analyzed using GraphPad Prism Software. Statistical analysis comparing the two groups was performed using Student's *t* test. Statistical analysis comparing different genotypes to WT controls was performed by Dunnett's multiple comparisons test. Data are depicted with bar graphs of the mean ± S.D.

Author contributions—L. K. F. and L. S. B. G. conceptualization; L. K. F. data curation; L. K. F., R. d. S. C., and S. M. R. formal analysis; L. K. F. and L. S. B. G. funding acquisition; L. K. F., M. M. Y., R. d. S. C., S. M. R., and V. F. L. investigation; L. K. F., M. M. Y., and S. M. R. methodology; L. K. F. writing-original draft; L. K. F. and L. S. B. G. writing-review and editing; G. W., E. A. R., and J. E. Y. resources; L. S. B. G. supervision.

Acknowledgments—We thank Rik van der Kant, Angels Almenar-Queralt, John W. Steele, and Bridget Kohlnhofer for scientific insight; Oswald Quehenberger and the UCSD Lipidomics Core for technical assistance; and Beatriz C. Freitas and Alysson R. Muotri for their astrocyte differentiation protocol.

References

1. Hardy, J. (1997) Amyloid, the presenilins and Alzheimer's disease. *Trends Neurosci.* **20,** 154–159 CrossRef Medline
2. Holtzman, D. M., Morris, J. C., and Goate, A. M. (2011) Alzheimer's disease: the challenge of the second century. *Sci. Transl. Med.* **3,** 77sr1 Medline
3. Hardy, J., and Selkoe, D. J. (2002) The amyloid hypothesis of Alzheimer's disease: progress and problems on the road to therapeutics. *Science* **297,** 353–356 CrossRef Medline
4. Corder, E. H., Saunders, A. M., Strittmatter, W. J., Schmechel, D. E., Gaskell, P. C., Small, G. W., Roses, A. D., Haines, J. L., and Pericak-Vance, M. A. (1993) Gene dose of apolipoprotein E type 4 allele and the risk of Alzheimer's disease in late onset families. *Science* **261,** 921–923 CrossRef Medline
5. Liu, C.-C., Liu, C.-C., Kanekiyo, T., Xu, H., and Bu, G. (2013) Apolipoprotein E and Alzheimer disease: risk, mechanisms and therapy. *Nat. Rev. Neurol.* **9,** 106–118 CrossRef Medline
6. Bertram, L., McQueen, M. B., Mullin, K., Blacker, D., and Tanzi, R. E. (2007) Systematic meta-analyses of Alzheimer disease genetic association studies: the AlzGene database. *Nat. Genet.* **39,** 17–23 CrossRef Medline
7. Jick, H., Zornberg, G. L., Jick, S. S., Seshadri, S., and Drachman, D. A. (2000) Statins and the risk of dementia. *Lancet* **356,** 1627–1631 CrossRef Medline
8. Yaffe, K., Barrett-Connor, E., Lin, F., and Grady, D. (2002) Serum lipoprotein levels, statin use, and cognitive function in older women. *Arch. Neurol.* **59,** 378–384 CrossRef Medline
9. Rockwood, K., Kirkland, S., Hogan, D. B., MacKnight, C., Merry, H., Verreault, R., Wolfson, C., and McDowell, I. (2002) Use of lipid-lowering agents, indication bias, and the risk of dementia in community-dwelling elderly people. *Arch. Neurol.* **59,** 223–227 CrossRef Medline
10. van der Kant, R., and Goldstein, L. S. (2015) Cellular functions of the amyloid precursor protein from development to dementia. *Dev. Cell* **32,** 502–515 CrossRef Medline
11. Grimm, M. O., Grimm, H. S., Pätzold, A. J., Zinser, E. G., Halonen, R., Duering, M., Tschäpe, J. A., De Strooper, B., Müller, U., Shen, J., and Hartmann, T. (2005) Regulation of cholesterol and sphingomyelin metabolism by amyloid-β and presenilin. *Nat. Cell Biol.* **7,** 1118–1123 CrossRef Medline
12. Liu, Q., Zerbinatti, C. V., Zhang, J., Hoe, H.-S., Wang, B., Cole, S. L., Herz, J., Muglia, L., and Bu, G. (2007) Amyloid precursor protein regulates brain apolipoprotein E and cholesterol metabolism through lipoprotein receptor LRP1. *Neuron.* **56,** 66–78 CrossRef Medline
13. Tamboli, I. Y., Prager, K., Thal, D. R., Thelen, K. M., Dewachter, I., Pietrzik, C. U., St George-Hyslop, P., Sisodia, S. S., De Strooper, B., Heneka, M. T., Filippov, M. A., Müller, U., van Leuven, F., Lütjohann, D., and Walter, J. (2008) Loss of γ-secretase function impairs endocytosis of lipoprotein particles and membrane cholesterol homeostasis. *J. Neurosci.* **28,** 12097–12106 CrossRef Medline
14. Pierrot, N., Tyteca, D., D'auria, L., Dewachter, I., Gailly, P., Hendrickx, A., Tasiaux, B., Haylani L. E., Muls, N., N'Kuli, F., Laquerrière, A., Demoulin, J. B., Campion, D., Brion, J. P., Courtoy, P. J., Kienlen-Campard, P., and Octave, J. N. (2013) Amyloid precursor protein controls cholesterol turnover needed for neuronal activity. *EMBO Mol. Med.* **5,** 608–625 CrossRef Medline
15. Wang, W., Mutka, A. L., Zmrzljak, U. P., Rozman, D., Tanila, H., Gylling, H., Remes, A. M., Huttunen, H. J., and Ikonen, E. (2014) Amyloid precursor protein α- and β-cleaved ectodomains exert opposing control of cholesterol homeostasis via SREBP2. *FASEB J.* **28,** 849–860 CrossRef Medline
16. Goldstein, J. L., DeBose-Boyd, R. A., and Brown, M. S. (2006) Protein sensors for membrane sterols. *Cell* **124,** 35–46 CrossRef Medline
17. Deane, R., Wu, Z., Sagare, A., Davis, J., Du Yan, S., Hamm, K., Xu, F., Parisi, M., LaRue, B., Hu, H. W., Spijkers, P., Guo, H., Song, X., Lenting, P. J., Van Nostrand, W. E., and Zlokovic, B. V. (2004) LRP/amyloid β-peptide interaction mediates differential brain efflux of Aβ isoforms. *Neuron* **43,** 333–344 CrossRef Medline
18. Zerbinatti, C. V., Wahrle, S. E., Kim, H., Cam, J. A., Bales, K., Paul, S. M., Holtzman, D. M., and Bu, G. (2006) Apolipoprotein E and low density lipoprotein receptor-related protein facilitate intraneuronal Aβ42 accumulation in amyloid model mice. *J. Biol. Chem.* **281,** 36180–36186 CrossRef Medline
19. Kim, J., Castellano, J. M., Jiang, H., Basak, J. M., Parsadanian, M., Pham, V., Mason, S. M., Paul, S. M., and Holtzman, D. M. (2009) Overexpression of low-density lipoprotein receptor in the brain markedly inhibits amyloid deposition and increases extracellular Aβ clearance. *Neuron* **64,** 632–644 CrossRef Medline
20. Basak, J. M., Verghese, P. B., Yoon, H., Kim, J., and Holtzman, D. M. (2012) Low-density lipoprotein receptor represents an apolipoprotein E-independent pathway of Aβ uptake and degradation by astrocytes. *J. Biol. Chem.* **287,** 13959–13971 CrossRef Medline
21. Liu, C.-C., Hu, J., Zhao, N., Wang, J., Wang, N., Cirrito, J. R., Kanekiyo, T., Holtzman, D. M., and Bu, G. (2017) Astrocytic LRP1 mediates brain Aβ clearance and impacts amyloid deposition. *J. Neurosci.* **37,** 4023–4031 CrossRef Medline
22. Nicolas, M., and Hassan, B. A. (2014) Amyloid precursor protein and neural development. *Development* **141,** 2543–2548 CrossRef Medline
23. Yuan, S. H., Martin, J., Elia, J., Flippin, J., Paramban, R. I., Hefferan, M. P., Vidal, J. G., Mu, Y., Killian, R. L., Israel, M. A., Emre, N., Marsala, S., Marsala, M., Gage, F. H., Goldstein, L. S., and Carson, C. T. (2011) Cell-surface marker signatures for the isolation of neural stem cells, glia and neurons derived from human pluripotent stem cells. *PLoS ONE* **6,** e17540 CrossRef Medline

24. Björkhem, I., Meaney, S., and Fogelman, A. M. (2004) Brain cholesterol: long secret life behind a barrier. *Arterioscler. Thromb. Vasc. Biol.* **24,** 806–815 CrossRef Medline
25. Pfrieger, F. W., and Ungerer, N. (2011) Cholesterol metabolism in neurons and astrocytes. *Prog. Lipid Res.* **50,** 357–371 CrossRef Medline
26. Nieweg, K., Schaller, H., and Pfrieger, F. W. (2009) Marked differences in cholesterol synthesis between neurons and glial cells from postnatal rats. *J. Neurochem.* **109,** 125–134 CrossRef Medline
27. Brown, M. S., and Goldstein, J. L. (1997) The SREBP pathway: regulation of cholesterol metabolism by proteolysis of a membrane-bound transcription factor. *Cell* **89,** 331–340 CrossRef Medline
28. Yang, C., McDonald, J. G., Patel, A., Zhang, Y., Umetani, M., Xu, F., Westover, E. J., Covey, D. F., Mangelsdorf, D. J., Cohen, J. C., and Hobbs, H. H. (2006) Sterol intermediates from cholesterol biosynthetic pathway as liver X receptor ligands. *J. Biol. Chem.* **281,** 27816–27826 CrossRef Medline
29. Zhang, Y., Sloan, S. A., Clarke, L. E., Caneda, C., Plaza, C. A., Blumenthal, P. D., Vogel, H., Steinberg, G. K., Edwards, M. S., Li, G., Duncan, J. A., 3rd., Cheshier, S. H., Shuer, L. M., Chang, E. F., Grant, G. A., *et al.* (2016) Purification and characterization of progenitor and mature human astrocytes reveals transcriptional and functional differences with mouse. *Neuron* **89,** 37–53 CrossRef Medline
30. Llorente-Cortés, V., Costales, P., Bernués, J., Camino-Lopez, S., and Badimon, L. (2006) Sterol regulatory element-binding protein-2 negatively regulates low density lipoprotein receptor-related protein transcription. *J. Mol. Biol.* **359,** 950–960 CrossRef Medline
31. van Dam, E. M., Ten Broeke, T., Jansen, K., Spijkers, P., and Stoorvogel, W. (2002) Endocytosed transferrin receptors recycle via distinct dynamin and phosphatidylinositol 3-kinase-dependent pathways. *J. Biol. Chem.* **277,** 48876–48883 CrossRef Medline
32. Kong, W., Wei, J., Abidi, P., Lin, M., Inaba, S., Li, C., Wang, Y., Wang, Z., Si, S., Pan, H., Wang, S., Wu, J., Wang, Y., Li, Z., Liu, J., and Jiang, J.-D. (2004) Berberine is a novel cholesterol-lowering drug working through a unique mechanism distinct from statins. *Nat. Med.* **10,** 1344–1351 CrossRef Medline
33. Woodruff, G., Reyna, S. M., Dunlap, M., Van Der Kant, R., Callender, J. A., Young, J. E., Roberts, E. A., and Goldstein, L. S. (2016) Defective transcytosis of APP and lipoproteins in human iPSC-derived neurons with familial Alzheimer's disease mutations. *Cell Rep.* **17,** 759–773 CrossRef Medline
34. Haass, C., Lemere, C. A., Capell, A., Citron, M., Seubert, P., Schenk, D., Lannfelt, L., and Selkoe, D. J. (1995) The Swedish mutation causes early-onset Alzheimer's disease by β-secretase cleavage within the secretory pathway. *Nat. Med.* **1,** 1291–1296 CrossRef Medline
35. Games, D., Adams, D., Alessandrini, R., Barbour, R., Berthelette, P., Blackwell, C., Carr, T., Clemens, J., Donaldson, T., and Gillespie, F. (1995) Alzheimer-type neuropathology in transgenic mice overexpressing V717F β-amyloid precursor protein. *Nature* **373,** 523–527 CrossRef Medline
36. Citron, M., Oltersdorf, T., Haass, C., McConlogue, L., Hung, A. Y., Seubert, P., Vigo-Pelfrey, C., Lieberburg, I., and Selkoe, D. J. (1992) Mutation of the β-amyloid precursor protein in familial Alzheimer's disease increases β-protein production. *Nature* **360,** 672–674 CrossRef Medline
37. Cai, X. D., Golde, T. E., and Younkin, S. G. (1993) Release of excess amyloid β protein from a mutant amyloid β protein precursor. *Science* **259,** 514–516 CrossRef Medline
38. Tamaoka, A., Odaka, A., Ishibashi, Y., Usami, M., Sahara, N., Suzuki, N., Nukina, N., Mizusawa, H., Shoji, S., and Kanazawa, I. (1994) APP717 missense mutation affects the ratio of amyloid β protein species (Aβ1–42/43 and Aβ 1–40) in familial Alzheimer's disease brain. *J. Biol. Chem.* **269,** 32721–32724 Medline
39. Suzuki, N., Cheung, T. T., Cai, X. D., Odaka, A., Otvos, L., Jr., Eckman, C., Golde, T. E., and Younkin, S. G. (1994) An increased percentage of long amyloid β protein secreted by familial amyloid β protein precursor (β APP717) mutants. *Science* **264,** 1336–1340 CrossRef Medline
40. Chen, A. K., Cheng, Z., Behlke, M. A., and Tsourkas, A. (2008) Assessing the sensitivity of commercially available fluorophores to the intracellular environment. *Anal. Chem.* **80,** 7437–7444 CrossRef Medline
41. Vassar, R., Bennett, B. D., Babu-Khan, S., Kahn, S., Mendiaz, E. A., Denis, P., Teplow, D. B., Ross, S., Amarante, P., Loeloff, R., Luo, Y., Fisher, S., Fuller, J., Edenson, S., Lile, J., *et al.* (1999) β-Secretase cleavage of Alzheimer's amyloid precursor protein by the transmembrane aspartic protease BACE. *Science* **286,** 735–741 CrossRef Medline
42. Choy, R. W., Cheng, Z., and Schekman, R. (2012) Amyloid precursor protein (APP) traffics from the cell surface via endosomes for amyloid β (Aβ) production in the trans-Golgi network. *Proc. Natl. Acad. Sci. U.S.A.* **109,** E2077–E2082 CrossRef Medline
43. Yamakawa, H., Yagishita, S., Futai, E., and Ishiura, S. (2010) β-Secretase inhibitor potency is decreased by aberrant β-cleavage location of the "Swedish Mutant" amyloid precursor protein. *J. Biol. Chem.* **285,** 1634–1642 CrossRef Medline
44. Young-Pearse, T. L., Bai, J., Chang, R., Zheng, J. B., LoTurco, J. J., and Selkoe, D. J. (2007) A critical function for β-amyloid precursor protein in neuronal migration revealed by *in utero* RNA interference. *J. Neurosci.* **27,** 14459–14469 CrossRef Medline
45. Kounnas, M. Z., Moir, R. D., Rebeck, G. W., Bush, A. I., Argraves, W. S., Tanzi, R. E., Hyman, B. T., and Strickland, D. K. (1995) LDL receptor-related protein, a multifunctional apoE receptor, binds secreted β-amyloid precursor protein and mediates its degradation. *Cell* **82,** 331–340 CrossRef Medline
46. Knauer, M. F., Orlando, R. A., and Glabe, C. G. (1996) Cell surface APP751 forms complexes with protease nexin 2 ligands is internalized via the low density lipoprotein receptor-related protein (LRP). *Brain Res.* **740,** 6–14 CrossRef Medline
47. Pietrzik, C. U., Yoon, I.-S., Jaeger, S., Busse, T., Weggen, S., and Koo, E. H. (2004) FE65 constitutes the functional link between the low-density lipoprotein receptor-related protein and the amyloid precursor protein. *J. Neurosci.* **24,** 4259–4265 CrossRef Medline
48. Trommsdorff, M., Borg, J. P., Margolis, B., and Herz, J. (1998) Interaction of cytosolic adaptor proteins with neuronal apolipoprotein E receptors and the amyloid precursor protein. *J. Biol. Chem.* **273,** 33556–33560 CrossRef Medline
49. Bu, G., Cam, J., and Zerbinatti, C. (2006) LRP in amyloid-β production and metabolism. *Ann. N.Y. Acad. Sci.* **1086,** 35–53 CrossRef Medline
50. Hass, S., Fresser, F., Köchl, S., Beyreuther, K., Utermann, G., and Baier, G. (1998) Physical interaction of ApoE with amyloid precursor protein independent of the amyloid Aβ region *in vitro*. *J. Biol. Chem.* **273,** 13892–13897 Medline
51. Kamal, A., Stokin, G. B., Yang, Z., Xia, C.-H., and Goldstein, L. S. (2000) Axonal transport of amyloid precursor protein is mediated by direct binding to the Kinesin light chain subunit of kinesin-I. *Neuron* **28,** 449–459 CrossRef Medline
52. Kamal, A., Almenar-Queralt, A., LeBlanc, J. F., Roberts, E. A., and Goldstein, L. S. (2001) Kinesin-mediated axonal transport of a membrane compartment containing β-secretase and presenilin-1 requires APP. *Nature* **414,** 643–648 CrossRef Medline
53. Schmidt, V., Sporbert, A., Rohe, M., Reimer, T., Rehm, A., Andersen, O. M., and Willnow, T. E. (2007) SorLA/LR11 regulates processing of amyloid precursor protein via interaction with adaptors GGA and PACS-1. *J. Biol. Chem.* **282,** 32956–32964 CrossRef Medline
54. Barrett, P. J., Song, Y., Van Horn, W. D., Hustedt, E. J., Schafer, J. M., Hadziselimovic, A., Beel, A. J., and Sanders, C. R. (2012) The amyloid precursor protein has a flexible transmembrane domain and binds cholesterol. *Science* **336,** 1168–1171 CrossRef Medline
55. McDonald, J. G., Smith, D. D., Stiles, A. R., and Russell, D. W. (2012) A comprehensive method for extraction and quantitative analysis of sterols and secosteroids from human plasma. *J. Lipid Res.* **53,** 1399–1409 CrossRef Medline
56. Mauch, D. H., Nägler, K., Schumacher, S., Göritz, C., Müller, E. C., Otto, A., and Pfrieger, F. W. (2001) CNS synaptogenesis promoted by glia-derived cholesterol. *Science* **294,** 1354–1357 CrossRef Medline
57. Karch, C. M., Cruchaga, C., and Goate, A. M. (2014) Alzheimer's disease genetics: from the bench to the clinic. *Neuron* **83,** 11–26 CrossRef Medline
58. Ryan, N. S., Nicholas, J. M., Weston, P. S. J., Liang, Y., Lashley, T., Guerreiro, R., Adamson, G., Kenny, J., Beck, J., Chavez-Gutierrez, L., de Strooper, B.,

Revesz, T., Holton, J., Mead, S., Rossor, M. N., and Fox, N. C. (2016) Clinical phenotype and genetic associations in autosomal dominant familial Alzheimer's disease: a case series. *Lancet Neurol.* **15,** 1326–1335 CrossRef Medline

59. Hsiao, K., Chapman, P., Nilsen, S., Eckman, C., Harigaya, Y., Younkin, S., Yang, F., and Cole, G. (1996) Correlative memory deficits, Aβ elevation, and amyloid plaques in transgenic mice. *Science* **274,** 99–102 CrossRef Medline
60. Mucke, L., Masliah, E., Yu, G.-Q., Mallory, M., Rockenstein, E. M., Tatsuno, G., Hu, K., Kholodenko, D., Johnson-Wood, K., and McConlogue, L. (2000) High-level neuronal expression of Aβ1–42 in wild-type human amyloid protein precursor transgenic mice: synaptotoxicity without plaque formation. *J. Neurosci.* **20,** 4050–4058 CrossRef Medline
61. Oddo, S., Caccamo, A., Shepherd, J. D., Murphy, M. P., Golde, T. E., Kayed, R., Metherate, R., Mattson, M. P., Akbari, Y., and LaFerla, F. M. (2003) Triple-transgenic model of Alzheimer's disease with plaques and tangles: intracellular Aβ and synaptic dysfunction. *Neuron* **39,** 409–421 CrossRef Medline
62. Mawuenyega, K. G., Sigurdson, W., Ovod, V., Munsell, L., Kasten, T., Morris, J. C., Yarasheski, K. E., and Bateman, R. J. (2010) Decreased clearance of CNS β-amyloid in Alzheimer's disease. *Science* **330,** 1774 CrossRef Medline
63. Siman, R., Card, J. P., Nelson, R. B., and Davis, L. G. (1989) Expression of β-amyloid precursor protein in reactive astrocytes following neuronal damage. *Neuron* **3,** 275–285 CrossRef Medline
64. Töpper, R., Gehrmann, J., Banati, R., Schwarz, M., Block, F., Noth, J., and Kreutzberg, G. W. (1995) Rapid appearance of β-amyloid precursor protein immunoreactivity in glial cells following excitotoxic brain injury. *Acta Neuropathol.* **89,** 23–28 CrossRef Medline
65. Almenar-Queralt, A., Falzone, T. L., Shen, Z., Lillo, C., Killian, R. L., Arreola, A. S., Niederst, E. D., Ng, K. S., Kim, S. N., Briggs, S. P., Williams, D. S., and Goldstein, L. S. (2014) UV irradiation accelerates amyloid precursor protein (APP) processing and disrupts APP axonal transport. *J. Neurosci.* **34,** 3320–3339 CrossRef Medline
66. Pietrzik, C. U., Busse, T., Merriam, D. E., Weggen, S., and Koo, E. H. (2002) The cytoplasmic domain of the LDL receptor-related protein regulates multiple steps in APP processing. *EMBO J.* **21,** 5691–5700 CrossRef Medline
67. Ulery, P. G., Beers, J., Mikhailenko, I., Tanzi, R. E., Rebeck, G. W., Hyman, B. T., and Strickland, D. K. (2000) Modulation of β-amyloid precursor protein processing by the low density lipoprotein receptor-related protein (LRP). Evidence that LRP contributes to the pathogenesis of Alzheimer's disease. *J. Biol. Chem.* **275,** 7410–7415 CrossRef Medline
68. Kang, D. E., Pietrzik, C. U., Baum, L., Chevallier, N., Merriam, D. E., Kounnas, M. Z., Wagner, S. L., Troncoso, J. C., Kawas, C. H., Katzman, R., and Koo, E. H. (2000) Modulation of amyloid β-protein clearance and Alzheimer's disease susceptibility by the LDL receptor-related protein pathway. *J. Clin. Invest.* **106,** 1159–1166 CrossRef Medline
69. Marzolo, M. P., and Bu, G. (2009) Lipoprotein receptors and cholesterol in APP trafficking and proteolytic processing, implications for Alzheimer's disease. *Semin. Cell Dev. Biol.* **20,** 191–200 CrossRef Medline
70. Israel, M. A., Yuan, S. H., Bardy, C., Reyna, S. M., Mu, Y., Herrera, C., Hefferan, M. P., Van Gorp, S., Nazor, K. L., Boscolo, F. S., Carson, C. T., Laurent, L. C., Marsala, M., Gage, F. H., Remes, A. M., *et al.* (2012) Probing sporadic and familial Alzheimer's disease using induced pluripotent stem cells. *Nature* **482,** 216–220 CrossRef Medline
71. Woodruff, G., Young, J. E., Martinez, F. J., Buen, F., Gore, A., Kinaga, J., Li, Z., Yuan, S. H., Zhang, K., and Goldstein, L. S. (2013) The presenilin-1 dE9 mutation results in reduced γ-secretase activity, but not total loss of PS1 function, in isogenic human stem cells. *Cell Rep.* **5,** 974–985 CrossRef Medline
72. Young, J. E., Boulanger-Weill, J., Williams, D. A., Woodruff, G., Buen, F., Revilla, A. C., Herrera, C., Israel, M. A., Yuan, S. H., Edland, S. D., and Goldstein, L. S. (2015) Elucidating molecular phenotypes caused by the SORL1 Alzheimer's disease genetic risk factor using human induced pluripotent stem cells. *Cell Stem Cell* **16,** 373–385 CrossRef Medline
73. Gore, A., Li, Z., Fung, H.-L., Young, J. E., Agarwal, S., Antosiewicz-Bourget, J., Canto, I., Giorgetti, A., Israel, M. A., Kiskinis, E., Lee, J.-H., Loh, Y.-H., Manos, P. D., Montserrat, N., Panopoulos, A. D., *et al.* (2011) Somatic coding mutations in human induced pluripotent stem cells. *Nature* **471,** 63–67 CrossRef Medline
74. Levy, S., Sutton, G., Ng, P. C., Feuk, L., Halpern, A. L., Walenz, B. P., Axelrod, N., Huang, J., Kirkness, E. F., Denisov, G., Lin, Y., MacDonald, J. R., Pang, A. W., Shago, M., Stockwell, T. B., *et al.* (2007) The diploid genome sequence of an individual human. *PLoS Biol.* **5,** e254 CrossRef Medline
75. Mali, P., Yang, L., Esvelt, K. M., Aach, J., Guell, M., DiCarlo, J. E., Norville, J. E., and Church, G. M. (2013) RNA-guided human genome engineering via Cas9. *Science* **339,** 823–826 CrossRef Medline
76. Ran, F. A., Hsu, P. D., Wright, J., Agarwala, V., Scott, D. A., and Zhang, F. (2013) Genome engineering using the CRISPR-Cas9 system. *Nat. Protoc.* **8,** 2281–2308 CrossRef Medline
77. D'Antonio, M., Woodruff, G., Nathanson, J. L., D'Antonio-Chronowska, A., Arias, A., Matsui, H., Williams, R., Herrera, C., Reyna, S. M., Yeo, G. W., Goldstein, L. S., Panopoulos, A. D., and Frazer, K. A. (2017) High-throughput and cost-effective characterization of induced pluripotent stem cells. *Stem Cell Reports* **8,** 1101–1111 CrossRef Medline
78. Quehenberger, O., Armando, A. M., Brown, A. H., Milne, S. B., Myers, D. S., Merrill, A. H., Bandyopadhyay, S., Jones, K. N., Kelly, S., Shaner, R. L., Sullards, C. M., Wang, E., Murphy, R. C., Barkley, R. M., Leiker, T. J., *et al.* (2010) Lipidomics reveals a remarkable diversity of lipids in human plasma. *J. Lipid Res.* **51,** 3299–3305 CrossRef Medline

Full-length amyloid precursor protein regulates lipoprotein metabolism and amyloid-β clearance in human astrocytes

Lauren K. Fong[1,4], Max M. Yang[1,4], Rodrigo dos Santos Chaves[1,4], Sol M. Reyna[1,4], Vanessa F. Langness[1,4], Grace Woodruff[1,4], Elizabeth A. Roberts[1,4], Jessica E. Young[1,3], and Lawrence S.B. Goldstein[1,2,4]*

Supporting Information, Figure 1

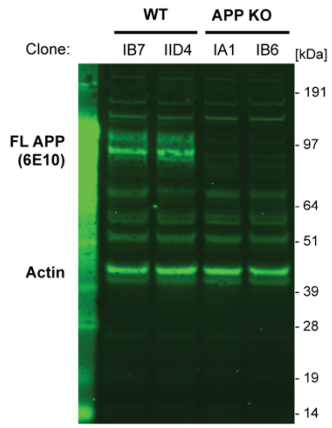

S-1: A full image of a western blot for FL-APP using the 6E10 antibody (expected ~100 kDA) and Actin (expected ~42 kDA) as a loading control in WT and APP-KO cells show that there are no truncated APP fragments detectable above background signal in the APP-KO cells.

ACKNOWLEDGEMENTS

Chapter 4, in full, is a reprint of the material as it appears in JBC 2018. Fong, L. K., Yang, M. M., Chaves, R. dos S., Reyna, S. M., Langness, V. F., Woodruff, G., Roberts, E. A., Young, J. E., and Goldstein, L. S. B. (2018) Full-length amyloid precursor protein regulates lipoprotein metabolism and amyloid-β clearance in human astrocytes. *J. Biol. Chem.* 10.1074/jbc.RA117.000441 The dissertation author was a co-author on this paper.

Chapter 5
Conclusion

Currently available AD treatments do not stop the progression of the disease but only help manage symptoms. The work in this dissertation was inspired by a search for better drugs. A drug screen performed in our lab was used to identify FDA (Food and Drug Administration) approved compounds which could be repurposed to lower pTau levels in human iPSC (hiPSC) derived neurons. Several cholesterol lowering drugs were identified as hits in this screen including a variety of statins and efavirenz. This caused us to become interested in the mechanism of how cholesterol lowering drugs act on pTau. We found that statins reduce cholesteryl ester levels which in turn increase proteasomal degradation of pTau. We found that statin induced reductions in pTau are highly correlated with statin induced reduction in Aβ. Using isogenic hiPSC lines carrying mutations in the cholesterol-binding domain of APP or APP knockout (KO) alleles we showed that while CE also regulate Aβ secretion, the effects of CE on Tau and Aβ are mediated by independent pathways. We additionally showed that a putative cholesterol binding site in APP mediates statin induced changes in Aβ secretion. Efavirenz is another drug that was identified in this screen which can lower CE levels. Efavirenz promotes neuronal cholesterol elimination by activating the neuron specific enzyme CYP46A1. Efavirenz showed lower astrocytic toxicity compared to statins and may allow us to target cholesterol metabolism while avoiding some of the side effects associated with statins. The details of this project can be found in the second chapter.

The second chapter raised many questions about the mechanism of how statins and CE influence Aβ secretion. These unanswered questions led me to the work

presented in the third chapter. In this chapter, we dug deeper into the mechanism of how cholesterol metabolism targeting drugs alter APP processing to Aβ. We used hiPSC derived neurons to show that atorvastatin treatment causes changes in APP fragmentation patterns that indicate that statins reduce processing by BACE1 and y-secretase. We modified a fluorescence complementation assay to show that atorvastatin increases full length APP (flAPP) dimerization and reduces full length APP interaction with BACE1. βCTF interaction with y-secretase catalytic subunits decreased as well after atorvastatin treatment. Together, these results suggest that cholesterol lowering drugs reduce APP processing to Aβ by increasing flAPP dimerization and inhibiting processing by BACE1 and y-secretase.

It is clear from the second and third chapters that cholesterol metabolism can influence APP processing. In the fourth chapter, we turn this question around and ask whether APP can influence cholesterol metabolism. Using APP KO hiPSC derived astrocytes, we show that flAPP plays a role in regulating endocytosis of LDL receptor ligands including cholesterol containing low density lipoproteins. This suggests that flAPP may function in maintenance of brain cholesterol homeostasis by regulating transport of cholesterol between different cell types in the brain.

Together, this work advances our understanding of the interplay between cholesterol metabolism, APP processing, and tau phosphorylation. Our work sheds light on a pathway which unites the variety of genetic and environmental factors that contribute to AD risk (cholesterol metabolism). Targeting cholesterol metabolic

pathways may be a promising approach in the search for drugs which can treat or prevent AD.

More work will be needed to determine whether SAD and FAD genetic risk factors can contribute to amyloid and tau pathology through alterations in brain cholesterol homeostasis. Additionally, well designed, long term clinical trials are needed to determine whether statins, ACAT inhibitors, efavirenz or other drugs that target brain cholesterol metabolism will be useful in AD treatment and prevention.